PATRÍCIA MANUELA AREIAS DA SILVA

THE SPINDLE ASSEMBLY CHECKPOINT: NEW INSIGHTS INTO ITS FUNCTION, REGULATION AND THERAPEUTIC IMPLICATIONS

Universidade do Algarve

Departamento de Ciências Biomédicas e Medicina

2017

PATRÍCIA MANUELA AREIAS DA SILVA

THE SPINDLE ASSEMBLY CHECKPOINT: NEW INSIGHTS INTO ITS FUNCTION, REGULATION AND THERAPEUTIC IMPLICATIONS

Doutoramento em Ciências Biomédicas

Trabalho efetuado sob orientação de:

Professor Doutor Hassan Bousbaa
Categoria –Professor Associado
Afiliação – IUCS, Instituto Universitário de Ciências da Saúde

Professor Doutor Álvaro Tavares
Categoria –Professor Auxiliar
Afiliação – Departamento de Ciências Biomédicas e Medicina da Universidade do Algarve

Universidade do Algarve
Departamento de Ciências Biomédicas e Medicina
2017

THE SPINDLE ASSEMBLY CHECKPOINT: NEW INSIGHTS INTO ITS FUNCTION, REGULATION AND THERAPEUTIC IMPLICATIONS

Declaração de autoria de trabalho

Declaro ser a autora deste trabalho, que é original e inédito. Autores e trabalhos consultados estão devidamente citados no texto e constam da listagem de referências incluída.

Patrícia Manuela Areias da Silva

(Patrícia Manuela Areias da Silva)

.

THE SPINDLE ASSEMBLY CHECKPOINT: NEW INSIGHTS INTO ITS FUNCTION, REGULATION AND THERAPEUTIC IMPLICATIONS

Para as minhas pessoas-sol, pelo brilho.

"There are many paths in the advancement of science, but the giant leaps in our Science of the Cell have been made by seeing. First we see and then we interpret and only then do we pursue mechanisms and theories. (...) The gift of the great microscopist is the ability to THINK WITH THE EYES AND SEE WITH THE BRAIN."

Daniel Mazia, 1996

The work presented in this thesis was conducted at:

Drug Discovery, Delivery & Toxicology Group | Mitosis & Cancer Biology

IINFACTS – Institute of Research and Advanced Training in Health Sciences and Technologies | iinfacts.cespu.pt

CESPU – Cooperativa de Ensino Superior e Universitário

Rua Central de Gandra, 1317

4585-116 Gandra PRD, Portugal

and

Oncobiology Research Group | The Cell Cycle and Cancer Biology Laboratory

CBMR – Centre for Biomedical Research | cbmr.ualg.pt

University of Algarve, FCT Bld. 8, Campus of Gambelas

8005-139 Faro, Portugal

and

Natural Products and Medicinal Chemistry Group

CIIMAR-UP - Interdisciplinary Centre of Marine and Environmental Research, University of Porto | ciimar.up.pt

Terminal de Cruzeiros do Porto de Leixões, Av. General Norton de Matos s/n

4450-208 Matosinhos, Portugal

FINANCIAL SUPPORT

Patrícia Manuela Areias da Silva was supported by a national PhD grant (SFRH/BD/90744/2012) from Fundação para a Ciência e Tecnologia (FCT).

The research described in this thesis was financially supported by CESPU (projects references: 02-GCQF-CICS-2011N; CheckTax-CESPU-2014; SpindlyTarget-CESPU-2016; AdoralLeuk-CESPU-2016 and MitOralC-CESPU-2016); and by national Portuguese funding through FCT (projects references: POCTI/BIA/PRO/60337/2004; PTDC/SAU-OBD/105234/2008; EXPL/BEX-BCM/1104/2013; PEst-OE/EQB/LA0023/2013; UID/BIM/04773/2013 CBMR).

ACKNOWLEDGEMENTS/AGRADECIMENTOS

I would like to express my gratitude to all the people and institutions that crossed my path and supported me during this wonderful journey and made this PhD thesis possible. In particular, I would like to deeply acknowledge to:

Professor Doutor Hassan Bousbaa, meu orientador, por ter acreditado desde início neste projeto e em mim. Obrigada pelo encorajamento, motivação e suporte incondicional. Pela partilha de conhecimento e pela liberdade de experimentação. Obrigada pela oportunidade de, uma vez mais, o ter como orientador. Sem dúvida, a pessoa que mais contribuiu para o meu crescimento científico.

Professor Doutor Álvaro Tavares, meu co-orientador, obrigada pelo constaste entusiasmo e otimismo. Pelos conhecimentos transmitidos e pelo apoio. Por acima de tudo, ter aceite embarcar nesta viagem mesmo antes de me conhecer. Espero que esteja orgulhoso dessa decisão.

Cláudia Florindo, da Unidade de Microscopia de Luz, do CMBR, um obrigado especial. Obrigada por me fazeres sentir em casa sempre que estava no Algarve; pelas conversas estimulantes e pela amizade. Agradeço tudo o que me ensinaste e todos os teus sábios conselhos. Obrigada pela semana intensa que passamos a fazer live-cell imaging. Sempre soube que formamos uma boa equipa.

Professor Luís Monteiro, Professor Convidado do Instituto Universitário de Ciências da Saúde (IUCS) e investigador do IINFACTS, CESPU, pela contribuição nesta tese, pelos conhecimentos transmitidos, nomeadamente na área da Patologia Oral, pelas palavras sempre carinhosas e pelo apoio.

Aos membros do grupo de investigação liderado pelo Professor Hassan Bousbaa (*Mitosis & Cancer Biology*), Professor Bruno Sarmento (*Drug Delivery*) e Professora Elizabeth Tiritan (*Applied Chemistry*), do IINFACTS, CESPU, pelos momentos partilhados ao longo destes quatro anos e pela troca de experiências. Um especial obrigado à Virgínia Gonçalves, por todo o apoio e amizade.

À Professora Maria Helena Vasconcelos, coordenadora do grupo de investigação *Cancer Drug Resistance*, do Instituto de Investigação e Inovação em Saúde da Universidade do Porto (i3S; IPATIMUP) e à Raquel Lima membro do grupo *Cancer Signalling & Metabolism* do i3S, pela disponibilidade e colaboração na Citometria de Fluxo e pelos reagentes cedidos.

À Professora Madalena Pinto, Professora Catedrática da Faculdade de Farmácia da Universidade do Porto (FFUP), coordenadora do Centro de Química Medicinal (CEQUIMED-UP) e, agora, do grupo de investigação *Natural Products and Medicinal Chemistry* do Centro Interdisciplinar de Investigação Marinha e Ambiental (CIIMAR-UP), por amavelmente ter disponibilizado o seu laboratório.

À Rita Reis, pelos momentos em que trabalhamos juntas, pela cumplicidade, pelo apoio e ensinamentos. Pela amizade e carinho que perduram.

À Joana Nunes, obrigada pela oportunidade de te ter conhecido. Sem dúvida das pessoas mais genuínas, alegres e contagiantes que conheço. Que sorriso fácil! Obrigada por todos os momentos.

À Ana Henriques, agradeço a ternura, o companheirismo e a humildade. Que a vida te sorria como mereces.

À Joana Fonseca, Sandra Marques e Nilza Ribeiro pela convivência, pelos momentos de descontração e pelo apoio.

À Francisca Araújo, pela amizade e pelo enorme carinho. Obrigada pelo teu apoio, pela disponibilidade imediata e pelo alento. Pelo conforto em todos os momentos. Acima de tudo, pela confiança.

À Vanessa Nascimento, pela energia contagiante. Pela boa disposição e pela amizade. Obrigada por tudo.

À Mariana Valente, Cláudia Andrade e Leonor Delgado por serem as amigas de sempre. Por estarem sempre cá, mesmo longe.

À Filipa e ao Nuno obrigada pela AMIZADE. Pela partilha constante; por estarem sempre aqui. Por me ouvirem em silêncio. Por todos os momentos, pelas aventuras e "viagens" inesquecíveis. Pelas pessoas maravilhosas que são e pelo crescimento conjunto.

À minha irmã, Paula, obrigada por seres a minha luz. Por estares sempre presente na minha vida e me apoiares incondicionalmente; pela tua disponibilidade e confiança em mim; pelo equilíbrio que me transmites.

À minha pequena princesa Beatriz, obrigada por colorires a minha vida. Pelo teu entusiasmo e sorriso fácil; pelos momentos de brincadeira libertadores. Obrigada pelas gomas e chocolates que colocavas ao lado do meu computador para impulsionar a escrita. Obrigada, acima de tudo, pela tua doce simplicidade e ternura que aquecem o meu coração.

Ao Eduardo, obrigada pelo carinho e pela boa disposição.

Aos meus Pais, agradeço pelo que sou hoje! Pelos princípios que me transmitiram e pela força que me dão em cada aventura. Pelo orgulho que têm em mim e por me darem asas para voar; pelo cuidado e pelo amor puro.

Á minha Avó, pelos sábios conselhos, pelo amor e pelo orgulho.

Agradeço ao Diogo, com especial ternura e amor, toda a paciência durante esta jornada (e todas as outras). Obrigada por compreenderes o que faço, por me apoiares sempre e por te orgulhares de mim tal como sou. Obrigada, do fundo do coração, por partilhares a tua vida comigo e me fazeres feliz a cada dia. Por seres o meu refúgio; pelo teu abraço que me renova a alma; por me lembrares que a vida é para ser vivida!

Em memória de Domingos Leite, agradeço partilha, a cumplicidade e o amor. É na adversidade que muitas vezes nos tornamos mais fortes. Obrigada pela confiança. Sei que estará orgulhoso.

Ao IINFACTS, CESPU e CBMR, Ualg pelo acolhimento, por disponibilizarem todas as infra-estruturas necessárias à realização desta tese e pelo financiamento. À Fundação para a Ciência e Tecnologia (FCT) por ter proporcionado esta aventura, ao me ter atribuído uma bolsa de doutoramento.

ABSTRACT

Genomic stability relies on the faithful chromosome segregation in mitosis, under the control of the Spindle Assembly Checkpoint (SAC). This surveillance mechanism monitors the nature of kinetochore-microtubule attachments (KT-MT) and prevents premature anaphase onset until all chromosomes achieve proper bipolar attachments and come under tension. To initiate anaphase and promote mitotic exit, the silencing of SAC is required.

In this study, we proposed to shed light into the function and regulation of the SAC mechanism and to explore its potential as therapeutic target for cancer therapy. For that, two questions were asked that define the main objectives of the present thesis: i) how SAC proteins are functionally related to motor proteins to regulate KT-MT attachments and SAC silencing? and ii) to what extent could SAC proteins constitute relevant cancer biomarkers and/or relevant targets to kill cancer cells, either alone or in combination with currently used antimitotics?

We found that RNAi-mediated co-depletion of the SAC protein Bub3 and the motor protein dynein partially restored functional KT-MT attachment, otherwise severely affect by individual depletion of each of the two proteins, leading to chromosome congression. An antagonistic relationship between Bub3 and dynein is suggested to ensure stable KT-MT attachments. In addition, we demonstrated that upon chromosome alignment at the metaphase plate, the core SAC proteins Mad1, Mad2, Bub1, BubR1, and Bub3 and the KMN components Hec1 and Mis12 are poleward transported by dynein, suggesting a role in SAC silencing.

Second, and in a therapeutic perspective, we dissected the dual role of Spindly (kinetochore regulator of dynein), in chromosome attachment and SAC silencing, as a strategy to potentiate tumor cell killing. We found an upregulation of Spindly in human cancer cell lines and in patient samples which are correlated with tumor proliferation. Interestingly, Spindly inhibition enhanced the cytotoxic response of paclitaxel- and cisplatin-mediated chemotherapy, and sensitized human tumor cells to death.

Overall, we provide new insight into the regulation of kinetochore-microtubule interactions by establishing a functional antagonistic relationship between Bub3 and dynein in regulating KT-MT attachment. Also, we provide new insight as to SAC components that are removed from the kinetochore by dynein during SAC silencing.

ABSTRACT

Finally, we propose Spindly as relevant target for cancer treatment and as a new biomarker for cancer proliferation and prognosis.

Keywords: spindle assembly checkpoint, kinetochore-microtubule interactions, Bub3, dynein, Spindly, cancer therapy.

RESUMO

A estabilidade genómica depende da fidelidade da segregação dos cromossomas, durante a mitose, sob o controlo do *checkpoint* mitótico. Este sofisticado mecanismo de controlo monitoriza o estado das ligações cinetocoro-microtúbulos e inibe o início prematuro da anafase até que todos os cromossomas estabeleçam uma ligação bipolar, através dos seus cinetocoros irmãos, com os microtúbulos provenientes de pólos opostos do fuso mitótico, culminando no seu alinhamento na placa metafásica, fenómeno designado de congressão. Nos cinetocoros não ligados ou ligados de forma incorrecta, a formação do complexo do *checkpoint* mitótico (MCC), constituído pela associação das proteínas Mad2, BubR1, Bub3 e Cdc20, inibe a activação do complexo promotor da anafase/ciclossoma (APC/C). A inibição do APC/C evita a degradação proteossómica dos substratos mitóticos ciclina B e securina, induzindo uma paragem na mitose e evitando a separação prematura das cromátides irmãs. Por sua vez, o início da anafase e a saída da mitose requerem o silenciamento do *checkpoint* mitótico.

A expressão anormal de componentes do *checkpoint* mitótico tem sido amplamente associada a vários tipos de cancro. Assim, a mitose como alvo no tratamento do cancro emergiu como um área de rápido avanço científico e várias proteínas envolvidas na sua regulação têm vindo a ser identificadas como possíveis alvos terapêuticos. Até à data, os fármacos que afectam a dinâmica dos microtúbulos como o paclitaxel, permanecem entre os quimioterápicos mais efetivos na clínica. Ao interferirem com a instabilidade dinâmica dos microtúbulos, estes agentes levam a uma activação crónica do *checkpoint* mitótico que ativaria o programa de morte celular. Infelizmente, o destino das células paradas em mitose sobre ação dos agentes anti-microtúbulos varia consideravelmente entre uma população de células tumorais e algumas células saem da mitose, escapando à morte celular. Não obstante, a resistência adquirida e a toxicidade, associada aos fármacos quimioterápicos em uso, permanecem uma preocupante limitação no sucesso da terapia do cancro. Assim, torna-se urgente compreender o mecanismo através do qual estes compostos atuam e travam a progressão das células tumorais, de forma a potenciar a sua acção e/ou desenvolver novas abordagens terapêuticas. Igualmente importante é a identificação de biomarcadores específicos que promovam uma detecção precoce e um diagnóstico efectivo.

RESUMO

No presente estudo propusemo-nos promover o conhecimento acerca da função e regulação do mecanismo do *checkpoint* mitótico e explorar o seu papel como potencial alvo terapêutico no tratamento do cancro. Para isso, duas questões principais foram colocadas, que definem os objetivos desta tese: (i) de que forma as proteínas do *checkpoint* mitótico estão funcionalmente relacionadas com as proteínas motoras dos microtúbulos, na regulação da ligação cinetocoro-microtúbulos e no silenciamento do checkpoint mitótico? e (ii) até que ponto as proteínas do *checkpoint* mitótico podem constituir relevantes biomarcadores e/ou alvos terapêuticos para eliminar as células tumorais, quer de forma isolada ou em combinação com os agentes anti-mitóticos correntemente em uso?

Para responder ao primeiro objetivo, propusemo-nos caracterizar, em células humanas em cultura, a relação funcional entre a proteína do *checkpoint* mitótico Bub3 e a proteína motora dineína, na ligação cinetocoro-microtúbulos, recorrendo à técnica de RNA de interferência, a ensaios funcionais e microscopia de alta resolução. A depleção, quer da proteína Bub3 quer da proteínas dineína, originou placas metafásicas incompletas com vários cromossomas desalinhados, confirmando o papel destas proteínas na ligação cinetocoro-microtúbulos. Surpreendentemente, a depleção simultânea das duas proteínas resultou na supressão parcial do fenótipo de desalinhamento e restaurou a congressão dos cromossomas. Consistente com estas observações, as ligações cinetocoro-microtúbulos estabelecidas nas células co-depletadas mostraram ser estáveis, produzindo tensão inter- e intra-cinetocoros, indicando que são funcionais. Sugerimos a existência de uma relação antagonística entre as proteínas Bub3 e dineína na regulação da estabilidade das ligações cinetocoro-microtúbulos. Ainda, propusemo-nos clarificar o papel da proteína dineína no silenciamento do *checkpoint* mitótico, nomeadamente no transporte de componentes do *checkpoint* dos cinetocoros ligados para os pólos do fuso mitótico. Recorrendo a dois ensaios de redução de ATP que mantêm a atividade motora da dineína mas que previne a libertação no pólo da proteína transportada, verificamos que os componentes do *checkpoint* mitótico Mad1, Mad2, Bub1, BubR1, and Bub3 são redistribuídos dos cinetocoros ligados para os pólos do fuso, pela ação motora da dineína. Esta redistribuição continua a ocorrer em células paradas em metafase, após tratamento com o inibidor do proteossoma MG-132, situação em que *checkpoint* deveria estar silenciado, indicando que estas células são capazes de reativar este mecanismo. Estes resultados foram corroborados *"in vivo"* pela observação em tempo real deste processo

recorrendo a uma proteína de fusão EGFP-Bub3. Curiosamente, foi verificado que um *pool* das proteínas Hec1 e Mis12 é igualmente transportado pela dineína para os pólos, sugerindo uma contribuição do complexo KMN (complexo proteico necessário para o estabelecimento da ligação cinetocoro-microtúbulo) no silenciamento do *checkpoint* mitótico.

Para responder ao segundo objetivo, e numa perspetiva terapêutica, exploramos o papel da proteína Spindly como potencial alvo terapêutico no tratamento do cancro. A Spindly é uma proteína necessária para a localização da dineína nos cinetocoros e está implicada na ligação dos cromossomas e no silenciamento do *checkpoint* mitótico. Inicialmente, verificamos uma sobreexpressão da Spindly quer em linhas celulares tumorais (PCR em tempo real) quer em amostras tumorais de pacientes (imunohistoquímica). Da análise imunohistoquímica verificou-se que a sobreexpressão da Spindly (+75% dos pacientes com carcinoma oral) estava correlacionada com um aumento da proliferação tumoral e com um mau prognóstico. As análises uni e multivariadas demonstraram que esta sobreexpressão constitui um indicador independente de prognóstico para a sobrevivência específica de cancro. Por outro lado, a depleção da Spindly, por RNA de interferência, revelou um aumento do efeito citotóxico de fármacos correntemente utilizados em quimioterapia, como o paclitaxel e a cisplatina, demonstrando sensibilizar as células tumorais para a morte celular. Estes resultados indicam que a supressão da Spindly poderá constituir uma estratégia válida e efectiva no tratamento do cancro. Como as concentrações utilizadas de paclitaxel e cisplatina utilizadas foram efetivamente reduzidas, esta estratégia poderá trazer benefícios clínicos, nomeadamente na superação dos efeitos secundários inerentes ao tratamento com estes fármacos. Estes resultados reforçam o potencial clinico da Spindly como um importante marcador de proliferação tumoral e o benefício de um co-tratamento com paclitaxel ou cisplatina na inibição da proliferação tumoral e na indução da morte celular.

Globalmente, o trabalho apresentado nesta tese contribuiu para estabelecer uma relação entre proteínas envolvidas na sinalização do *checkpoint* mitótico e as proteínas da maquinaria da ligação cinetocoro-microtúbulos; clarificou quais as proteínas transportadas dos cinetocoros para os pólos do fuso, pela dineína na promoção do silenciamento do *checkpoint* mitótico e identificou novos componentes sujeitos a este transporte; e identificou a proteína Spindly como potencial biomarcador e alvo terapêutico no tratamento do cancro, como adjuvante dos fármacos quimioterápicos em

uso. Permitiu, ainda, estabelecer uma ponte sólida entre a investigação fundamental e a investigação aplicada ao relacionar aspetos da função e regulação do mecanismo do *checkpoint* mitótico com as implicações terapêuticas resultantes da sua modelação.

Palavras-chave: *checkpoint* mitótico, interações cinetocoro-microtúbulos, Bub3, dynein, Spindly, terapia anti-cancro.

LIST OF CONTENTS

LIST OF FIGURES

Chapter 1: General Introduction

Chapter 3. Shedding light on Spindle Assembly Checkpoint regulation and function

Chapter 4. Exploring the potential therapeutic implications of Spindle Assembly Checkpoint for cancer therapy

LIST OF TABLES

Chapter 4. Exploring the potential therapeutic implications of Spindle Assembly Checkpoint for cancer therapy

LIST OF ABBREVIATIONS, ACRONYMS AND SYMBOLS

a.a	Aminoacids
APC/C	Anaphase promoting complex/cyclosome
A549	Human lung adenocarcinoma epitelial cells
ATM	Ataxia telangiectasia mutated
ATP	Adenosine triphosphate
ATR	Rad3-related
AZ/DOG	Sodium azide/2-deoxyglucose
BCA	Bicinchoninic Acid
Bub	Budding uninhibited by benzimidazole
BubR1	Budding uninhibited by benzimidazole-related 1
BuGZ	Microtubule-associated zinc finger protein
CAKs	Cdk-activating kinases
CCAN	Constitutive centromere-associated network
Cdc	Cell division cycle
Cdks	Cyclin-dependent kinases
CH	Calponin-homology
Chk	Checkpoint kinase
CIN	Chromosomal instability
cDNA	Complementary deoxyribonucleic acid
CENP	Centromere-associated protein
CKIs	Cdk inhibitors
CLASP	CLIP-associated protein
CLIP	Cytoplasmic linker proteins
C-Mad2	Closed Mad2
CO_2	Carbon dioxide
CPC	Chromosomal passenger complex
CSS	Cancer-specific survival
CT	Chemotherapy
DAPI	4′,6-diamidino-2-phenylindole
DHC	Dynein Heavy Chain
DLC	Dynein light chain

DLIC	Dynein light intermediate chain
DMEM	Dulbecco's Modified Eagle's Medium
DNA	Deoxyribonucleic acid
DIC	Dynein intermediate chain
DiM	Death in mitosis
DTT	Dithiothreitol
EBs	End Binding proteins
ECL	Enhanced Chemiluminescence
EDTA	Ethylenediamine tetraacetic acid
EGFP	Enhanced green fluorescent protein
FBS	Fetal bovine serum
FITC	Fluorescein isothiocyanate
G0	Gap0
G1	Gap1
G2	Gap2
GDP	Guanosine diphosphate
GFP	Green fluorescent protein
GTP	Guanosine triphosphate
h	Hours
HCl	Hydrochloric acid
Hec1	Highly expressed in cancer
HOK	Human oral keratinocytes
HPAEpiC	Normal pulmonary alveolar epithelial cells
HRP	Horseradish peroxidase
K-fiber	Kinetochore-fiber
KMN	KNL-1/Mis12 complex/Ndc80 complex
KT-MT	Kinetochore-microtubule
Lis-1	Lissencephaly-1
Mad	Mitotic arrest deficient
MAPK	Mitogen activated protein kinase
MAPs	Microtubule-associated proteins
MCAK	Centromere-associated kinesin
MCC	Mitotic checkpoint complex
MG-132	Carbobenzoxy-Leu-Leu-leucinal

LIST OF ABBREVIATIONS, ACRONYMS AND SYMBOLS

ml	Milliliter
mM	Millimolar
M phase	Mitosis
MPF	Mitosis-Promoting Factor
Mps1	Monopolar spindle 1 kinase
MRP	Multidrug-resistance protein
MTAs	Microtubule-targeting agents
MTOC	Microtubule-organizing center
MT	Microtubule
MTT	3-(4, 5-dimethylthiazolyl-2)-2,5-diphenyltetrazolium bromide
mRNA	Messenger ribonucleic acid
min	Minutes
NaCl	Sodium chloride
NCI-H460	Non-small cell lung cancer
NDGA	Nordihydroguaiaretic acid
NEBD	Nuclear envelope breakdown
nm	Nanometer
nM	Nanomolar
NS	No statistical significance
NSCLC	Non-small cell lung cancer
NuMA	Nuclear Mitotic Apparatus protein
O-Mad2	Open-Mad2
OSCC	Oral squamous cell carcinoma
PARP-1	Poly [ADP-ribose] polymerase 1
PBS	Phosphate-buffered saline
PCM	Pericentriolar material
PE	Plating efficiency
PI	Propidium iodide
Plk	Polo-like kinase
PMD	Post-mitotic death
PP	Protein phosphatase
PTM	Post-translational modification
PTX	Paclitaxel
qRT-PCR	Quantitative real-time polymerase chain reaction

RNA	Ribonucleic acid
RNAi	RNA interference
RNase	Ribonuclease
Rod	Rough deal
RPMI	Roswell Park Memorial Institute
RT	Room temperature
RRZZ	Rod/ZW10/Zwilch
S-phase	Synthesis-phase
SAC	Spindle assembly checkpoint
Saline G	Isotonic salt solution with glucose
SD	Standard deviation
SDS	Sodium dodecyl sulfate
sec	Seconds
shRNAs	Short hairpin RNAs
siRNA	Small interfering RNA
SG	Sugery
Thr	Threonine
Tyr	Tyrosine
TMA	Tissue microarray
Tris	Tris(hidroximetil)aminometano
TUNEL	Terminal deoxynucleotidyl transferase-mediated nick end labeling
ZW10	Zeste White 10
+TIPs	Microtubule plus-end-tracking proteins
γ-TuRC	γ-tubulin ring complex
°C	Degree Celsius
µg	Microgram
µM	Micromolar
µm	Micrometer

THESIS OUTLINE

This thesis is organized into **six chapters** and **one appendix**.

Chapter 1 provides a general introduction in light of the current literature. An overview of the cell cycle, its regulation and control are addressed. A particular emphasis is given to mitosis, from the description of the events to the molecular machinery of the mitotic spindle. Kinetochore-microtubules interactions and error correction are described in detail. Spindle Assembly Checkpoint (SAC) activation and silencing mechanisms are presented, together with the link between SAC and tumorigenesis. Lastly, targeting mitosis for cancer therapy was focused, providing an overview of the current approaches, their limitations and future directions.

Chapter 2 describes the project motivation and the specific aims**.**

Chapters 3 and **4** are related to the experimental work and are structured according to two main aims. In chapter 3 we describe the work performed on the regulation and function of SAC. In particular, chapter 3 unveils a functional interaction between the SAC protein Bub3 and the microtubule motor dynein in regulating kinetochore-microtubule attachments and elucidates the role of kinetochore dynein in SAC silencing mechanism. In chapter 4 we describe the work concerning the relevance of SAC components in cancer therapy. In this chapter, we explore the dual role of Spindly protein in chromosome attachment and SAC silencing as a strategy to potentiate tumor cell killing. The consequences of Spindly depletion on the viability of tumor cells treated with clinically relevant doses of paclitaxel and cisplatin are reported. Importantly, the pattern of Spindly expression in patient samples from oral cancer and its potential correlation to clinicopathologic significance are stated. A rationale for combination chemotherapy is discussed, providing a novel and possibly effective approach for therapeutic intervention in cancer.

Chapter 5 provides overall conclusions and perspectives for future research.

In **Chapter 6** a list of all cited references is available.

Lastly, the **Appendix** contains the legends of the movies that were provided in digital support.

The information presented in the chapters 2 and 3 is published or submitted for publishing in international peer review scientific journals, according to the following list:

Patrícia M.A. Silva, Maria Leonor Delgado, Nilza Ribeiro, Cláudia Florindo, Álvaro A. Tavares, Carlos Lopes, Barbas do Amaral, Hassan Bousbaa and Luís Silva Monteiro. Spindly Expression, Prognostic Significance and Therapeutic Implications in Oral Squamous Cell Carcinoma. International Journal of Cancer. 2017. (*submitted*).

Patrícia M.A. Silva, Nilza Ribeiro, Raquel Lima, Cláudia Andrade, Vânia Diogo, Joana Teixeira, Cláudia Florindo, Álvaro A. Tavares, Helena Vasconcelos and Hassan Bousbaa. Suppression of Spindly Delays Mitotic Exit and Exacerbates Cell Death Response of Cancer Cells Treated with Low Doses of Paclitaxel. Cancer Letters. 2017;394:33-42. DOI: 10.1016/j.canlet.2017.02.024.

Patrícia M.A. Silva, Álvaro A. Tavares and Hassan Bousbaa. Co-silencing of human Bub3 and dynein highlights an antagonistic relationship in regulating kinetochore-microtubule attachments. FEBS Letters. 2015;589(23):3588-94. DOI: 10.1016/j.febslet.2015.10.017.

Patrícia M.A. Silva, Rita M. Reis, Victor M. Bolanos-Garcia, Claudia Florindo, Álvaro A. Tavares and Hassan Bousbaa. Dynein-dependent transport of spindle assembly checkpoint proteins off kinetochores toward spindle poles. FEBS Letters. 2014;588(17):3265-73. DOI: 10.1016/j.febslet.2014.07.011.

The presented work was divulgated through the following communications in scientific meetings:

Patrícia M.A. Silva; Maria Leonor Delgado; Carlos Lopes; Hassan Bousbaa; Luís Silva Monteiro. Spindly Expression in Oral Squamous Cell Carcinomas. 6th World Congress of the International Association of Oral Oncology. 17-20 May 2017. Bangalore, India. (Poster)

Patrícia M.A. Silva. "A mitose como alvo terapêutico contra o cancro." I Congresso Nacional de Ciências Biomédicas Laboratoriais. Instituto Politécnico de Bragança. 28-30 October, 2016. Bragança, Portugal. (Oral communication)

Patrícia M.A Silva, Diogo V, Teixeira J, Ribeiro N, Lima RT, Vasconcelos MH, Florindo C, Tavares AA and Bousbaa H. Targeting Spindly as Antimitotic Strategy to Induce Cancer Cell Death. 2nd ASPIC International Congress. 28-29 April, 2016. Porto, Portugal. (Poster)

Patrícia M.A Silva, Reis RM, Bolanos-Garcia VM, Florindo C, Tavares AA, Bousbaa H. Tracking dynein-mediated transport of spindle assembly checkpoint proteins from kinetochore to spindle pole. Conferência Internacional de Microscopia e Microanálise (INCOMAM´14), XLVIII Congresso da Sociedade Portuguesa de Microscopia. Faculdade de engenharia da Universidade do Porto (FEUP). 6-7 November, 2014. Porto, Portugal. (Oral communication)

Patrícia M.A Silva, Tavares AA, Bousbaa H. Functional relationship between the mitotic checkpoint protein Bub3 and the molecular motor dynein in regulating kinetochore-microtubule attachment. EMBO Conference Series - Microtubules: Structure, Regulation and Functions. 28-31 May, 2014. EMBL Heidelberg, Germany. (Poster)

CHAPTER 1

GENERAL INTRODUCTION

1. THE EUKARYOTIC CELL DIVISION CYCLE

1.1. Cell cycle overview

The cell cycle can be defined as a highly ordered and tightly regulated process by which a parental cell reproduces and gives rise to two genetically identical daughter cells. Therefore, it is a vital process during the development of multicellular organisms and for the maintenance of adult tissues, by providing the renewal of old or damaged cells.

Classically, the eukaryotic cell cycle can be divided in two major phases: the longest, called interphase, during which the cell grows and replicates the chromosomal DNA; and the shorter phase, mitosis, where the segregation of replicated chromosomes and their equal distribution takes place (**Figure 1.1**).

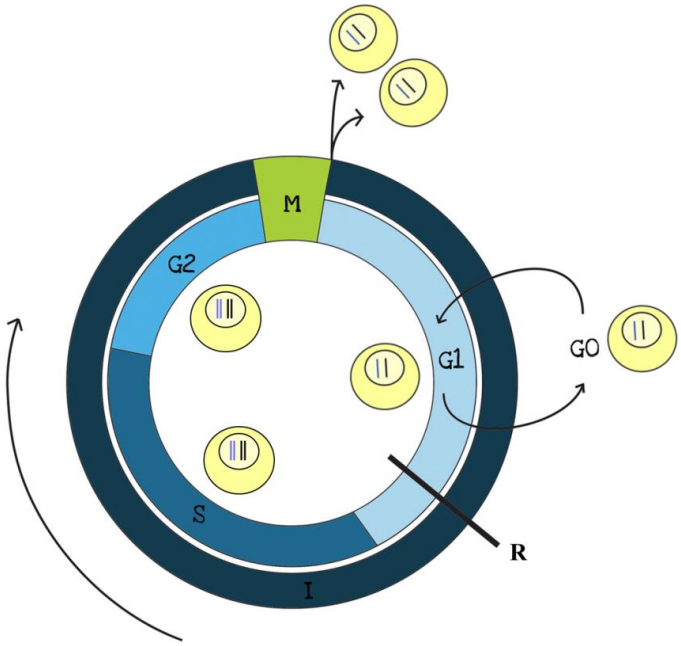

Figure 1.1. Illustration of the eukaryotic cell cycle. Resting non-dividing cells are called in G0 and may entre G1 phase, pass the restriction point (R) and go through cell cycle under mitogen stimuli. The cell cycle is divided in two major phases, the interphase (I, dark blue), which comprises the G1-, S- and G2-phases, and mitosis (M, green). During the Gap phases, G1 and G2, the cell continuously grows and synthetizes components for the S-phase and mitosis, respectively. At the S-phase the DNA and centrosomes are replicated. At mitosis (M phase) the cell contents are equally distributed between the two new daughter cells.

The interphase is the period between two consecutive mitosis and contemplates the orderly phases Gap1 (G1), the synthesis-phase (S-phase), and the Gap2 (G2). During the G1, the biosynthetic activity of the cell is quite pronounced, namely the synthesis of enzymes required for the following S-phase. The membrane, structural proteins,

cytoplasmic organelles and RNAs are duplicated, resulting in the cell size doubling, although the chromosomes are in only single copies *per* cell. The major control of cell proliferation is positioned at late G1 and is called restriction point. Regulated primarily by extracellular growth factors, the fate of the most cells is dictated at this point. In the presence of suitable growth factors, cells go past the restriction point, and become committed to proceed through S-phase and continuing cycling. In contrast, if proper growth factors are not available, cells exit from the cell cycle becoming quiescent, a reversible non-proliferating resting state called Gap0 (G0). Some cells can stay for long periods without proliferating, remaining metabolically active, although they cease growth and have reduced rates of protein synthesis; while others remain at G0 for their entire lifespan. During the S-phase, centrosomes and DNA are replicated, and each chromosome has now two sister chromatids. At the G2 phase, the cell continues to grow and synthetize macromolecules in preparation for mitosis.

Mitosis, or M-phase, culminates into the nuclear division, and is followed by the cytoplasmic division, or cytokinesis, where the formed daughter cells are completely individualized.

1.2. Cell cycle regulation and control

The ordering of cell cycle events is orchestrated by a complex regulatory network that controls the accurate timing and direction of duplication and division of cellular components. By ensuring the unidirectionality, the occurrence of later events is dependent of the successful completion of earlier events. For instance, DNA replication should begin and end before the distribution of cell contents at mitosis. Through signal transduction pathways, the cell cycle control system allows events separated either in time or space to be connected between the different phases.

Cell cycle central regulators are a family of serine/threonine kinases known as Cyclin-dependent kinases (Cdks) [1, 2], which catalyze the phosphorylation of protein substrates inducing changes in their enzymatic activity or the interaction with other proteins. Cdks concentration is constant throughout the cell cycle and regulation of their activity depends primarily on fluctuations in levels of the regulatory subunits termed cyclins. These bind tightly to Cdks and stimulate their catalytic activity. In addition to cyclin binding, complete activation of Cdks requires a phosphorylation of a threonine residue 160 (Thr 160) adjacent to the kinase active site, catalyzed by Cdk-activating

kinases (CAKs). In contrast, Cdks inhibition could be modulated by interactions with Cdk inhibitors (CKIs), working as brakes to halt cell cycle progression under adverse conditions, and by inhibitory phosphorylation at tyrosine residue 15 (Tyr 15) and threonine residue 14 (Thr 14) of Cdks. Changes in the phosphorylation of these sites are particularly critical in the activation of mitotic Cdks, at the onset of mitosis. Phosphorylation of Tyr 15 by kinase Wee1, or phosphorylation of both Tyr 15 and Thr 14 by kinase Myt1, inactivates the M-phase cyclin-Cdk complex. In turn, dephosphorylation of the inhibitory sites by the phosphatase Cdc25C leads to complex reactivation and allows entry into mitosis [3, 4].

Cyclins are produced and degraded according to the cell cycle stage, resulting in the formation of specific complexes cyclin-Cdk which controls the progression of cell cycle (**Figure 1.2**). Cyclins can be divided in four classes: G1 cyclins (D in vertebrates), G1/S cyclins (E in vertebrates), S cyclins (A in vertebrates) and G2/M cyclins (A and B in vertebrates) [5, 6].

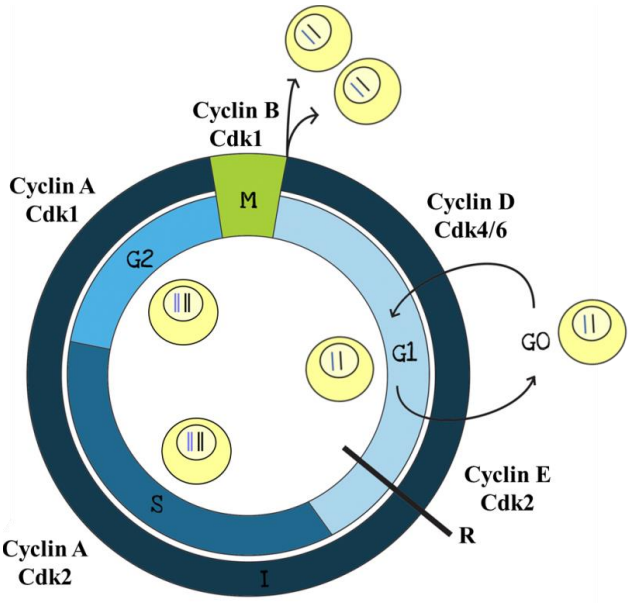

Figure 1.2. Different cyclin-Cdk complexes formed along the cell cycle stages in vertebrates. Cyclin D-Cdk4 or -Cdk6 controls the cell cycle entry at G1; Cyclin E-Cdk2 monitors the G1/S phase, initiating the process of DNA replication; Cyclin A-Cdk1 or -Cdk2 stimulates the DNA replication at S-phase and promotes early mitotic events; Cyclin B-Cdk1 promotes mitosis entrance and its degradation is required for mitotic exit.

G1 cyclins contributes to stimulate and control the cell cycle entrance in response to extracellular factors. G1/S cyclins rise in late G1 and fall in early S-phase, triggering cell progression through restriction point and initiating the process that leads to DNA

and centrosomes replication. S cyclins are responsible for stimulate the DNA replication, remaining high throughout S-phase, and also at G2 and early mitosis to promote the initial mitotic events. The association between cyclin B with Cdk1 (initially known as p34Cdc2) forms a complex called Mitosis-Promoting Factor (MPF), critical for mitosis onset. Cyclin B rises as the cell approaches mitosis and it is responsible for the cellular changes that occur in early stages (described in the next section), while their degradation leads to the mitotic exit. Cyclin levels regulation depends on cyclin gene expression and their degradation by the ubiquitin-proteolytic system, thereby modulating different Cdks activity [7]. Indeed, the irreversibility of the cell cycle is achieved by proteolytic destruction of cyclins and this post-translational mechanism is particularly important at the metaphase to anaphase transition, during mitosis, where the sister chromatids separation and mitosis exit are triggered by cyclin B destruction and consequent inactivation of Cdk1. Cyclin B is targeted for degradation after ubiquitination (addition of multiple copies of ubiquitin) by the anaphase-promoting complex/cyclosome (APC), followed by destruction on the proteasome.

To ensure that genetically normal cells are produced, there are control mechanisms at each phase transition called checkpoints that detect errors in the execution of a cell cycle event, leading to an arrest until the damage is repaired. These checkpoints are positioned before key cell cycle events like DNA replication and sister chromatids separation (**Figure 1.3**) and are critical for the maintenance of genomic fidelity [8]. An attenuation of their function contributes to genomic instability that may benefit the development of cancer cells [9-11]. The major cell cycle checkpoints can be grouped in two classes according to their function in DNA damage, during the interphase, or in mitosis progression. DNA damage checkpoints have evolved as a network of cellular signaling pathways to ensure accuracy of DNA replication and, in turn, prevent progression into mitosis with damaged DNA. These cell cycle checkpoints arrest or delay cell cycle progression either in: the G1 phase, before DNA replication; in S-phase, during DNA replication; or in G2 phase, before mitosis [12, 13, 11]. Cells respond to DNA damage by inducing repair mechanisms or, in the presence of excessive and irreparable damage, by promoting cell death. For instance, if DNA damage occurs at G1, the G1 checkpoint induces the rapid stabilization and accumulation of the tumor suppressor p53 and cells with damaged DNA are restricted from entering S-phase until the damage is removed [14]. The Ataxia Telangiectasia Mutated (ATM) kinase is

activated by DNA double strand breaks (DSBs), acting as a transducer of DNA damage signals, and triggers the G1 checkpoint by phosphorylating and activating the Checkpoint Kinase 2 (Chk2) [15]. In turn, Chk2 inhibits Cdc25A, a phosphatase that removes inhibitory phosphorylation of the cyclin A-Cdk2 and cyclin E-Cdk2 complexes, preventing cells from proceeding into S-phase [16]. ATM also induces phosphorylation and stabilization of p53, reducing its affinity for the negative regulator, the ubiquitin ligase Mdm2 [17, 18]. Stabilized p53 induces the transcription of the CKI p21 that binds and inhibits cyclin A-Cdk2 and cyclin E-Cdk2 complexes [19]. In case the damage cannot be repaired, this mechanism is capable of triggering apoptosis or senescence. The intra-S checkpoint delays or slows down DNA replication during S-phase in order to minimize replication errors. The damage is sensed by the ATM and Rad3-related (ATR) kinase which by activating Checkpoint Kinase 1 (Chk1) induces Cdc25A proteosomal degradation, blocking further progression through S-phase [20, 21]. ATR and Chk1 also trigger the G2/M checkpoint, which prevents cells with damaged DNA from entering mitosis, therefore minimizing chromosome missegregation [22]. The checkpoint operating during mitosis is termed spindle assembly checkpoint (SAC) and controls the successful bipolar attachment of all chromosomes with spindle microtubules and the consequent alignment at metaphase plate before cell transition to anaphase [23] (described in detail in section 4).

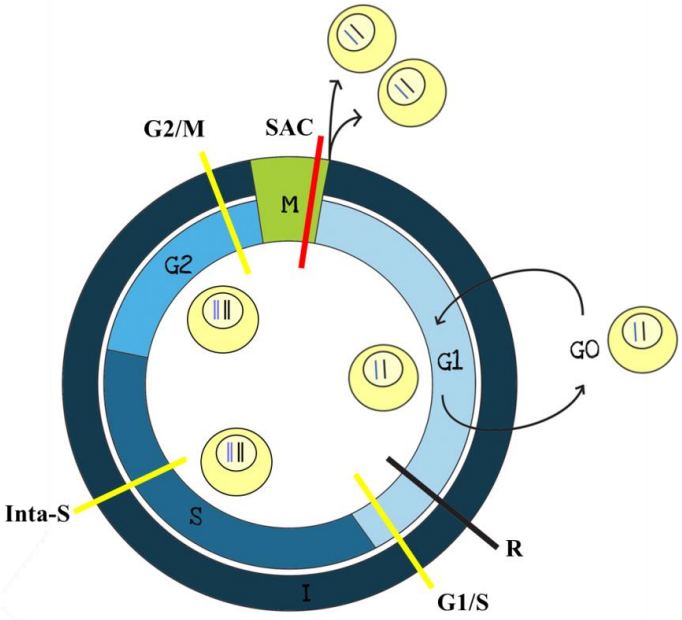

Figure 1.3. Localization of the cell cycle checkpoints. Yellow lines represent the DNA damage-activated checkpoints (G1/S, intra-S and G2/M), positioned to detect DNA lesions before, during and after DNA replication; and the red line the mitotic checkpoint (SAC), which ensures that all chromosomes are aligned and correctly attached to the spindle microtubules before segregate. R represents the restriction point.

2. MITOSIS

2.1. General description

Mitosis represents one of the most important and fascinating events of the cell cycle, since the genomic material, duplicated in interphase are equally distributed by the new formed daughter cells, ensuring the accuracy of genome transmission.

Based on structural changes, mitosis can be divided into five continuous stages: prophase, prometaphase, metaphase, anaphase and telophase (**Figure 1.4 and 1.5**).

At the beginning of prophase, the filaments of chromosomal DNA start to condense, originating recognizable chromosomes and making visible the two sister chromatids held together by a constricted region known as centromere. Simultaneously, centrosomes separate and start to migrate towards opposite sides of cell to initiate the bipolar microtubules array for the mitotic spindle assembly. The end of prophase and the onset of prometaphase is marked by the nuclear envelope breakdown (NEBD), allowing a dynamic interaction between chromosomes and spindle microtubules. Spindle microtubules attach to sister chromatids at the kinetochore, a specialized protein complex assembled on centromeric DNA. At this moment, the microtubules from opposite spindle poles, defined by centrosomes, start to attach to kinetochores of dispersed chromosomes in a classical process called “search and capture”. The metaphase is achieved when all captured chromosomes have established bipolar attachments with microtubules from opposite spindle poles, becoming bi-oriented, and reaches the alignment at the equatorial region of the spindle in a process known as congression. The metaphase to anaphase transition is the most dramatic event of mitosis. At anaphase A, the cohesion between the sister chromatids are swiftly lost and the separated chromatids are pulled towards opposite poles of the spindle, leading to their segregation. At anaphase B, the mitotic spindle elongates and the two poles move farther apart from of each other, completing the segregation. During the telophase, the spindle is disassembled, leaving a single centrosome associated with one set of chromosomes. The nuclear envelope reorganizes and repackages the already decondensing chromosomes, and other nuclear components, in two daughter nuclei. In addition, a contractile furrow starts to form between the nuclei and splits the cell in two due to actin and myosin action, characterizing the cytokinesis step.

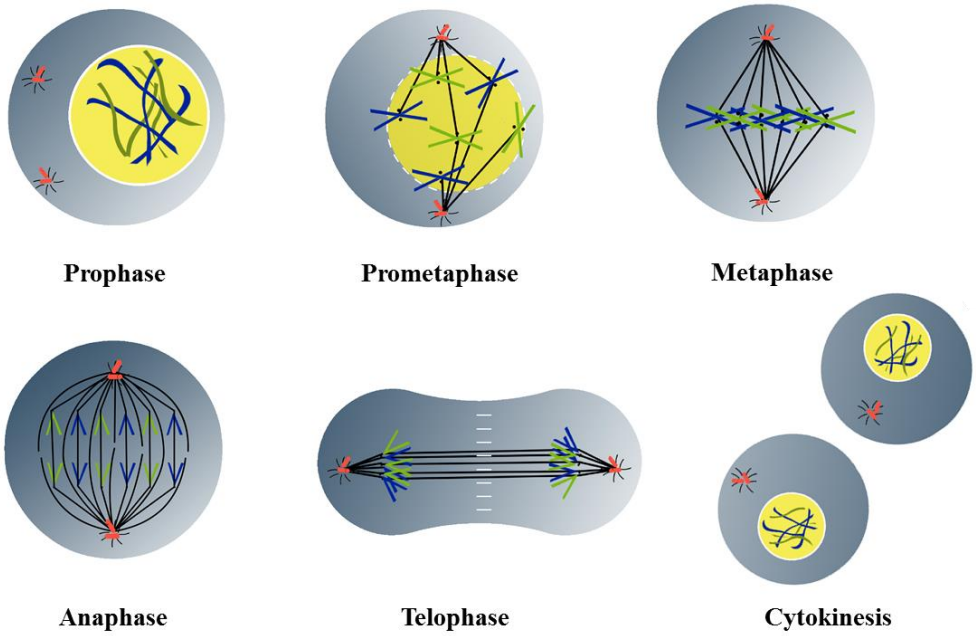

Figure 1.4. Schematic representation of the mitotic stages and cytokinesis. In prophase the chromosomal DNA (blue and green lines) starts to condense, to generate well-defined chromosomes, and the centrosomes (orange) initiate the migration towards opposite sides of the cell to assemble the future bipolar spindle. The envelope nuclear breakdown (white line surrounding the nucleus in yellow) sets the beginning of prometaphase, and microtubules (black) from opposite spindle poles can now interact and capture chromosomes, thought their kinetochores (black points positioned on each chromosome arm). At metaphase, all chromosomes have established a bipolar attachment with microtubules and are aligned at the equatorial plane of the cell. During anaphase, the cohesion between sister chromatids is dissolved and they separate into opposite spindle poles. At telophase, the spindle is disassembled, the nuclear envelope reorganizes around each group of decondensing chromosomes. At the same time, the division of cytoplasm (cytokinesis) gives rise to independent daughter cells.

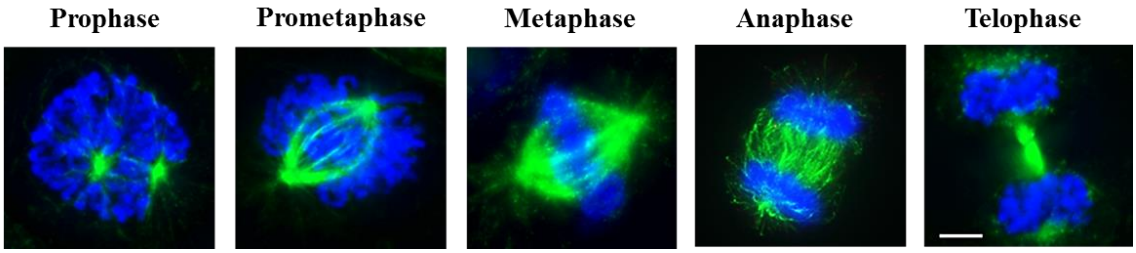

Figure 1.5. Representative immunofluorescence images from culture cells showing the different mitotic phases. Cells were stained with an anti-α-tubulin antibody to visualize spindle microtubules (green) and the DNA was stained with DAPI (blue). Bar = 5 µm.

2.2. Mitotic apparatus

Early in mitosis, the mitotic spindle starts to assemble to allow chromosomes alignment at the spindle equator in metaphase, and to separate equally the sister

chromatids to daughter cells in anaphase. The spindle itself is a macromolecular machine composed of an array of dynamic microtubules, nucleated at centrosomes, and associated motor and non-motor proteins responsible for their assembly and maintenance and coordination of diverse mitotic events.

2.2.1. Centrosomes

The centrosome of animal cells is a large organelle consisting of a pair of centrioles, positioned orthogonally to each other, and surrounded by amorphous pericentriolar material (PCM) [24]. Each centriole is a short cylindrical array of nine microtubule triplets, associated with centrosome integrity and with recruitment of centrosomal proteins. The PCM is a fibrous scaffold lattice mainly composed by a specialized tubulin called γ-tubulin, which assembles into a multisubunit γ-tubulin ring complex (γ-TuRC) to serve as a nucleation template for microtubule formation [25, 26] **(Figure 1.6)**.

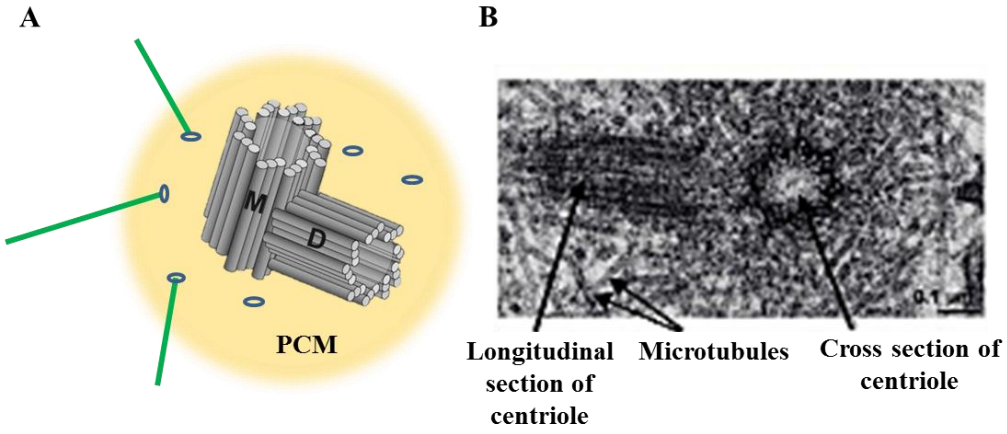

Figure 1.6. Simplified scheme of the centrosome and the centriole ultra-structure. (A) A centrosome is composed of a pair of centrioles (in gray, M - mother and D - daughter) embedded in a cloud of amorphous pericentriolar material (in yellow, PCM). Each centriole is a cylindrical structure composed of nine microtubule arrays, and each array consists of three microtubules. The main component of PCM is a specialized tubulin called γ-tubulin, which assembles into a multisubunit γ-tubulin ring complex (in blue, γ-TuRC) to serve as a nucleation template for microtubule formation (in green). (Adapted from [27]) **(B)** Electron micrograph of animal centriole. A longitudinal and a cross-section, illustrating the ninefold radial symmetry of microtubules, are shown (Adapted from [28]).

For this reason, centrosomes are referred as the major microtubule-organizing center (MTOC), in higher eukaryotes, nucleating polarized microtubule arrays with their plus-ends extending outward, to originate the mitotic spindle, a typical bipolar microtubule-based structure [29, 30]. Microtubules can also be directly nucleated from chromatin

[31] and kinetochores [32]. In addition to their role in microtubules nucleation and spindle architecture, the centrosome has emerged as an important site of cell cycle regulation and plays a major role in diverse cellular functions, orchestrating G1/S transition and DNA damage, the entry into mitosis, anaphase onset and cytokinesis [33, 26, 34]. Especially at mitosis, the centrosomes have the critical role to mediate the strictly balanced bipolar separation of chromosomes.

Certain proteins are permanently associated with the centrosome core structure such as γ-tubulin, the γ-TuRC and centrin, remaining after treatment with microtubule depolymerizing agents such as nocodazole or colchicine, while others are temporarily associated, to perform centrosome-specific functions, such as the Nuclear Mitotic Apparatus protein (NuMA) which become the most significant centrosome-associated protein after NEBD [35]. NuMA is a multifunctional protein playing a significant role in the organization of the mitotic apparatus, and translocates from the nucleus to spindle poles at the onset of mitosis to form a crescent-shaped complex around centrosomes tethering microtubules into the accurate bipolar organization. This translocation occurs in a dynein-mediated mechanism, a molecular motor associated with microtubules [36, 37]. Interestingly, some kinases, such as the mitogen activated protein kinase (MAPK), and phosphatases seems to utilize centrosomes only as a docking or platform station [38]. A proteomic-based approach has identified several centrosomes proteins from human purified centrosomes grouped into structural proteins, regulatory molecules and heat shock proteins [39].

In interphase, at G1, a single centrosome is positioned into the cytoplasm and closely associated with the nucleus. At S-phase, concomitantly with DNA synthesis, the centrosome duplicates in an accurate and semi-conservative process divided into four main stages: disengagement of the pair of centrioles, centriole duplication, centrosome elongation and sister centrosome separation (reviewed in [40, 41]). Centrosome separation is related to the spatial separation of centrosome material around the nucleus which is driven by plus- and minus-end directed microtubule motor proteins. Polo-like kinases (Plks) have been clearly implicated in several events of centrosomes cycle (reviewed in [42]).

2.2.2. Microtubules

Microtubules (MTs) are hollow cylindrical polymers of α- and β-tubulin heterodimer subunits. Typically, microtubules are arranged in a head-to-tail configuration into 13 laterally associated protofilaments to form a 25 nm diameter structure [43]. In each protofilament all tubulin dimers are oriented in the same way, with β-tubulin exposed at one end (plus-end) and α-tubulin at the other end (minus-end), making microtubules natural polar structures (**Figure 1.7**) [44]. This polarity is central to the ability of motor proteins to move cargo to specific locations *in vivo* [45].

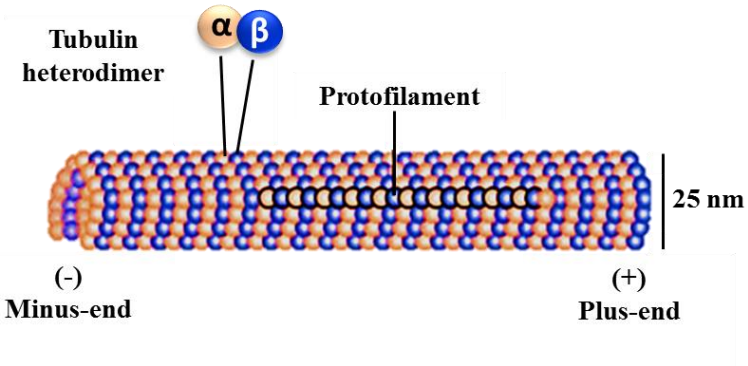

Figure 1.7. Microtubule structure. Illustration of a 25 nm wide polymer composed of α- (orange circles) and β-tubulin (blue circles) subunits. In each protofilament all tubulin dimers are oriented in the same way with α-tubulin exposed at minus-end and β-tubulin at plus-end, creating polar structures (Adapted from [46]).

Microtubules behavior is highly dynamic, since they are capable of polymerizing (growing) and depolymerizing (shortening) over many cycles, resulting in a versatility of cellular functions, including cell division, polarization and migration. The stochastic switch of microtubules between growing and shortening states is termed dynamic instability and results from the ability of β-tubulin to bind and hydrolyze guanosine triphosphate (GTP) to guanosine diphosphate (GDP). Although each α- and β-tubulin monomer binds to one guanine nucleotide, the nucleotide in α-tubulin is non-exchangeable (N-site nucleotide) and non-hydrolysable, while the one in β-tubulin is exchangeable in the unassembled dimer (E-site nucleotide), becoming hydrolyzed to GDP and non-exchangeable within the microtubule lattice (**Figure 1.8**) [47]. GTP to GDP hydrolysis occurs very fast, during or soon after subunit addition, and the GDP-bound β-tubulin makes microtubules less stable and prone to depolymerization. However, the hydrolysis occurs with a delay after a tubulin dimer has been incorporated

into the microtubule end and it is accepted that the newly formed microtubule tip contains a cap of GTP-tubulin (GTP-cap), which has stabilizing properties, ensuring the stability of whole microtubule. In the presence of the GTP-cap, the microtubule continues growing while their lost leads to rapid microtubule shrinkage. The transition from polymerization to depolymerization, with rapid loss of GTP-tubulin subunits and oligomers from the microtubules end, is referred to as a catastrophe, and the reverse transition is referred to as a rescue (**Figure 1.8**) [48, 49]. In a steady state, when microtubules length is constant, there is continuous incorporation of tubulin subunits into microtubules plus-end and release of subunits at the minus-end, in a unidirectional flux, known as treadmilling [50, 51].

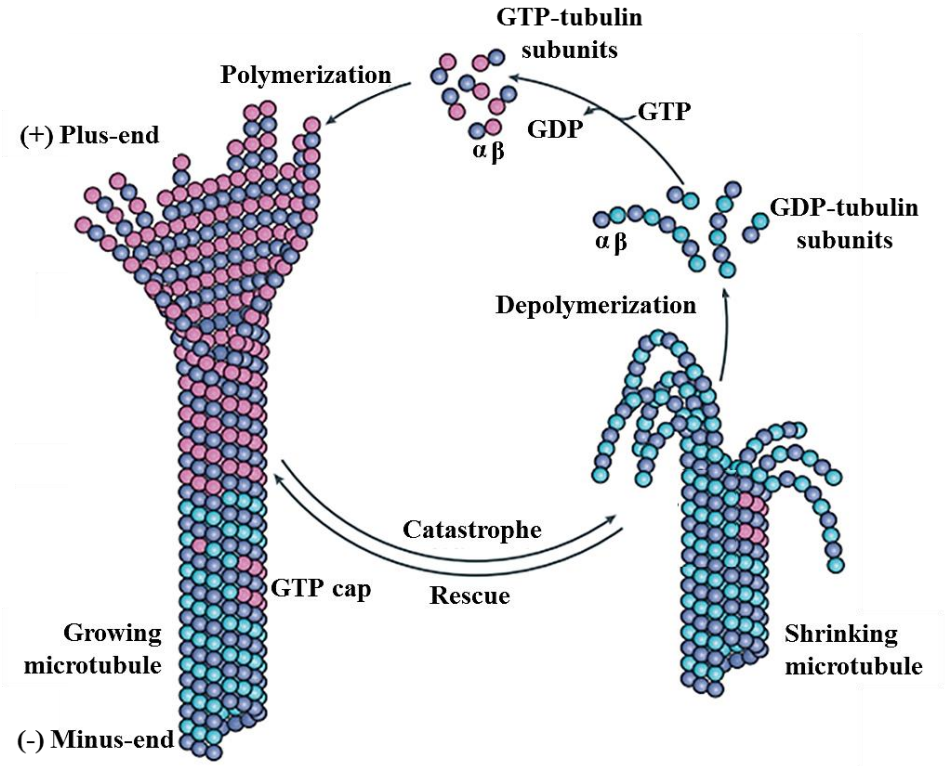

Figure 1.8. Microtubules behavior. The cycle of tubulin assembly (polymerization) and disassembly (depolymerization) is powered by hydrolysis of the GTP bound to β-tubulin, which enables microtubules to switch between catastrophes and rescues. GTP-bound tubulin dimers are incorporated into growing (polymerizing) microtubules. GTP hydrolysis occurs, with a delay, after a GTP-tubulin dimer incorporates into the sheet-like structure of growing microtubule tips. Growing microtubule ends thus maintain a stabilizing GTP cap, the loss of which leads to a catastrophe and rapid depolymerization, resulting in shrinkage of the microtubule (Adapted from [49]).

Microtubules of the mitotic spindle are arranged into a symmetric and fusiform structure at metaphase, with the slow-growing minus-ends oriented toward the poles and the faster-growing plus-ends pointed to the cell cortex [52]. According to the

orientation of the plus-ends, spindle microtubules are divided into three classes: astral, interpolar and kinetochore microtubules (**Figure 1.9**). Astral microtubules arise from centrosomes and radiate out into the cytoplasm with the plus-ends contacting with the cell cortex and are thought to contribute to spindle pole separation and positioning within the cell. Interpolar microtubules emanates from centrosomes towards the cell center and interdigitate at spindle midzone, connecting the two poles and conferring spindle stability [53, 54]. Kinetochore microtubules have a function to connect the spindle poles to chromosomes, at kinetochores, in an initial lateral attachment that is then converted into a mature end-on attachment for chromosomes bi-orientation, creating a distinct bundle known as kinetochore-fiber (K-fiber) [55]. Within the three classes of microtubules, the K-fibers are the more stable and the less dynamic, resistant to cold treatment [56] .

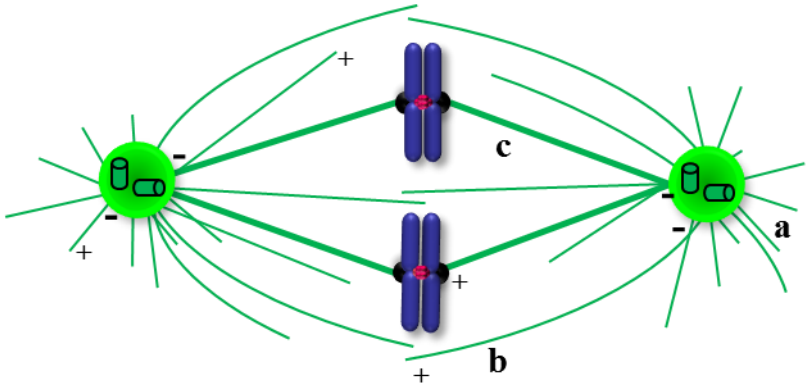

Figure 1.9. Mitotic spindle structure. Illustration of spindle showing its symmetric and fusiform shape, in which microtubules slow-growing minus-ends (-) are oriented toward the poles and the faster-growing plus-ends (+) oriented to the cell cortex. Three different classes of microtubules are shown: astral microtubules (a), interpolar microtubules (b) and kinetochores microtubules (c) creating the k-fiber.

2.2.3. Microtubule-associated proteins (MAPs)

The dynamic instability of microtubules and their connections with cellular structures are controlled by numerous factors, which can be broadly grouped into microtubule-associated proteins (MAPs). MAPs are defined as proteins that specifically bind to microtubules, at least transiently, either *in vitro* or *in vivo*. The targets are soluble tubulin subunits, microtubule lattice and/or microtubule ends, and can be divided in two major classes: non-motor and motor MAPs [49]. Among these, a specialized MAPs, known as microtubule plus-end-tracking proteins (+TIPs), are

distinguished by their ability to concentrate at growing microtubule ends [57], affecting the polymerization rate. For example, the end-binding protein 1 (EB1) increases the microtubules polymerization by inducing a structural change near the plus-end and by recruiting additional +TIPs [58, 59]. Microtubule polymerases such as member of XMAP215/Dis1 and CLIP-associated proteins (CLASP) recruit tubulin dimer subunits to the plus-end, increasing the rate of tubulin addition to growing tips [60]. In addition, CLASPs have been shown to suppress microtubules catastrophe [61] and cytoplasmic linker protein-170 (CLIP-170) has been shown to promote microtubule rescue [62].

Non-motor microtubule associated proteins are involved in the control of cell cycle progression, mediation of motor function and regulation of microtubule nucleation, organization and dynamics. It could be found at different structures including microtubule lattice, microtubule ends, kinetochores, centrosomes, spindle poles, central spindle, and midbody [63].

In contrast to non-motor proteins, the microtubules-based motors proteins couple the chemical energy of ATP hydrolysis to mechanical force production and movement [64]. These cargo-transporting motors include members of the kinesin superfamily and dyneins. Most kinesin family members transport cargoes towards the microtubules plus-end (plus-end directed motors) whereas dyneins transports cargo towards the minus-end (minus-end directed motors) [65].

Kinesins (kinesin-1 to kinesin-14) play an important role at different stages of cell division [66] and in the intracellular vesicles and organelle transport [67]. They have a well-conserved globular domain that contains both a catalytic core for the ATP hydrolysis and the binding sites for microtubules. Members of this family are essential for bipolar spindle formation in all eukaryotes, since in its absence or lack of function centrosomes do not separate and result in monopolar spindles.

Kinesin-8 family members, accumulate at microtubule ends on the basis of their ATP hydrolysis-driven movement inducing catastrophe. Members of the kinesin-4 family decrease overall turnover at the microtubule plus-end, stabilizing microtubules at a specific length in contexts such as the mitotic spindle and cell cortex. The mitotic centromere-associated kinesin (MCAK), a kinesin-13 family member, is able to diffuse one-dimensionally along microtubules and induce depolymerization at either the plus- or minus-end; its overexpression causes spindle defects [68]. The Kinesin-5, Eg5, is a plus-end directed motor consisting of two motor dimers oriented in an anti-parallel manner with a pair of motor domains (heads) on either end [69]. By cross-linking

microtubules, kinesin-5 plus-end directed motility is activated and induces antiparallel microtubule sliding and it is also involved in centrosome separation at prophase to initiate the bipolar spindle assembly [70, 71].

Basic microtubule-binding regions present in the kinesin tails can enhance motor processivity and the ability of motors to remain attached to microtubule ends, as has been shown for the kinesin-8 family members kinesin-related protein 3 (KIP3) and KIF18A and the kinetochore kinesin-7 member centromere protein E (CENP-E).

Although at least 14 classes of kinesins have been identified, the dyneins fall into only two major classes, axonemal and cytoplasmic. Axonemal dynein is involved in the regulation of microtubule sliding in the axonemes of cilia and flagella while cytoplasmic dynein is implicated in a versatility of cellular functions including intracellular transport, cell polarization and directed cell movement, and in mitosis [72].

Two forms of cytoplasmic dynein have been identified: cytoplasmic dynein 1 and cytoplasmic dynein 2, according to their distributions and functions within the cell. While cytoplasmic dynein 1 is found in all microtubule-containing cells and is associated with several cellular compartments such as Golgi apparatus, lysosomes, endosomes and RNA-containing complexes and kinetochores; cytoplasmic dynein 2 is found almost exclusively within and around the base of cilia and flagella.

Structurally, dynein forms a massive multisubunit complex (>500 KDa) comprised of a homodimer of two identical heavy chains (DHC) and several additional subunits, including intermediate (DIC), light intermediate (DLIC) and light chains (DLC), which are usually associated with the cargo-binding. The DHC forms two prominent structures, an N-terminal domain consisting in the base of the molecule, to which most of the accessory subunits bind, and a motor domain [72]. The motor domain contains six discernible AAA ATPase units, that form into a ring-like structure, identifying the DHC as a divergent member of the AAA+ family of ATPases [73] that bind to microtubules and hydrolyze ATP for force production **(Figure 1.10)**.

During mitosis, cytoplasmic dynein 1 (hereinafter dynein) localizes at three distinct mitotic loci: cell cortex and spindle poles reflecting their role in spindle formation/integrity and spindle rotation/positioning and at kinetochores where dynein has involved in MT-attachment [74-77], chromosome movement [78-81] and regulation of the SAC response [82-84]. Accordingly, dynein accumulates at kinetochores prior to MT attachment [77] and as chromosomes achieve bipolar attachment and approach the metaphase plate becomes less prominent being visible along spindle fibers and at

spindle poles [83, 84], consistent with dynein involvement in SAC silencing. After chromosome congression dynein is undetectable at kinetochores [84, 74].

Most of the activities described above are carried out by dynein working in conjunction with dynactin, a multi-subunit protein complex working as dynein cofactor, and several adaptor proteins that link dynein-dynactin to specific cargos [85]. ZW10, LIS-1, nudE/nudEL, nudC, and Spindly have been identified as dynein partners required either for dynein functions and localization at kinetochores (reviewed in [86]).

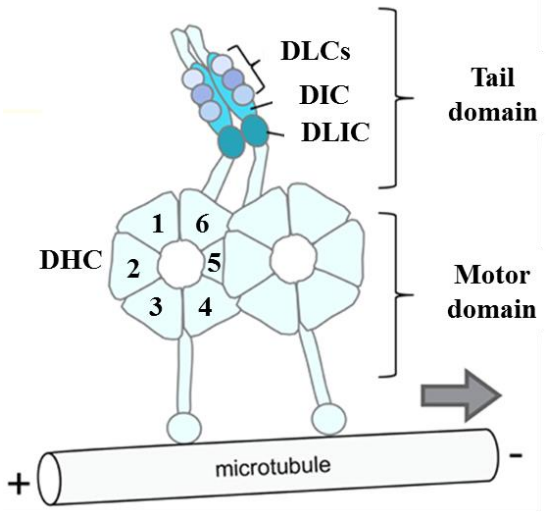

Figure 1.10. Cytoplasmic structural organization of the dynein. Dynein is a complex of two heavy chains (DHC), two intermediate chains (DIC), two light intermediate chains (DLIC), and three light chains (DLC). The motor domain comprises six AAA+ ATPase modules (1-6) that form a ring, and a stalk that contains the microtubule domain. The N-terminal tail domain interacts with the smaller non-catalytic subunits, and is responsible for dimerization and cargo interaction. The arrow indicates the direction of movement along microtubules (Adapted from [87]).

3. THE KINETOCHORE

3.1. Kinetochore structure

The kinetochore is at the heart of microtubules attachment to chromosomes and the first insights into their structure were provided by classical electron microscopy studies [88]. The observation of the vertebrate chromosomes ultrastructure revealed that kinetochores have a trilaminar proteinaceous morphology (**Figure 1.11**) [89-92]. The innermost layer, known as the inner kinetochore plate, is a disk of densely packed material, continuous with the centromeric heterochromatin [93]. This region is thought

to be responsible for the assembly and size determination of a robust kinetochore. The outer kinetochore plate is an electron-dense DNA-free structure that constitutes the primary site of attachment for spindle microtubules. With a questionable existence, a third lighter middle layer separates and connects the inner and outer regions of the kinetochore [91]. At the outer plate surface, in the absence or presence of a few attached microtubules, is visible an expanded filamentous meshwork called fibrous corona [94, 95], containing a dynamic network of mainly transient proteins implicated in microtubule capture, dynamics and SAC response.

The size and complexity of kinetochores differ considerably among different species, as well as, the number of attached microtubules. Indeed, S. *cerevisiae* kinetochore binds just one microtubule, S. *pombe* bind up to four, D. *melanogaster* on average bind eleven and vertebrate kinetochores typically bind fifteen to twenty-five microtubules [96, 97].

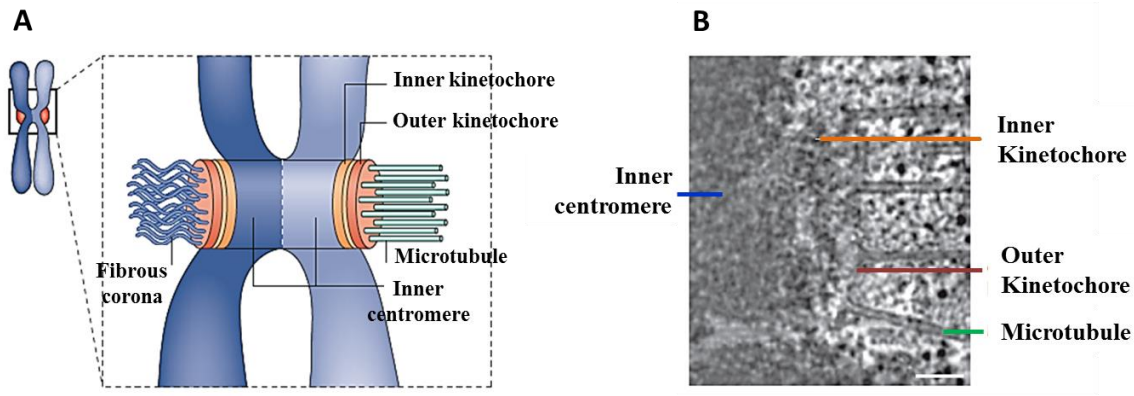

Figure 1.11. Vertebrate kinetochore ultrastructure. (A) A schematic of a mitotic chromosome with paired sister chromatids; the chromatid on the right is attached to microtubules and the chromatid on the left is unattached. The inner kinetochore, the outer kinetochore, the inner centromere and the fibrous corona, which is detectable on the unattached kinetochore, are highlighted. **(B)** Electron micrograph of a human kinetochore (image courtesy of Y. Dong and B. McEwen, State University of New York at Albany, USA). The micrograph represents a single slice from a tomographic volume of a high-pressure frozen mitotic cell and has been labelled as in (A) to highlight the key structural features of the kinetochore. Scale bar, 100 nm (Adapted from [98]).

3.2. Molecular composition of kinetochore

To identify functional components of the kinetochore, a combination of genetics, RNA interference (RNAi)-based screens and biochemistry was used in model organisms. The studies conducted in budding yeast were particularly successful given their short centromeric DNA sequence and although most kinetochore proteins show

limited homology between species, vertebrate counterparts of many of the proteins have been identified in model organisms.

The organization and molecular composition of the human kinetochore appear to be conserved among eukaryotes, and there are more than one hundred kinetochore proteins, localized at specific domains, identified until now. The assembly of kinetochore components occurs in a stepwise manner from the heterochromatin to the outer kinetochore plate, although a less linear hierarchy occurs at the outer kinetochore and fibrous corona. Here, the assembly of components is mainly transient and is influenced by the microtubule attachment status and local signaling pathways (**Figure 1.12**).

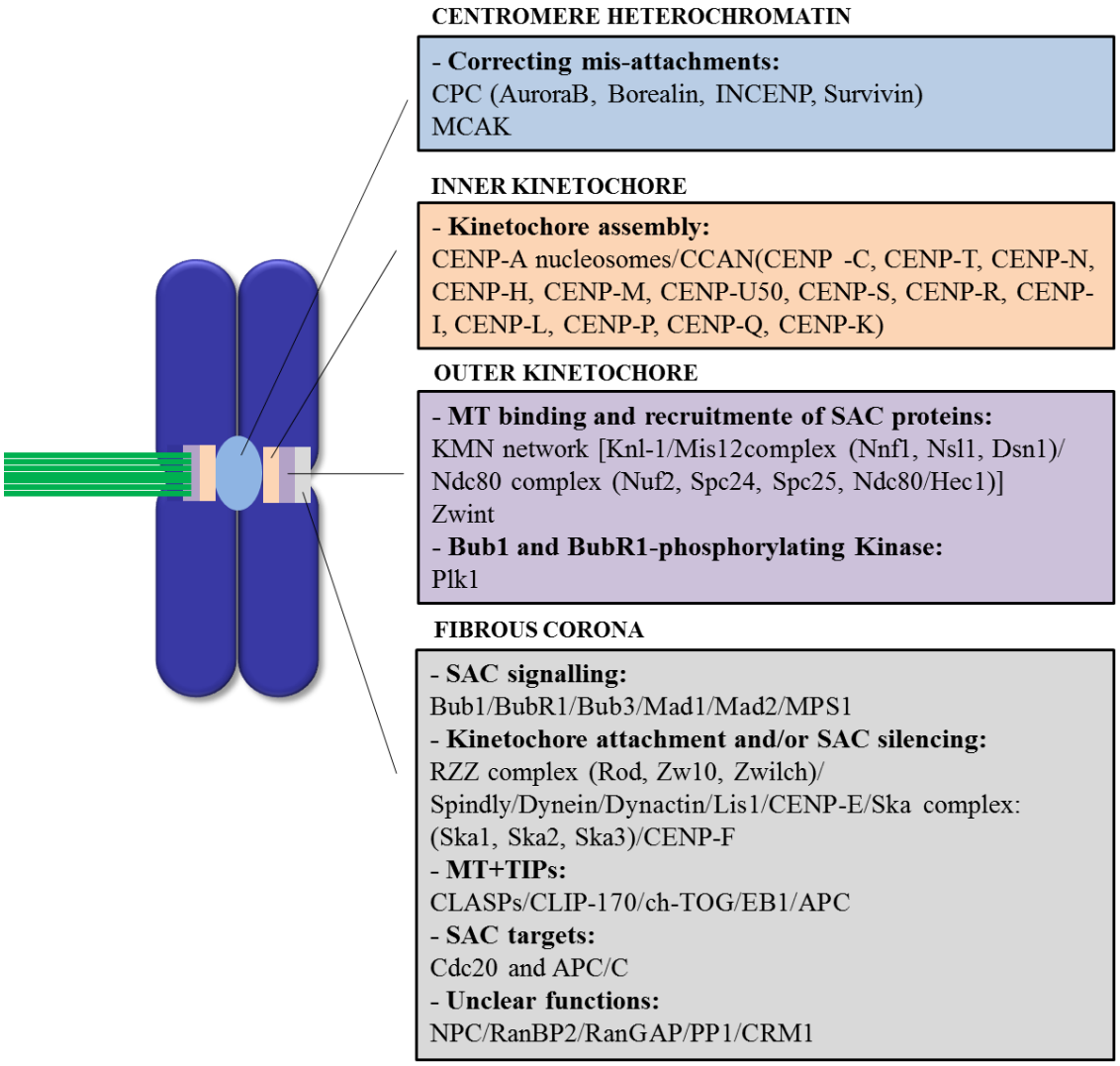

Figure 1.12. Overview of protein complexes that build the kinetochore in animal cells. The kinetochore is built on the centromere as a trilaminar protein-rich structure: the inner kinetochore, the outer kinetochore and the fibrous corona. Proteins that compose each kinetochore layer are grouped by function (APC/C, anaphase promoting complex/cyclosome; Bub1BubR1-Bub3, budding uninhibited by benzimidazole; Cdc20, cell division cycle 20; CENP, centromere protein; CLASP, CLIP-associating protein; CLIP170, cytoplasmic linker

protein-170; CPC, chromosome passenger complex; EB1, end-binding protein-1; INCENP, inner centromere protein; kMTs, kinetochore microtubules; LIS1, lissencephaly-1; Mad1-Mad2, mitotic-arrest deficient; MCAK, mitotic centromere-associated kinesin; MPS1, multipolar spindle-1; MT, microtubules; NPC, nuclear pore complex; PLK1, polo-like kinase-1; RanBP2, Ran-binding protein 2; RanGAP, Ran-GTPase-activating protein; RZZ, Rod (rough deal); SAC, spindle assembly checkpoint; Ska1–3, spindle and kinetochore-associated proteins; Zw10, zeste white 10-Zwilch complex; Zwint, Zw10 interactor (Adapted from [99]).

The main component of centromeric heterochromatin is the chromosomal passenger complex (CPC), composed of Aurora B, INCENP, Borealin and Survivin, which is one of the most widely studied and highly conserved hetero-tetrameric complexes.

A fundamental determinant of the inner kinetochore identity is the centromere protein (CENP)-A, a histone H3 homologue and one of the core subunits of nucleosomes. In humans, CENP-A associates with several additional inner kinetochore proteins collectively known as constitutive centromere associated network (CCAN). CCAN allows the assembly of the outer kinetochore domain, the microtubule binding and in deposition of new CENP-A [100-102]. Given their function, depletion of components of the CCAN often leads to cell-cycle arrest, kinetochore-assembly defects, severe chromosome missegregation and loss of kinetochore function (reviewed in [98]).

The outer kinetochore is the microtubule-binding interface, and its core is the KMN network. KMN is composed of Knl-1 protein (Blinkin / Spc105 in human and budding yeast, respectively) and the two sub-complexes Mis12 (composed of four proteins Mis12/Nnf1/Nsl1/Dsn1) and Ndc80 (containing the four proteins Ndc80 (Hec1 in mammals)/ Nuf2/Spc24/Spc25)) [98]. In metazoans, the Ndc80 complex associates with kinetochores prior to nuclear envelope breakdown and forms a rod-like structure with two globular heads at each end separated by a long coiled-coil region. The globular regions of Ndc80 and Nuf2, localizes at the outer kinetochore domain and bind directly to microtubules while the globular regions of Spc24 and Spc25 are oriented towards the inner kinetochore plate. The crystal structure of the globular domain of the Ndc80 subunit has revealed that it is folded into a calponin-homology (CH) domain, also exhibited by the microtubule binding region of the plus-end-associated protein EB1 suggesting an ancient evolutionary origin for this fold.

Ndc80 complex localization at vertebrate kinetochores is influenced by both the Mis12 complex and the CCAN [101, 103]. The Ncd80 affinity to microtubules is weak, but when in association with Mis12 complex and Knl1protein the microtubule-binding affinity is synergistically increased [104]. The association of Ndc80 complexes with

spindle microtubules is critical for chromosome segregation and their depletion or inactivation causes the most severe chromosome segregation defect.

Localized at the kinetochore fibrous corona are the proteins involved in SAC signaling pathway, like Bub1, BubR1, Bub3, Mad1, Mad2 and Mps1; the SAC targets Cdc20 and APC/C; components involved in kinetochore-microtubules attachment and/or SAC silencing like RZZ complex (Rod, Zw10, Zwilch), Spindly, dynein, dynactin, Lis1, CENP-E, CENP-F and Ska complex (Ska1, Ska2, Ska3); and microtubule-plus-end-tracking proteins (+TIPs) like CLASPs, CLIP-170, ch-TOG, EB1 and APC. The role of the majority of outer kinetochore proteins are discussed in following topics. Together, all these kinetochore proteins create an environment that allows efficient chromosome alignment at the metaphase plate and promote proper chromosome segregation.

4. KINETOCHORE-MICROTUBULE INTERACTIONS

4.1. Kinetochore-microtubule binding, chromosome capture and bi-orientation

Proper kinetochore capture by spindle microtubules is achieved in a stepwise manner. After nuclear envelope breakdown at prometaphase, chromosomes are released into the cytosol and become accessible to the microtubules from the mitotic spindle. These, probe the cytoplasm, through episodes of lengthening and shortening of their plus ends, to search and capture chromosomes [105, 106]. This “search and capture” model remains the cornerstone of spindle assembly, 31 years later after being proposed. Nevertheless, over the last few years, functional and proteomic-based analysis of the kinetochore-microtubule interface has increased our understanding of the molecular mechanism of chromosome attachments to the spindle and shed light on kinetochore bi-orientation [98, 107]. Different studies have demonstrated that the plus ends of microtubules bind to kinetochores through the KMN protein network. Removal of any of the KMN network components leads to the disruption of the binding scaffold for microtubules at the outer kinetochore plate [108, 103]. Initial capture results in the binding of one kinetochore to the lateral surface of the microtubules, followed by rapid poleward movements of attached chromosome along highly dynamic astral

microtubules (**Figure 1.13**). This movement is probably powered by the motor activity of the cytoplasmic dynein [78, 109, 77, 81, 79], recruited to kinetochore by the RZZ complex via Spindly [110-115]. The high density of microtubules near the spindle pole will contribute to the conversion of the lateral attachments to mature end-on attachments (**Figure 1.13**). RZZ complex and Spindly were reported to be required for this conversion [113]. Furthermore, the Ska complex was also shown to be involved in stable end-on kinetochore-microtubule (KT-MT) attachments in vertebrate cells [116-118]. Due to the polar ejection forces, the now mono-attached chromosome is forced to move towards the spindle equator, a process known as chromosome congression, with the unattached sister-kinetochore facing the microtubules from the opposing pole, resulting in its end-on attachment [119]. Besides this simplified mechanism, in metazoan cells, mono-oriented chromosomes could be transported towards the spindle equator by gliding alongside microtubules attached to other already bi-oriented chromosomes, driven by the kinetochore-bound CENP-E, a plus end-directed microtubule motor of the kinesin-7 family [120] and by chromokinesins kinesin-10 (Kid/NOD) and kinesin-4 (Kif4/Xklp1) that push the chromosome arms away from the centrosome [121-123]. Indeed, how a spatially selective activities mediated by the kinetochore motors, dynein and CENP-E, ensure chromosome congression were recently reported [80] and was associated with microtubule (de)tyrosination, one of the tubulin post-translational modification (PTM) (**Figure 1.14**) [124, 125]. Accordingly, dynein has a preference for tyrosinated astral microtubules and counteracts chromokinesin-mediated polar ejection forces. By bringing chromosomes to the vicinity of the spindle-pole-localized Aurora A kinase, dynein prevents premature stabilization of erroneous end-on attachments and contributes to the local activation of CENP-E. At the pole, CENP-E interacts with detyrosinated microtubules (modified α-tubulin lacking the C-terminal tyrosine), becoming dominant over dynein to move chromosomes towards the equator (**Figure 1.14**). This model is linked to the emerging concept that tubulin PTMs are a part of the so-called tubulin code [126, 127], that is read by the molecular motors and determines the preferences for particular tubulin PTMs [124].

In addition, RanGTP-induced diffusible gradients [128, 129] and adaptive changes in chromosome architecture [130, 131] has been proposed as facilitators of kinetochore-based chromosome motility during early mitosis. Nonetheless, these recent mechanisms have been organically incorporated into the search and capture model, which even so still sustains their basic principles and simplicity.

Invariably, chromosomes are successfully aligned at the metaphase plate once they become bi-oriented, a condition known as amphitelic attachment, with full microtubule occupancy.

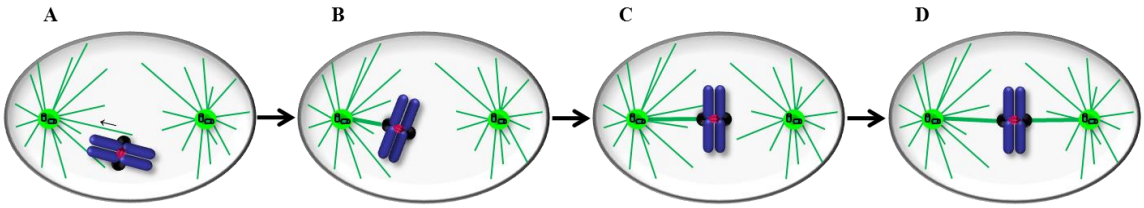

Figure 1.13. Chromosome biorientation during prometaphase. When the nuclear envelope breaks down, the kinetochore is captured by the lateral surface of microtubules emanating from a spindle pole **(A)**, resulting in its transport toward that pole (arrow). The high density of microtubules near the pole contributes to the maturation of the lateral attachment to end-on attachment, with the kinetochore tethered at the plus end of the microtubules **(B)**. Polar ejection forces and/or gliding alongside microtubules attached to other already bi-orientated chromosome (not represented in the figure) drive the mono-orientated chromosome toward the metaphase plate **(C)**, resulting in its bi-orientation **(D)** [99].

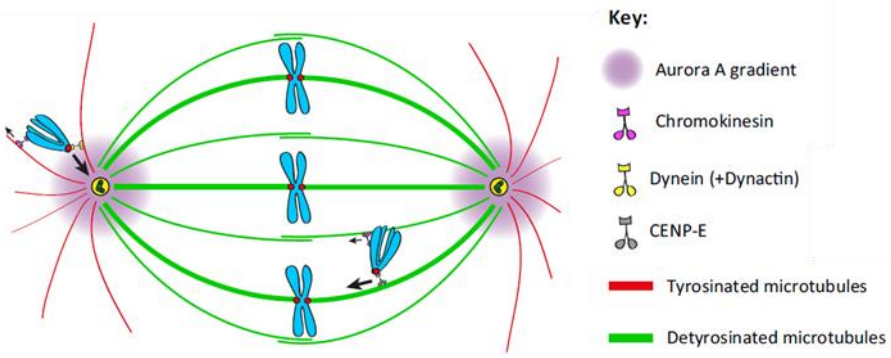

Figure 1.14. Schematic representation of the impact of tubulin tyrosination/detyrosination on the regulation of motor proteins responsible for chromosome movements in mitosis. Dynein/dynactin have a preference for tyrosinated astral microtubules and counteract chromokinesin-mediated polar-ejection forces. By bringing chromosomes to the vicinity of the spindle-pole-localized Aurora A kinase, dynein/dynactin prevent premature stabilization of erroneous end-on attachments and contributes to the local activation of CENP-E. At the pole, CENP-E interacts with detyrosinated microtubules, becoming dominant over dynein to move chromosomes towards the equator. Thus, the levels of microtubule (de)tyrosination provide the direction albias for CENP-E-mediated chromosome transport and regulate the dynein/CENP-E activity switch that facilitates chromosome congression (adapted from [124]).

4.2. Correction of kinetochore-microtubules attachment errors

It is known that the amphitelic attachment, achieved when sister kinetochores are attached to opposite poles of the spindle, is the only geometry that ensures an accurate segregation of sister-chromatids to daughter cells, at anaphase. However, due to the stochastic nature of the widely accepted "search and capture" mechanism, and to the chromosome position within the cell and the geometry of their sister-kinetochores relative to microtubules at the onset of prometaphase, other connections can occur and compromise the proper segregation of chromosomes. There are three possibilities for kinetochore-microtubules mis-attachments: monotelic, syntelic, and merotelic (**Figure 1.15**) [132, 133]. Monotelic kinetochore attachment occurs when one sister kinetochore is unattached while the other is attached to microtubules from just one pole. This is common in early mitosis and it is a normal condition at the very beginning of prometaphase. Syntelic attachment is observed, although rarely, when the two sister kinetochores are bound to microtubules from the same spindle pole. Both monotelic and syntelic attachments activate the SAC, due to reduced tension at sister-kinetochores, and are generally corrected and converted into amphitelic configurations. Merotelic attachments occur when one sister kinetochore binds to microtubules from both poles, frequently in early prometaphase. These attachments do not interfere with chromosome alignment during prometaphase and are not always detected by the SAC. Nevertheless, they rarely cause chromosome mis-segregation, as they are usually corrected before anaphase onset by an Aurora B-dependent mechanism [132-134].

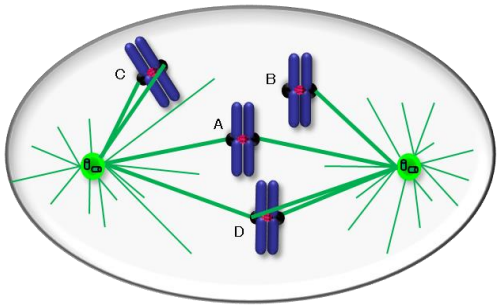

Figure 1.15. Biorientation and kinetochore attachment errors. (A) In amphitelic attachment, sister kinetochores are correctly attached to the microtubules emanating from the opposite poles of the spindle, leading to chromosome bi-orientation. **(B)** In monotelic attachment, the chromosome is mono-oriented as one kinetochore is attached to the microtubules from one spindle pole, while its sister is unattached. **(C)** In syntelic attachment, the chromosome is mono-oriented but, in this case, both sister kinetochores are attached the microtubules from the same spindle pole. **(D)** In merotelic attachment, one sister kinetochore is attached to microtubules from both spindle poles, the chromosome is improperly bi-oriented and, if left uncorrected, can produces an anaphase lagging chromosome (Adapted from [99]).

Proper tension across the sister kinetochores contributes to the detection and correction of merotelic and syntelic attachment errors. Sister kinetochores in amphitelic attachments are under tension, which results from the pulling forces of the spindle microtubules in opposite directions. Pioneering micromanipulation experiments from Nicklas and co-workers suggested that the mechanical tension at kinetochores increases the occupancy of microtubule attachment sites, which contributes to stabilizing kinetochore to microtubules attachments [135, 136]. It is widely accepted that tension is the signal that distinguishes different attachment states of sister kinetochores and that the Aurora B kinase, the mammalian homologue of the budding yeast Ipl1 kinase, acts as a tension sensor to correct mis-attachments by destabilizing them [134, 137]. Aurora B localizes to the inner centromere and regulates the interactions between the kinetochores and microtubules through phosphorylation of the Ndc80 complex and the member of the kinesin-13 family of microtubule depolymerases, MCAK [138]. A spatial separation model was proposed that might explain how tension mediates correction of mis-attachments by Aurora B kinase [139]. The low tension at the syntelically attached kinetochores and the unbalanced tension resulting from merotelic orientation would locate the kinetochores close to a peak of Aurora B kinase activity in the inner centromere, which release microtubules as a consequence of Ndc80 and MCAK phosphorylation. Indeed, phosphorylation of the Ndc80 complex weakens its affinity for microtubules while phosphorylated MCAK catalyses depolymerization at the ends of microtubules [104, 140]. The selective destabilization of incorrect chromosome attachments provides a new chance to bi-orient. Bi-orientation increases the distance between the kinetochores and the inner centromere, due to the forces exerted by spindle microtubules in opposite directions. As a consequence, Aurora B becomes spatially separated from its substrates and the attachments are stabilized. In this spatial separation model, a constitutively active phosphatase, such as PP1 (protein phosphatase 1) in budding yeast and PP1γ and PP2A in vertebrates, would dephosphorylate Aurora B substrates allowing for rapid re-attachment [137]. It was also reported that Mps1 kinase phosphorylates Borealin/DasraB on residues that are crucial for Aurora B activity and chromosome alignment. Other models are possible for the mechanisms by which Aurora B regulates kinetochore-microtubule attachments, stressing the need to clarify the molecular nature of the processes through which improper attachments are detected and corrected [134, 137]. It was recently reported that disturbing the microtubules-binding Dam1 and Ska1 complexes, other additional

Aurora B substrates, destabilizes kinetochore-microtubules attachments even in tension absence [141].

The polo-like kinase 1 (Plk1), localized at kinetochores during prometaphase [142, 143], has also been implicated in the correction of attachment errors, stimulating the kinetochore activity of both kinetochore-microtubules stabilizers and destabilizers. Plk1 activity is required for the initial formation of stable kinetochore-microtubules attachments, probably by phosphorylating the KT-MT stabilizing protein BubR1 [144, 145]. Paradoxically, Plk1 phosphorylates and stimulates the microtubule depolymerase activity of kinesin family member 2B (KIF2B), required to destabilize KT-MT attachments and efficiently correct errors [146, 147].

Unexpectedly, it has been proposed that Aurora A kinase contribute to error correction, by opposing the stabilizing effect of the elevated polar ejection forces close to the spindle poles. Through inhibitory phosphorylation of the kinetochore subtract Ndc80/Hec1, Aurora A increases the incidence of kinetochore-microtubules mis-attachments, in a balanced activity with polar ejection forces, giving the chance for a corrected attachment similar to its counterpart Aurora B on centromeres [148]. Dynein also contributes to prevent error formation by counteracting the role of chromokinesins in the stabilization of end-on kinetochore-microtubule attachments [149, 150], while promoting Aurora-A-mediated kinetochore-microtubule destabilization, in a balanced process of forces [151].

5. THE SPINDLE ASSEMBLY CHECKPOINT

The spindle assembly checkpoint (SAC) is a constitutive surveillance mechanism in eukaryotic dividing cells that is extremely sensitive to defects in kinetochore attachment. It prevents chromosome misssegregation by delaying the metaphase to anaphase transition until all chromosomes are correctly connected to the spindle microtubules, bi-oriented and aligned at the metaphase plate [23]. The SAC consists of a signalling cascade that represents the primary cell-cycle control mechanism in mitosis and is activated immediately after mitosis entrance, every cell cycle. Accurate activity of this checkpoint mechanism is crucial for equal segregation of the genetic material into the two daughter cells and thus, for the effective reduction of the error rate occurring during cell division. Failure in SAC function has been suggested as a possible

cause of aneuploidy in several tumor types [152, 153]. Moreover, SAC contributes to the temporal organization of the cell cycle, since the cell only progresses to the next phase when its requirements are satisfied. The SAC molecular pathway involves the detection of the attachment error and the generation of the signal that inhibits mitosis progression, error correction, and SAC silencing.

5.1. Molecular components and checkpoint activation

The proteins of the SAC molecular pathway can be divided in to two groups: i) proteins that form the "*bona fide"* SAC components and ii) proteins of the attachment, APC/C regulatory, correction, and SAC silencing machineries, with which true SAC proteins must interact to monitor attachments and cell cycle progression [98]. The distinction between the two groups of proteins was elegantly expressed in an opinion article [154].

The *bona fide* SAC proteins are comprised of Mad1, Mad2, BubR1, Bub1, Bub3, Mps1, which have been initially identified in budding yeast [23, 98]. Homologues for these proteins have also been identified in higher organisms, including mammals. These proteins were shown to share a high degree of both sequence and functional homology with their yeast counterparts. Functional disruption studies through dominant-negative mutants, antibody injection or RNA interference (RNAi) completely compromised the spindle checkpoint activity, causing chromosome misssegregation, aneuploidy and escape from mitotic arrest in the presence of microtubule poisons such as nocodazole and taxol [155].

Whenever unattached kinetochores are present, the Mad2, BubR1, and Bub3 proteins localize there to generate, in association with Cdc20, the Mitotic Checkpoint Complex (MCC) [156], a "wait anaphase signal" that diffuses through the cytosol (**Figure 1.16**) [157, 158]. This keeps APC/C inhibited, an E3 ubiquitin ligase that regulates many cell cycle processes, preventing it from ubiquitinating Securin (Pds1 in budding yeast) and Cyclin B from targeting them for destruction by the 26S proteasome. By preventing Securin and Cyclin B degradation, sister-chromatid cohesion and the mitotic state are maintained, respectively. A "Mad2-template" model was proposed as the mechanism by which the cytosolic inhibitory signal is propagated away from the kinetochore [159]. According to this model, Mad2 can adopt either an open (O-Mad2) or closed (C-Mad2) conformation [159-161]. A constitutively C-Mad2 bound

to Mad1 serves as template or receptor at unattached kinetochore for cytosolic O-Mad2 to switch this latter to C-Mad2 bound to Cdc20 form. The C-Mad2/Cdc20 complex leaves the kinetochore and acts as a structural equivalent of Mad1/Mad2 to convert more O-Mad2 into Cdc20 bound C-Mad2 in the cytosol, resulting in signal amplification (**Figure 1.16**) [159, 162]. This model starts with an early nuclear envelope breakdown when the level of the MCC complex is not yet sufficient to prevent anaphase. Recently, some elegant studies focused on SAC understanding shed light into this mechanism and suggested novel theories, especially concerning MCC-APC/C activity. It was described that C-Mad2 induces a conformational modification in Cdc20, enhancing its binding with N-terminus of BubR1, already bound to Bub3 which, in turn, inhibits the APC/C [163]. Moreover, Bub3 has emerged as a promoter and an enhancer of two different interactions between BubR1 and Cdc20 to sustain the anaphase inhibitor signal [164].

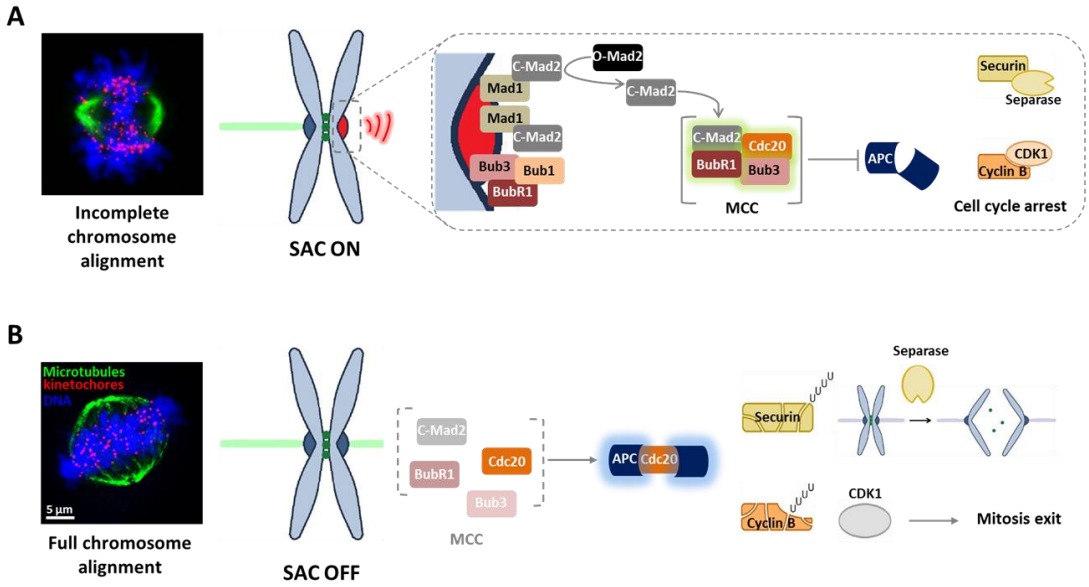

Figure 1.16. Molecular view of spindle assembly checkpoint (SAC) pathway. (A) Immunofluorescence image of a prometaphase cell, stained for microtubules (green), kinetochores (red) and for DNA (blue), showing the presence of unaligned chromosomes. Under these conditions, at early mitosis, when chromosomes are not aligned or improperly attached to microtubules, the SAC is turned on and the Mad1/c-Mad2 complex, localized at unattached kinetochore, recruits and converts cytosolic o-Mad2 into c-Mad2, which together with Bub3, BubR1 and Cdc20 forms the mitotic checkpoint complex (MCC), leading to anaphase promoting complex/cyclosome (APC/C) inhibition. Thus, the mitotic substract cyclin B remains associated with Cdk1 as does securin with separase, resulting in mitotic arrest. **(B)** Immunofluorescence image of a metaphase cell, stained as in (A), showing all chromosomes aligned at the metaphase plate. At this stage, SAC is turned off and MCC is disassembled, allowing APC/C activation by Cdc20 and subsequent ubiquitylation (U) of cyclin B and securin. As a result, separase can cleave cohesins to promote sister chromatid separation, while Cdk1 becomes inactive which promotes exit from mitosis (Adapted from [165]).

Once the last chromosome becomes bi-oriented, the "wait anaphase" is no longer produced, consistent with SAC silencing, and Cdc20 is released to trigger APC/C activation, which in turn ubiquitinates Securin and Cyclin B, targeting them to proteasome degradation. Degradation of Securin, an inhibitor of the protease separase, leads to cohesin proteolysis and sister chromatid separation, whereas Cyclin B degradation leads to the inactivation of cyclin-dependent kinase 1 (Cdk1), which drives mitotic exit.

Protein phosphorylation and dephosphorylation have probably a major role in the transduction and the amplification of SAC signals. In this respect, however, the exact role of the kinase activity of the checkpoint proteins Bub1, BubR1, and (to a lesser extent) Mps1 in SAC signaling has long been controversial. Contradictory results were reported regarding the requirement of these checkpoint kinases in the SAC, probably due to the variability between the different assays used to assess the SAC response or inefficient depletion of the endogenous proteins [166, 167]. Bub1 was reported to phosphorylate Cdc20, inhibiting its ability to activate the APC/C [168], suggesting a model in which Bub1 kinase contributes to amplify or strengthen the SAC signal in the presence of few unattached kinetochores [169]. Other studies have shown that the Bub1 kinase activity is not sufficient to complete SAC function [170]. Less certain is the contribution of the BubR1 kinase activity to the SAC. It was reported that BubR1 kinase activity is activated by binding to CENP-E tail and inactivated upon CENP-E binding to microtubules [171]. Conflicting studies had reported mixed results as to whether BubR1 kinase activity is required for efficient chromosome capture and congression [172-174]. There is no doubt regarding the necessity of Mps1 kinase activity for SAC activity as its inhibition overrides the SAC [175, 176]. Mps1-mediated direct phosphorylation of Knl1 is required for Bub1 and Bub3 kinetochore localization [177, 178].

Mps1 kinase activity was also shown to be involved in the error correction during chromosome bi-orientation [179]. Moreover, Mps1 phosphorylates Borealin that in turn directs the activity of Aurora B [180], in agreement with its role in regulating chromosome attachment and alignment. Phosphorylation of Mad1 has been reported to be Mps1-dependent [181], but the role of the Mad1 phosphorylation in the SAC remains to be determined.

5.2. Mechanisms of checkpoint silencing

SAC silencing implies preventing the generation of the "wait anaphase" signal upon stable chromosome attachment. This presumes the existence of a regulatory link between chromosome bi-orientation and silencing mechanisms. Several models for SAC silencing mechanism were proposed [182, 183].

The first model suggests that MCC production is halted by dynein-dependent stripping of SAC components from the attached kinetochore [82]. Upon kinetochore-microtubule attachment, the minus-end directed motor dynein actively transports, along spindle microtubules, SAC proteins such as Mad2 and BubR1 away from the attached kinetochore, towards spindle poles **(Figure 1.17)**. Consistently with this mechanism, cells arrest in mitosis with high kinetochore-associated Mad2 levels following depletion of the dynein light intermediate chain 1 (LIC1) or after microinjection of 70.1 anti-dynein antibodies [184, 82].

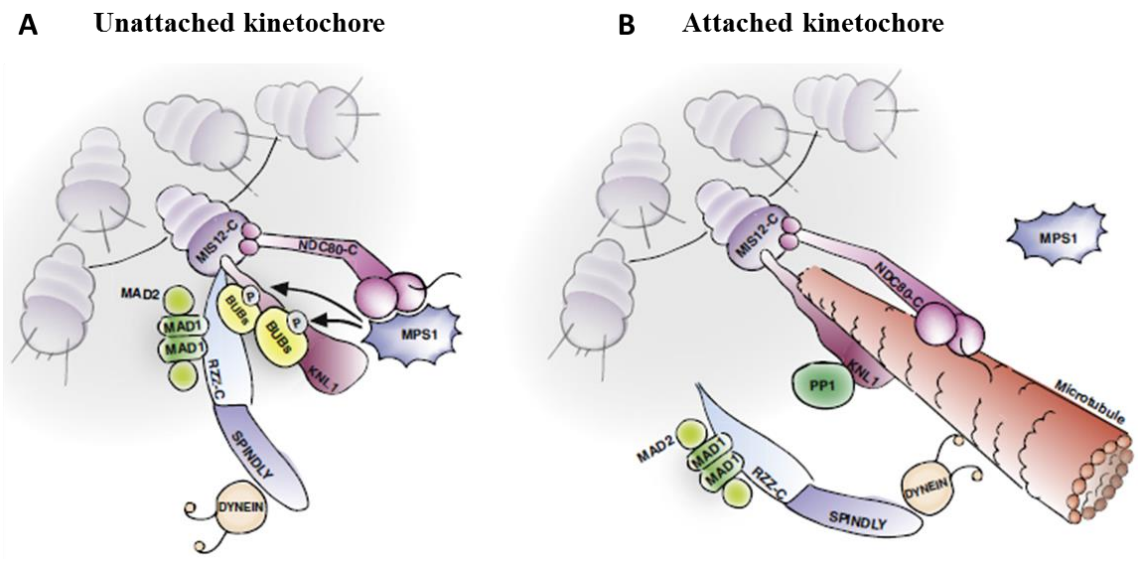

Figure 1.17. SAC protein recruitment to and removal from kinetochores. (A) SAC proteins Mps1, Mad1, Mad2 and the Bubs (Bub1, Bub3 and BubR1) localize to the unattached kinetochore by interacting with members of the KMN complex (consisting of the Knl1, Mis12 and Ndc80 complexes). **(B)** Upon microtubule binding, several mechanisms, namely dynein-mediated protein stripping, and Mps1 removal by microtubules, contribute to removal of the SAC proteins (Adapted from [185]).

By recruiting dynein to kinetochores Spindly, a 605 aa protein consisting of two coiled coil domains, plays a critical role in checkpoint silencing [186, 114, 187]. Spindly kinetochore localization depends on the RZZ complex, since ZW10 knockdown

leads to their abrogation [114]. Recently, it was reported that Spindly undergoes farnesylation at C-terminal cysteine residue, a post-translational lipid modification, to interact with RZZ and, hence, to target kinetochores [188, 189]. Spindly inhibition causes chromosome alignment defects, loss of dynein-dynactin kinetochore localization and a severe prometaphase delay, consistent with permanent SAC activation [114, 190, 186]. Curiously, in Spindly-depleted cells, where kinetochore dynein is absent, Mad1 and Mad2 were found to dissociate from kinetochores following microtubule attachments, and the SAC is silenced without poleward transport. This observation suggests an existence of kinetochore dynein-independent mechanism, probably dependent on the KMN network that has the ability to couple both silencing and attachment mechanisms [186].

Another silencing mechanism is the inhibition exerted by the $p31^{comet}$ protein on Mad2, preventing it from inhibiting the APC/C^{Cdc20} in mammalian cells [191, 192]. By binding the dimerization interface of Mad2, the $p31^{comet}$ protein prevents Mad2 activation and promotes the dissociation of the Mad2/Cdc20 complex [192]. Indeed, HeLa cells that recover from a SAC-dependent nocodazole-induced block are delayed in mitosis under conditions of low $p31^{comet}$ expression. Accordingly, overexpression of $p31^{comet}$ abrogates the SAC-dependent mitotic arrest in HeLa cells treated with microtubule poisons [192]. Additionally, phosphorylation of Mad2 was reported to inhibit its interaction with APC/C^{Cdc20} or Mad1, suggesting its implication in SAC silencing [193]. Although the regulatory mechanism whereby Mad2 becomes phosphorylated and silences the SAC upon kinetochore attachment is still unknown, it is possible that the phosphorylated form of Mad2 facilitates its binding by $p31^{comet}$ and/or makes it competent to be transported by dynein during kinetochore stripping.

An alternative silencing mechanism, namely in countering MCC production, was related to the protein phosphatases PP1 and PP2A [194, 195, 178, 196]. Both have been proposed to dephosphorylate the Mps1-targeted repeat motifs in Knl1 leading to kinetochore SAC signaling inhibition [195, 178]. Although PP1γ binds the KMN directly, via motifs in Knl1, PP2A-B56 connects to Knl1 indirectly by binding to BubR1, which in turn interacts with the Bub1/Bub3 dimer [197-200].

6. ROLE OF THE SPINDLE ASSEMBLY CHECKPOINT IN TUMORIGENESIS

The discovery of SAC and its relevance to genetic stability **(Figure 1.18)**, together with the fact that many cancer cells exhibit weakened SAC activity, had initially prompted many scientists to search for mutations in SAC genes in several tumors, in order to establish a relationship between SAC and tumorigenesis and, eventually, to anticipate the prevention, diagnosis and cancer treatment [153].

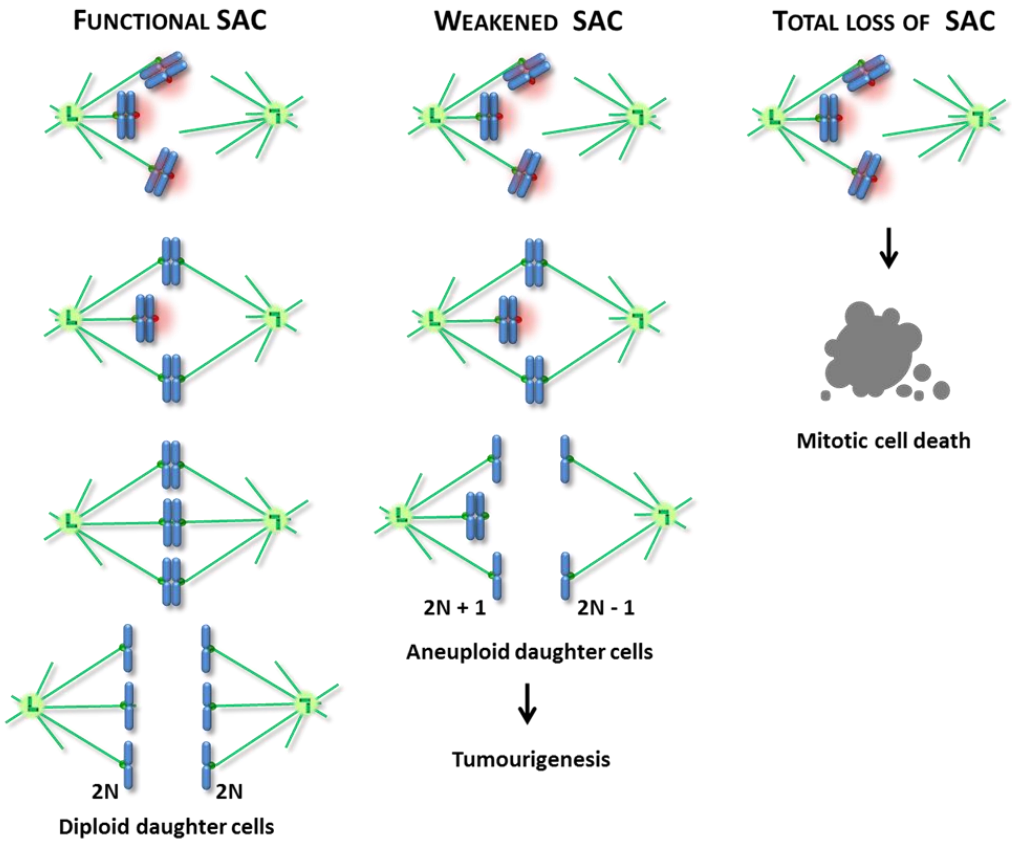

Figure 1.18. Different cell fates according to SAC activity status. Cells with a functional SAC (left) detect unattached or mis-attached kinetochores and an arrest in mitosis is sustained until correct attachment is achieved, resulting in accurate chromosome distribution between daughter cells. In cells with a weakened SAC (middle), a sustained arrest in mitosis could not be ensured in the persistence of errors in kinetochore attachment and, missegregation occurs resulting in aneuploid daughter cells which could potentiate tumorigenesis. Cells with complete loss of SAC activity (right) exit mitosis prematurely, and die as a result of massive aneuploidization (Adapted from [201]).

Although the first identification of mutations in the SAC genes BUB1 and BUB1B in human colorectal cancer cell lines was encouraging [202], genetic lesions on SAC

components revealed to be rather rare in a large number of aneuploid cancers with weakened SAC activity, suggesting that epigenetic alterations are responsible for the SAC impairment [203]. Indeed, many studies reported altered expression of SAC components in various tumors. Moreover, mice with heterozygous SAC genes, hence with low levels of SAC proteins, have a weakened SAC activity, exhibit a high frequency of aneuploid cells and develop tumors [204-206]. Although mutations or altered expression levels of SAC genes were reported in many aneuploid cancers, it remains to be elucidated whether these alterations are directly responsible for SAC weakening. It is likely that the decreased levels of some SAC components, known to have a role in chromosome congression, may contribute to aneuploidy in cancer cells. For instance, Bub1-, BubR1- or Bub3-depleted cells were reported to exhibit chromosome congression defects [207-210]. While the presence of a compromised SAC and its contribution to aneuploidy in many tumors had gained a widespread acceptance, a number of studies reported that the SAC is fully functional in most aneuploid cancer cells [211, 212]. Aneuploid cell lines were shown to arrest in response to microtubule damage for longer than non-transformed cells and, interestingly, they only rarely enter anaphase in the presence of unaligned chromosomes [212]. A study analyzing the consequences of gradual increases in chromosome segregation errors in the viability of tumor cells and normal human fibroblasts, found that partial inhibition of SAC proteins BubR1 and Mps1,both involved in checkpoint activation and chromosome alignment, sensitizes the tumor cell lines to low doses of taxol due to increased severity of chromosome segregation errors, therefore suggesting that a weak spindle checkpoint and an increase in chromosome segregation errors might selectively kill tumor cells [213]. One possible explanation to this controversy is that the SAC status varies between cancer types depending on the putative underlying molecular alterations. For instance, different expression profiles of SAC genes were reported in different cancer lines, with the same genes showing increased expression in some cancers and decreased expression in others. Moreover, efficient SAC activity is based on the equilibrium between its components and their expression levels; therefore, the SAC status in a given tumor would be influenced by the extent to which this equilibrium is affected by the overall alterations in the expression profile of all SAC genes in that tumor. Taken together, it appears that the SAC activity in aneuploid cancer cells is sufficient to prevent premature anaphase under normal growth conditions. However, its ability to sustain an artificially prolonged arrest, such as the one imposed by microtubule poisons,

would depend on the nature of the molecular alterations in the SAC components or in the components of other mechanisms that allow premature satisfaction of the SAC, such as those responsible for microtubule dynamics or for correcting chromosome attachment errors.

Independently of the controversy around the SAC status in cancer cells and its role in the occurrence of chromosome instability and tumorigenesis, there is no doubt that complete SAC inactivation is lethal to cells due to massive chromosome misssegregation [214, 215]. As the SAC is only required during mitosis, its targeting obviously represents a promising therapeutic strategy to selectively kill dividing cells, which could circumvent the resistance to or the side effects caused by the anti-cancer agents currently in use, such as those that target microtubules. In this respect, SAC components with no functional roles outside of mitosis constitute the suitable targets [216].

7. TARGETING MITOSIS IN CANCER THERAPY

7.1. Classical Antimitotic drugs

Antimitotic drugs block mitosis progression and have been extensively used in cancer chemotherapy as they restrict cancer cells growth and spread. Classical antimitotic drugs targets microtubule dynamics, and for this reason are referred as microtubules-targeting agents (MTAs) and have carrying a proven history of clinical efficacy [217].

MTAs are typically divided in two major classes: microtubule-stabilizing and microtubule-destabilizing agents [218]. The former class consists of taxanes (eg. paclitaxel and docetaxel) that are currently used in clinical treatment for a wide range of cancers namely advanced breast, non-small cell lung, androgen-independent prostate, and ovarian cancers [219]; and the second class concerns to Vinca alkaloids (eg. vinblastine, vincristine and vinorelbine) that have shown antitumor activity in Hodgkin and non-Hodgkin lymphoma, Kaposi sarcoma, acute leukemias, neuroblastoma, rhabdomyosarcoma, Wilms tumor, and testicular, breast, and non-small cell lung cancers [217]. Although taxanes and Vinca alkaloids are amongst the most popular MTAs, a more recent class of microtubules-stabilizing agents are the epothilones (A and B) which bind at the taxane-binding site on microtubules [220]. The ixabepilone, a

semi-synthetic analog of epothilone B, was FDA-approved, in 2007, for clinical use in the treatment of metastatic breast cancer [221].

Both of these agents disturb the dynamic of microtubules and causes abnormal spindle formation, by interfering with assembly and disassembly of tubulin subunits [222, 223]. The taxanes inhibit microtubules depolymerization, by binding to β-tubulin subunits, stabilizing them while the Vinca alkaloids prevent microtubules assembly, destabilizing the whole filament. Cells exposed to MTAs arrest in mitosis due to chronic activation of the SAC [224]. Following a prolonged mitotic arrest cells respond to mitotic inhibition by different ways: die in mitosis via apoptosis, divide unequally producing aneuploid daughter cells or exit mitosis without dividing, a process known as slippage. After slippage cells can enter into an abnormal G1 state, followed by cell death, arrest in a tetraploid G1 state (interphase arrest), or continue to proliferate (cell cycle progression) (**Figure 1.19**) [212, 225].

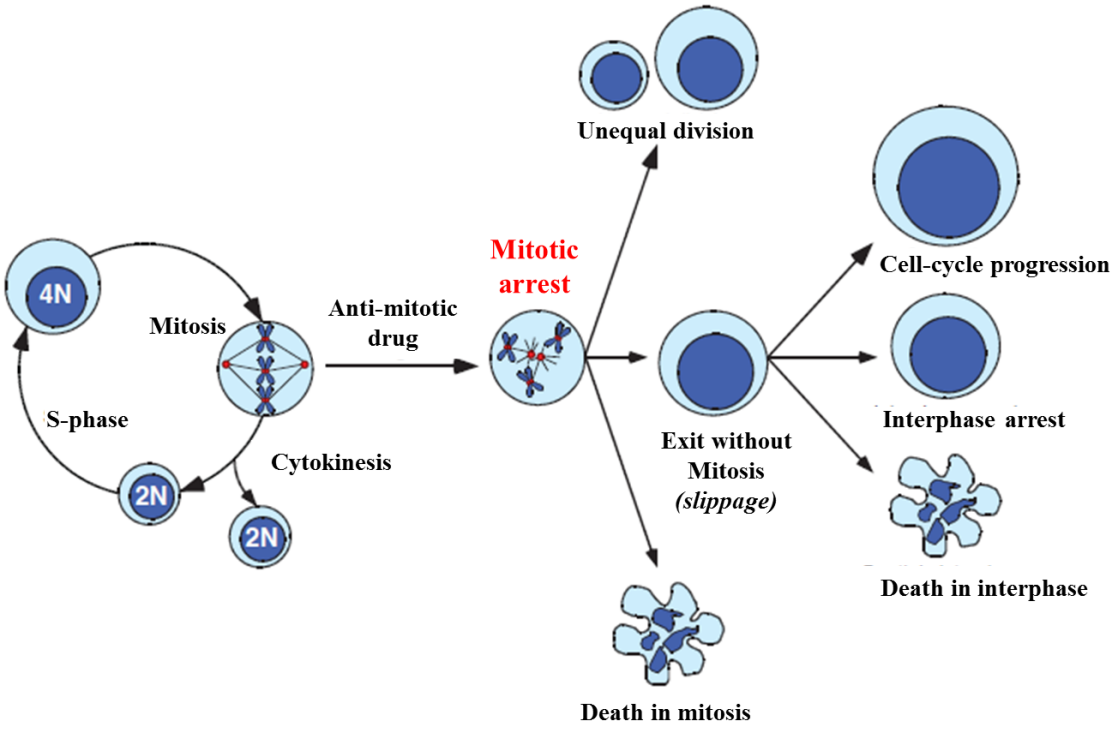

Figure 1.19. Cell fate in response to anti-mitotic drug treatment. When cells are exposed to an anti-mitotic agent, they arrest in mitosis due to chronic activation of the spindle assembly checkpoint. They then undergo one of several fates. Cells might die directly in mitosis, or divide unequally to produce aneuploid daughter cells. Alternatively, cells might exit mitosis without undergoing division (slippage). In this case, cells might then die in interphase, arrest in interphase indefinitely or enter additional cell cycles in the absence of division (Adapted from [225]).

Thus, the fate of cells exposed to antimitotic agents is, in part, determined by the length of the mitotic arrest and their ability to activate apoptosis. It was proposed that cell fate is determined by two competing networks that run in parallel upon exposure to MTAs, one that involves accumulation of cell death signal, and another that promotes gradual cyclin B degradation [226]. Therefore, the network that reaches first its threshold will determine the fate of the mitosis-arrested cell. For instance, if cyclin B decreases below the threshold level (that sustains the mitotic state) first, then the cell will exit mitosis (slippage). Slippage is linked to resistance to anti-mitotic agents due to impaired SAC activity in many cancers. In SAC defective cancers, cyclin B degradation threshold would be readily reached which favours slippage and aneuploid cells are produced.

Actually, to predict how a given tumor will respond to antimitotic therapy remains a great challenge and no tools are yet available. Indeed, using a high-throughput automated time-lapse light microscopy approach it was shown that cancer cells display profound intra- and interline variation following prolonged exposure to antimitotic drugs, resulting in multiple cell fates within a cell population [212].

Throughout the years, MTAs have proven their efficacy in cancer treatment. However, several limitations such as adverse side effects and drug resistance remain to restrict their clinical potential [227]. The most frequent adverse side effects are associated with neuro and hematological toxicity since, unfortunately, MTAs do not distinguish between malignant and normal cells. Neurotoxicity can be explained by the high content of microtubules in axons, which are vital for the transport in neurons [228] and the hematological toxicity, or myelosuppression, can result from the impairment of normal rapidly dividing cells, namely the bone marrow cells [229, 230]. To the other hand, drug resistance can emerge due to mutations at drug binding sites, changes in microtubule dynamics and in expression of tubulin isotopes, modifications in microtubule-regulatory proteins and efflux activity of the P-glycoprotein and the multidrug-resistance protein MRP1 that involves the transport of drugs out of the cell, thus dropping the intracellular drug concentration. Accordingly, several screens have been performed to identify markers of resistance or sensitivity to paclitaxel. A diverse array of candidates has been identified, such as proteasome subunits, cyclin G1, and solute carriers transporters [231-238], although no validated biomarker that predicts which patients will benefit from paclitaxel therapy was discovered.

7.2. Second generation of Antimitotic drugs

Due to the abovementioned disadvantages that limit MTAs efficacy, a novel generation of antimitotic drugs is being developed, in a mitosis-selective approach, that inhibit mitosis without affecting microtubules dynamics in non-dividing cells [239].

Several mitotic-related components have been proposed as drug target candidates, and the front-runners include the plus end-directed motor protein Eg5 (kinesin-5) and Aurora and Polo-like kinases.

Eg5, involved in centrosome separation at prophase, initiates the bipolar spindle assembly [70, 71]. Inhibition of their motor activity results in assembly of a monopolar spindle, leading to impairment on chromosome congression and chronic SAC activation, followed by cell death [240, 241]. Notably, Eg5 inhibition showed to effectively kill paclitaxel-resistant cell lines [242], making this protein a suitable anti-cancer target. Indeed, a diversity of selective Eg5 inhibitors has been developed and some of them have entered clinical trials. Despite the initial expectative and although limited cytotoxicities have been found in patients treated with Eg5 inhibitors, only partial responses have been reported so far [243], suggesting that these agents should be used in combination with other cytotoxic drugs. Moreover, mutations in Eg5 have been reported as inducers of resistance to Eg5 inhibitors [244-246]. Also, increased expression of Kif15 allows cancer cells to overcome a mitotic delay induced by Eg5 inhibition [247].

Aurora kinases play a key role in the control of mitosis. Defects in these kinases activity are related with chromosomal instability and aneuploidy, and they are frequently deregulated in human cancers. Aurora A is found overexpressed in breast, ovary, lung, bladder, stomach, pancreas, head-and-neck, and colon cancers whereas Aurora B is overexpressed in breast cancer, NSCLC, glioblastoma, and prostate cancer [248-250]. A role for Aurora C in tumorigenesis has not been established until now. Due to their recognition as potential targets for cancer treatment, around 30 Aurora kinase inhibitors have reached different stages of pre-clinical and clinical development [251]. Despite the demonstrated antitumor activity in several cancer cell lines and xenografts models in clinic the results are still disappointing [252, 253].

Amongst of Polo-like kinases family, Plk1 has the most studied kinase and plays a central role in mitosis being required for their initiation, maintenance, and completion [254]. Overexpression of Plk1 has been found in a diversity of human cancers, such as

glioma [255], thyroid carcinoma [256], head and neck squamous cell carcinoma [257], melanoma [258], colorectal [259], esophageal [260], ovarian [261], breast [262], and prostate cancers [263] and it was associated with poor prognosis [264-266]. Plk1 suppression by RNAi, antibodies or kinases inhibitors has shown an efficient inhibition of cancer cells proliferation and an induction of apoptosis [267, 268], suggesting that Plk1 could be an attractive target for cancer therapy. Moreover, from the discovery of Plk1 is highly expressed in primary tumor tissues [269], its role as an oncogene gain additional relevance [270, 271]. Several studies point Plk1 targeting as a novel approach for overcoming drug resistance in cancer chemotherapy and to sensitize tumor cells to radiation. For example, it was reported that Plk1 silencing could enhance the sensitivity to cisplatin in human TP53-mutated epidermal squamous carcinoma cells by upregulating p73a [272] or potentiate the neoplastic effect of paclitaxel, causing synergistic effects in breast cancer cell lines and in human breast cancer xenografts [273]. In addition, Plk1 inhibition showed to suppresses cell growth and enhances radiation sensitivity in medulloblastoma cells [274]. The BI2536, a small molecule inhibitor of Plk1, it was also reported as could enhance the inhibition of imatinib and nilotinib on chronic myeloid leukemia cell growth [275]. Unfortunately, so far, the small molecule inhibitors of Plk1 have not achieved a satisfactory therapeutic effect in clinical trials [276], probably due to dose-limiting toxicities. In accordance, there is a study revealing that reduced efficacy of the Plk1 inhibitor BI2536 on progressive hepatocellular carcinoma was due to low intratumoral drug levels [277].

The kinesin motor protein CENP-E has been added to the list of potential antimitotic targets. Apparently, CENP-E functions are restricted to mitosis namely in chromosome congression, as described above, and in SAC response by modulating BubR1 function [278, 279] a critical MCC component. In agreement, CENP-E inhibition leads to mitotic delay with several misaligned chromosomes and has been shown to elicit anti-tumor effects in mouse models of spontaneous tumor formation and in mice bearing xenografts of human tumor cells [280, 281]. Overexpression of CENP-E was found in human melanoma and cervical cancer [282, 283]. Notably, an increase in CENP-E levels was linked to epothilone B resistance in A549 lung cancer cells, suggesting CENP-E protein expression could potentially act as a predictive biomarker to identify patients more likely to benefit from treatment with microtubule-stabilizing drugs [284]. Small-molecules inhibitors of CENP-E are under evaluation and some of them has reached phase I of clinical trials [243, 285].

Mps1 is a dual-specificity protein kinase that binds to kinetochores. Mps1 is required to sustain SAC functions and promotes correct kinetochore-microtubule attachment [286]. Due to its function in mitosis, Mps1 is an appealing target for anti-cancer therapies. High levels of Mps1 are found in many types of human malignancies including glioblastoma, anaplastic thyroid carcinoma, breast and lung cancers [287-291]. Overexpressed Mps1 correlates with a shorter period of recurrence and survival time suggesting that Mps1 might also be an independent biomarker indicative of cancer prognosis [288]. Inhibition of Mps1 leads to SAC abrogation, thereby leading to shortened mitosis, chromosome misssegregation, aneuploidy or polyploidy and cell death [180] Mps1 reduced levels have showed to increase tumor cells sensitivity to paclitaxel, resulting from severe chromosome missegregation, leading to cell death [213]. Although several chemical inhibitors of human Mps1 kinase activity led to promising results, none has fulfilled clinical premise [292]. The first phase I clinical trials of oral Mps1 inhibitors (BAY1161909, BAY1217389) in combination with paclitaxel are still underway (ClinicalTrials.govID: NCT02138812, NCT02366949).

Overall, most of this new generation of antimitotic drugs that reach clinical trials, has been showing the lack of anti-microtubules-related side effects but the effectiveness to kill tumor cells stayed behind. These unexpected results could be, in part, related with the hidden mechanism underlying MTAs-mediated cytotoxicity. Nonetheless, antimitotic drugs are still subject of intense research that aims to improve maximal clinical benefit with reduced toxicity through new strategy of drug design, formulation and delivery or taking advantages of combinatorial drugs regimens. Another important issue is the improvement of strategies to more effectively target heterogenic tumor cell populations and the identification of which tumor/patients are most likely to respond to anti-cancer drugs, highlighting the role of the emerging era of pharmacogenomics.

7.3. MCC components as potential anticancer targets

Anti-mitotic activity can be achieved either by inhibiting mitotic exit or by forced mitotic exit, depending on the targeted SAC component. The rational of this approach is that: i) inhibiting mitotic exit should maximize the time that tumor cells spend in mitosis, ultimately leading to their death; and, alternatively, ii) forcing tumor cells to exit mitosis prematurely should inevitably result in their death as a consequence of massive chromosome misssegregation. Both approaches were tested in human cancer

cells, with varying degrees of success. It should be noted that there are two functionally different groups of SAC components, that elicit two different types of response upon inhibition: i) the core SAC components (Aurora B, Mps1, Bub1, BubR1, Bub3, Mad2, and Mad1) which are involved in the generation of the diffusible inhibitory signal, and whose inhibition results in forced mitotic exit; and ii) the SAC components (Plk1, Hec1, Mis12, Knl1, Rod/Zwilch/Zw10, Ska1-3, CENP-E Spindly and dynein) which are involved in kinetochore-microtubule attachment and/or chromosome congression but are not required for SAC signal generation, and whose inhibition elicits a mitotic arrest. In principle, most SAC components are potential targets [216].

Focusing on MCC components, to date, only one inhibitor is available in preclinical studies.

Mad2 is a key component of the MCC, with central role in SAC signal amplification in response to unattached kinetochores. Overexpression of Mad2 was found in breast, renal, lung, salivary, esophageal, pancreatic, gastric, colorectal, hepatocellular, bladder, cervical and oral cancer and in retinoblastoma and osteosarcoma [291, 293-299]. RNAi targeting of Mad2 caused massive chromosome missegregation and apoptosis in colorectal cancer cells, and reduced growth of xenograft tumors [300, 215]. In contrast, in gastric cancer, Mad2 inhibition showed an increase of proliferation, apoptosis inhibition and multidrug resistance by regulating the activation of phosphorylated survivin [301]. Downregulation of Mad2 has been associated with worse prognosis and as a driver of resistance to conventional chemotherapeutics drugs, such as paclitaxel or cisplatin [302-306]. Interestingly, an overcome of cisplatin resistance in non-small cell lung cancer with Mad2 silencing siRNA delivered systemically using EGFR-targeted chitosan nanoparticles was recently described [307]. Through fluorescence polarization-based screen, the first small molecule inhibitor of Mad2 (M2I-1), was proposed as targeting the binding of Mad2 to Cdc20. Cellular studies revealed that M2I-1 weakens the SAC response, indicating that the compound might be active in cells [308].

BubR1 is a serine/threonine protein kinase that binds to kinetochores, and is involved in SAC signaling in response to a lack of tension on kinetochores. BubR1-depleted cells are unable to maintain stable KT-MT attachments, consistent with their role to regulate the switching from lateral to end-on attachment [207, 208]. BubR1 was reported as overexpressed in several human cancers, including gastric adenocarcinoma, hepatocellular, urothelial bladder, esophageal, cervix, ovarian, thyroid, renal, lung,

prostate, colorectal and oral squamous cell carcinomas and pediatric glioblastoma [145, 309-311, 296, 312-318, 295]. Overexpression of BubR1 was reported as associated with disease progression and poor survival in human lung adenocarcinoma patients. Moreover, BubR1 knockdown inhibited metastasis and prolonged overall survival, suggesting that therapeutic strategies targeting BubR1 may prove efficacious as single agents [319]. RNAi-mediated knockdown of BubR1 showed to restores cancer cell sensitivity to paclitaxel [145, 213]. A natural diterpenoid, Pharicin A, was reported to inhibit BubR1autophosphorylation, leading to impaired spindle checkpoint functions and inhibition of proliferation of leukemia and solid tumor-derived cells. Also, Pharicin A was showed to induce mitotic arrest in paclitaxel-resistant Jurkat and U2OS cells [320].

In human cells, Bub3 is shown to be required for the establishment of accurate KT-MT attachments, since RNAi-mediated Bub3 repression leads to persistent chromosome misalignment phenotype [208, 207, 321]. Moreover, Bub3-depleted cells or BUB3 null embryos exit prematurely from mitosis as a result of SAC activation failure [208], leading to anaphases with lagging chromosomes [208] and micronuclei formation [322]. Indeed, a role of Bub3 as a tumor suppressor was reported in *Drosophila melanogaster* tumorigenic model [323]. These findings suggested that Bub3 repression is associated with chromosomal instability (CIN) and aneuploidy [205], a hallmark of most solid tumors. Variations in Bub3 expression were reported in human tumors being upregulated in breast [324, 325], gastric [318], cervical [283] and salivary gland [326] cancers and downregulated in pediatric glioblastoma [309]. However, the clinicopathological significance of Bub3 deregulation is still missing. Suppressing Bub3 in HeLa cervical carcinoma cells seems to produces paclitaxel resistance [327].

Cdc20 is the main target of SAC activity, whose inhibition leads to mitotic arrest and an extended apoptotic cell death. Its overexpression was found in breast, hepatocellular, head and neck, pancreatic, bladder, cervical and gastric cancers [283, 328-332]. An inhibition of cancer cells growth, due to mitotic arrest, and an improvement of cytotoxic activity of both paclitaxel and irradiation were reported after Cdc20 knockdown [333] [334] as well as an significant inhibition of hepatocellular carcinoma growth in the orthotopic liver tumor model [335]. In histological samples from Oral Squamous Cell Carcinoma (OSCC), Cdc20 overexpression was linked to a poor prognosis, suggesting Cdc20 as a novel independent prognostic factor, as well as a molecular marker to categorize high-risk OSCC subgroups [332].

Overall, the abovementioned reports reinforce that targeting the MCC components, may be promising target for antimitotic activity. Also, combinatorial regimen between SAC components and conventional antimitotic drugs could be an attractive therapeutic avenue of exploration of new cancer therapies.

CHAPTER 2

MOTIVATION AND AIMS

MOTIVATION AND AIMS

The spindle assembly checkpoint (SAC) is the major safeguard mechanism for protecting cells against chromosome missegregation at anaphase by monitoring the status of kinetochore-microtubule (KT-MT) attachments [99]. SAC signaling pathway is activated by unattached or misattached kinetochores, and it is silenced after these kinetochores form stable end-on microtubule attachments [99]. Bub and Mad proteins are key players for effective SAC response. Nonetheless, the role of SAC proteins was expanded with the discovery that BubR1, Bub1, and Bub3 are themselves implicated in the regulation of KT-MT attachment [207], besides their role in SAC signaling. In higher eukaryotes, KT-MT attachments are mainly mediated by the minus-end directed motor dynein [78, 109, 79, 81], and the plus-end directed kinesin motor CENP-E [120, 151]. The link between SAC signaling and KT-MT binding machinery is still not completely understood. Dynein was also reported as involved in SAC silencing, namely in the stripping of SAC proteins from the attached kinetochores towards spindle poles [82, 336]. An open issue is to clarify which components are poleward transported by dynein, to switch off the SAC signal, since the reported results remains controversial.

Hence, the first aim of this thesis was focused on SAC function and regulation (Chapter 3), with two specific objectives:

(i) To establish a relationship between the SAC protein Bub3 and the microtubule motor dynein in regulating kinetochore-microtubule attachment and chromosome congression;
(ii) To elucidate the role of dynein-mediated transport of SAC components off kinetochores to promote SAC silencing.

Targeting mitosis in cancer cells leads to mitotic arrest, due to chronic SAC activation, and frequently to cell death [225]. This explains the proven success of the anti-microtubule drugs, taxanes and Vinca alkaloids, in the clinical treatment of several human cancers [217]. Despite this and given their limitations, conventional antimitotic drugs are still subject of intense research that aims to enhance their efficacy while minimizing their toxicity. Although it seems hard to achieve, efforts have recently focused on the use of molecularly targeted agents, either alone or in combination with standard therapies such as taxanes, in order to improve survival and quality of life

outcomes. Moreover, effective clinical use of the novel targets and/or combined therapies will require the development of predictive biomarkers and patient stratification which, in turn, will require an in-depth understanding of the molecular mechanisms behind how these drugs kill cancer cells.

Accordingly, the second aim of this thesis was directed to therapeutic implications of spindle assembly checkpoint targeting (Chapter 4), with two specific objectives:

(i) To explore the potential of Spindly, a kinetochore regulator of dynein, as a target for cancer therapy, either alone or in a combination therapy

ii) To explore the potential of Spindly as diagnostic/prognostic biomarker of cancer.

These two aims allow to establish a bridge between the basic and applied research which is important for future progress namely in SAC function, regulation and therapeutic implications, at a translational view.

CHAPTER 3

SHEDDING LIGHT ON SPINDLE ASSEMBLY CHECKPOINT REGULATION AND FUNCTION

According to the objectives highlighted in the previous section, this chapter is divided into two parts:

3.1. Co-silencing of human Bub3 and dynein highlights an antagonistic relationship in regulating kinetochore-microtubule attachments;

3.2. Dynein-dependent transport of spindle assembly checkpoint proteins off kinetochores toward spindle poles.

3.1. Co-silencing of human Bub3 and dynein highlights an antagonistic relationship in regulating kinetochore-microtubule attachments

The information presented in this section was based in the following published paper:

Patrícia M.A. Silva, Álvaro A. Tavares and Hassan Bousbaa. Co-silencing of human Bub3 and dynein highlights an antagonistic relationship in regulating kinetochore-microtubule attachments. FEBS Letters. 2015;589(23):3588-94.

1. Abstract

We previously reported that the spindle assembly checkpoint protein Bub3 is involved in regulating kinetochore-microtubule (KT-MT) attachments. Also, Bub3 was reported to interact with the microtubule motor protein dynein. Here we examined how this interaction contributes to KT-MT attachments. Depletion of Bub3 or dynein induced misaligned chromosomes, consistent with their role in KT-MT attachments. Unexpectedly, co-silencing of both proteins partially suppressed the misalignment phenotype and restored chromosome congression. Consistent with these observations, KT-MT attachments in co-depleted cells were stable, able to drive chromosome congression, and produce inter- and intra-kinetochore stretch, indicating they are functional. We suggest that a mutual antagonism exists between Bub3 and dynein to ensure optimal KT-MT attachments.

Keywords: Bub3, dynein, Spindly, kinetochore-microtubule interactions, chromosome congression, antagonistic interaction.

2. Introduction

Faithful chromosome segregation in mitosis relies on appropriate kinetochore-microtubule (KT-MT) attachments, under the surveillance of the spindle assembly checkpoint (SAC). The SAC prevents anaphase onset until all chromosomes accomplish proper bipolar attachments and come under tension. Core components of the SAC proteins include, among others, the evolutionary conserved Mad2, Bub3, and BubR1, which form the mitotic checkpoint complex (MCC) with Cdc20 whenever unattached or improperly attached kinetochores are present. As a consequence, Cdc20 is unable to activate the anaphase promoting complex/cyclosome (APC/C) and anaphase is blocked [99, 23]. Besides this surveillance role, SAC components were also involved in the regulation of KT-MT attachments [207]. For instance, we previously reported that Bub3 is required for the establishment of stable end-on KT-MT attachments. Yet, the relationship between Bub3 and other proteins involved in the same process of KT-MT attachments remains unknown. A good candidate for this relationship is the cytoplasmic dynein. Dynein was reported to interact with Bub3 [337, 338]. Although there is still no clear demonstration of a direct role of dynein in the formation of stable KT-MT attachments, in many reports, displacement of kinetochore dynein was reported to delay chromosome congression and the formation of load-bearing attachments. For instance, inhibition of dynein results in unstable KT-MT attachments and interferes with metaphase chromosome alignment [339, 340]. Here, we studied the functional relationship between Bub3 and dynein in regulating KT-MT attachments.

3. Materials and Methods

3.1. Cell culture and siRNA transfection

HeLa cells, HeLa cells stably expressing EGFP-Bub3 [341], and HeLa cells stably expressing EGFP-CENP-A (a gift from Dr. Lars Jansen, IGC, Lisboa, Portugal) were cultured in Dulbecco's Modified Eagle's Medium (DMEM, Biochrom, São Mamede de Infesta, Portugal), supplemented with 10% fetal bovine serum (FBS, Biochrom), and maintained at 37°C, in a 5% CO_2 humidified atmosphere. For HeLa cell lines stably expressing EGFP-Bub3 and EGFP-CENP-A, the medium was supplemented with 400

µg/ml of a selective agent G418 and 1 µg/ml Blasticidin (Sigma-Aldrich Co., Saint Louis, MO, USA) respectively.

For transfection with siRNAs, cells were seeded in 22 mm poly-L-lysine-coated coverslips in 6-well plates containing DMEM and, 24 hours later, transfected using INTERFERin siRNA Transfection Reagent (PolyPlus, New York, USA) according to the manufacturer's instructions. The culture medium was replaced 6 hours after transfection with fresh DMEM. Validated siRNA duplexes against Dynein Heavy Chain (DHC) and Bub3 (Santa Cruz Biotechnology, Dallas, USA) were used at a final concentration of 13.3 nM and 6.7 nM, respectively. A validated siRNA sequence against Spindly [342] was synthetized by Sigma-Aldrich and was used at a final concentration of 100 nM. Microscopic analysis was performed 48 or 72 hours post-transfection.

3.2. Cell extracts and Western Blotting

For total cell extracts, cells were harvested by centrifugation and resuspended in lysis buffer (50 mM Tris pH 7.5; 150 mM NaCl; 1 mM EDTA; 1% Triton-100) containing a protease inhibitor cocktail (Sigma-Aldrich). Protein quantification was performed using a BCA™ Protein Assay Kit (Pierce Biotechnology), according to the manufacturer's instructions. A total of 15 µg of protein lysate was resuspended in SDS-sample buffer (375 mM Tris pH 6.8; 12% SDS; 60% Glycerol; 0.12% Bromophenol Blue; 600 nM DTT), boiled for 3 minutes at 100°C and proteins were separated on a 7.5% SDS-PAGE gel. After electrophoresis, proteins were transferred to a nitrocellulose membrane (Amersham) by semidry transfer system (Hoefer). Membrane was blocked with 5% nonfat dried milk in TBST (50 mM Tris pH 7.5; 150 mM NaCl, 0.05% Tween-20) for 1 hour at room temperature (RT) with mild agitation. Primary antibodies were diluted, in 1% nonfat dried milk, as follows: mouse anti-Bub3 (1:1000, 611731 clone 31, BD Biosciences); mouse anti-DIC (1:200, D5167 clone 70.1, Sigma-Aldrich); rabbit anti-Spindly (1:3000, gift from Dr. R. Gassmann, IBMC, Portugal), rabbit anti-α-tubulin (1:1500, ab15246, Abcam) and mouse anti-α-tubulin (1:5000, T568 Clone B-5-1-2, Sigma-Aldrich). After washing in TBST, membrane was probed, for 1 hour at RT, with horseradish peroxidase (HRP)-conjugated secondary antibodies, diluted at 1:1500 (anti-mouse, Vector) or at 1:1000 (anti-rabbit, Sigma). Proteins were visualized using the Enhanced Chemiluminescence (ECL) method and the relative signal intensity of the

bands was determined as normalized against α-tubulin intensity levels using ImageJ 1.4v software (http://rsb.info.nih.gov/ij/).

3.3. Immunofluorescence

Cells were fixed in fresh 2% paraformaldehyde (Sigma-Aldrich) in phosphate-buffered saline (PBS) for 12 minutes, rinsed three times 5 minutes in PBS and permeabilized with 0.5% Triton X-100 in PBS for 7 minutes. Alternatively, cells were fixed in -20ºC cold methanol for 10 minutes and rehydrated twice in PBS. Non-specific binding sites were blocked with 10% FBS in PBST (PBS plus 0.05% Tween-20) for 30 minutes at RT. Then cells were incubated for 1 hour with primary antibodies diluted in PBST containing 5% FBS as follows: human anti-CREST (1:4500, gift from Dr. E. Bronze-da-Rocha, IBMC, Porto, Portugal); mouse anti-Hec1 (1:600, ab3616, Abcam); rabbit anti-Spindly (1:3000, gift from Dr. R. Gassmann, IBMC, Portugal); rabbit anti-α-Tubulin (1:100, Abcam); mouse anti-γ-Tubulin (1:1500, T6557, Clone GTU-88, Sigma-Aldrich) mouse anti-α-Tubulin (1:2500, Sigma-Aldrich). After washing in PBST, cells were incubated with secondary antibodies for 1 hour. All secondary antibodies were used at 1:1500 (Molecular Probes), with the exception of Alexa Fluor 647-conjugated secondary antibody which was used at 1:2000 (Molecular Probes). DNA was stained with 2 μg/ml 4′,6-diamidino-2-phenylindole (DAPI, Sigma-Aldrich) diluted in Vectashield mounting medium (Vector, H-1000).

3.4. Functional assays for kinetochore-microtubule attachments

To assess cold-stable microtubules, cells in culture medium were incubated at 4°C for 5 minutes and processed immediately for immunofluorescence with anti-α-tubulin and anti-Hec1 antibodies. Inter-kinetochore distance was measured between Hec1 spots on kinetochore pairs of bi-oriented chromosomes. Kinetochore stretching (intra-kinetochore distance) was obtained by subtracting the distance between CENP-A spots (inner kinetochore marker) from the distance of Hec1 spots (outer kinetochore marker), using GFP-CENP-A expressing HeLa cell line. More than 50 kinetochore pairs from 10 cells were analyzed. To evaluate the ability of KT-MT attachments to drive chromosome congression, cells were first incubated with 1 μM nocodazole (Sigma-Aldrich) for 1 hour to depolymerize microtubules, in the presence of 10 μM of the proteasome inhibitor MG-132 (Sigma-Aldrich) in order to arrest cells at metaphase-

anaphase boundary. Then cells were released into medium in the presence of MG-132 for 1 hour before immunostaining [208]. Nocodazole washout gives cells the opportunity to nucleate a new set of microtubules and MG-132 give chromosomes time to achieve successful bipolar KT-MT attachments and to align at the equator to (re)organize a metaphase plate. More than 750 mitotic cells were counted for each condition.

3.5. Image acquisition and processing

Phase-contrast images were acquired with a 10x objective, on a Nikon TE 2000U microscope, using a DXM1200F digital camera and with Nikon ACT-1 software (Melville, NY). Fluorescence images were acquired with Plan Apochromatic 63x/NA 1.4 objective on an Axio Observer Z.1 SD microscope, coupled to an AxioCam MR3 digital camera (Carl Zeiss, Germany). Z-stacks were acquired at 0.4-µm intervals and images were processed using ImageJ software after deconvolution with AxioVision Release 4.8.2 SPC software. Insets are representative of each condition with 2-4 stacks projection.

Quantification of kinetochore fluorescence signals was performed as previously described except that values were normalized to Hec1 fluorescence intensities [208]. Each value was derived from at least 300 kinetochores in ten representative cells. For quantification of cold-stable microtubules, unattached and attached kinetochores were counted in 5 representative cells as previously described except that Hec1 staining was used to identify kinetochores in image Z-stacks [208]. More than 90 kinetochores were counted per cell.

3.6. Statistical analysis

Data are presented as the means ± standard deviation (SD) of at least three independent experiments. Statistical analysis was performed using an unpaired Student *t*-test in GraphPad Prism version 6 (GraphPad software Inc., CA, USA). The level of significance was set at probabilities of $*p < 0.05$, $**p < 0.01$, $***p < 0.001$ and $****p < 0.0001$.

4. RESULTS AND DISCUSSION

4.1. Bub3 and dynein are not mutually interdependent for kinetochore localization

To study the relationship between Bub3 and dynein in KT-MT attachment, we performed single and double depletions using validated siRNAs (**Figure 3.1A and B**). An important question that needed to be clarified first was whether depletion of one protein affects kinetochore localization of the other. This possibility was excluded as Bub3 properly localized to kinetochores in dynein-depleted cells, as did dynein in Bub3-depleted cells (**Figure 3.1B**). Thus, the chromosome misalignment phenotype known to result from depletion of one protein is not a consequence of depletion of the other.

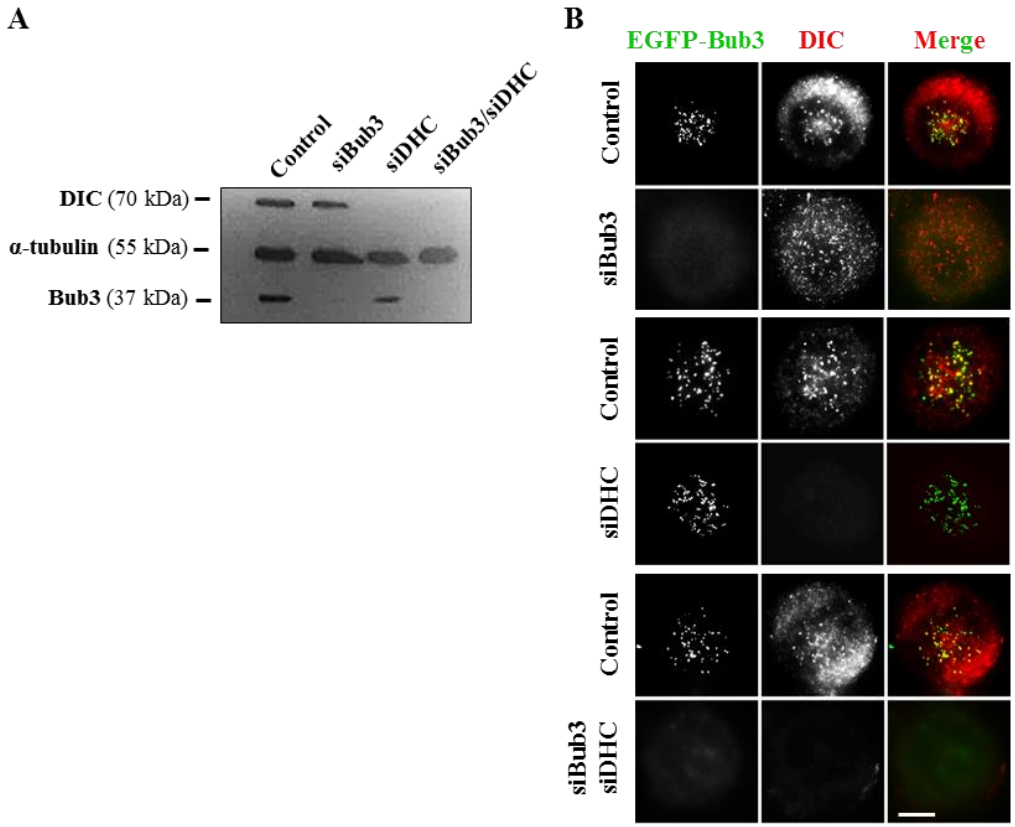

Figure 3.1. Bub3 and dynein depletion are not interdependent for kinetochore localization. **(A)** Immunoblots showing efficient siRNA-mediated individual (siBub3 and siDHC) and co-depletion of Bub3 and dynein (siBub3/siDHC). Note that the levels of one protein are not affected by depletion of the other. **(B)** Immunofluorescence images showing that (top panel) depletion of Bub3 (siBub3) did not affect kinetochore localization of dynein (DIC), and (middle panel) depletion of dynein (siDHC) did not affect kinetochore localization of Bub3 (EGFP-Bub3); (bottom panel) shows depletion of both proteins (siBub3siDHC). Cells were treated with 1µM nocodazole prior immunofluorescence to create conditions where Bub3 and dynein are maximally enriched at kinetochores. Bar, 5µm.

4.2. Dynein depletion partially suppresses chromosome misalignment phenotype associated with Bub3 depletion

We then proceeded to the analysis of chromosome congression in the absence of both Bub3 and dynein in order to determine if a relationship exists between the two proteins. For that, we determined the ability of chromosomes to align at spindle midzone and to form a defined metaphase plate in Bub3/dynein co-depleted cells. Cells were treated with the anaphase inhibitor MG-132 prior to immunostaining in order to give chromosomes enough time to reach the metaphase plate [208, 207, 215]. Most mitotic cells in control were blocked in metaphase (91.0±0.7%) and had all chromosomes aligned (**Figure 3.2A and B**). In contrast, the majority of mitotic Bub3-depleted cells (62.0±1.5%) that reached metaphase exhibited misaligned chromosomes (**Figure 3.2A and B**), consistent with defective KT-MT attachments we previously reported [208]. In dynein-depleted cells, we observed three distinct mitotic figures: metaphases with misaligned chromosomes (36.2±7.2%), full metaphases (26.2±3.1%), and mitotic cells with no defined organization that we scored as disorganized metaphases (37.6±2.4%) (**Figure 3.2A and B**). While the presence of metaphases with misaligned chromosomes reflects the dynein role in initial attachments and probably in their conversion into end-on attachment [74, 75, 340], the disorganized figures displayed abnormal mitotic spindle morphology with no focused spindle poles, probably reflecting dynein role in spindle organization and centrosomes separation [109, 78]. Nevertheless, the metaphases with misaligned chromosomes and full metaphases showed bipolar spindles with focused poles as judged by the centrosome marker γ-tubulin (**Figure 3.2C**). Quantification of metaphases in MG-132-treated Bub3/dynein co-depleted cells showed a significant increase in full metaphases, from 38.4±1.5% in Bub3- and 26.2±3.1% in dynein-depleted to 47.4±8.1% after depletion of both proteins (**Figure 3.2A and B**). This increase was accompanied with a concomitant decrease in metaphase with misaligned chromosomes, with a drop from 61.7±1.5% in Bub3 and 36.2±4.6% in dynein single knockdown to 22.4±1.8% in the absence of both proteins. The percentage of disorganized metaphases did not seem to be affected by the co-depletion.

Then, we sought to clarify whether the contribution of dynein to the rescue of chromosome alignment observed in Bub3/dynein co-depletion was specific to its kinetochore pool, or it is due to the multiple roles of its cytosolic pool in mitotic spindle

organization. To selectively deplete dynein from kinetochore, we used validated siRNAs against Spindly, a protein required for dynein recruitment to kinetochores [343]. As expected, dynein was absent from kinetochore after Spindly depletion (**Figure 3.S1A and B**). We also certified that Bub3 and Spindly were not interdependent for kinetochore localization (**Figure 3.S1C and D**). In MG-132-treated Bub3/Spindly co-depleted cells, the severity of chromosome misalignment was clearly attenuated, compared to Spindly depletion, with a net increase in well-defined metaphase plates having few to no misaligned chromosomes (**Figure 3.2D and E**).

Collectively, these observations indicate that co-depletion of Bub3 and dynein suppresses, at least partially, the misalignment phenotype generated by depletion of each protein individually, which probably underlies an antagonistic interaction. Of note, as a dynein-recruitment independent role in chromosome alignment has been proposed for Spindly [186], we do not exclude the possibility that Bub3/Spindly co-depletion is also rescuing alignment defects that are not necessarily dependent on dynein.

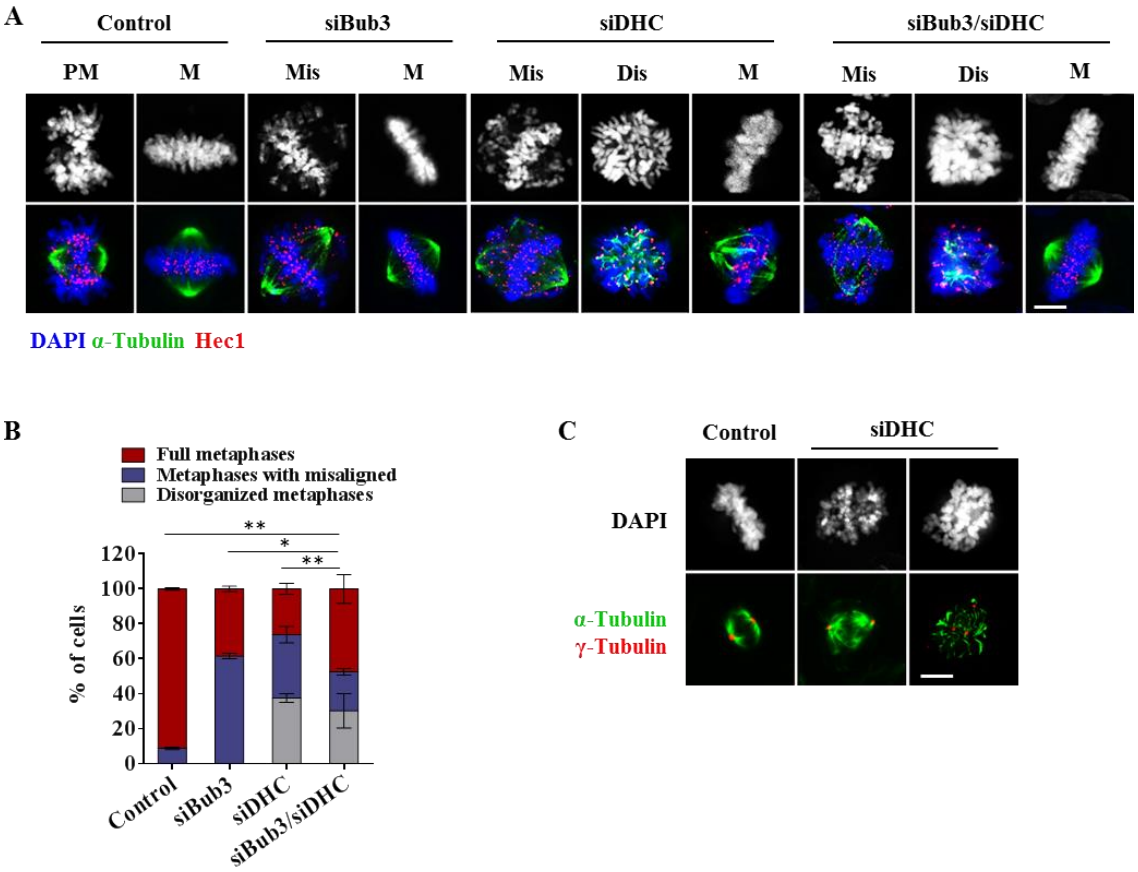

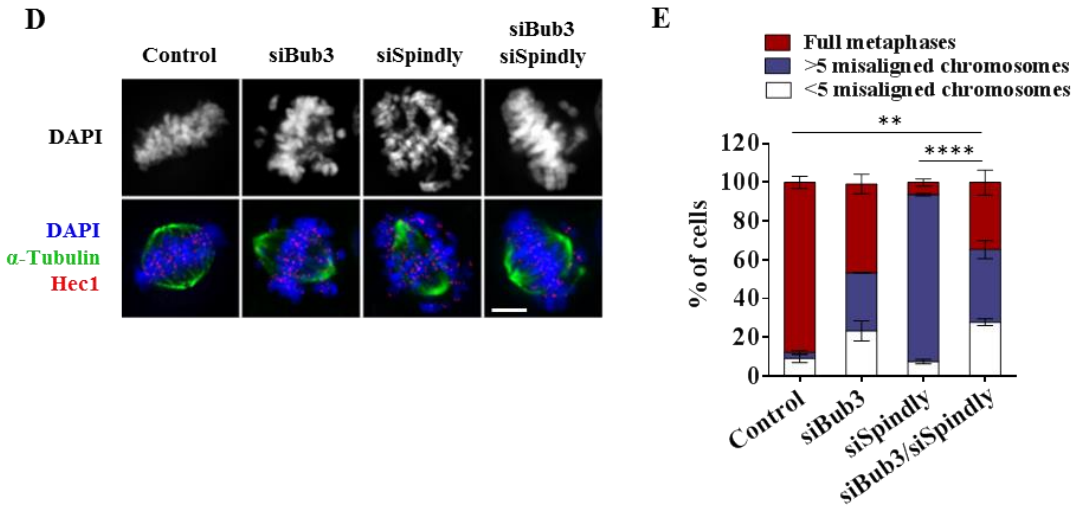

Figure 3.2. Bub3 and dynein co-depletion rescues chromosome alignment. (A) Immunofluorescence images showing misalignment phenotype after individual (siBub3 and siDHC) and co-depletion of Bub3 and dynein (siBub3/siDHC) showing many misaligned chromosomes in a cell depleted of Bub3 (siBub3) or dynein (siDHC). Co-depletion (siBub3/siDHC) suppressed the misalignment phenotype. Microtubules (green) were stained with anti-α-tubulin antibody, kinetochores (red) with anti-Hec1 antibody, and DNA (blue) with DAPI. PM = prometaphase; M = metaphase; Mis = misaligned; Dis = disorganized. **(B)** Quantification of data shown in (A). **(C)** Immunofluorescence images of control and siDHC-treated cells, stained for α-tubulin to visualize spindle microtubules (green) and for γ-tubulin to localize spindle pole position (red). In siDHC cells, metaphase plates with misaligned chromosomes (middle) exhibited a defined bipolar spindle similar to control (left), while disorganized metaphases (right) displayed abnormal spindle morphology and thus were excluded from this study. **(D)** Immunofluorescence images showing many misaligned chromosomes in a cell depleted of Bub3 (siBub3) or Spindly (siSpindly). Co-depletion (siBub3/siSpindly) greatly improved chromosome alignment. Cells were processed as in (A). **(E)** Quantification of data shown in (D). *p < 0.05, **p < 0.01, ***p < 0.001 and ****p < 0.0001. Bar, 5 μm.

4.3. Kinetochore-microtubule attachments in Bub3/dynein co-depleted cells are stable and functional enough to restore the alignment

Successful chromosome congression relies on stable and functional KT-MT attachments. We asked whether the apparent rescue of chromosome alignment upon Bub3/dynein depletion was due to a rescue of stable and functional KT-MT attachments. For that, we performed functional assays to test the robustness of KT-MT attachments and their ability to generate tension and to drive chromosome movement and alignment in co-depleted cells.

The robustness of kinetochore-attached microtubules (or K-fibers) was tested after a brief exposure of cells to low temperature. Low temperature induces disassembly of unstable, but not stable, K-fibers [56]. After cold treatment, metaphases in Bub3- or

dynein-depleted cells exhibited few cold-resistant K-fibers and many unattached kinetochores, as judged by Hec1/tubulin immunostaining (**Figure 3.3A**). Instead, unattached kinetochores were rather rare or absent in metaphases of co-depleted cells, almost indistinguishably from control metaphases, indicating that robust KT-MT connections were restored.

Robustness of KT-MT attachments in co-depleted cells was further assessed for their ability to generate tension across sister-kinetochores due to poleward forces exerted by microtubules on kinetochores. Tension between kinetochores can be appreciated by measuring inter- and intra-kinetochore distances [344]. Inter-kinetochore distance reflects centromere stretching and intra-kinetochore distance reflects stretching at the kinetochore itself [345, 346]. Inter-kinetochore distance was found to be smaller in siBub3 cells (1.39 ± 0.09 μm) and in siDHC cells (1.56 ± 0.10 μm), compared to control cells (2.08 ± 0.37 μm), in agreement with previous data **(Figure 3.3B)** [340, 79, 207]. In co-depleted cells, inter-kinetochore distance slightly increased to reach 1.66 ± 0.19 μm. Although it did not reach control values, this slight increase underlies an improvement in KT-MT attachments. Interestingly, a clear improvement of intra-kinetochore distance (kinetochore stretching) was found in co-depleted cells (68.33 ± 0.02 nm), compared to Bub3-depleted cells (45.00 ± 0.07 nm) (**Figure 3.3C**). Here, intra-kinetochore stretching was restored to levels indistinguishable from control (68.50 ± 0.05 nm). Intra-kinetochore stretch can occur at low levels of inter-kinetochore stretch and reflects the attachment of dynamic microtubules, ultimately leading to satisfaction of the SAC [345]. Taken together, these observations strongly indicate that Bub3 and dynein co-depletion restores robust and dynamic KT-MT attachments that are able to generate tension.

Finally, we were concerned whether the restored KT-MT attachments in co-depleted cells were functional and, thus, able to drive chromosome congression. For that, we assessed their ability to drive chromosome movement and alignment after a nocodazole treatment/washout assay in the presence of MG-132. After 45 minutes of recovery, up to 80% of mitotic control cells have formed full metaphases, while only 12% in Bub3- and 20% in dynein-depleted mitotic cells exhibited full alignment (**Figure 3.3D**). However, upon co-depletion, up to 40% of mitotic cells reaching full metaphases, indicating that Bub3/dynein co-depletion restores functional KT-MT attachments that are able to drive chromosome congression.

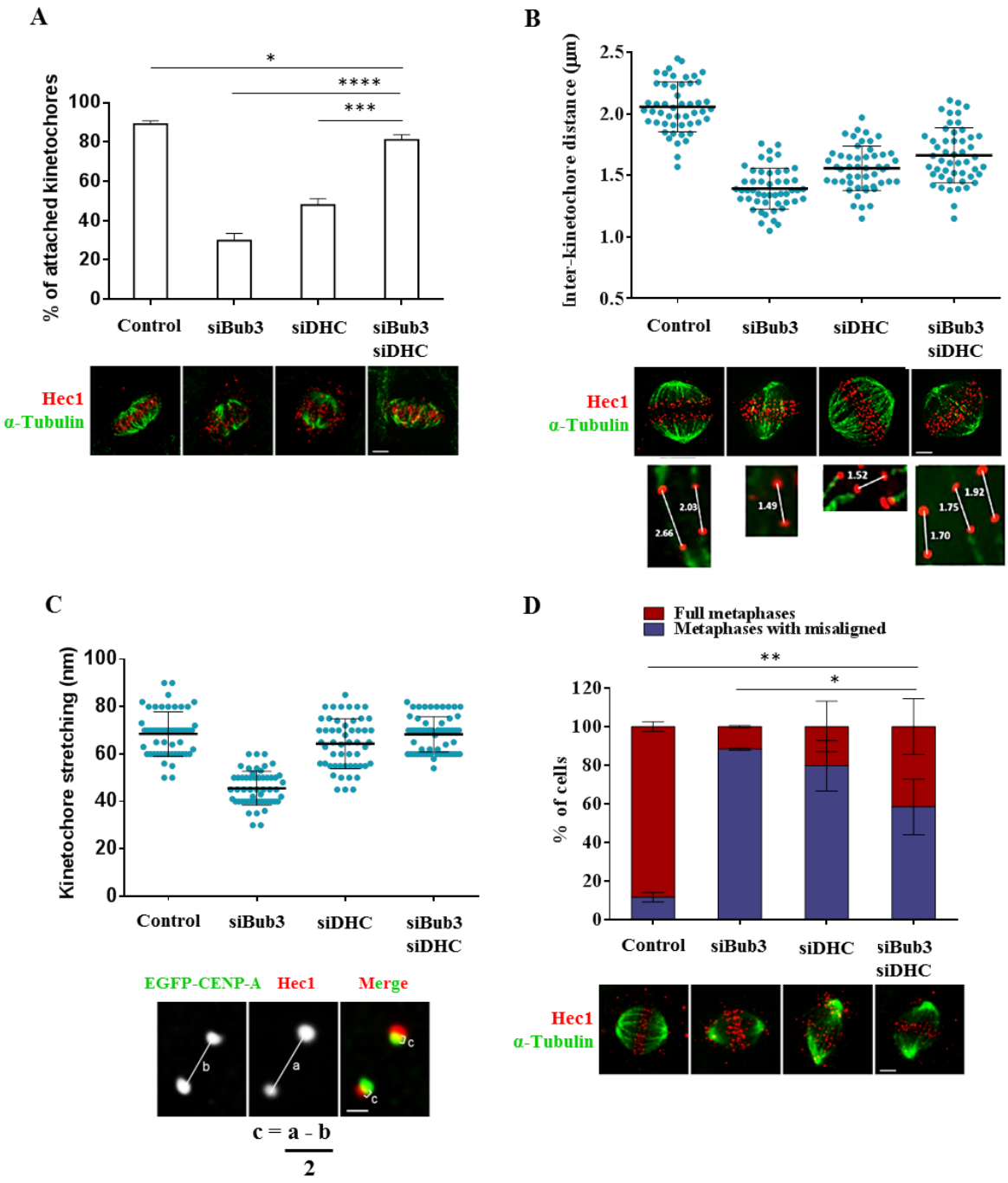

Figure 3.3. Bub3 and dynein co-depletion rescues stable and functional Kinetochore-microtubule attachments. (A) (Top) Quantification of cold-stable microtubules (as percentage of attached kinetochores per cell) after individual (siBub3 and siDHC) and co-depletion of Bub3 and dynein (siBub3/siDHC). (Bottom) Representative immunofluorescence images of (A) showing several unattached kinetochores (free Hec1 red spots) in cells depleted of Bub3 (siBub3) or dynein (siDHC), whereas most kinetochores were attached (Hec1 red spots with attached green fibers) in siBub3/siDHC cells, similarly to control. **(B)** Distance between Hec1 spots of aligned sister kinetochore pairs, showing a slight increase in inter-kinetochore distance in siBub3/siDHC cells, comparatively to individual depletions. Lower images and insets are representative of each condition. **(C)** Kinetochore stretching (intra-kinetochore distance), of bi-oriented kinetochores, showing an increase in intra-kinetochore distance in siBub3/siDHC, comparatively to individual depletions. Kinetochore stretching (c) was measured by subtracting the distance between inner kinetochore CENP-A spots (b) from that between outer kinetochore

Hec1 spots (a) and divided by two, as illustrated in the lower image. **(D)** Cells were treated with nocodazole to depolymerize microtubules in the presence of MG132, released into fresh culture medium containing MG132 for 45 minutes, and stained for α-tubulin (green) and Hec1 (red). The ability of cells to form a metaphase plate was significantly improved in siBub3/siDHC cells, comparatively to siBub3 cells. *$p < 0.05$, **$p < 0.01$, ***$p < 0.001$ and ****$p < 0.0001$. Bar in A-C, 5 µm; bar in D, 1 µm.

4.4. How to explain this unexpected antagonistic interaction between Bub3 and dynein and what would be its functional significance?

At first glance, the question may seem difficult to answer. Indeed, given the role of Bub3, and most probably also of dynein, in promoting end-on attachments, one should expect a rather worst chromosome misalignment phenotype in the absence of both proteins. Nevertheless, in light of previous reports, involvement of dynein in intriguing antagonistic relationships is not too surprising. For instance, depletion of dynein restored bipolar spindles in cells depleted of the drosophila homolog of human CLASP, a protein required to incorporate tubulin subunits into microtubule plus-ends, suggesting an unexpected antagonistic role of the two proteins in kinetochore-microtubule plus-end dynamics [347]. Similarly, depletion of the drosophila motor protein CENP-E partially suppressed the unstable KT-MT attachments associated with the depletion of the SAC protein BubR1 [348]. As both proteins are implicated in stable KT-MT attachments, the restoration of stable attachments upon their co-depletion revealed, again, an intriguing antagonistic interaction. Interestingly, alleviation of chromosome alignment defects has been also surprisingly seen upon co-depletion of Spindly and Rod/ZW10/Zwilch (RZZ) complex by allowing constitutive binding of Ndc80 complex to microtubules [187].
One possible explanation for the antagonistic interaction is that Bub3 and dynein are functioning in parallel pathways to promote KT-MT attachments and that the two pathways might, either directly or indirectly, mutually restrain the activity of each other. Particularly consistent with this possibility is the partial suppression of the misalignment phenotype associated with Bub3 depletion when dynein was also removed. The restoration of full metaphase after the double knockdown could result from a restoration of balance between residual Bub3/dynein or from other regulators of KT-MT interactions.

As to the functional significance of this antagonistic interaction, first we believe that this crosstalk is the result of direct interactions between Bub3 and dynein as both proteins were reported to interact in human [338]. The crosstalk between Bub3 and

dynein activities may serve to fine-tune KT-MT interactions, probably to achieve optimal end-on attachments. It may also serve to link the state of KT attachment to the SAC signaling machinery in order to ensure that efficient KT-MT attachments are established before anaphase resumes. Additionally, the crosstalk would allow dynein to probe when SAC proteins need to be transported away from kinetochores to promote SAC silencing. In this respect, Bub3 itself is a dynein cargo during the step of SAC silencing according to our previous report [341]. Future work will be needed to understand the mechanistic aspect of this crosstalk.

5. Acknowledgments

This work was supported by grants from CESPU (02-GCQF-CICS-2011N; CheckTax-CESPU-2014) and from FCT - Fundação para a Ciência e a Tecnologia under the project CEQUIMED-PEst-OE/SAU/UI4040/2014; Patrícia M.A. Silva is a PhD fellowship holder from FCT (SFRH/BD/90744/2012). We thank both anonymous Reviewers for their comments and constructive criticism.

6. Supplementary figures

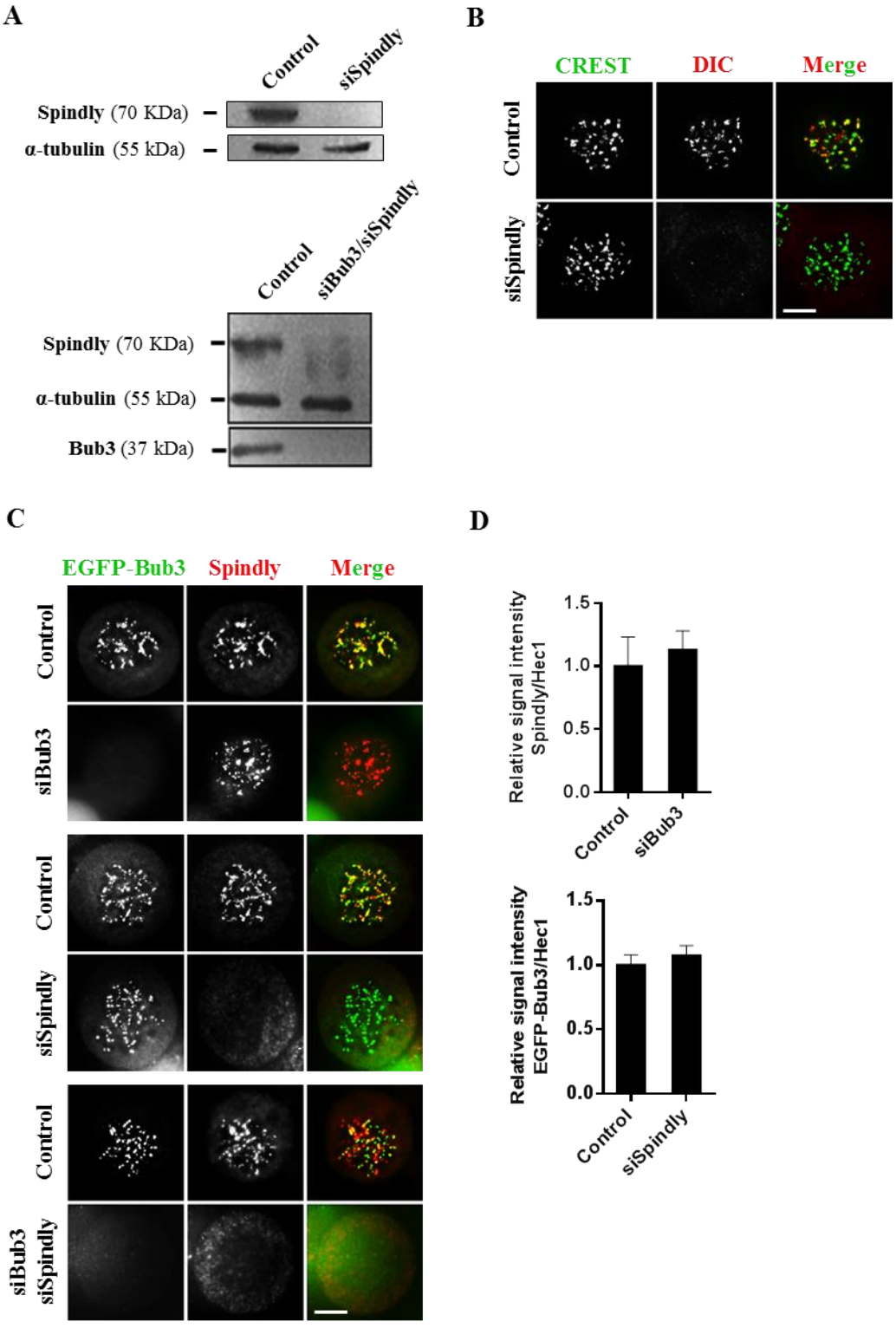

Figure 3.S1. Displacement of kinetochore dynein as mediated by spindly depletion. (A) Immunoblots showing efficient siRNA-mediated depletion of Spindly (siSpindly, top blot), and efficient co-depletion of Bub3 and Spindly (siBub3/siSpindly, bottom blot). **(B)** Immunofluorescence images showing efficient delocalization of dynein (DIC) from kinetochores after depletion of Spindly (siSpindly). CREST serum was used as kinetochore

marker (green). **(C)** Immunofluorescence images showing that (top panel) depletion of Bub3 (siBub3) did not affect kinetochore localization of Spindly, and (middle panel) depletion of Spindly (siSpindly) did not affect kinetochore localization of Bub3 (EGFP-Bub3); (bottom panel) shows depletion of both proteins. Cells in B, and C were treated with 1 μM nocodazole prior immunofluorescence to create conditions where Bub3, dynein and Spindly are maximally enriched at kinetochores. **(D)** Quantification of kinetochore staining intensity of Spindly in Bub3-depleted cells (top), and of EGFP-Bub3 in Spindly-depleted cells (bottom). Bar, 5 μm.

3.2. Dynein-dependent transport of spindle assembly checkpoint proteins off kinetochores toward spindle poles

The information presented in this section was based in the following published paper:

Patrícia M.A. Silva, Rita M. Reis, Victor M. Bolanos-Garcia, Claudia Florindo, Álvaro A. Tavares and Hassan Bousbaa. Dynein-dependent transport of spindle assembly checkpoint proteins off kinetochores toward spindle poles. FEBS Letters. 2014;588(17):3265-73.

1. Abstract

A predominant mechanism of spindle assembly checkpoint (SAC) silencing is dynein-mediated transport of certain kinetochore proteins along microtubules. There are still conflicting data as to which SAC proteins are dynein cargoes. Using two ATP reduction assays, we found that the core SAC proteins Mad1, Mad2, Bub1, BubR1, and Bub3 redistributed from attached kinetochores to spindle poles, in a dynein-dependent manner. This redistribution still occurred in metaphase-arrested cells, at a time when the SAC should be satisfied and silenced. Unexpectedly, we found that a pool of Hec1 and Mis12 also relocalizes to spindle poles, suggesting KMN components as additional dynein cargoes. The potential significance of these results for SAC silencing is discussed.

Keywords: Mitotic checkpoint, checkpoint silencing, cytoplasmic dynein, Mad1, Mad2, Bub1, BubR1, Bub3, Hec1.

2. Introduction

Accurate chromosome segregation relies on the activity of the spindle assembly checkpoint (SAC) [23], a surveillance mechanism that monitors the status of kinetochore-microtubule attachment and prevents anaphase onset until all chromosomes are bipolarly attached to the mitotic spindle and aligned at the metaphase plate [349]. Inhibition of anaphase onset is achieved by the SAC through downregulation of the APC/C (anaphase promoting complex/cyclosome). The latter is an E3 ubiquitin ligase required for targeting cyclin B1 and securin for degradation by the 26S proteasome, thereby delaying cell in mitosis and preventing precocious sister-chromatid separation. APC/C inhibition is predominantly achieved by the MCC, the mitotic checkpoint complex that forms between the SAC proteins Mad2, BubR1 and Bub3, and the cofactor and activator of APC/C, Cdc20 [157]. It is widely believed that unattached or improperly attached kinetochores provide the catalytic platform for the formation of the anaphase inhibitor MCC [350, 23].

SAC components also include the evolutionary conserved proteins Mad1, and the kinases Bub1, Mps1, and Aurora B. These proteins localize to kinetochores and participate in the recruitment, activation, or formation of the MCC. Kinetochore levels of these proteins fall upon microtubule attachment [349]. Once all kinetochore-microtubule attachments are efficiently established, SAC must be extinguished in order to allow for mitotic progression, a process known as SAC silencing. Extinguishing SAC requires that assembly of new MCC is prevented and existing inhibitory complexes are disassembled in order to release Cdc20 and, thus, alleviate APC/C inhibition [351, 352] [353]. A predominant mechanistic model of SAC silencing postulates the removal of proteins that are required for SAC activation from attached kinetochores via stripping (also known as streaming) [353]. Stripping is mediated by the minus-end directed microtubule motor dynein, which transports certain SAC proteins off kinetochores towards spindle poles along kinetochore-microtubules. Using an ATP depletion assay that maintained dynein activity but prevented release of its cargo from spindle poles, Howell et al. were the first to report that Mad2 and BubR1 (as well as CENP-E, dynein itself and 3F3/2 antigens) are transported to spindle poles, and that inhibition of dynein prevented Mad2 removal from attached kinetochores [82]. Subsequent studies also based on ATP depletion have catalogued several kinetochore components for their ability to be transported by dynein [336]. While it is consensual that Mad1, Mad2, and

spindly (which is required for dynein kinetochore binding) are dynein cargoes, there is conflicting data concerning the poleward transport of Bub1 and BubR1 [336, 82]. Furthermore, whether all SAC components are transported to spindle poles upon checkpoint silencing is not known yet.

In an attempt to clarify these issues, we used two ATP depletion assays to assess the poleward transport of SAC proteins, focusing the analysis on those that are relevant to the generation of the anaphase inhibitory signal. Through this approach, we confirm the dynein-dependent transport to spindle poles of Mad1 and Mad2; we clarify that Bub1 and BubR1 are indeed dynein cargoes; and propose Bub3 as additional dynein cargo. We also report that the poleward transport of these SAC proteins persists in metaphase arrested cells, a situation when the cells are in a SAC inactive state with all chromosomes bipolarly attached. Interestingly, we further propose dynein-dependent poleward transport of the KMN components Hec1 and Mis12.

3. Materials and Methods

3.1. Cell culture, drug treatment, and RNAi

HeLa cells were cultured in DMEM (PAA Laboratories, E15-883), supplemented with 10% FBS (GIBCO, 10500-064) and 1% antibiotic/antimycotic (GIBCO, 12605-028) and maintained at 37°C, in a 5% CO_2 humidified atmosphere. EGFP-Bub3 stably-expressing HeLa cell line was generated by inserting the hBub3 cDNA in frame into pIC113 vector [354]. Clones expressing near endogenous levels of EGFP-Bub3 were selected and maintained in culture under 400 µg/ml of G418 (Sigma-Aldrich, A1720-1G).

MG-132 (Sigma-Aldrich, 2211-5MG) was used at 10 µM for 60 minutes; nocodazole (Sigma-Aldrich, M1404-2MG) was used at 1 µM for 60 minutes; nordihydroguaiaretic acid (Biomol, BML-EI101-0001) was used at 30 µM for 30 minutes as described [336]. The ATP inhibition assay was performed as described [82].

Dynein knockdown was performed using validated siRNA oligoduplexes against Dynein Heavy Chain [355] (Santa Cruz Biotechnology, sc-43738). Spindly knockdown was performed using validated siRNAs sequence [186] that was synthetized by (Sigma-Aldrich). Cells were transfected as previously described [208], except that INTERFERin siRNA Transfection Reagent (PolyPlus, 409-10) was used. For immunoblotting, cells were collected by centrifugation, lysed, and resuspended on SDS-

sample buffer containing protease inhibitors (Sigma-Aldrich cocktail, P2850-1ML), and loaded onto a 7.5% SDS-PAGE and western blots were processed and analyzed as described [208].

3.2. Immunofluorescence

Cells were fixed for 12 min in freshly prepared 2% paraformaldehyde (Sigma-Aldrich, 158127-500G) in phosphate-buffered saline (PBS), permeabilized with 0.5% Triton X-100 in PBS for 7 min, rinsed in PBS and blocked with 10% FBS in PBST (PBS plus 0.05% Tween-20) for 30 min. Cells were then incubated for 1 hour with primary antibodies diluted in PBST with 5% FBS. After three washes in PBST for 5 minutes each, cells were incubated with fluorescently-labeled secondary antibodies for 1 hour, and then washed three times 5 minutes in PBST. DNA was stained with 2µg/ml DAPI (Sigma-Aldrich, D9542-5MG) diluted in Vectashield mounting medium (Vector, H-1000).

Images were acquired on a Spinning Disc AxioObserver Z.1 SD confocal microscope (Carl Zeiss, Germany), coupled to an AxioCam MR3, and with a Plan Apochromatic 63x/NA 1.4 objective. Z-stacks were acquired at 0.5 µm intervals, deconvolved using AxioVision Release 4.8.2 SPC software, and projected using ImageJ software (http://rsbweb.nih.gov/ij/).

3.3. Antibodies

Primary antibodies used were: mouse anti-Mad2L1 (1:200, Sigma-Aldrich, WH0004085M1-100UG); mouse anti-Bub1 (1:400, Abcam, ab54893); mouse anti-BubR1 (1:1000, BD Biosciences, 612503); rabbit anti-Cdc20 (1:1000, Sigma, C5497); rabbit anti-Mad1 (1:100, gift from Dr. Kuan-The, NIH, USA); human anti-CREST (1:4500, gift from Dr. Bronze-da-Rocha, IBMC, Portugal); mouse anti-Hec1 (1:600, Abcam, ab3613); rabbit anti-α-Tubulin (1:100, Sigma, T5168); mouse anti-dynein intermediate chain (1:200, Sigma, D5167); mouse anti-Spindly (1:100, Sigma, WH0054908M1-100UG); rabbit anti-Spindly (1:3000, gift from Dr. R. Gassmann, IBMC, Portugal). Alexa Fluor 488- and 568-conjugated secondary antibodies were used at 1:1500, and 647-conjugated secondary antibody which was used at 1:2500 (Molecular Probes). Horseradish peroxidase (HRP)-conjugated secondary antibodies was used at 1:1500 (Vector).

3.4. Live-cell imaging

HeLa cells stably expressing EGFP-Bub3 were seeded on glass bottom dish (Bioptechs) and synchronized in S phase using a double thymidine (2.5 mM) block of 24 hours, with a 12 hours interval between the blocks. Cells were filmed 8–10 hours after the final release as they entered mitosis, on a Delta Vision microscope, using a 100x/NA 1.4 Plan Apo objective, and an EMCCD camera (Cascade2_1k) with gain 75. Time-lapse images were acquired every minute (7 stacks at 1 μm intervals).

4. Results

We were particularly interested in understanding the behavior of *bona fide* SAC proteins in terms of their dynein-dependent removal from attached kinetochores during SAC silencing.

We first examined Mad1 and Mad2 as it has been established that these proteins function as dynein cargoes. After treatment of HeLa cells with sodium azide/2-deoxyglucose (AZ/DOG), we observed a strong accumulation of Mad2 at spindle poles in all prometaphase and metaphase cells analyzed, while Mad2 was undetectable at attached kinetochores (**Figure 3.4A**). Mad1 redistribution from kinetochores to spindle poles mirrored that of Mad2 (**Figure 3.4B**), in accordance with previous reports [336, 186, 82]. Treatment with nordihydroguaiaretic acid (NDGA) showed similar results (data no shown).

BubR1 has been shown previously to redistribute to spindle poles in an ATP reduction assay [82]. However, a subsequent study using NDGA treatment reported that BubR1 did not accumulate at spindle poles and therefore ruled out the role of BubR1 as dynein cargo [336]. In an attempt to clarify this crucial aspect of SAC signaling, we treated HeLa cells with AZ/DOG or with NDGA followed by staining of BubR1. In the NDGA assay, BubR1 was observed at kinetochores but not at spindle poles, behaving much like untreated cells (**Figure 3.4C**), thus suggesting that BubR1 is insensitive to NDGA in the experimental conditions here described. In the 30 minutes AZ/DOG assay, we were unable to detect BubR1 at kinetochores and at spindle poles (**Figure 3.S2A**). However, in a recovery experiment, 10 minutes after AZ/DOG washout, BubR1 readily reappeared on kinetochores (**Figure 3.S2A**). In order to clarify whether BubR1 stability was affected by AZ/DOG, making it inaccessible to the antibodies, we reduced the AZ/DOG incubation time to 10 minutes. Under such conditions BubR1 was consistently observed at spindle poles with a clear loss from both unaligned and aligned

kinetochores (**Figure 3.4D**), suggesting that BubR1 was affected by ATP reduction at longer incubation periods. Although definition of how exactly BubR1 is affected by ATP reduction requires further investigation, our results suggest that BubR1 relocalizes to spindle poles upon kinetochore attachment and that conflicting results from previous studies is due to differences in the experimental protocols used by different authors. Such discrepancies extend to the study of Bub1, which has been reported to function as dynein cargo in AZ/DOG but not in NDGA assays [336, 356]. Our data shed light into this process as they consistently show that Bub1 leaves the kinetochores toward spindle poles after 30 minutes incubation with the inhibitors (**Figure 3.4E**) thus supporting the view that Bub1 functions as dynein cargo. Bub3 is a crucial kinetochore partner of Bub1 and BubR1 that is required for efficient kinetochore-microtubule attachments [208].

Bub3 forms part of the MCC; binds to the recently identified protein BuGZ [357, 358] and is required for SAC activation and silencing. Given the multiple roles of Bub3 in SAC signaling, we set out to investigate whether Bub3 is poleward transported by dynein upon kinetochore-microtubule attachment. For this, we used a HeLa cell line stably expressing EGFP-Bub3. Thirty minutes after treatment with AZ/DOG (**Figure 3.4F**) or NDGA (data not shown), we observed EGFP-Bub3 at spindle poles, while a pool was retained at attached kinetochores in all prometaphases and metaphases analyzed (**Figure 3.4F**). The persisting EGFP-Bub3 pool at kinetochores was not due to insufficient inhibition as Mad2 was depleted from kinetochores within the same treated cells (**Figure 3.4G**). Importantly, extension of the incubation time with the inhibitors gave the same results (data not shown). Although the possibility that EGFP-Bub3 competed with the endogenous version cannot be ruled out, our data support the idea of the normal retention of a Bub3 pool at aligned kinetochores until the onset of anaphase [359]. The possibility of our observations being the result of an incomplete enzymatic reaction is remote given the time scale of mitosis in HeLa cells and the fact the assays were performed for up to 45 minutes. Comparable incubation times for ATP reduction assays have been reported by others [186] thus allowing a fair and meaningful comparison of our experiments with such reports.

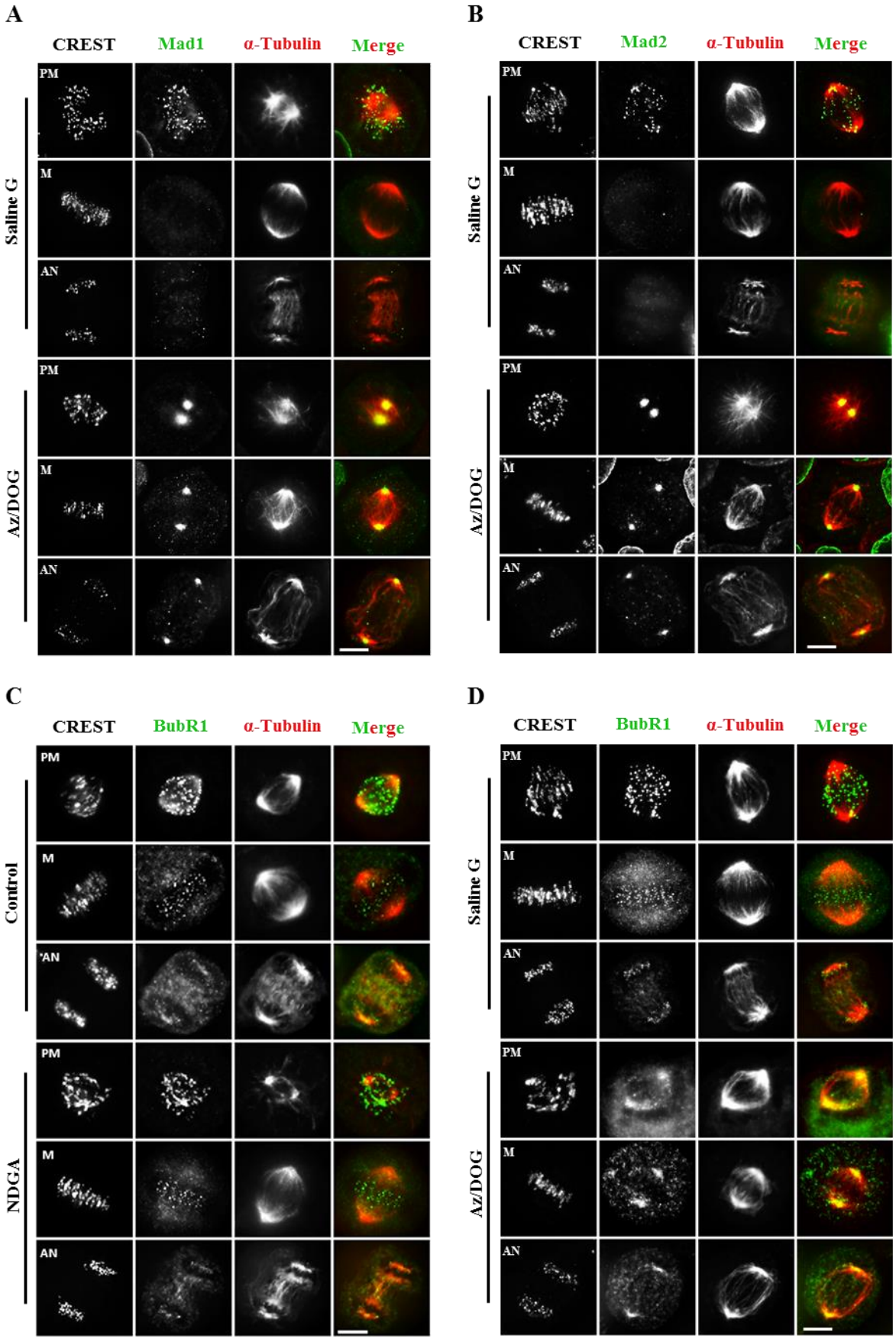
A
CREST
Mad1
α-Tubulin
Merge
Saline G
Az/DOG
PM
M
AN
B
CREST
Mad2
α-Tubulin
Merge
Saline G
Az/DOG
PM
M
AN
C
CREST
BubR1
α-Tubulin
Merge
Control
NDGA
PM
M
AN
D
CREST
BubR1
α-Tubulin
Merge
Saline G
Az/DOG
PM
M
AN

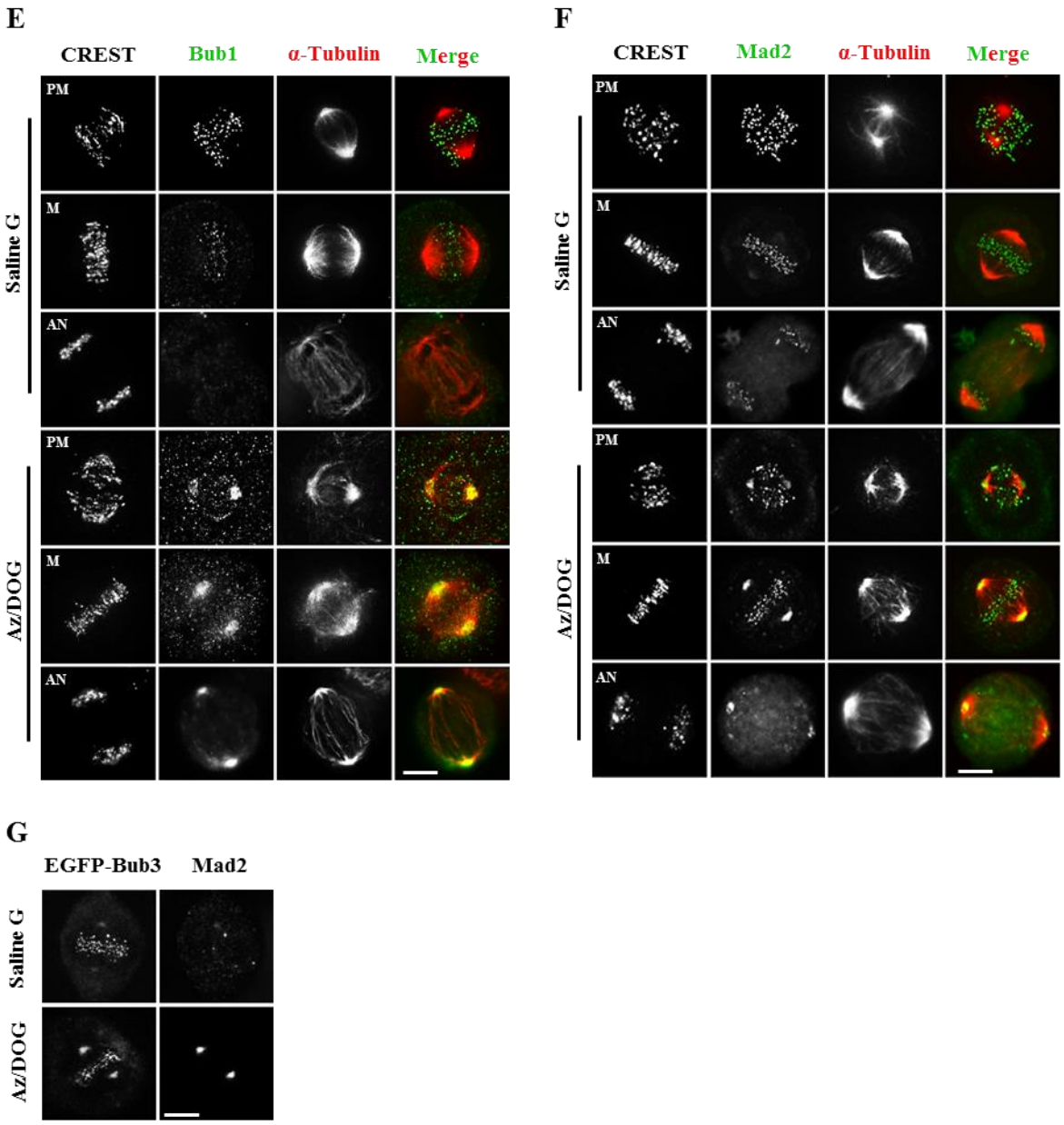

Figure 3.4. SAC proteins accumulate at spindle poles upon ATP reduction. (A) ATP reduction was performed by 30 minutes incubation either with isotonic salt solution with glucose (Saline G) or with sodium azide/2-deoxyglucose (AZ/DOG) [82]. Cells were stained with anti-Mad2, CREST as kinetochore marker, and anti-tubulin to localize spindle pole position. **(B)** Cells were treated as in (A) except that they were stained for Mad1. **(C)** ATP reduction was performed by 30 minutes incubation with nordihydroguaiaretic acid (NDGA) and cells were stained for BubR1, CREST, and tubulin. **(D)** Cells were treated as in (A) except that they were incubated for 10 minutes only with AZ/DOG and stained for BubR1. **(E)** Cells were treated as in (A) except that they were stained for Bub1. **(F)** Cells were treated as in (A) except that a HeLa line stably expressing EGFP-Bub3 was used to visualize Bub3 spindle pole relocalization, with a persistent pool at kinetochores. **(G)** A cell treated as in (A) showing that the persistence of the EGFP-Bub3 kinetochore pool is not due to insufficient inhibition as Mad2 was completely removed from kinetochores in the same cell. PM = Prometaphase; M = Metaphase; Bars, 5 µm.

Interestingly, we observed that upon AZ/DOG or NDGA treatment, Mad1, Mad2, BubR1, Bub1, and Bub3 accumulate at spindle poles from prometaphase through anaphase (**Figure 3.4**), suggesting that their poleward transport may occur even in cells with the checkpoint satisfied. This was particularly clear in the case of Mad2 in metaphase when this protein was absent from attached kinetochores [360]. To assess if this could be the case of other SAC proteins, we treated cells with the proteasome inhibitor MG-132 to arrest cells in metaphase before performing the ATP reduction assay. In these conditions, all SAC proteins were still able to accumulate at spindle poles (**Figure 3.5A**). We took advantage of the HeLa cell line stably expressing EGFP-Bub3 to perform live-cell imaging experiments in order to monitor spindle pole relocalization of Bub3 upon ATP reduction. In control cells, the behavior of EGFP-Bub3 is consistent with the cellular distribution pattern described for endogenous Bub3 throughout mitosis (**Figure 3.5B and movie 3.1**) [208]. We noted, however, that mitotic progression stopped almost instantaneously upon addition of AZ/DOG, indicating that it is affected by ATP reduction. This aspect was not appreciated before in the previous works that used ATP reduction assays, which precludes any comparison with such reports. We therefore monitored mitotic progression by time-lapse microscopy, and once cells reached the desired mitotic phase AZ/DOG was added to the medium and cells immediately filmed. Under these conditions, EGFP-Bub3 was observed to immediately accumulate to spindle poles with a pool retained at kinetochores (**Figure 3.5B**), confirming the results described above Moreover, while no accumulation of EGFP-Bub3 at spindle poles was apparent in MG-132 metaphase-arrested cells during the 30 min of filming, addition of AZ/DOG to these MG-132-pretreated cells resulted in immediate EGFP-Bub3 relocalization to the poles (**Figure 3.5B and movie 3.2**).

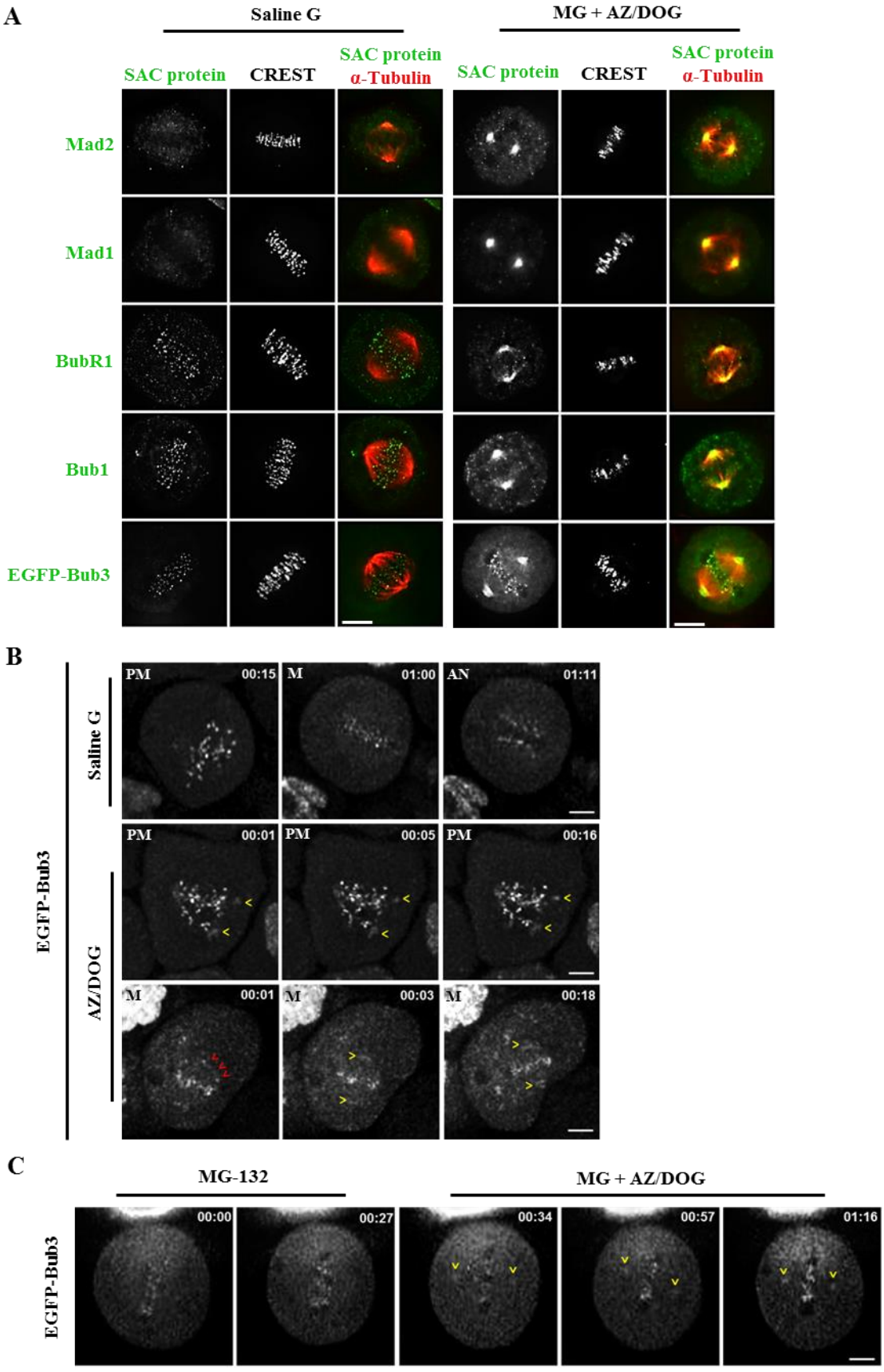

Figure. 3.5. Poleward transport of SAC proteins still occurs at metaphase. (A) HeLa cells were pre-treated with MG-132 for 1 hour, subjected to ATP reduction assay, and stained for

Mad2, Mad1, BubR1, or Bub1. For Bub3, the EGFP-Bub3 expressing HeLa line was used. CREST was used to localize kinetochore position, and anti-tubulin to localize spindle pole position. **(B)** Selected 1 μm Z-stacks collected every minute in time-lapse experiments using HeLa cells stably expressing EGFP-Bub3. Control saline G cells (top) show intense EGFP-Bub3 staining on prometaphase (PM) kinetochores and reduced staining on metaphase (M) and anaphase (AN) kinetochores. EGFP-Bub3 relocalizes to spindle poles (yellow arrowheads) almost instantaneously upon AZ/DOG treatment in prometaphase (middle) and metaphase (bottom). The red arrows indicate EGFP-Bub3 foci streaming towards the pole. **(C)** HeLa cells stably expressing EGFP-Bub3 were treated with MG132 and filmed for 30 minutes, then AZ/DOG was added and the cells were further filmed for 60 minutes. EGFP-Bub3 relocalized to spindle poles (yellow arrowheads) at the start of filming. Time is shown in hours:minutes. Bar, 5 μm.

We then inhibited dynein in order to establish if poleward transport of the aforementioned SAC proteins was dependent on this motor protein. Inhibition of dynein was achieved either by direct RNAi depletion or by preventing its kinetochore localization through RNAi depletion of Spindly, a protein indispensable for the kinetochore localization of dynein (**Figure 3.S2B**). Our results show that dynein inhibition abolished spindle pole relocalization of Mad1, Mad2, BubR1, Bub1, and Bub3 following AZ/DOG treatment (**Figure 3.6**). Also, we found that dynein-inhibited cells, without or with AZ/DOG treatment, did not retain SAC proteins on kinetochores of aligned chromosomes. Instead, these proteins accumulated only on misaligned kinetochores (**Figure 3.6**). The same results were obtained in cells co-depleted of dynein and spindly in order to maximize dynein depletion from kinetochores, therefore ruling out the possibility that residual dynein delocalised SAC proteins from kinetochores (**Figure 3.6**). These results support the idea of the existence of a dynein-independent mechanism of protein stripping from attached kinetochores during SAC silencing [187, 114, 186]. Moreover, we noted that Cdc20 was not subjected to poleward transport (data not shown) which is in good agreement with similar, previous observations [336].

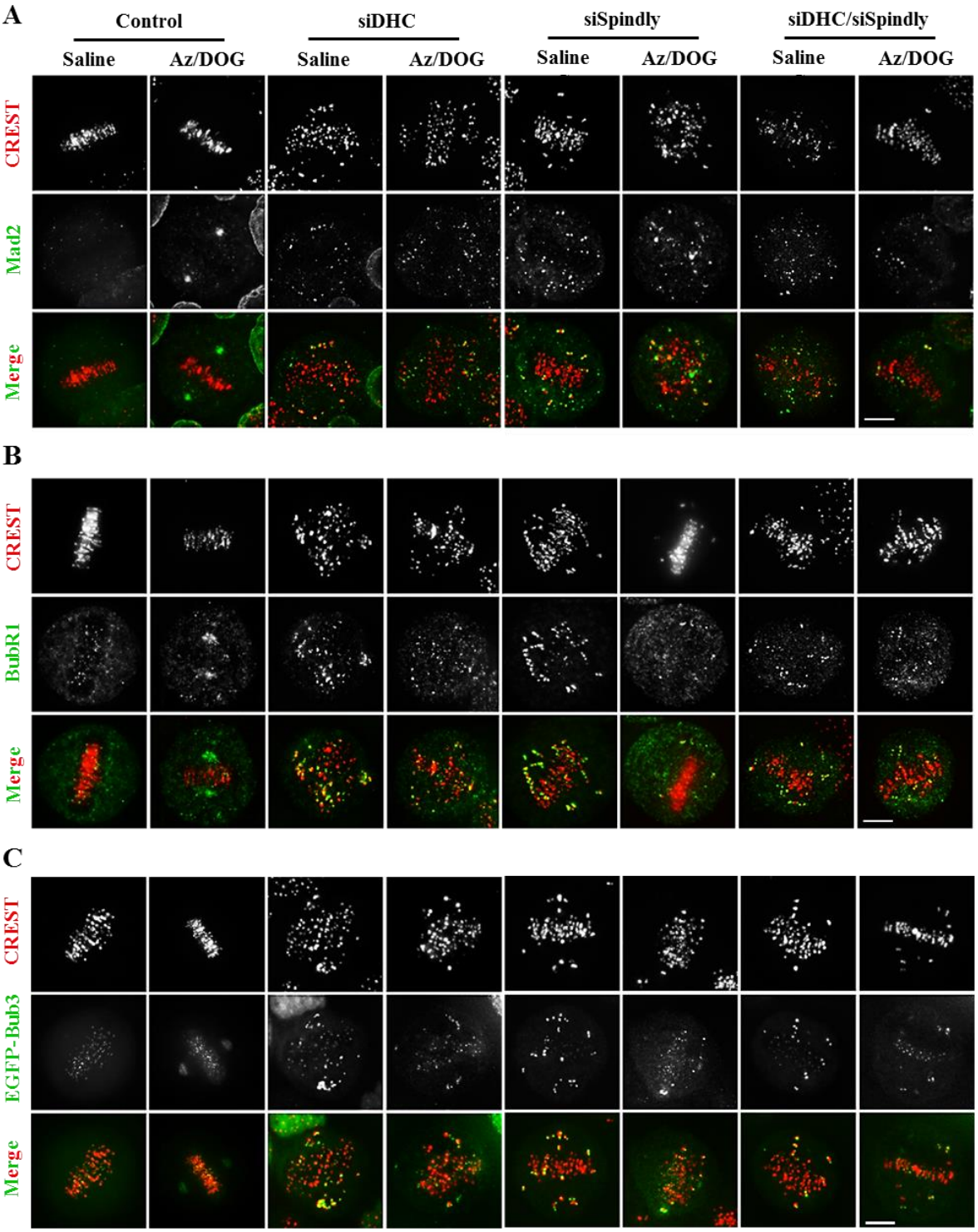

Figure 3.6. Poleward transport of SAC proteins is suppressed upon dynein depletion. Cells were depleted of dynein (siDHC), spindly (siSpindly), or both (siDHC/siSpindly), subjected to ATP reduction assay, and stained for **(A)** Mad2, **(B)** BubR1 and **(C)** Bub3 (analyzed using the EGFP-Bub3 expressing cell line). Note that in all cases, SAC proteins accumulate on unaligned but not on aligned kinetochores. Mad1 behaves identically to Mad2 (not shown); and Bub1 behaves identically to Bub3 (not shown). Bars, 5 μm.

An unexpected result from our analyses concerned the protein Hec1, a subunit of the outer kinetochore KMN network that constitutes the core site for microtubule attachment. In the present study we first intended to use Hec1 as kinetochore marker instead of CREST. Interestingly, we noted that 30 minutes after AZ/DOG treatment, Hec1 accumulated at spindle poles and a pool remained at attached kinetochores, in a manner that mirrored Bub3 localization (**Figure 3.7A**). The localization of Hec1 to spindle poles was prevented upon dynein inhibition (**Figure 3.7A**), thus suggesting that Hec1 function as an additional dynein cargo [114, 336]. Similar results were obtained for the other component of the KMN network, Mis12, except that its spindle pole localization was not observed at prometaphase but only when a metaphase plate became evident (**Figure 3.7B**).

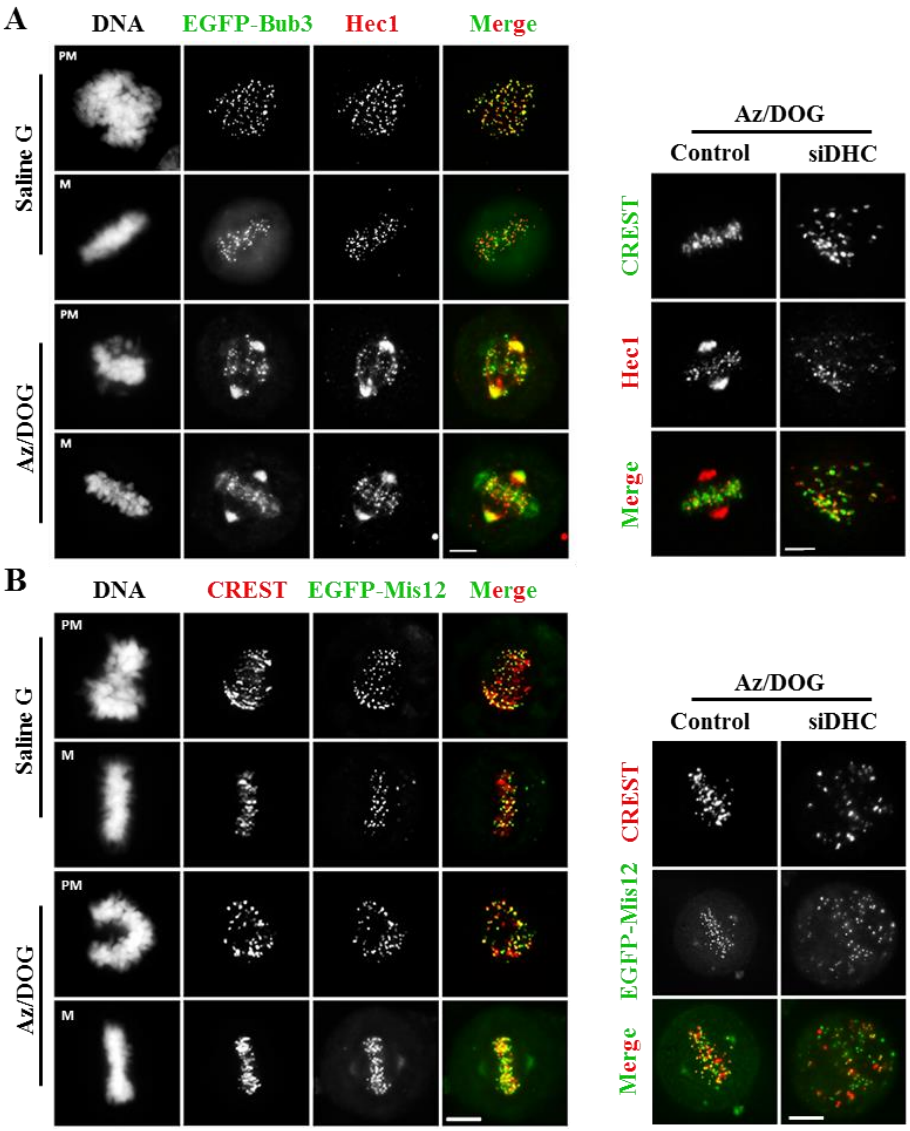

Figure 3.7. KMN components are dynein-dependent cargoes. (A) EGFP-Bub3 expressing HeLa cells were subjected to ATP reduction assay and stained for Hec1. (Left) Upon the assay, Hec1 redistributes to spindle poles with a pool left on kinetochores, mirroring the behavior of Bub3. (Right) Dynein depleted cells (siDHC) were subjected to ATP reduction assay and

stained for Hec1 and CREST. Note the absence of Hec1 at spindle poles in cells depleted of dynein. **(B)** HeLa cells were transiently transfected with pBABEblast YFP-Mis12 construct and subjected to ATP reduction assay. (Left) Upon the assay, Mis12 redistributed to spindle poles with a pool left on kinetochores. (Right) YFP-Mis12 expressing cells were depleted of dynein (siDHC) and subjected to ATP reduction; CREST was used as kinetochore marker. Note the absence of Mis12 at spindle poles in cells depleted of dynein PM = Prometaphase; M = Metaphase; Bars, 5 μm.

5. Discussion

Unattached kinetochores activate and accumulate critical SAC components such as Mad1, Mad2, Bub1, BubR1, and Bub3. Binding of Mad2 to Mad1 to the kinetochore induces significant conformational changes that promote Mad2 binding to Cdc20, which in turn makes Cdc20 unable to activate the APC/C [159]. Additionally, the Mad2-Cdc20 complex associates with Bub3 and BubR1 to form the MCC, the protein assembly that acts as a pseudosubstrate to inhibit the APC/C [361, 362, 163]. Bub1 is required to recruit all the above SAC components to the kinetochore and contributes to APC/C inhibition through Cdc20 phosphorylation [353, 168].

We used two previously described ATP reduction assays [336, 82] which prevent release of dynein and its cargoes from spindle poles, in order to identify core SAC proteins that are transported off kinetochores toward spindle poles. We found that Mad1, Mad2, Bub1, BubR1, and Bub3 accumulated at spindle poles following treatment with the inhibitors. This poleward transport was dynein-dependent as it was abolished upon dynein inhibition. The result confirmed that Mad1 and Mad2 function as dynein cargoes, a feature shown in earlier reports [336, 186, 82]. We argue that the discrepancy between previous studies concerning BubR1 and Bub1 function as dynein cargoes is due to differences in the experimental approaches, a concern that has been expressed by others [336, 82]. We found that BubR1 was the only SAC protein which was insensitive to NDGA but not to AZ/DOG as co-staining of NDGA-treated cells showed BubR1 only at kinetochores while Bub3 was relocalized to spindle poles (**Figure 3.S2A**). We have also determined that Bub3 is a new dynein cargo that is poleward transported upon kinetochore attachment, suggesting a role in SAC silencing. Such role seems consistent with Bub3 direct involvement in the MCC complex whose assembly must be prevented to relieve inhibition exerted on the APC/C thus allowing mitotic progression. Interestingly, the SAC proteins were not retained at aligned kinetochores upon dynein depletion, supporting the existence of a dynein-independent mechanism for SAC silencing as previously suggested [187, 114, 186]. Also, it should

be noted that spindle pole accumulation of SAC proteins reported in the present study depends on the specific treatment we used to inhibit dynein cargo release at the poles; such poleward transport needs, however, to be confirmed under physiological conditions upon chromosome attachment.

We found that ATP depletion assays performed on cells arrested at metaphase after pretreatment with MG-132 still resulted in a poleward transport of all the SAC proteins reported in this study, in a manner that mirrored that of ATP depletion assays without prior MG-132 treatment. This poleward relocalization was dynein-dependent as it was abolished by dynein inhibition. These finding suggests that metaphase cells with complete chromosome alignment are still competent to generate a SAC signal. This is consistent with the recently reported ability to reestablish SAC activity after initial silencing, [363] and with the persistence of SAC activity observed in MG-132-treated mitotic cells and in proteasome deficient cells [364, 365]. As MG-132-treated cells can be arrested in metaphase with kinetochores that develop normal tension, [366] it was assumed that the kinetochores in these cells would be depleted of Mad2, a condition that should inactivate the SAC [336]. Although the absence of Mad2 poleward stripping in metaphase-arrested cells, in a previously reported ATP reduction assay, seems to support this assumption, [336, 82] Zeng et al. showed that cells treated with the proteasome inhibitor MG-132 were unable to sustain a prolonged metaphase arrest after depletion of Mad2, suggesting that MG132-mediated metaphase arrest may depend on continued inhibition of APC/C by the SAC [367]. The latter notion would explain why SAC components could be detected at spindle poles of metaphase-arrested cells in our ATP depletion assays. Intriguingly, it is unclear how SAC proteins appeared at spindle poles in a stage when their levels are lowered since all kinetochores are attached and under tension, particularly in the case of Mad2, which leaves the kinetochore upon attachment [360].

Interestingly, and contrary to what has been reported, [114, 336] we observed that a pool of Hec1, a subunit of the outer kinetochore KMN network that constitutes the core site for microtubule attachment, [104] accumulated at spindle pole in a dynein-dependent manner. Hec1 is one of four proteins of the outer kinetochore Ndc80 complex that together with the KNL-1 protein and the Mis-12 complex form the conserved KMN (KNL-1/Mis-12/Ndc80) network that constitutes the core microtubule binding site at the kinetochore [104]. The observed dynein-dependent relocalization of Hec1 to spindle poles is consistent with early studies where Hec1 was reported to

localize at the centrosome [368, 369]. As Mis-12 exhibited similar behaviors, it is tempting to speculate that KMN streaming from kinetochores would partially disassemble the docking platform that recruits SAC proteins, therefore contributing to SAC silencing by preventing further assembly of anaphase inhibitors. At the same time, a significant pool of KMN components must be retained at kinetochores in order to ensure the efficient attachment and chromosome transport at anaphase onset. This is consistent with the decrease in Hec1 kinetochore levels following an ATP reduction assay, [108] and with the recently reported disassembly of all KMN components at the onset of anaphase [370]. We have previously shown that Bub3 is required for efficient kinetochore-microtubule attachment [207, 208]. Accordingly, the pool of Bub3 retained at the kinetochores, as observed in the present study, might serve to sustain attachment during metaphase and anaphase.

In summary, this report presents evidence of additional SAC components to be subjected to dynein-mediated transport to the spindle pole. We also show that poleward transport still occurs in metaphase-arrested cells consistent with the reported SAC reactivation ability at metaphase [371], and that a pool of Hec1 and Mis12, may function as additional dynein cargoes, thus providing new insights into the contribution of the KMN network to SAC silencing.

6. Acknowledgments

This work was supported by grant to H.B. from CESPU (02-GCQF-CICS-2011N); by grants to A.T. from national Portuguese funding through FCT - Fundação para a Ciência e a Tecnologia FCT (POCTI/BIA/PRO/60337/2004 and PTDC/SAU-OBD/105234/2008); by grant to C.F. EXPL/BEX-BCM/1104/2013; by FCT ref. PEst-OE/EQB/LA0023/2013; Patrícia M.A. Silva. is a PhD fellowship holder from FCT (SFRH/BD/90744/2012). We thank Dr. I. Cheeseman for providing the pIC113 vector and the pBABEblast YFP-Mis12 construct. We acknowledge the generous gift of anti-spindly antibody from Dr. R. Gassmann.

7. Supplementary figures

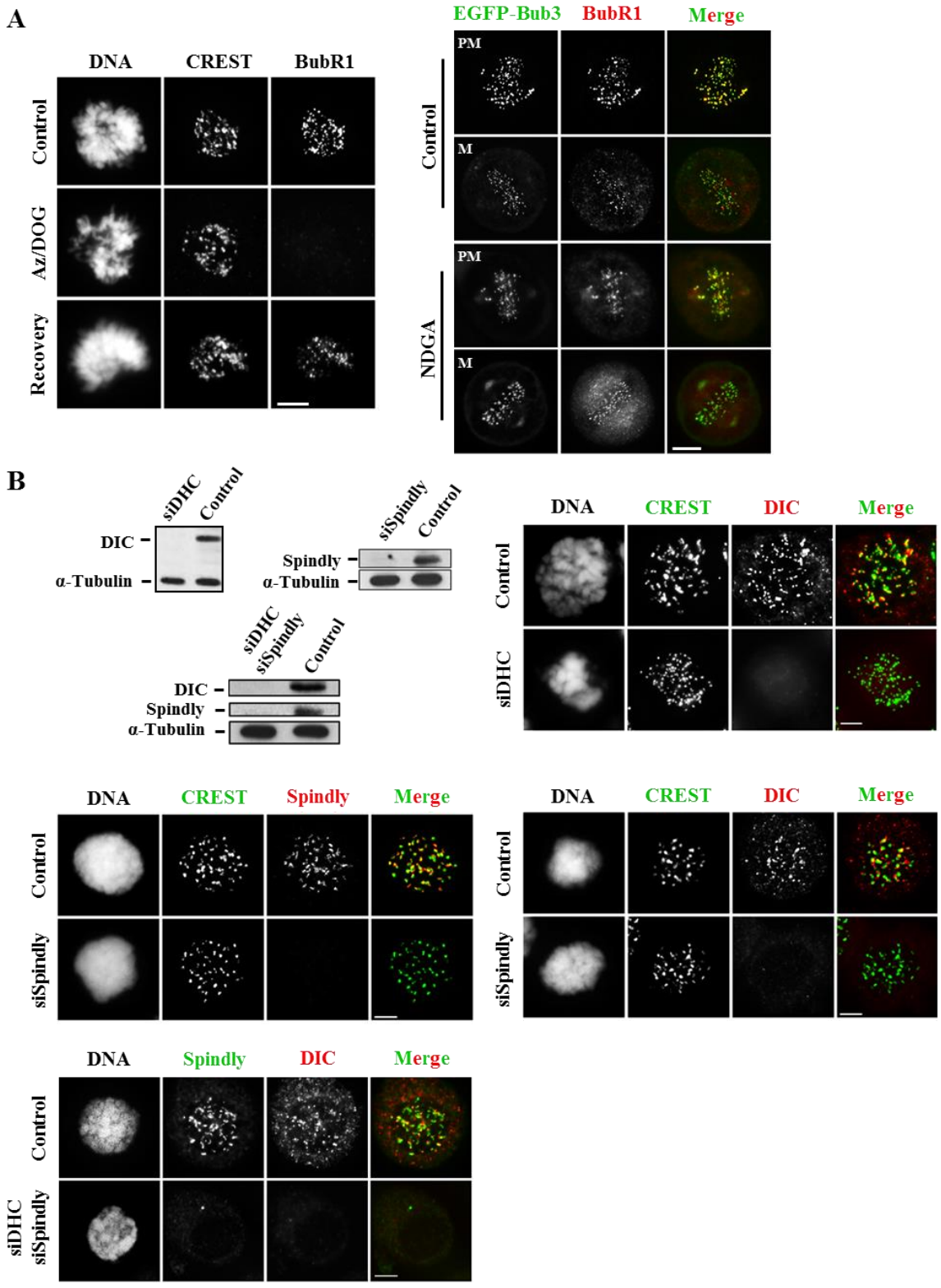

Figure 3.S2. (A) BubR1 is insensitive to sodium azide/2-deoxyglucose assay. (Left) Cells were treated for 30 minutes with sodium azide/2-deoxyglucose (AZ/DOG) and stained for CREST and BubR1. Alternatively, treated cells were allowed to recover for 10 minutes after AZ/DOG washout (Recovery) before immunostaining. (Right) A NDGA-treated cell showing BubR1 only

at kinetochores while Bub3 was relocalized to spindle poles. Bar, 5 μm. **(B)** Efficiency of RNAi-mediated depletion of dynein and spindly. (Top left) Representative western blots showing depletion of dynein (siDHC) as assessed by an anti-dynein intermediate chain [184] antibody, spindly (siSpindly), or both (siDHC/siSpindly). Tubulin was used as loading control. (Top right) siDHC-treated cells were incubated with nocodazole (to create conditions where dynein is maximally enriched at kinetochores) prior to immunostaining for dynein to confirm efficient depletion. **(**Bottom left**)** Spindly RNAi cells were treated with nocodazole and immunostained to confirm efficient spindly depletion. (Bottom right) Spindly RNAi cells were treated with nocodazole and stained with anti-DIC to confirm that dynein was efficiently prevented from localizing to kinetochores.

CHAPTER 4

EXPLORING THE POTENTIAL THERAPEUTIC IMPLICATIONS OF SPINDLE ASSEMBLY CHECKPOINT FOR CANCER THERAPY

According to the objectives highlighted in Chapter 2, this chapter is divided into two parts:

4.1. Suppression of Spindly Delays Mitotic Exit and Exacerbates Cell Death Response of Cancer Cells Treated with Low Doses of Paclitaxel;

4.2. Spindly Expression, Prognostic Significance and Therapeutic Implications in Oral Squamous Cell Carcinoma.

4.1. Suppression of Spindly Delays Mitotic Exit and Exacerbates Cell Death Response of Cancer Cells Treated with Low Doses of Paclitaxel

The information presented in this section was based in the following published paper:

Patrícia M.A. Silva, Nilza Ribeiro, Raquel Lima, Cláudia Andrade, Vânia Diogo, Joana Teixeira, Cláudia Florindo, Álvaro A. Tavares, Helena Vasconcelos and Hassan Bousbaa. Suppression of Spindly Delays Mitotic Exit and Exacerbates Cell Death Response of Cancer Cells Treated with Low Doses of Paclitaxel. Cancer Letters. 2017;394:33-42.

1. Abstract

Microtubule-targeting agents (MTAs) are used extensively for the treatment of diverse types of cancer. They block cancer cells in mitosis through the activation of the spindle assembly checkpoint (SAC), the surveillance mechanism that ensures accurate chromosome segregation at the onset of anaphase. However, the cytotoxic activity of MTAs is limited by premature mitotic exit (mitotic slippage) due to SAC silencing. Here we have explored the dual role of the protein Spindly in chromosome attachments and SAC silencing to analyze the consequences of its depletion on the viability of tumor cells treated with clinically relevant doses of paclitaxel. As expected, siRNA-mediated Spindly suppression induced chromosome misalignment and accumulation of cells in mitosis. Remarkably, these cells were more sensitive to low-doses of paclitaxel. Sensitization was due to an increase in the length of mitotic arrest and high frequency of multinucleated cells, both correlated with an exacerbated post-mitotic cell death response as determined by cell fate profiling. Thus, by affecting both SAC silencing and chromosome attachment, Spindly targeting offers a double-edged sword that potentiates tumor cell killing by clinically relevant doses of paclitaxel, providing a rationale for combination chemotherapy against cancer.

Keywords: Spindly; paclitaxel; cancer cells; spindle assembly checkpoint; apoptosis; cell cycle

2. Introduction

Attachment between kinetochores and microtubules during prometaphase is monitored by the spindle assembly checkpoint (SAC) that halts the metaphase-to-anaphase transition until all chromosomes are fully attached and properly bioriented at the metaphase plate [99, 372]. SAC is activated by the presence of unattached or misattached kinetochores. As a consequence, a diffusible mitotic checkpoint complex (MCC) is formed between the proteins Mad2, BubR1, Bub3, and Cdc20, which promotes the inhibition of the anaphase-promoting complex/cyclosome (APC/C) [157]. APC/C is an E3 ubiquitin ligase that targets securin and cyclin B1 for degradation, thereby promoting sister-chromatid separation and mitotic exit [373]. Once all chromosomes are correctly aligned at the metaphase plate, SAC is switched off in a process called SAC silencing, which in turn relieves the inhibition of APC/C required for the completion of mitosis [99]. Several mechanisms have been proposed to contribute to SAC silencing, including the dissociation of MCC [374, 375], and the stripping of SAC proteins from the kinetochore by a dynein motor [82, 299].

Microtubule-targeting agents (MTAs) such as paclitaxel remain amongst the most effective cancer chemotherapeutics used in the clinic [217]. By preventing mitotic spindle assembly, MTAs delay cells in mitosis through chronic activation of SAC [349]. The fate of cells held in mitosis by MTAs is influenced by the duration of the mitotic arrest, and varies greatly between cancer cells [376, 377]. Prolonged mitotic arrest can lead to cell death in mitosis (DiM) through the accumulation of an apoptotic signal from the intrinsic pathway [226]. However, some cells can prematurely degrade cyclin B, before the accumulation of the apoptotic signal, and, thus, exit mitosis back to interphase without chromosome segregation, through a process known as mitotic slippage. Depending on the robustness of a still unclear post-mitotic response, these cells may either undergo post-mitotic death (PMD), or enter a new cell cycle [212]. Therefore, having a control over the different cell fates should influence the effectiveness of MTAs in cancer therapy. For instance, delaying mitotic exit should allow more time for death signals to accumulate thereby shifting cancer cell fates to death.

Spindly protein is a kinetochore-specific regulator of dynein and functions in chromosome alignment and SAC signaling [112]. Knockdown of Spindly was reported to cause unstable kinetochore-microtubule interactions, severe chromosome alignment

defects, and extensive prometaphase delay [343, 114]. Importantly, kinetochore dynein-mediated removal of Spindly is critical for checkpoint silencing [186, 187].

Our goal was to shift the fate of cancer cells exposed to clinically relevant doses of paclitaxel towards death. To achieve this goal, we investigated Spindly´s dual role in chromosome alignment and in SAC silencing, exploring the possibility of targeting Spindly as a strategy to delay mitotic exit in paclitaxel-based treatment. We show, for the first time, that targeting cancer cells with a combination of Spindly downregulation and clinically relevant doses of paclitaxel significantly promotes tumor cells death. This significant cell death response is due to an increase in the length and frequency of mitotic arrest and to severe multinucleation of treated tumor cells. The results provide a rationale for a promising future combination chemotherapy.

3. Materials and methods

3.1. Cell lines and culture conditions

HPAEpiC (human pulmonary alveolar epithelial cells), Calu-3 (human lung adenocarcinoma) and A549 (human adenocarcinoma alveolar basal epithelial) cells were grown in DMEM medium with 10% fetal bovine serum (FBS, Biochrom) and 1% non-essential amino acids (Sigma-Aldrich Co., Saint Louis, MO, USA). NCI-H460 (human non-small cell lung cancer) cells were grown in RPMI-1640 culture medium (Lonza, Basel, Switzerland) with 5% FBS. Cells were maintained at 37°C in a 5% CO_2 humidified incubator and all experiments were performed when exponentially growing cells presented more than 95% viability.

3.2. RNA isolation and quantitative real-time PCR

Total RNA was extracted using the PureZOL™ RNA Isolation Reagent (Bio-Rad Laboratories, Inc. Hercules, CA, USA), according to the manufacturer's instructions and quantified through spectrophotometry (NanoDrop 2000, Thermo Scientific, Waltham, MA, USA). cDNA synthesis was performed using the iScript™ cDNA Synthesis Kit (Bio-Rad), following supplier's instructions and was amplified using iQ™ SYBR Green Supermix Kit (Bio-Rad) on iQ Thermal Cycler (Bio-Rad), according to the following program: initial denaturing step at 95.0°C for 3 min; 40 cycles at 94.0°C for 20 sec; 60.0°C for 30 sec and 72.0°C for 30 sec. The melt curve included temperatures from 65.0 to 95.0°C, with increments of 0.5°C for 5 sec. Primers, used at

final concentration of 10 µM, were as follows: Spindly: forward 5´-CTC AAA GAG GCT GAA GAA GAG-3´ and reverse 5´-TGT TCA TAA CTC TCA GTC ATG G-3´; Actin: forward 5´- AAT CTG GCA CCA CAC CTT CTA -3´ and reverse 5´- ATA GCA CAG CCT GGA TAG CAA-3´. Experiments were performed in triplicate for each data point. Data were acquired with CFX ManagerTM Software (version 1.0, Bio-Rad) and the results were analyzed according ΔCT and normalized against actin expression levels, which was used as control template. A fold value of mRNA level ≥ or ≤ 1.5 relatively to that of normal cells was considered as over- or underexpression, respectively.

3.3. Gens analyzed in this study

To avoid gene symbol homonymy and species confusion [378], we list here gene symbols and their NCBI ID numbers. Genes under study included Spindly (SPDL1; NCBI ID# 54908), Actin (ACTB; NCBI ID#60), α-Tubulin (TUBA1B; NCBI ID# 10376), PARP-1 (PARP1; NCBI ID# 142) and Cyclin B1 (CCNB1; NCBI ID# 891).

3.4. siRNAs transfection

For siRNAs transfection, cells were seeded in 22 mm poly-l-lysine-coated coverslips in 6-well plates or in 6-well dishes containing complete culture medium and, 24 hours later, transfected using INTERFERin siRNA Transfection Reagent (PolyPlus, New York, USA) according to the manufacturer's instructions. The culture medium was replaced 24 hours post-transfection with fresh medium. A validated siRNA sequence against Spindly (synthetized by Sigma-Aldrich) or a validated negative control siRNA (AllStars Negative Control siRNA, Qiagen, Germantown MD, USA) was used at a final concentration of 100 nM [186, 321].

3.5. Cell extracts and Western blotting

Total cell protein extracts were prepared and Western blot analysis carried out as previously described [321]. The primary antibodies used were: rabbit anti-Spindly (1:3000, gift from Dr. R. Gassmann, IBMC/i3S, Portugal); rabbit anti-cyclin B1 (1:500, C8831, Sigma-Aldrich); mouse anti-PARP-1 (1:2000, H-250, sc-7150, Santa Cruz Biotechnology); rabbit anti-α-tubulin (1:2000, Abcam) and mouse anti-α-tubulin (1:5000, T568 Clone B-5-1-2, Sigma-Aldrich). Horseradish peroxidase (HRP)-

conjugated secondary antibodies were diluted at 1:1500 (anti-mouse, Vector) or at 1:1000 (anti-rabbit, Sigma-Aldrich). The protein signal intensity quantification was performed using ImageJ 1.4v software (http://rsb.info.nih.gov/ij/) and normalized against α-tubulin expression levels.

3.6. Indirect immunofluorescence

Cells grown on coverslips were fixed in fresh 2% (w/v) paraformaldehyde (Sigma-Aldrich) in phosphate-buffered saline (PBS) for 12 min, rinsed three times in PBS, and permeabilized with 0.5% Triton X-100 (Sigma-Aldrich) in PBS for 7 min. Alternatively, to visualize spindle microtubules, cells were immediately fixed in -20°C cold methanol (Sigma-Aldrich) for 10 min and rehydrated twice for 5 min in PBS. Then, cells were blocked with 10% FBS in PBST (0.05% Tween-20 in PBS) for 30 min at room temperature, followed by 1 hour incubation with primary antibodies diluted in 5% FBS in PBST. The following primary antibodies were used: human anti-CREST (1:4000, gift from E. Bronze-da-Rocha, University of Porto, Portugal); mouse anti-α-tubulin (1:2500, T568 Clone B-5-1-2, Sigma-Aldrich) and rabbit anti-Spindly (1:3000, gift from Dr. R. Gassmann, IBMC/i3S, Portugal). After washing in PBST, cells were incubated for 1 hour with Alexa Fluor 488 and 568 conjugated secondary antibodies (Molecular Probes, Eugene, OR, USA), diluted at 1:1500. DNA was stained with 2μg/ml 4′,6-diamidino-2-phenylindole (DAPI, Sigma-Aldrich) diluted in Vectashield mounting medium (Vector, H-1000, Burlingame, CA, USA).

3.7. Mitotic index determination

Mitotic index, the percentage of mitotic cells over the total cell population, was determined by cell-rounding under phase-contrast microscopy in 48 hours control- or Spindly siRNA-treated cells. Alternatively, mitotic index was determined under fluorescence microscope after DNA staining with DAPI. Paclitaxel (Sigma-Aldrich) was used at concentrations ranging from 0-100 nM. This clinically relevant dose range of paclitaxel were adapted from previous studies on breast cancer cell lines [379] and on lung cancer cell lines [380]. Nocodazole (Sigma-Aldrich) was used as a positive control at 1 μM. For each condition, more than 2000 cells were counted from random microscope fields.

3.8. Cell viability assay

Cell viability was determined with MTT (3-(4, 5-dimethylthiazolyl-2)-2,5-diphenyltetrazolium bromide) assay (Sigma-Aldrich). A total of $5x10^4$ control- and Spindly siRNA-treated cells were seeded in 96-well plate, allowed to attach for 6 hours and treated with paclitaxel (0-100 nM). Forty-eight hours later, cells were placed in fresh FBS-free medium and 20 µl MTT reagent (5mg/ml in PBS) was added and incubated at 37 °C and 5% CO_2 for 4 hours. The purple formazan crystals were solubilized with a detergent solution (89% (v/v) 2-Propanol, 10% (v/v) Triton X-100, 1% (v/v) HCl 3.7%), for 2 hours. Optical density was measured at 570 nm in a microplate reader (Biotek Synergy 2, Winooski, VT, USA) and retrieved through the Gen5 software (version 1.07.5, Biotek, Winooski, VT, USA). Cell viability was calculated relative to control siRNA-treated cells.

3.9. Colony forming assay

A total of 500 cells from 24 hours control- or Spindly siRNA-transfected cell cultures were seeded in six-well plates, allowed to attach for 6 hours, and treated with 4 nM of paclitaxel. Forty-eight hours later, paclitaxel was removed by washing cells twice with PBS, then fresh medium was added and cells were allowed to grow for 10 days. The recovered colonies were fixed for 5 min with 3.7% (w/v) paraformaldehyde in PBS, and stained for 20 min with 0.05% (w/v) violet crystal (Merck Millipore, Billerica, MA, USA) in distilled water. The number of colonies was counted on duplicate dishes from three independent experiments. The plating efficiency (PE) was calculated as the percentage of the number of grown colonies over the number of cells seeded in control. For each condition, the survival fraction was determined as the number of colonies over the number of cells seeded × 1/PE.

3.10. Flow cytometry

For cell cycle analysis, cells were harvested, washed twice in PBS and fixed in 70 % ice-cold ethanol at 4°C until analysis. Cells were then resuspended in 5 µg/ml propidium iodide and 100 µg/ml RNase in PBS for 30 min, and analyzed in the flow cytometer. Cell distribution in G0/G1, S, or G2/M phases was determined using the Watson pragmatic fitting algorithm of FlowJo software (version 10.1, Williamson Way, Ashland, USA), after excluding cell debris and aggregates. For apoptosis detection,

cells were harvested and further processed with the "Annexin V-FITC Apoptosis Detection Kit" (eBioscience, Vienna, Austria) according to manufacturer's instructions. Data was analyzed with FlowJo software, version 10. All flow cytometry analysis was carried out using a BD Accuri™ C6 Flow cytometer (BD Biosciences, Qume Drive, San Jose, CA) and analysis at least 20.000 events per sample.

3.11. TUNEL assay

Terminal deoxynucleotidyl transferase-mediated nick end labeling (TUNEL) assay was performed using DeadEnd Fluorometric TUNEL System (Promega, Madison, WI, USA), according to the manufacturer's instructions. DNA was stained with 2μg/ml DAPI in Vectashield mounting medium. The level of cells undergoing cell death was determined by scoring TUNEL-positive cells in a total of 500 cells under fluorescence microscope, from at least ten random microscopic fields, for each experimental condition.

3.12. Live Cell imaging

Live-cell imaging experiments were performed as previously described [381]. Briefly, NCI-H460 cells were seeded onto LabTek II chambered cover glass (Nunc, Penfield, NY, USA) containing 1 ml of culture medium, allowed to attach for 24 hours at 37 °C with 5% CO_2. Then, cells were transfected with control (control siRNA) or Spindly (siSpindly) siRNAs, or treated with 10 nM of paclitaxel, in RPMI without phenol red supplemented with 5% FBS. Time-lapse imaging was performed soon after siRNA or 10 nM paclitaxel addition. For siSpindly and paclitaxel co-treatment, paclitaxel 10 nM was added 24 hours after siRNA-transfection. In this case, Time-lapse imaging was initiated immediately after addition of siRNA-Spindly transfection solution. Images were captured at 10 minutes intervals up to 72 hours under differential interference contrast (DIC) optics, with a 63x objective on an Axio Observer Z.1 SD inverted microscope, equipped with an incubation chamber with the temperature set to 37 °C and an atmosphere of 5% CO_2. Movies were generated from the time-lapse images using ImageJ software (version 1.44, Rasband, W.S., ImageJ, U. S. National Institutes of Health, Bethesda, MD, USA). The number of cells arrested at mitosis, apoptotic, or bypassed cytokinesis was scored. Mitotic cells and cell death were easily scored based on changes in cell morphology by DIC imaging. Mitotic entry was characterized by cell rounding and cell death by cell retraction and blebbing of the

plasma membrane. Cell death was classified as death in mitosis (DiM) when mitotic cells died before cell division, or as post-mitotic death (PMD) when death occurred following cell division.

3.13. Microscopy analysis and Image Processing

Phase-contrast microscopy images were recorded with a 10x objective, on a Nikon TE 2000-U microscope (Amsterdam, Netherlands), using a DXM1200F digital camera (Amsterdam, Netherlands) and with Nikon ACT-1 software (version 2.62, Melville, NY, USA). Fluorescence images were acquired with Plan Apochromatic 63x/NA 1.4 objective or with 40x objective on an Axio Observer Z.1 SD microscope (Carl Zeiss, Germany), coupled to an AxioCam MR3. Z-stacks were acquired with 0.4μm intervals and after image deconvolution with AxioVision Release SPC software (version 4.8.2, Carl Zeiss, Germany) they were processed using ImageJ (version 1.44, Rasband, W.S., ImageJ, U. S. National Institutes of Health, Bethesda, MD, USA).

3.14. Statistical analysis

Statistical analysis was performed using an Unpaired Student t-test or an ordinary two-way ANOVA with Tukey's multiple comparisons test, in GraphPad Prism version 6 (GraphPad software Inc., CA, USA). Alpha value was 0.05 and the confidence interval 95%. Data are presented as the means ± standard deviation (SD) of at least three independent experiments. The level of significance was set at probabilities of $*^{/\#}p < 0.05$, $**^{/\#\#}p < 0.01$, $***^{/\#\#\#}p < 0.001$ and $****^{/\#\#\#\#}p < 0.0001$.

4. Results

4.1. Spindly is overexpressed in lung cancer cells

To gain insight into the relevance of Spindly as potential antimitotic target for cancer therapy, we first examined its expression in lung cancer cell lines. Analysis of Spindly mRNA levels by qRT-PCR showed that this gene was overexpressed in the tested cancer cell lines compared with mRNA levels in the non-tumor cell line (**Figure 4.1A**). There was a 2.9 ± 0.4, 4.6 ± 0.2, and 5.4 ± 0.2 fold increase in Spindly expression in NCI-H460, Calu-3, and A549 cell lines, respectively, compared with Human Pulmonary Alveolar Epithelial Cells (HPAEpiC). Western blot analysis showed

that Spindly was also upregulated at protein level (**Figure 4.1B**). Spindly overexpression was also found in glioblastoma, colorectal and oral cancer cell lines (Silva and Bousbaa, unpublished data). Analyzing published databases from the publicly available Oncomine database confirmed Spindly upregulation in lung cancer [382] and, interestingly, in many other cancers (www.oncomine.org). This result highlights the relevance of targeting Spindly for cancer therapy.

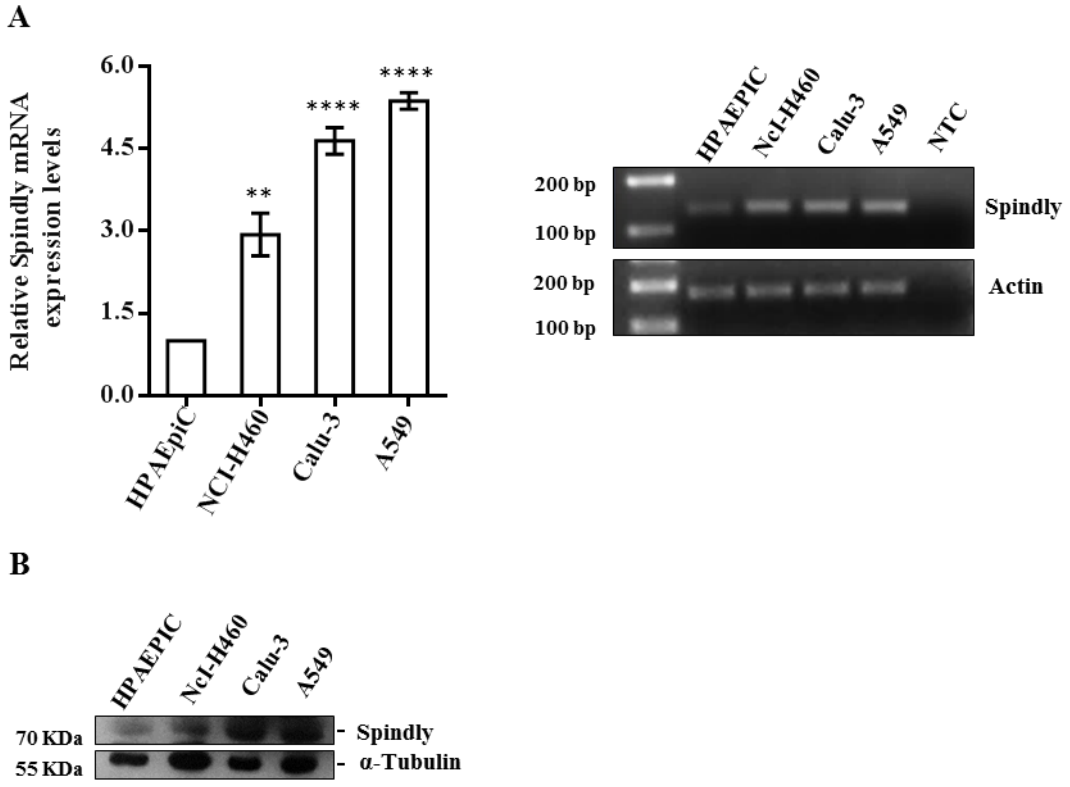

Figure 4.1. Spindly is overexpressed in lung cancer cells. **(A)** Relative expression of Spindly mRNA as determined by RT-PCR in NCI-H460, Calu-3 and A549 cell lines, comparatively to non-tumor HPAEpiC (left); a representative 2% agarose gel image of PCR products is shown (right). Actin served as a loading control. **(B)** Representative Western blot showing differential expression at protein levels in the cell lines analyzed in (A). Tubulin served as a loading control. $^{**}p < 0.01$ and $^{****}p < 0.0001$ normal *vs* cancer cell lines.

4.2. Depletion of Spindly protein levels from lung cancer cells

There are many studies exploring the possibilities of RNA interference (RNAi) to silence genes with therapeutic applications. RNAi can be achieved locally by delivering synthetic siRNAs, or using shRNAs delivered via viral particles, or following transfection of plasmid DNAs [383, 384]. We used validated siRNA duplexes [186, 321] to deplete the expression of Spindly in NCI-H460 and A549 cancer cells. Efficient Spindly repression was ascertained by immunofluorescence for Spindly kinetochore

staining of prometaphase cells as confirmed by its colocalization with the kinetochore marker CREST (**Figure 4.S1A**). Spindly depletion value of 98.9% and 98.4% was achieved as determined by immunoblotting against total NCI-H460 and A549 cell extracts, respectively (F**igure 4.S1B**). Furthermore, and according to Spindly depletion phenotype reports, Spindly silencing resulted in a severe chromosome misalignment (Supplementary figure S1A) and an increased mitotic index (Supplementary figure S1C) [321, 114]. These results indicate that the previously validated Spindly siRNA is suitable for subsequent studies on NCI-H460 and A549 cancer cell lines, namely, to determine whether Spindly targeting can render paclitaxel-mediated therapy more effective.

4.3. Depletion of Spindly extends the length of mitotic arrest induced by paclitaxel

We reasoned that if SAC silencing is delayed by Spindly depletion, then the mitotic delay induced by paclitaxel would be extended, thereby providing more time for paclitaxel to exert its cytotoxic effect. The NCI-H460 cell line was selected to address this hypothesis due to its suitability for *in vivo* microscopy and for quantitative evaluation of morphological changes. Cells were transfected with control or Spindly siRNAs, 24 h post-transfection cells were treated with paclitaxel and the length of mitotic arrest was determined by time-lapse imaging. Mitosis in control siRNA-treated cells spent an average of 34.3 ± 7.3 min (n=30) from nuclear envelope breakdown to anaphase onset. In contrast, we found that Spindly-depleted cells spent more time in mitosis (628.1 ± 403.7 min, n=31) before mitotic exit or cell death (see below). These results are in good agreement with previous report [114]. We have observed that paclitaxel-treated cells spent 115.0 ± 142.1 min in mitosis (n=32); and, interestingly, the duration of mitosis was extended to 332.6 ± 220.9 min when paclitaxel was added after Spindly depletion (n=35) (**Figure 4.2A**). Notably, this prolongation of mitosis was concomitant with an increase in the mitotic index in cells treated with the combination siSpindly plus paclitaxel (41.8%), when compared to the residual accumulation of mitotic cells in 10 nM paclitaxel-treated cells (13.1%). Massive accumulation in mitosis (68.0% of total cells) was only achieved with a minimum of 100 nM paclitaxel (**Figure 4.2B**). Our results demonstrate that preventing SAC silencing through Spindly depletion increases the length and the frequency of the mitotic arrest of cells treated with low doses of paclitaxel.

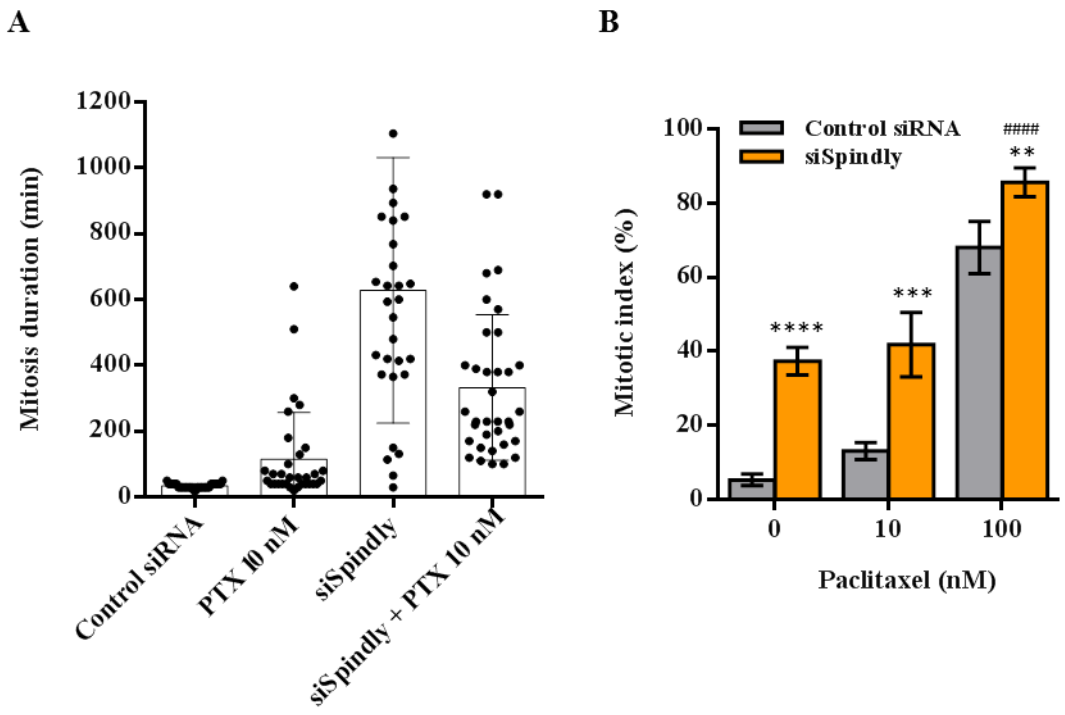

Figure 4.2. Spindly inhibition increases the duration of the mitotic block and the mitotic index under low doses paclitaxel treatment. **(A)** Mitosis duration as determined by time-lapse microscopy, in the absence or presence of 10 nM paclitaxel (PTX 10 nM) both for control- or Spindly siRNA-transfected cells. Each spot represents one NCI-H460 cell. **(B)** Mitotic index of control siRNA- or siSpindly-treated cells, in the absence or presence of paclitaxel. Cells were treated with control or Spindly siRNA for 48 hours, or 24 if Spindly siRNA was used in combination with paclitaxel. Mitotic Index was established upon DNA staining. $^{**}p < 0.01$, $^{***}p < 0.001$ and $^{****}p < 0.0001$ individual or combination treatments *vs* control siRNA; $^{\#\#\#\#}p < 0.0001$ combination treatment *vs* siSpindly.

4.4. Spindly depletion exacerbates the cytotoxic activity of paclitaxel

As Spindly depletion led to much longer mitotic arrest in paclitaxel-treated cells, we asked whether this would result in an exacerbated cytotoxicity. To address this question, NCI-H460 and A549 cells were transfected with Spindly siRNAs, 24 h post-transfection cells were treated with various concentrations of paclitaxel. An MTT assay was performed 72 h post-transfection. In control siRNA-treated cells, viability was only marginally compromised at low doses of paclitaxel (<10 nM), and >50 nM of paclitaxel was required in order to significantly affect cell viability (**Figure 4.3A**). However, viability was drastically reduced by low doses of paclitaxel when Spindly was also downregulated. The results indicate that sensitivity to paclitaxel is significantly increased when Spindly is suppressed.

The increased sensitivity to paclitaxel of Spindly-depleted cells was also assessed by using a long-term (10 days) clonogenic assay. Sublethal concentrations of paclitaxel (4 nM) greatly compromised colony formation in Spindly-depleted cells, when compared to control siRNA-treated cells (**Figure 4.3B**). Our results led us to conclude that that suppressing Spindly sensitizes human tumor cells to cytotoxic effect induced by clinically relevant doses of paclitaxel.

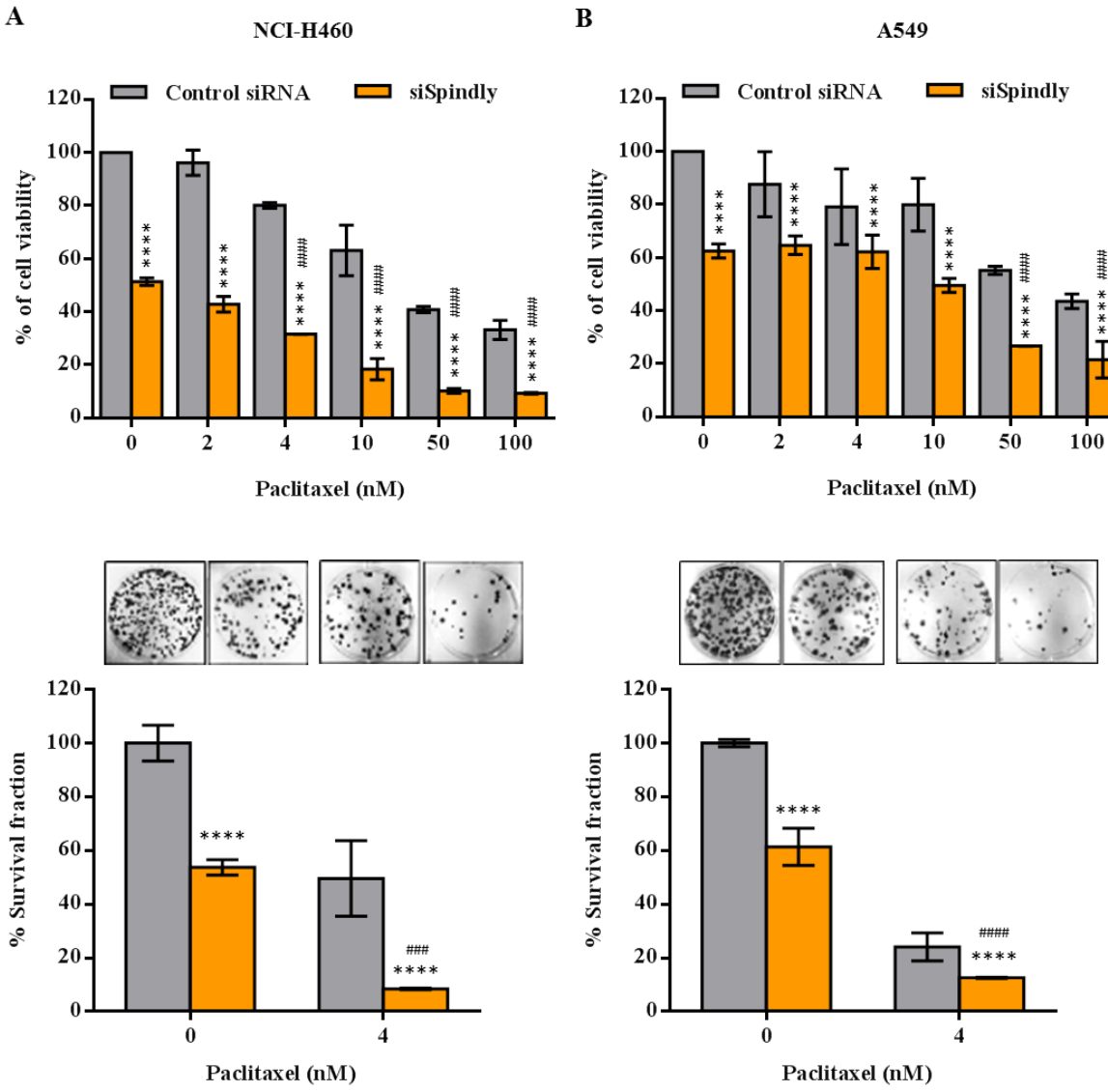

Figure 4.3. Spindly depletion enhances paclitaxel-mediated cytotoxicity. **(A)** NCI-H460 (left) and A549 (right) cell viability, as determined by MTT assay. Twenty-four hours post-transfection with control or Spindly siRNA, paclitaxel (PTX) was added at the indicated concentrations (0-100 nM) and cells were incubated for an extra 48 hours. **(B)** NCI-H460 (left) and A549 (right) cells were treated as in (A), washed and allowed to grow for 10 days. Cells were then stained with crystal violet. Results are the mean ± SD from three independent experiments, expressed as % of survival fraction. Representative images of surviving colonies (top) are shown for each condition. ****$p < 0.0001$ individual or combination treatments *vs* control siRNA; $^{###}p < 0.001$ and $^{####}p < 0.0001$ combination treatment *vs* siSpindly.

4.5. Spindly suppression promotes death of low doses paclitaxel-treated cancer cells

In an attempt to understand the reason of the increased sensitivity to paclitaxel due to Spindly abolition we performed live-cell imaging experiments. Again, the NCI-H460 was selected in this study for the aforementioned reasons. We aimed to directly determine the survival fate of each NCI-H460 arrested cell by time-lapse imaging over 72 h time course as described above. Control- and Spindly-depleted cells were incubated with a sublethal dose (10 nM) of paclitaxel and imaged over a 72 h time course. All unperturbed NCI-H460 cells underwent normal cell cycling and division (n=30) (**Figure 4.4A and movie 4.1**). Spindly depletion induced cell death in 93% of cells (n=31) (**Figure 4.4A and movie 4.2**), while only 8% of cells (n=32) died after treatment with 10 nM paclitaxel (**Figure 4.4A and movie 4.3**). The same amount of the antimitotic drug triggered near-maximal cell death (86% of cells, n=35) in Spindly-suppressed NCI-H460 cells (**Figure 4.4A and movie 4.4**).

Cell death fell into two categories according to the stage of cell cycle at which it occurred: cell death in mitosis (DiM) when cells died during mitosis; and post-mitotic death (PMD) when death occurred following cell division. We have adopted DiM and PMD for standardization concern with previous report [212]. Of 93% of Spindly-depleted cells that died, 90% underwent DiM while 3% only underwent PMD after the first division (**Figure 4.4B**); cells that survived (7%) remained in interphase for the duration of the imaging. Most of the paclitaxel-treated cells survived and continued cycling (84%), 8% stayed in interphase without cycling and only 8% underwent PMD (**Figure 4.4B**). For cells in which we used the combination treatment, 86% died. Most of these dead cells (72%) underwent PMD (mainly following the first division), the remaining 14% underwent DiM. Importantly, all the survivors (14%) were arrested in interphase for the duration of the imaging (**Figure 4.4B**).

The strong tendency to die after cell division upon the combination treatment was confirmed by a two-fold decrease in cyclin B levels and a strong PARP-1 cleavage activity, supporting mitotic exit, and cell death, respectively (**Figure 4.4C and D**). In conclusion, Spindly targeting significantly increases post-mitotic death in paclitaxel-based treatment.

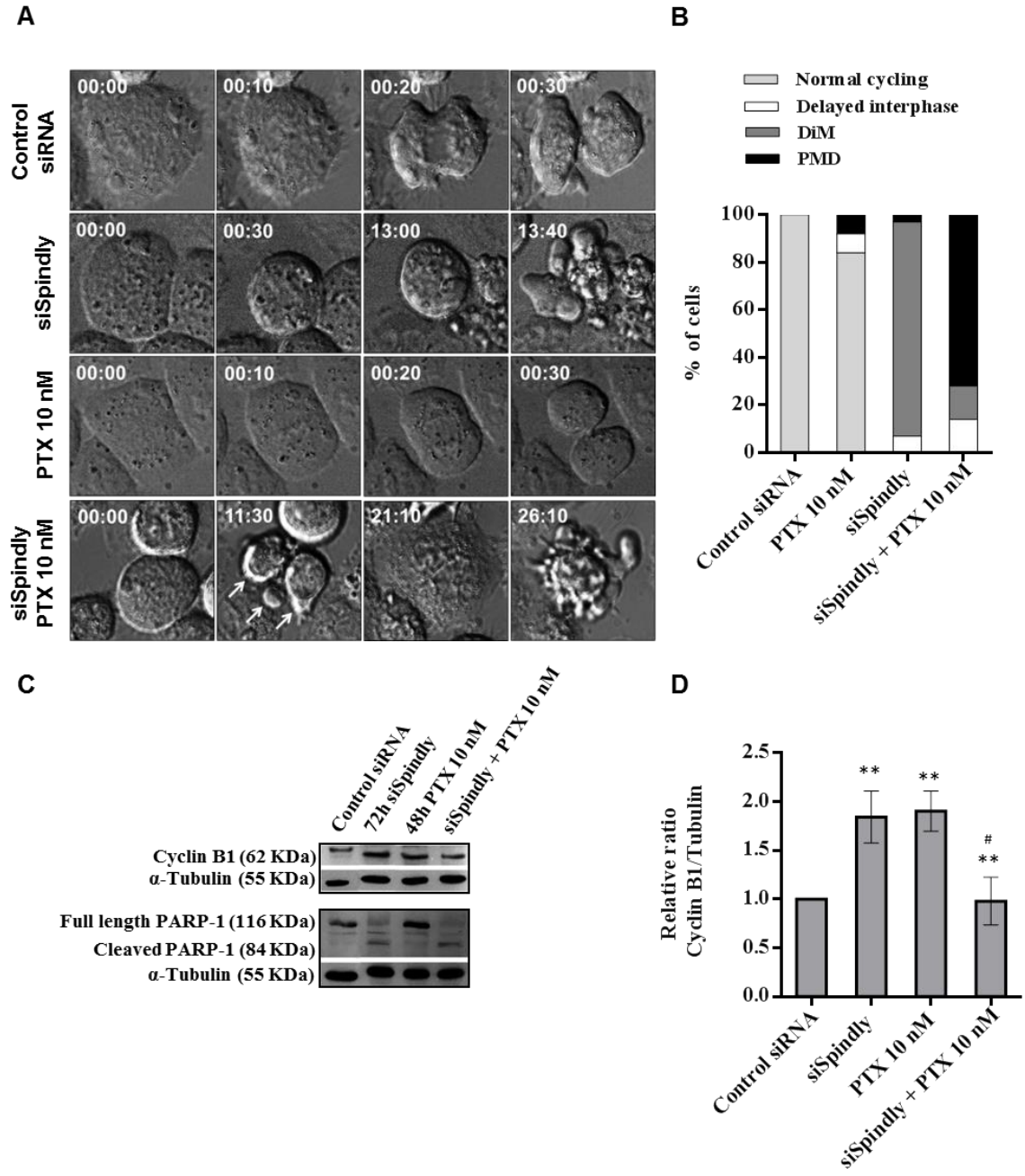

Figure 4.4. A combination of low dose paclitaxel and Spindly depletion promotes post-mitotic death in tumor cells. **(A)** Representative time-lapse sequences of NCI-H460 treated with control or Spindly siRNAs, either alone or in combination with 10 nM of paclitaxel (see section 2.12 for live-cell imaging details). It can be observed a control siRNA-treated cell and a paclitaxel-treated cell (PTX 10 nM) spending ~30 minutes in mitosis before cytokinesis; a siSpindly-treated cell is shown undergoing membrane blebbing >13 h upon mitotic block; a siSpindly plus paclitaxel-treated cell (siSpindly + PTX 10 nM) underwent post-mitotic death 26 h:10 min after mitotic exit (white arrows). Cell death occurred more than 11h after the mitotic block. Numbers indicate times in 00hours:00minutes. Movies are available as supplementary materials. **(B)** Quantification of cell fates for each condition in (A). **(C)** Cyclin B1 levels (top) and PARP-1 activity (bottom) as determined by immunoblotting against protein extracts from NCI-H460 treated as in (A). Protein extraction was performed at the indicated time. For the combination, cells were treated with siRNA for 24h, then with paclitaxel for further 48h before protein extraction. **(D)** Ratio of Cyclin B1/tubulin for quantification of Cyclin B1 levels shown in (C). Results are the mean ± SD from three independent experiments. For Western blots α-

tubulin was used as a loading control. $^{**}p < 0.01$ individual or combination treatments *vs* control siRNA; $^{\#}p < 0.05$ combination treatment *vs* siSpindly.

Paclitaxel kills cancer cells mainly through the induction of apoptosis [226, 385]. The majority of cells that died, either by DiM or PMD, presented membrane blebbing characteristic of apoptosis. In addition to the aforementioned PARP-1 activity, apoptosis was further confirmed by TUNEL assay. Spindly depletion plus 10 nM paclitaxel resulted in more TUNEL-positive cells (30.1 ± 3.2%) than Spindly siRNA or paclitaxel alone (20.3 ± 3.6 % and 1.6 ± 0.6, respectively) (**Figure 4.5A and B**). Using an Annexin-V FITC and propidium iodide co-staining, we re-confirmed the apoptotic response by flow cytometry (**Figure 4.5C and D**). Therefore, a combination of clinically relevant doses of paclitaxel with suppression of Spindly enhances the apoptotic response of tumor cells.

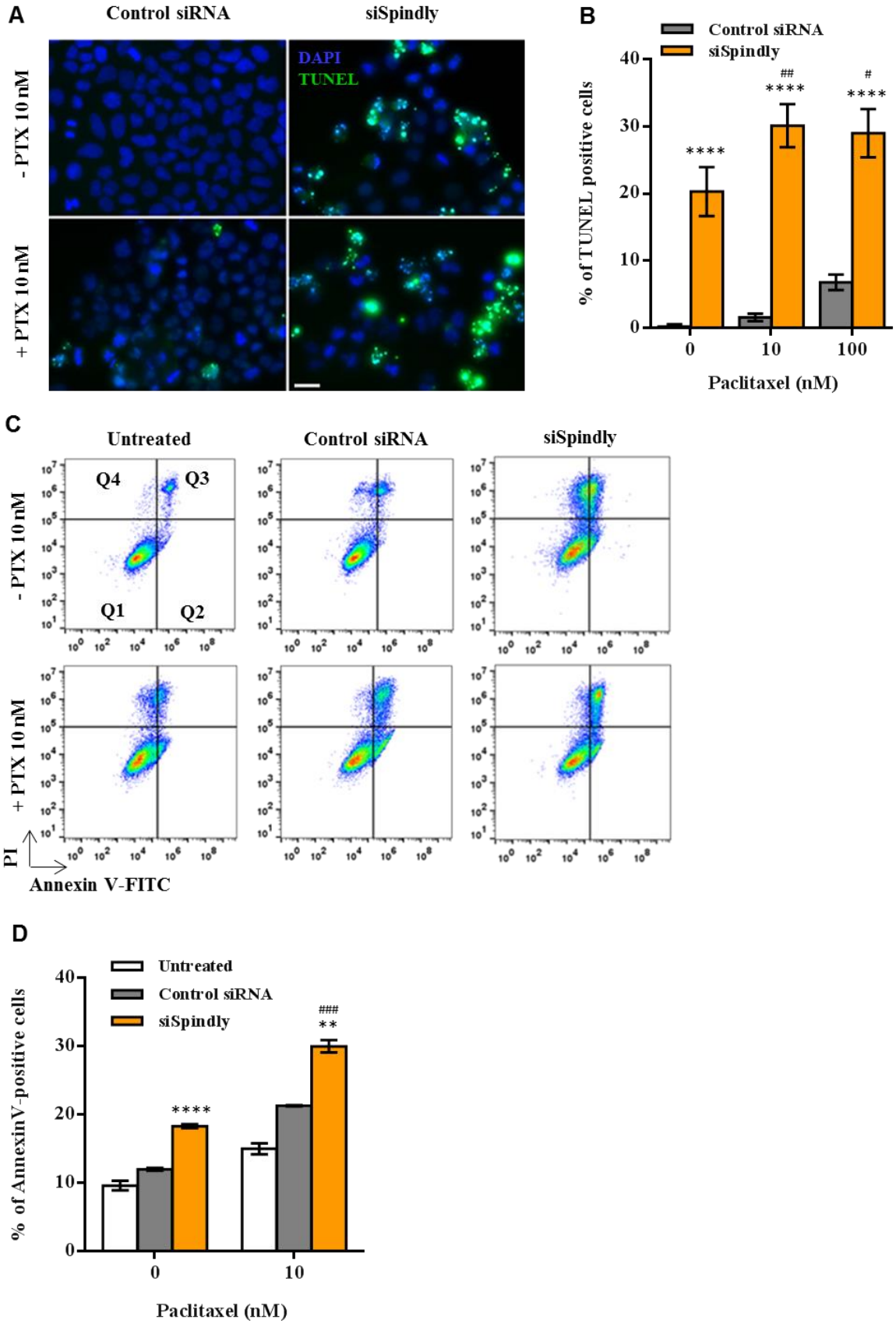

Figure 4.5. Tumor cells treated with low doses of paclitaxel exhibits increased apoptosis upon Spindly inhibition. NCI-H460 cells were treated with control or Spindly siRNAs, either alone (- PTX 10 nM) or in combination with 10 nM of paclitaxel (+ PTX 10 nM). (A) Cells stained with TUNEL to detect apoptotic cells (green). DNA (blue) was stained with DAPI.

Bar = 5 µm. **(B)** Quantification of data shown in (A). **(C)** Representative cytogram from flow cytometry analysis of apoptosis by Annexin V/PI co-staining to confirm results presented in (A) and (B). The quadrants Q were defined as Q1=live (Annexin V- and PI-negative), Q2=early stage of apoptosis (Annexin V-positive/PI-negative), Q3= late stage of apoptosis (Annexin V- and PI-positive) and Q4=necrosis (Annexin V-negative/PI-positive). **(D)** Quantification of Annexin V-positive cells from the data shown in (C). Results are the mean ± SD from three independent experiments. ****$p < 0.0001$ individual or combination treatments *vs* control siRNA; $^{\#}p < 0.05$, $^{\#\#}p < 0.01$ and $^{\#\#\#}p < 0.001$ combination treatment *vs* siSpindly.

4.6. Spindly depletion potentiates multipolar spindle and multinucleation phenotype of paclitaxel-based treatment leading to cell death

In order to gain a mechanistic understanding of the increased frequency of cell death induced by paclitaxel in Spindly depletion background, we investigated the precise impact of the combination on cell cycle progression and mitosis execution. Cells were processed for immunofluorescence and stained with α-tubulin antibody to visualize mitotic spindle microtubules, and stained with DAPI for DNA. The microscopy analysis revealed major alterations in both the morphology of mitotic spindle and interphasic nuclei. We found that 56.8 ± 7.5% and 49.7 ± 10.7% of spindles were multipolar in mitotic cells depleted of Spindly or treated with 10 nM paclitaxel, respectively. The remainder exhibited near-normal bipolar spindles (**Figure 4.6A**). Interestingly, treatment of Spindly-depleted cells with 10 nM paclitaxel exacerbated this phenotype as 96.0 ± 5.1% of spindles were multipolar. Paclitaxel was only able to induce comparable frequency of multipolar spindles if used at higher concentrations (> 100 nM). Similar behavior was observed when the morphology of interphasic nuclei was analyzed. While only 20% of cells exposed to individual treatments were multinucleated, 76.5 ± 7.4% of cells were multinucleated in the combination treatment (**Figure 4.6B**). We further confirmed this result using flow cytometry analysis to analyze the cell cycle profile (**Figure 4.6C**). Spindly knockdown plus 10 nM paclitaxel resulted in an increased cell population with >4N DNA content (>G2), compared to untreated cells or to cells exposed to individual treatments.

Overall, the results indicate that under Spindly depletion background, severe chromosome missegregation within a multipolar spindle is induced in low-dose paclitaxel-treated cells, generating multinucleated cells probably as a result of failure in cytokinesis, and leading eventually to cell death.

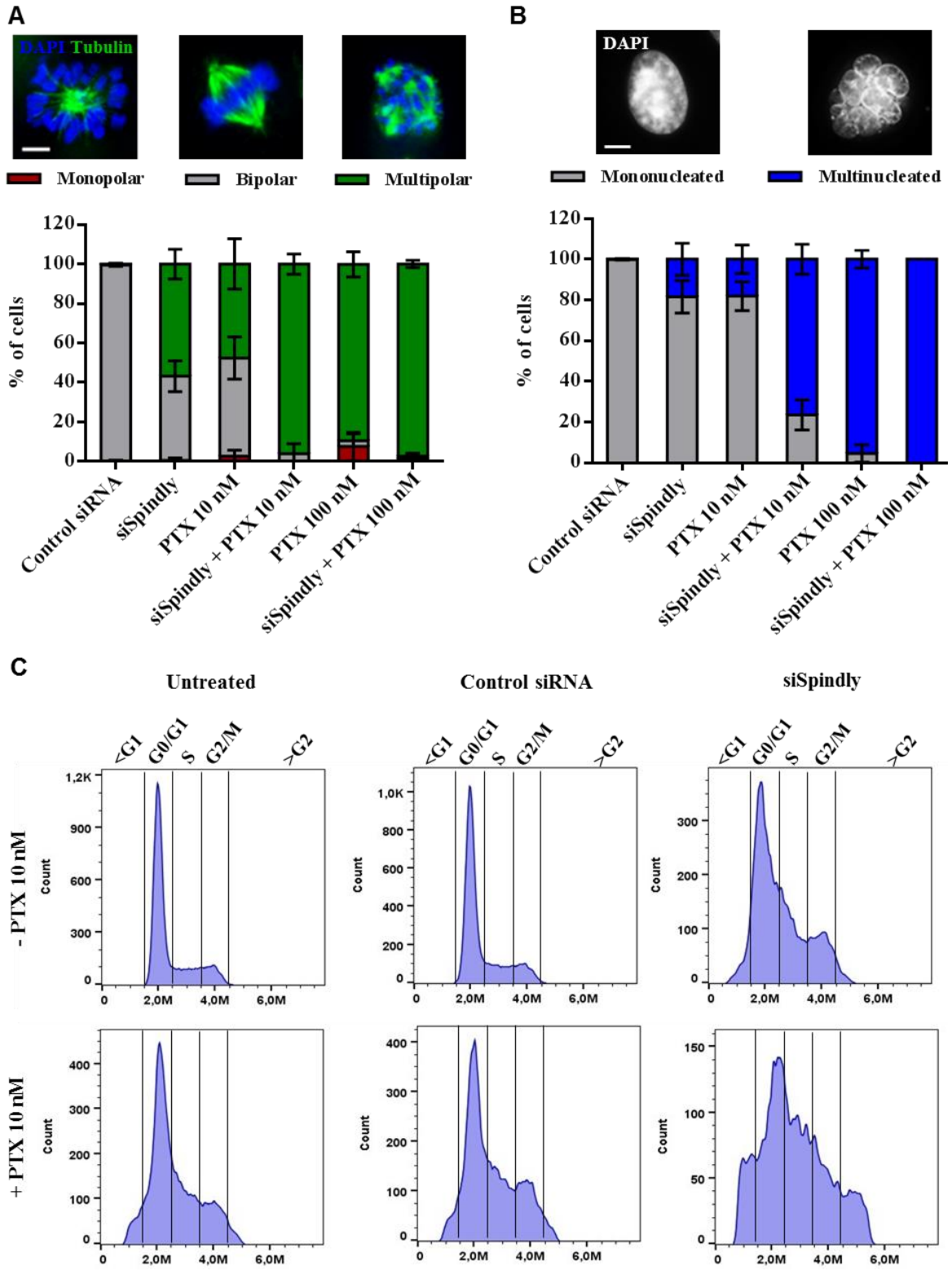

Figure 4.6. Spindly inhibition enhances multipolar spindles and multinucleation induced by low doses paclitaxel. (A) Quantification (graph) of mitotic spindle morphology (upper images, DAPI and tubulin -staining) after treatment with control or Spindly siRNAs, either alone or in combination with 10 and 100 nM of paclitaxel (PTX). Bar = 5 µm. **(B)** Quantification (graph) of nuclear morphology (upper images, DAPI staining) in NCI-H460

treated as in (A). **(C)** Confirmation of data in (B) by flow cytometry analysis. Results are the mean ± SD from three independent experiments.

5. Discussion

Despite the broad clinical use of microtubule targeting agents (MTAs), the associated hematopoietic and neurologic toxicities as well as the intrinsic or acquired drug resistance remain a significant problem limiting their overall effectiveness. Here we present data that support a rationale for targeting Spindly to potentiate the effectiveness of paclitaxel at clinically relevant doses, thus providing a novel and possibly effective approach for therapeutic intervention in cancer.

In the present study, depletion of Spindly created misaligned chromosomes and lengthened mitosis, consistent with previous reports [114, 343]. As predicted, we found that depletion of Spindly rendered cells remarkably more sensitive to low doses of paclitaxel. Sensitization to paclitaxel was due to an enhanced antimitotic activity resulting, primarily, from an increase in the duration of mitotic delay. This was correlated with the extent of multinucleation and cell death response. Cell death consisted predominantly of post-mitotic death (PMD) as revealed by cell fate profiling.

Paclitaxel induces SAC-dependent mitotic delay at high doses by inhibiting microtubule dynamics but at low doses, clinically relevant concentrations, it induces aneuploidy without mitotic arrest [386, 379]. It is possible that at low doses of paclitaxel, cells exhibit the same kinetics of chromosome attachment to the mitotic spindle as control cells, and the SAC is inactivated [345]. In this regard, due to its dual role in chromosome attachment and SAC silencing, targeting Spindly would have two consequences on cell division that would potentiate the effect of low doses of paclitaxel. On one hand, suppression of Spindly induces misattached chromosomes which activate the SAC and, consequently, block cells in mitosis. On the other hand, Spindly suppression prevents SAC silencing and, hence, mitotic exit, resulting in a lengthening of mitotic arrest. Both consequences, mitotic block and sustained SAC activation, create maximal conditions for apoptotic signal accumulation, thereby sensitizing tumor cells to cell death by clinically relevant doses of paclitaxel.

The fate of cells exposed to antimitotic agents is determined by the length of the mitotic arrest and their ability to activate apoptosis [376]. As long as SAC is activated, rapid cyclin B1 degradation is prevented and cells are trapped in mitosis, allowing accumulation of apoptotic signals. However, cyclin B1 levels decline by slow and

continuous degradation that ultimately leads to SAC slippage which, if it happens before accumulation of sufficient cell death signal, drives cells out of mitosis, with the possibility of giving rise to surviving progeny cells [387, 212] . Therefore mechanisms that activate SAC and delay its silencing, such as Spindly inhibition, may increase the length of mitotic arrest induced by MTAs, allowing apoptotic signals to accumulate and irreversibly marking cell for death, even after mitotic slippage. It was proposed that enhancing chromosome missegregation and aneuploidy could be a strategy to sensitize cancer cells to MTAs [213]. Indeed, gross chromosome missegregation is not compatible with cell viability [215]. The high frequency of aneuploidy and cell death response that resulted from Spindly depletion plus paclitaxel treatment in our study confirms the relevance of such strategy to cancer cell killing. In this regard, the misattachment phenotype associated with Spindly depletion might potentiate the aneuploidy induced by low doses of paclitaxel. We therefore propose that future drug candidates against Spindly be added to the list of the so-called second-generation antimitotic drugs that block mitotic progression by disrupting spindle assembly, like inhibitors against mitotic kinesins (e.g. Eg5 and CENP-E), and mitotic kinases (e.g. Plk1) [239]. Spindly inhibitors would have the advantage of acting on mitotic exit and not only on spindle assembly like the Eg5, CENP-E, and Plk1 inhibitors. In fact, blocking mitotic exit was reported to be better cancer therapeutic target than perturbing spindle assembly [377]. Although our results indicate that Spindly targeting alone was sufficient for an efficient cell killing, based on the reported limited success of second-generation antimitotics in clinical trials [388, 389], we believe that candidates for Spindly inhibitors would provide a better clinical benefit if combined with the most successful chemotherapy drugs in history such as paclitaxel.

Intriguingly, Spindly depletion led to DiM while the combination with paclitaxel induced PMD. It is possible that the longer mitotic arrest provided by Spindly depletion favors DiM due to accumulation of pro-apoptotic signal to a level that dictates cell death while cells are still in mitosis. On the other hand, in the combination treatment, subtle perturbations in microtubule dynamics and kinetochore-microtubule attachments, induced by low doses of paclitaxel, might induce Spindly-independent SAC silencing, leading to mitotic exit. Indeed, although mitotic delay in the combination was increased, its duration was shorter when compared to Spindly-depleted cells. At the same time, these cells have already accumulated enough apoptotic signals to irreversibly undergo post-mitotic death.

As SAC inactivation drives precocious mitotic exit and cell death as a result of massive chromosome missegregation, its modulation has been tested for cancer therapy experiments in many reports [390]. The overall conclusion is that, to be effective in cancer therapy, a complete abrogation of SAC is needed, which is difficult to achieve in vivo [391, 215]. On another hand, incomplete inactivation of SAC activity confers strong resistance to SAC-dependent antimitotic drugs in various cancer cell lines [392, 212]. Together with the aforementioned reasons, this highlights the advantages of targeting Spindly in triggering cancer cell death more effectively than modulating SAC directly.

In conclusion, we have explored the dual role of Spindly in chromosome attachment and SAC silencing to increase the effectiveness of clinically relevant doses of paclitaxel. We show that the suppression of Spindly sensitizes human tumor cells to death by low doses of paclitaxel by increasing the length of mitotic arrest and the frequency of aneuploidy. We thus propose Spindly inhibition as valid and valuable strategy in rational combination cancer therapy with paclitaxel. As low doses of paclitaxel can be used, this strategy might provide therapeutic benefits by overcoming problems of resistance and side effects. Additionally, SAC-deficient cancer cells resist cell killing by antimitotics because they prematurely exit mitosis, before initiation of apoptosis [377]. Preventing SAC silencing in these cells, through Spindly inhibition, might help circumvent this resistance.

6. Acknowledgements

This work was funded by CESPU – Cooperativa de Ensino Superior Politécnico e Universitário under the project “SpindlyTarget-CESPU-2016”. Patrícia M.A. Silva is a PhD fellowship holder from FCT (SFRH/BD/90744/2012), and partially supported by national Portuguese funding through FCT - Fundação para a Ciência e a Tecnologia, project ref. UID/BIM/04773/2013 CBMR.

7. Supplementary figures

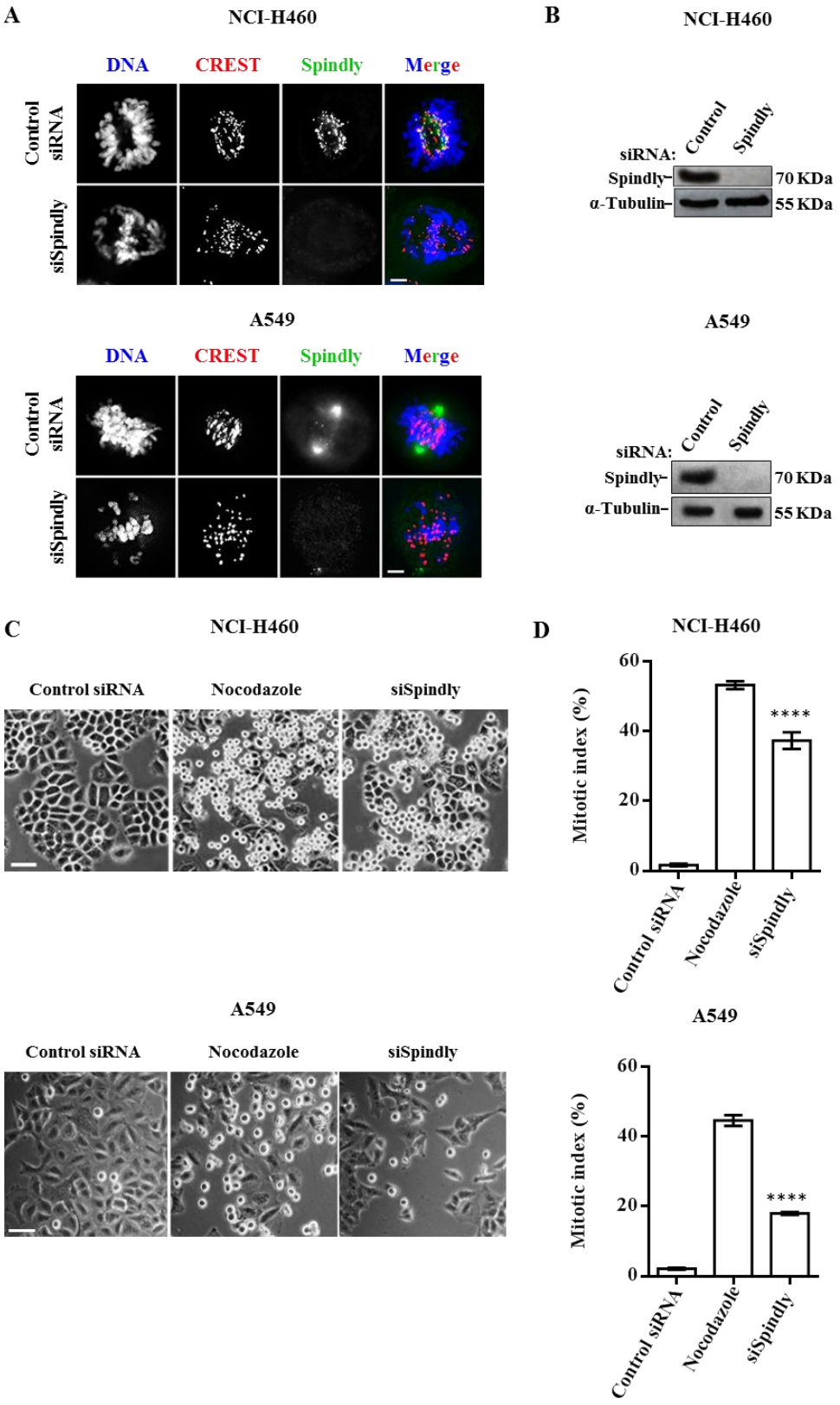

Figure 4.S1. Spindly depletion resulted in a significant increase in mitotic arrested lung cancer cells. NCI-H460 and A549 cells were transfected with control (control siRNA) or Spindly (siSpindly) siRNAs for 48 hours. **(A)** The expected Spindly kinetochore staining was exhibited by control siRNA-treated cells but was absent from siSpindly-treated cells, indicating

efficient Spindly depletion. Cells were immunostained with CREST and anti-Spindly antibodies to localize kinetochores (in red) and Spindly (in green), respectively. DNA is shown in blue (DAPI). Bar = 5 µm. **(B)** Representative immunoblots from NCI-460 (top) and A549 (bottom) cell extracts showing efficient Spindly downregulation upon transfection with siRNAs. α-tubulin was used as a loading control. **(C)** Representative phase contrast microscopy fields showing an accumulation of NCI-H460 and A549 mitotic cells (rounded-shape) upon transfection with Spindly siRNAs (siSpindly). Nocodazole was used as a positive control of antimitotic activity. Bar = 20 µm. **(D)** Determination of mitotic index (percentage of mitotic cells over the total of cell population) from the data shown in (C). Results are the mean ± SD from three independent experiments. ****$p < 0.0001$ control siRNA *vs* siSpindly.

4.2. Spindly Expression, Prognostic Significance and Therapeutic Implications in Oral Squamous Cell Carcinoma

The information presented in this section was based in the following submitted paper:

Patrícia M.A. Silva, Maria Leonor Delgado, Nilza Ribeiro, Cláudia Florindo, Álvaro A. Tavares, Carlos Lopes, Barbas do Amaral, Hassan Bousbaa and Luís Silva Monteiro. Spindly Expression, Prognostic Significance and Therapeutic Implications in Oral Squamous Cell Carcinoma. International Journal of Cancer. (*submitted*).

1. Abstract

The spindle assembly checkpoint (SAC) ensures genomic stability by preventing chromosome segregation at metaphase to anaphase transition in the presence of unattached or improperly attached chromosomes to mitotic spindle. Anaphase onset requires SAC silencing, a process that involves the protein Spindly. The aim of this study was to analyze the expression pattern of Spindly, its clinicopathological significance in patients with oral squamous cell carcinoma (OSCC), and its potential as therapeutic target. Immunostaining of tissue microarrays from OSCC patients demonstrated > 75% patients had high levels of Spindly expression. Both univariate and multivariate analyses showed that high expression of Spindly was an independent prognostic indicator for cancer-specific survival. Importantly, Spindly overexpression was associated with increased cellular proliferation. Moreover, Spindly was found to be upregulated in OSCC cell lines comparatively to their normal counterpart. RNAi-mediated knockdown of Spindly compromises cell viability of OSCC cells and, interestingly, enhances their chemosensitivity to cisplatin. Overall, the data suggest promising clinical potential of Spindly as marker of cancer proliferation and prognosis, and highlights the potential therapeutic benefit of combining Spindly inhibition with cisplatin.

Keywords: Spindly; gene expression; oral squamous cell carcinoma; cisplatin; combinatorial therapy

2. Introduction

Oral squamous cell carcinoma (OSCC) is the most common oral cancer worldwide, with a still dismally low survival rate [393, 394]. Like in other cancers, genetic and epigenetic events govern the multistep process of OSCC progression [395]. Therefore, identifying the changes that occur at the molecular and biological levels during oral cancer development could provide a mean for understanding the disease mechanisms, as well as for earlier diagnosis and the delivery of more efficacious and safer therapies, thereby improving health management.

Spindly is a regulator of dynein at kinetochores during mitosis and is also involved in chromosome alignment and spindle assembly checkpoint (SAC) signaling [112, 114]. The SAC monitors the attachment of chromosomes to spindle microtubules and prevents anaphase onset until all chromosomes have achieved bipolar attachments and are properly aligned at the metaphase plate [99]. The transition from metaphase to anaphase requires SAC silencing, a process that involves kinetochore dynein-mediated removal of the 605-aa protein Spindly [341, 187, 186]. Knockdown of Spindly induces chromosome alignment defects and extensive prometaphase delay, consistent with its role in chromosome attachment and SAC silencing [396, 114].

The expression of many SAC components has been reported to be altered in cancer, and some of these components have been identified as suitable targets for the clinical treatment of cancer [99, 397]. To the best of our knowledge there is, however, no information available about the impact of Spindly in oral or any other cancer pathogenesis and clinical outcome. Thus, this is the first study where the patterns of Spindly expression were analyzed in OSCC patient samples, as well as its potential correlations between clinicopathologic significance, and its potential use in chemotherapy. We found that Spindly was highly expressed in OSCC patients with a significant correlation with tumor proliferation, and that this high expression inversely correlated with overall survival. More importantly, knockdown of Spindly significantly increased sensitivity of OSCC cells to cisplatin treatment. The prognostic and therapeutic relevance of these results are discussed.

3. Materials and Methods

3.1. Patients and tissue specimens

Tissue samples from primary OSCC (ICD 10: C00-06), were retrospectively collected from 2000 to 2006, at the Hospital de Santo António (HSA) - Centro Hospitalar do Porto, Portugal. The study was approved by institutional ethical board of the hospital (Investigation, Formation and Teaching Department – DEFI; 024/CES/03) and performed in accordance with the Declaration of Helsinki. The clinical characteristics of the OSCC patients are described in detail in Table 4.S1. Clinical follow-up information was obtained from the patients' records.

3.2. Immunohistochemistry processing and evaluation

Immunohistochemistry was performed on tissue microarray (TMA) sections as previously described [398], using the NovoLink Polymer Detection System (Novocastra, Leica Biosystems Newcastle Ltd.). The primary antibodies used were a rabbit anti-human Spindly diluted at 1:500 (HPA044700, Sigma-Aldrich), and a rabbit anti-human Ki-67 diluted at 1:100 (clone MIB1, Dako, Glostrup, Denmark). Positive (oral mucosa) and negative (omission of primary antibody) controls were included.

Immunohistochemical expression of Spindly was evaluated by two authors blinded to clinicopathological characteristics, who recorded the intensity of staining [0 (negative), 1 (weak), 2 (moderate) and 3 (strong)]. Discordant cases were reviewed to achieve a consensus. We used the concordant result score out of at least two of the three cores examined per case, and when this was not possible, the case was excluded. For data analysis, score 0/1 was considered as low expression and scores 2/3 as high expression for Spindly marker [399]. The proliferative status of the tumors was evaluated by the percentage of Ki-67 positive nuclear staining and classified as tumors with low (0–49% of stained cells) or high (50–100% of stained cells) cellular proliferation activity [299].

3.3. Cell culture

Oral squamous cell carcinoma cell lines SCC-09 and SCC-25 were grown in DMEM-F12 culture medium (Biochrom, São Mamede de Infesta, Portugal) with 10% fetal bovine serum (FBS, Biochrom), and supplemented with 40 ng/ml hydrocortisone

(Sigma-Aldrich, St. Louis, MO, USA). Human oral keratinocytes (HOK) were grown in an oral keratinocyte medium (Innoprot, Derio, Biscaia, Spain) according to the manufacturer's instructions. Cells were maintained at 37°C in a 5% CO_2 humidified atmosphere.

3.4. Real-time PCR

For isolation of total RNA, cDNA synthesis and amplification we performed as previously described [299]. Primers, used at final concentration of 10 µM, were as follows: Spindly: forward 5´-CTC AAA GAG GCT GAA GAA GAG-3´ and reverse 5´-TGT TCA TAA CTC TCA GTC ATG G-3´; Actin: forward 5´- AAT CTG GCA CCA CAC CTT CTA -3´ and reverse 5´- ATA GCA CAG CCT GGA TAG CAA-3´. The housekeeping gene Actin was used as an internal control to normalize the expression levels of Spindly. Three experiments were performed in triplicate.

3.5. siRNA transfection

Cells were seeded in 22 mm poly-l-lysine-coated coverslips in 6-well plates, allowed attaching for 24 hours, and transfected using INTERFERin siRNA Transfection Reagent (PolyPlus, New York, USA) according to the manufacturer's instructions. The culture medium was replaced 24 hours post-transfection with fresh medium. A validated siRNA sequence [186, 321] against Spindly (synthetized by Sigma-Aldrich) and a validated negative control siRNA (AllStars Negative Control siRNA, Qiagen, Germantown MD, USA) were used at a final concentration of 100 nM.

3.6. Cell extracts and western blotting

Western blot analysis was as previously described [321]. Briefly, cells were collected by trypsinization and resuspended on lysis buffer supplemented with protease inhibitors cocktail (Sigma-Aldrich). A total of 20 µg of denatured proteins were separated onto a 7.5% polyacrylamide gel. The primary antibodies were as follows: rabbit anti-Spindly (1:3000, gift from Dr. R. Gassmann, IBMC/I3S, Portugal) and mouse anti-α-tubulin (1:2500, Sigma-Aldrich). (HRP)-conjugated secondary antibodies were diluted at 1:1500 (anti-mouse, Vector) or at 1:1000 (anti-rabbit, Sigma). The quantification of signal intensity was performed using ImageJ 1.4v software and normalized against α-tubulin expression levels.

3.7. Cell viability assay

Cell viability was determined through (3-(4, 5-dimethylthiazolyl-2)-2,5-diphenyltetrazolium bromide) MTT (Sigma-Aldrich) assay. A total of $0.06x10^6$ siRNA-treated cells were seeded in 96-well plate, allowed to attach for 6 hours and treated with 1-200 µM cisplatin. After 24 hours, cells were placed in fresh FBS-free medium and 20 µl of MTT reagent (5mg/ml in PBS) was added and incubated at 37°C and 5% CO_2 for 4 hours. Then, a solubilization solution (89% (v/v) 2-Propanol, 10% (v/v) Triton X-100, 1% (v/v) HCl 3.7%) was added for 2 hours. The optical density was measured at 570 nm in a microplate reader (Biotek Synergy 2, Winooski, VT, USA) and retrieved through the Gen5 software (version 1.07.5, Biotek, Winooski, VT, USA). Cell viability was calculated relative to control siRNA-treated cells.

3.8. Colony formation assay

A total of 1000 siRNAs-transfected cells were seeded in six-well plates, allowed to attach for at least 6 hours, and treated with 1 and 2 µM of cisplatin. Twenty-four hours later, to remove cisplatin, cells were washed twice with PBS and then incubated in fresh medium for 10 days. The recovered colonies were fixed with 3.7% paraformaldehyde in PBS, for 5 min, and stained with 0.05% (w/v) Violet Crystal (Merck Millipore, Billerica, MA, USA) in distilled water, for 20 min. The number of colonies was counted on duplicate dishes from three independent experiments. The plating efficiency (PE) was calculated as the percentage of the number of colonies formed over the number of cells seeded, in control siRNA-treated cells. The survival fraction was determined as the number of colonies over the number of cells seeded × 1/PE, for each condition.

3.9. Statistical analysis

For immunohistochemistry evaluation, the associations between categorical variables were evaluated by Chi-square tests. Cancer-specific survival (CSS) was defined as the time interval (months) between primary treatment and death from oral cancer or last follow-up. Survival curves were plotted using Kaplan–Meier method, and their prognostic effect was tested using the Log-rank test. Variables with significant influence in the univariate analyses were entered into Cox proportional hazards model to investigate their independent effects. Differences were considered statistically

significant at $p < 0.05$. Statistical analysis was performed using IBM SPSS Statistics version 22.0 software (IBM Corporation, NY, USA).

For cell culture assays, statistical analysis was performed using an Unpaired Student t-test or an Ordinary Two-way ANOVA with Tukey's multiple comparisons test, in GraphPad Prism version 6 (GraphPad software Inc., CA, USA). Data are presented as the means ± standard deviation (SD) of at least three independent experiments. The level of significance was set at probabilities of *p < 0.05, **p < 0.01, ***p < 0.001 and ****p < 0.0001.

4. Results

4.1. Spindly is differentially expressed in OSCC tissues

The localization and expression of Spindly in paraffin-embedded OSCC samples were examined by immunohistochemical analysis. Spindly staining was mainly cytoplasmic in epithelial cells (**Figure 4.7**). Spindly expression was detected in all of the 61 (100%) OSCC tissue microarrays (**Table 4.1**). High levels of Spindly expression were detected in 75.4% of the tumor samples; the remainder expressed only weak levels. In contrast, adjacent non-tumor epithelial cells showed no staining or only low and marginal staining (**Figure 4.7**).

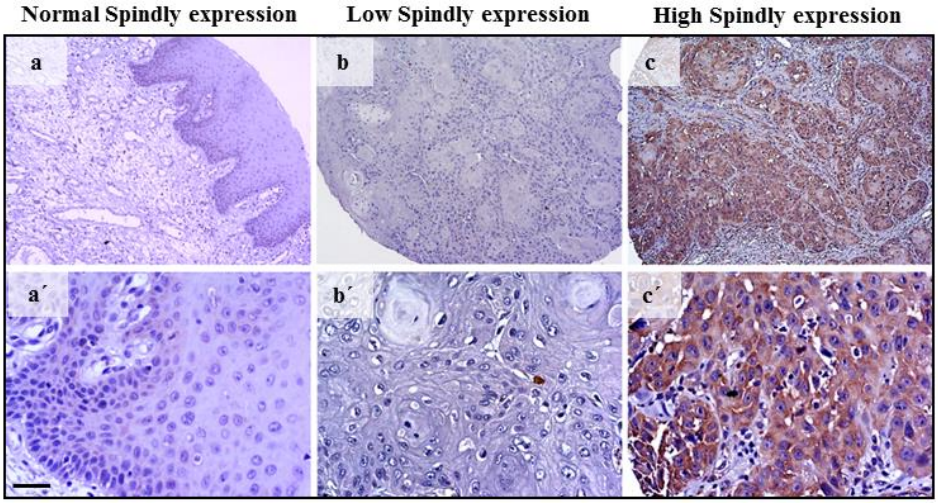

Figure 4.7. Immunohistochemical expression and localization pattern of Spindly ioral squamous cell carcinoma. Normal oral mucosa stained for Spindly at low (a) and high (a') magnification; Squamous cell carcinoma with low expression of Spindly at low (b) and high (b´) magnification; and with high expression of Spindly at low (c) and high (c') magnification.

Note the cytoplasmic spindly staining of epithelial cells, homogenously distributed by the tumor islands. Low magnification (x 100); high magnification (x 400). Scale bar = 20 µm

Table 4.1. Clinicopathological characteristics of the OSCC patients and its association with Spindly expression.

		Spindly expression		P^a
		Low expression	High expression	
Characteristic	**N (%)**	**N (%)**	**N (%)**	
All cases	61 (100)	15 (24.6)	46 (75.4)	
Gender				
Female	16 (26.2)	3 (18.8)	13 (81.2)	NS (0.528)
Male	45 (73.8)	12 (26.7)	33 (73.3)	
Age				
<62 years	26 (42.6)	7 (26.9)	19 (73.1)	NS (0.715)
≥62 years	35 (57.4)	8 (22.9)	27 (77.1)	
Consumption habits				
No habits	16 (30.2)	5 (31.2)	11 (68.8)	
Alcohol	5 (9.4)	1 (20.0)	4 (80.0)	NS (0.531)
Tobacco	12 (22.6)	1 (8.3)	11 (91.7)	
Alcohol + tobacco	20 (37.7)	4 (20.0)	16 (80.0)	
Tumor location				
Lip	7 (11.5)	3 (42.9)	4 (57.1)	
Floor of the mouth	5 (8.2)	2 (40.0)	3 (60.0)	
Tongue	26 (42.6)	5 (19.2)	21 (80.8)	
Buccal mucosa	4 (6.6)	1 (25.0)	3 (75.0)	NS (0.600)
Retromolar trigone	6 (9.8)	0 (0.0)	6 (100.0)	
Hard palate	7 (11.5)	2 (28.6)	5 (71.4)	
Gingiva	6 (9.8)	2 (33.3)	4 (66.7)	
Tumor size				
T1	17 (27.9)	6 (35.3)	11 (64.7)	
T2	27 (44.3)	7 (25.9)	20 (74.1)	NS (0.414)
T3	3 (4.9)	0 (0.0)	3 (100.0)	
T4	14 (23.0)	2 (14.3)	12 (85.7)	
N *status*				
N0	37 (60.7)	12 (32.4)	25 (67.6)	
N1	11 (18.0)	2 (18.2)	9 (81.8)	NS (0.315)
N2	11 (18.0)	1 (9.1)	10 (90.9)	
N3	2 (3.3)	0 (0.0)	2 (100.0)	

Abbreviations: SG= surgery; RT=radiotherapy; CT=chemotherapy; NS=No statistical significance. [a]Chi-square test.

Table 4.1. *(continued)*

		Spindly expression		P^a
		Low expression	High expression	
Characteristic	**N (%)**	**N (%)**	**N (%)**	
Stage				
I	12 (19.7)	5 (41.7)	7 (58.3)	
II	21 (34.4)	7 (33.3)	14 (66.7)	NS (0.109)
III	12 (19.7)	2 (16.7)	10 (83.3)	
IV	16 (26.2)	1 (6.2)	15 (93.8)	
Treatment modality				
SG	33 (54.1)	12 (36.4)	21 (63.6)	
SG + RT	18 (29.5)	3 (16.7)	15 (83.3)	**0.042**
CT + other	10 (16.4)	0 (0.0)	10 (100.0)	
Tumor grade				
G1	37 (60.7)	13 (35.1)	24 (64.9)	
G2	22 (36.1)	2 (9.1)	20 (90.9)	NS (0.057)
G3	2 (3.3)	0 (0.0)	2 (100.0)	
Margin *status*				
Free of tumor	32 (59.3)	9 (28.1)	23 (71.9)	
Tumor proximity	13 (24.1)	4 (30.8)	9 (69.2)	NS (0.906)
With tumor	9 (16.7)	2 (22.2)	7 (77.8)	
Vascular invasion				
Absent	57 (93.4)	15 (26.3)	42 (73.7)	NS (0.237)
Present	4 (6.6)	0 (0.0)	4 (100.0)	
Perineural permeation				
Absent	52 (85.2)	14 (26.9)	38 (82.6)	NS (0.309)
Present	9 (14.8)	1 (11.1)	8 (88.9)	
Lymphatic invasion				
Absent	48 (78.7)	12 (25.0)	36 (75.0)	NS (0.886)
Present	13 (21.3)	3 (23.1)	10 (76.9)	

Abbreviations: SG= surgery; RT=radiotherapy; CT=chemotherapy; NS=No statistical significance. [a]Chi-square test.

4.2. High levels of Spindly expression correlate with tumor proliferation and poor prognostics

Statistical analysis was performed to identify association between Spindly expression levels and clinicopathological parameters of OSCC. Apart from treatment modality, no significant correlation was found between Spindly levels and the assessed clinicopathologic factors (**Table 4.1**). Moreover, we evaluated whether Spindly expression was associated with patient prognosis. The follow-up mean time for the 61 patients was 43.8 ± 33.1 months with a range from 1 to 142 months. Kaplan-Meier curves with univariate analyses showed that the patients with the highest Spindly

expression levels had a much reduced survival time than those with the lowest expression levels (P < 0.048) (**Table 4.2 and Figure 4.8**).

Table 4.2. Univariate analysis of cancer-specific survival (CSS) according to the clinicopathological characteristics and Spindly expression in OSCC.

Characteristic	N	Dead	CSS[a]	*p*[b]
Gender				
Female	16	8	50.0	NS
Male	45	13	71.1	(0.134)
Age				
<62 years	26	12	53.8	NS
≥62 years	36	9	74.3	(0.156)
Consumption habits				
No habits	16	6	62.5	
Alcohol	5	1	80.0	NS
Tobacco	12	4	66.7	(0.827)
Alcohol + tobacco	20	9	55.0	
Location				
Lip	7	1	85.7	
Floor of the mouth	5	2	60.0	
Tongue	26	8	69.2	NS
Buccal mucosa	4	1	75.0	(0.870)
Retromolar trigone	6	3	50.0	
Hard palate	7	3	57.1	
Gingiva	6	3	50.0	
Tumor size				
T1	17	1	94.1	
T2	27	9	66.7	**<0.001**
T3	3	1	66.7	
T4	14	10	28.6	
N *status*				
N0	37	6	83.8	
N1	11	5	54.5	**<0.001**
N2	11	9	18.2	
N3	2	1	50.0	
Stage				
I	12	0	100.0	
II	21	5	76.2	**0.001**
III	12	5	58.3	
IV	16	11	31.2	

Abbreviations: SG= surgery; RT=radiotherapy; CT=chemotherapy; NS=No statistical significance. [a]Percentage of cases without event at 3 years of follow-up. [b]Log-rank test.

Table 4.2. *(continued)*

Characteristic	N	Dead	CSS[a]	*p*[b]
Treatment modality				
SG	33	4	87.9	
SG + RT	18	10	44.4	**<0.001**
CT + other	10	7	30.0	
Tumor grade				
G1	37	9	75.7	NS (0.206)
G2	22	11	50.0	
G3	2	1	50.0	
Margin status[c]				
Free of tumor	32	8	75.0	NS (0.329)
Tumor proximity	13	5	61.5	
With tumor	9	5	44.4	
Vascular invasion				
Absent	57	20	64.9	NS (0.872)
Present	4	1	75.0	
Perineural permeation				
Absent	52	17	67.3	NS (0.372)
Present	9	4	55.6	
Lymphatic invasion				
Absent	48	17	64.6	NS (0.876)
Present	13	4	69.2	
Ki-67 expression				
Low	30	9	70.0	NS (0.186)
High	20	10	50.0	
Spindly expression				
Low expression	15	2	86.7	**0.048**
High expression	46	19	58.7	

Abbreviations: SG= surgery; RT=radiotherapy; CT=chemotherapy; NS=No statistical significance. [a]Percentage of cases without event at 3 years of follow-up. [b]Log-rank test.

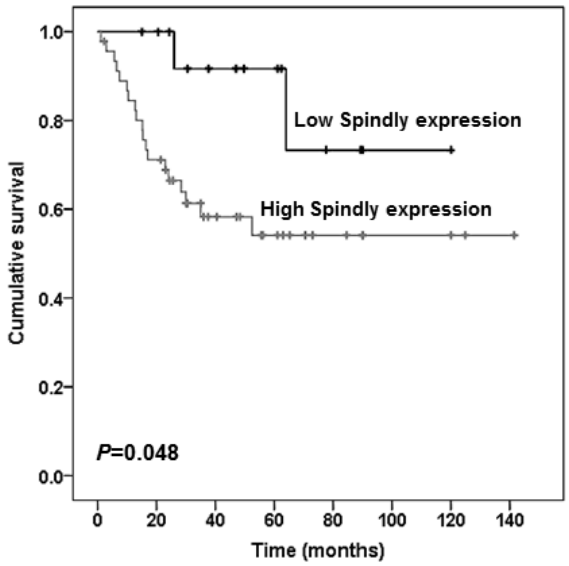

Figure 4.8. Figure Kaplan–Meier curves for overall patient´s survival according to Spindly expression.

The cumulative 5-year survival rate was only 54.1% for the high Spindly group, while it was 91.7% for the low Spindly group. Tumor size, N status, tumor stage, and treatment modality were also statistically significant prognostic factors in univariate analysis ($p < 0.001$). Inclusion of these characteristics, together with Spindly expression values, into multivariable Cox proportional hazards regression model, showed that Spindly expression level was an independent prognostic factors for OSCC ($P < 0.041$) (**Table 4.3**).

Table 4.3. Multivariate analysis of cancer-specific survival (CSS).

Variable	HR (95% CI)	*P*
Stage		
I+II	1	
III	0.317 (0.016-6.110)	0.447
IV	0.191 (0.012-3.088)	0.244
Tumor size		
T1	1	
T2	13.455 (1.368-132.378)	0.026
T3	12.262 (0.379-396.844)	0.158
T4	32.261 (3.123-333.211)	0.004
N *status*		
N0	1	
N1	5.008 (0.343-73.133)	0.239
N2	23.925 (2.362-242.286)	0.007
N3	3.138 (0.156-63.277)	0.456
Treatment modality		
SG	1	
SG + RT	3.873 (0.972-15.434)	0.199
CT + other	2.766 (0.585-13.087)	0.055
Spindly expression		
Low expression	1	
High expression	6.427 (1.080-38.264)	**0.041**

Abbreviations: HR=hazard ratio; CI= confidence interval; NS=No statistical significance; SG= surgery; RT=radiotherapy; CT=chemotherapy.

Interestingly, when we investigated the relationship between Spindly expression and OSCC proliferation using Ki-67 expression, we detected high Spindly level in 100% of high proliferative (n=20) and in 63.3% (n=19) of low proliferative tumors (n=30). This highlights a strong association between Spindly expression and increased cellular proliferation ($p = 0.002$). Our data indicates that Spindly expression is associated with increased tumor cell proliferation, as well as with a greatly increased risk pointing to Spindly as a marker of poor prognosis.

4.3. Spindly is highly expressed in OSCC cell lines

In order to study if Spindly could be a potential target for cancer therapy in vitro, we first conducted a quantitative real-time PCR to investigate the expression of Spindly on OSCC cell lines at the mRNA level. The SCC-09 and SCC-25 oral cancer lines exhibited a higher expression of Spindly mRNA than their normal cell counterpart HOK (human oral keratinocytes) (**Figure 4.9**). Therefore, Spindly expression is upregulated in OSCC lines.

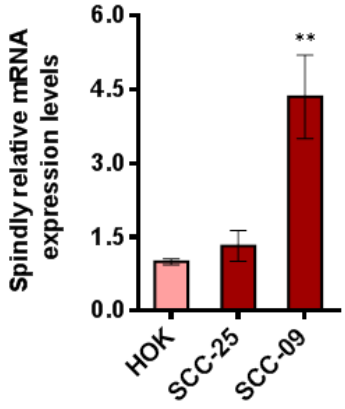

Figure 4.9. Spindly gene expression in oral cancer cell lines. Spindly mRNA levels were analyzed by quantitative real-time PCR in oral cancer cell lines SCC-09 e SCC-25 comparatively to normal human oral keratinocytes (HOK).

4.4. Spindly depletion enhances sensitivity of OSCC cells to cisplatin

Cisplatin is amongst the most potent chemotherapeutic agents currently in use, exerting its cytotoxic action through the formation of intra-strand DNA crosslink adducts [400]. However, intrinsic or acquired resistance is a major limitation of cisplatin-based chemotherapy. The aforementioned overexpression of Spindly in OSCC tissues and cell lines prompted us to analyze whether Spindly knockdown enhances cytotoxicity of OSCC cells to cisplatin treatment. We first certified that efficient Spindly knockdown (> 90%) was achieved in the OSCC lines by use of previously validated siRNA oligonucleotides (**Figure 4.10A**) [186]. OSCC cells were transfected with Spindly siRNAs, 24 h post-transfection cells were treated with various concentrations of cisplatin for further 24 h, and then processed for MTT assay. As shown by the dose-response histograms in **Figure 4.10B and C**, in control siRNA-treated cells, viability was only marginally compromised at doses <10 μM cisplatin, while exposure doses as high as > 50 μM cisplatin were required in order to significantly affect cell viability. However, viability was drastically reduced by doses <10 μM cisplatin when Spindly was also downregulated. The results indicate that sensitivity to cisplatin treatment is significantly increased when combined with Spindly depletion. To further confirm our observations, a long-term (10 days) clonogenic assay was performed to evaluate cancer cell killing efficiency of the combination therapy. Low concentrations of cisplatin (1 to 2 μM) greatly compromised colony formation in Spindly-depleted cells, when compared to individual treatments (**Figure 4.10D and E**),

consistent with data in MTT assay. The data indicates that Spindly knockdown sensitizes OSCC cells to cytotoxic effect induced by clinically relevant doses of cisplatin.

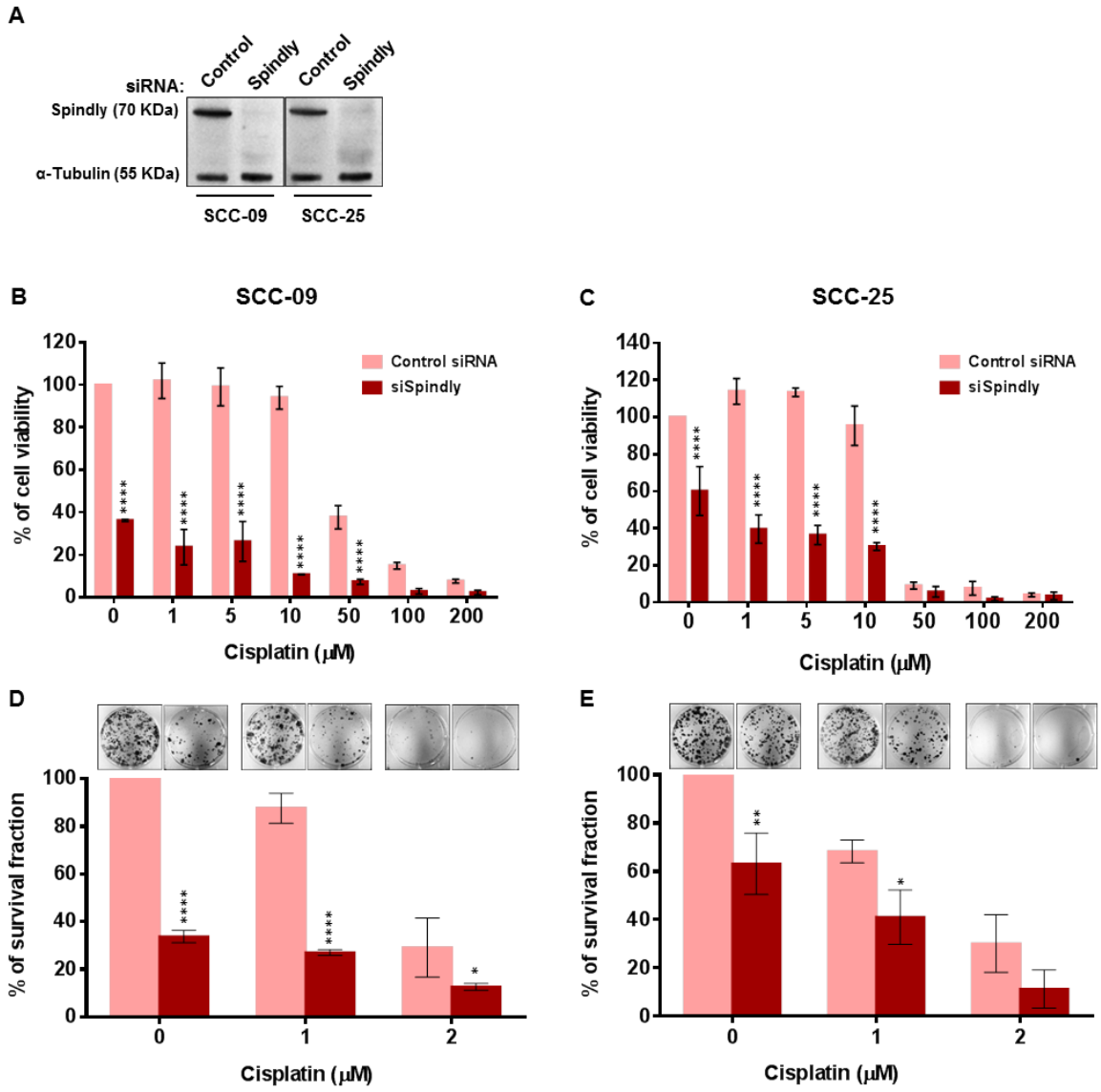

Figure 4.10. Spindly depletion potentiates cisplatin-mediated cytotoxicity. (A) Representative immunoblots from SCC-09 and SCC-25 cell extracts showing efficient Spindly downregulation upon cell transfection with siRNAs. α-tubulin was used as a loading control. Cells were transfected with control (control siRNA) or Spindly (siSpindly) siRNAs for 48 hours. **(B and C)** Twenty-four hours post-transfection with control (control siRNA) or Spindly siRNA (siSpindly), cisplatin was added at the indicated concentrations and cells were incubated for 24 hours. SCC-09 (B) and SCC-25 (C) cell viability was determined by MTT assay. **(D and E)** Cells were treated as in B and C, washed in PBS and remained for 10 days in culture. After crystal violet staining, the number of colonies was counted. Results are the mean ± SD from three independent experiments, expressed as % of survival fraction. Representative images of surviving colonies (Top) are shown for each condition. *p < 0.05, **p < 0.001 and ****p < 0.0001 individual or combination treatments vs control siRNA.

5. Discussion

In this study, we provided the first report of Spindly upregulation in cancer, namely in OSCC cell lines and OSCC tissue specimens. Overexpression of Spindly was significantly associated with tumor cell proliferation and, interestingly, was inversely correlated with the survival time of OSCC patients, highlighting the potential of Spindly as an independent marker of poor prognostic in OSCC. Moreover, we found that Spindly depletion significantly enhanced the chemosensitivity of OSCC cells to clinically relevant doses of cisplatin, pointing to Spindly as a potential target in a drug combination strategy to circumvent resistance to cisplatin treatment.

Chromosomal instability (CIN) plays a key causative role in many malignancies and is often found in OSCC, with complex structural and numerical variations [401, 402]. Abnormal karyotype in OSCC cells arises from defects in chromosome segregation, frequently in the form of lagging chromosomes [403]. Spindly is a transient kinetochore protein required for efficient chromosome attachment to microtubules and plays a key role in SAC silencing [114, 396]. Indeed, depletion of Spindly by RNAi induces chromosome misalignment and caused cells to arrest in prometaphase [187]. It may be possible that overexpression of Spindly affects proper chromosome attachments and occasionally leads to lagging chromosomes thereby contributing to CIN. Changes in karyotype through CIN appear to confer proliferative advantages as a result of massive gene dosage imbalances [404]. Strikingly, in the present study, Spindly overexpression was strongly associated with increased cellular proliferation, suggesting a function of Spindly upregulation in the pathogenesis of OSCC. Thus, the link between the biological function of Spindly, CIN, and the pathogenesis of OSCC disease deserves to be investigated.

Cisplatin is currently used as a potent chemotherapeutic agent in a wide variety of malignant solid tumors including OSCC [405]. However when used as a single agent is limited by intrinsic or acquired resistance. While the molecular mechanisms of such resistance remain poorly understood, cisplatin-based combination therapy has been the focus of intense research. As a consequence, combinatorial therapy has been applied as novel therapeutic strategy and has proven to be more effective while minimizing cisplatin resistance [406]. Our *in vitro* data suggests therapeutic implications for Spindly. We found that cytotoxicity of low doses of cisplatin was strongly increased in OSCC cells

depleted of Spindly. This suggests Spindly as suitable target in a combination strategy to sensitize OSCC to low doses of cisplatin, thus providing therapeutic benefits by overcoming problems of resistance and side effects. Further study is needed to clarify the detailed mechanism regulating cell growth by a combination of Spindly inhibition and cisplatin.

In conclusion, in this study, Spindly was found to be overexpressed in OSCC. This upregulation was correlated with tumor proliferation and shown to be an independent poor prognosis factor. Depletion of Spindly sensitized OSCC to clinically relevant doses of cisplatin. We thus propose Spindly inhibition as promising strategy in rational combination with cisplatin for OSCC therapy.

6. Acknowledgments

This work was funded by CESPU – Cooperativa de Ensino Superior Politécnico e Universitário under the projects “SpindlyTarget-CESPU-2016”, “AdoralLeuk-CESPU-2016”, and “MitOralC-CESPU-2016”. Patrícia M.A. Silva is a PhD fellowship holder from FCT (SFRH/BD/90744/2012).

7. Supplementary table

Table 4.S1. Clinicopathological characteristics of the OSCC patients.

Characteristic	N (%)
All cases	61 (100)
Gender	
Female	16 (26.2)
Male	45 (73.8)
Age	
<62 years	26 (42.6)
≥62 years	35 (57.4)
Consumption habits[a]	
No habits	16 (26.2)
Alcohol	5 (8.2)
Tobacco	12 (19.7)
Alcohol + tobacco	20 (32.8)
Tumor location	
Lip mucosae	7 (11.5)
Floor of the mouth	5 (8.2)
Tongue	26 (42.6)
Buccal mucosa	4 (6.6)
Retromolar trigone	6 (9.8)
Hard palate	7 (11.5)
Gingiva	6 (9.8)
Tumor size	
T1	17 (27.9)
T2	27 (44.3)
T3	3 (4.9)
T4	14 (23.0)
N *status*	
N0	37 (60.7)
N1	11 (18.0)
N2	11 (18.0)
N3	2 (3.3)
Stage	
I	12 (19.7)
II	21 (34.4)
III	12 (19.7)
IV	16 (26.2)
Treatment modality	
SG	33 (54.1)
SG + RT	18 (29.5)
CT + other	10 (16.4)

Abbreviations: SG= surgery; RT=radiotherapy; CT=chemotherapy. [a] Not available in the 8 cases. [b] Not available in the 7 cases.

Table 4.S1. *(continued).*

Characteristic	N (%)
Tumor grade	
G1	37 (60.7)
G2	22 (36.1)
G3	2 (3.3)
Margin *status*[b]	
Free of tumor	32 (52.5)
Tumor proximity	13 (21.3)
With tumor	9 (14.8)
Vascular invasion	
Absent	57 (93.4)
Present	4 (6.6)
Perineural permeation	
Absent	52 (85.2)
Present	9 (14.8)
Lymphatic invasion	
Absent	48 (78.7)
Present	13 (21.3)

Abbreviations: SG= surgery; RT=radiotherapy; CT=chemotherapy. [a] Not available in the 8 cases.
[b] Not available in the 7 cases.

CHAPTER 5

GENERAL CONCLUSIONS AND FUTURE PERSPECTIVES

In present work we have achieved the main goals we had set up in the beginning, namely (1) to shed light into the function and regulation of the SAC mechanism and (2) to explore its potential as therapeutic target for cancer therapy.

Concerning SAC function and regulation we proposed:

(i) To establish a relationship between the SAC protein Bub3 and the microtubule motor dynein in regulating kinetochore-microtubule attachment and chromosome congression and

(ii) To elucidate the role of dynein-mediated transport of SAC components off kinetochores to promote SAC silencing.

Interestingly, we found a functional and antagonistic relationship between Bub3 and dynein to ensure stable KT-MT attachments and chromosome congression, establishing a link between SAC signaling and KT-MT binding machinery. Indeed, several studies have contributed to unveil a number of proteins involved in SAC signaling pathway and in mediation of KT-MT interactions and some of them were shown to participate in more than one functional activity. Here, beside dynein, the function of Bub3 in the regulation of KT-MT attachments might involve other interactors that define the molecular context in which this regulation is performed at the KT-MT interface. Hence, a possible further approach is to perform a proteomics-based analysis to identify novel partners of Bub3 to arrive to a better mechanistic understanding of Bub3's role in the regulation of KT-MT attachments during mitosis.

We also showed that the core SAC proteins Mad1, Mad2, Bub1, BubR1, and Bub3 and a pool of KMN components Hec1 and Mis12 are poleward transported in a dynein-dependent manner, after successful chromosome attachment, contributing to extinguish the inhibitory SAC signal and to allow cell cycle progression. These results contributed to clarify which proteins are truly dynein cargoes and to unveil new proteins subjected to the poleward transport, namely KMN components, providing first insights into the contribution of the KMN network to SAC silencing. Moreover, we found that dynein-inhibited cells did not retain SAC proteins on kinetochores of aligned chromosomes. Instead, these proteins accumulated only on misaligned kinetochores, supporting the existence of a dynein-independent mechanism of protein stripping from attached kinetochores during SAC silencing. Indeed, in human cells, unlike direct dynein inhibition, depletion of Spindly (that abolishes kinetochore dynein localization) does not

block the removal of Mad2 SAC protein from attached kinetochores [114], suggesting additional mechanisms for SAC silencing. To the other hand, in Drosophila Spindly-depleted cells, high levels of Mad2 and RZZ were found on bi-oriented and stretched metaphase kinetochores [112]. Further studies, conducted by Gassmann *et al.*, using Spindly motif mutants, that target normally to kinetochores but prevent dynein recruitment, indicated that kinetochore dynein is essential for SAC silencing in the presence of Spindly but a second mechanism silence the checkpoint in their absence [186]. In fact, dynein-dependent removal of checkpoint proteins from kinetochores does not appear to be a conserved mechanism for SAC silencing, as no obvious Spindly/RZZ homologs are present in lower eukaryotes such as yeast and the reason for these discrepancies might be due to different kinetochore structures in the different species. In line with this, it would be interesting for future progress to explore the probably alternative SAC silencing mechanism operating when dynein is absent. Overall, these results contribute to expand the scientific knowledge about SAC mechanism, based on a fundamental research which constitutes a fuel for applied research.

Focusing on SAC targeting in a therapeutic perspective, we proposed:

(i) To highlight the potential of Spindly, a kinetochore regulator of dynein, as a target for cancer therapy;

(ii) To explore the therapeutic benefit of combining Spindly inhibition with currently used chemotherapeutic drugs.

First, we found Spindly overexpression both in human tumor cell lines and in patient samples from oral cancer. Importantly, Spindly overexpression was significantly correlated with tumor proliferation and worse prognosis, making Spindly expression pattern an independent prognostic indicator for cancer-specific survival and a marker of cell proliferation. Since Spindly is involved both in chromosome attachment and in SAC silencing we hypothesize that potentiate chromosome attachment errors and block mitotic exit, through Spindly inhibition, could result in improvement of cytotoxicity mediated by current chemotherapeutic drugs, namely paclitaxel and cisplatin. We found that Spindly inhibition plus low doses of paclitaxel or cisplatin co-treatment potentiates cell death, pointing Spindly inhibition as valid and valuable strategy in rational combination cancer therapy. Given the disappointed results in clinical trials from the new generation of antimitotics and in light of our results, we believed that the drug

concentration is a crucial factor in the response to antimitotics. For instance, although taxanes have been widely used in the clinic for over a decade, a divergence between *in vitro* and *in vivo* data exists on this drug's therapeutic action [407]. It is probably related with the selected drug concentration used in cell culture experiments, forgetting the availability of drug in *vivo*. It is possible that the clinical efficacy of paclitaxel is not in fact due to mitotic arrest, but an enhancement of aneuploidy related with drug concentration used. In response to paclitaxel treatment, abnormal DNA contents and cell death were found at low drug concentrations, where a robust mitotic arrest was not apparent [408], suggesting that antimitotic agents that elicit their effect via prolonged mitotic arrest are only cytotoxic at a high concentration. Moreover, the percentage of mitotic cells in tumors is significantly lower than the percentage found in cell cultures but the number of aneuploid cells is higher. So, potentiates chromosome missegregation and aneuploidy could be a more efficient strategy to induce tumor cells killing rather than an exclusive mitotic arrest. Our results showed effectively that Spindly inhibition enhance the chromosome missegregation, in cells treated with paclitaxel, leading to cell death. Different from paclitaxel, a microtubule-targeting agent, cisplatin interfere with DNA replication which kills the fastest proliferating cells. Although the final result from Spindly and paclitaxel or cisplatin co-treatment was transversal, since induces cell death, further studies are needed to clarify the detailed mechanism regulating cell growth by a combination of Spindly inhibition and cisplatin.

The promising our *in vitro* results lead us to believe that the *in vivo* experiments on mouse xenografts models would strengthen our findings towards a future therapeutic use. Accordingly, it would be relevant to assess the ability of siRNA-mediated Spindly inhibition to inhibit tumor progression, in a murine subcutaneous tumor model, and to evaluate the effect of Spindly inhibition as an adjuvant of paclitaxel and cisplatin. This combination would minimize undesired toxicity to normal cells, as low doses of drugs would be used. Importantly, since siRNAs offers some restrictions due to its specific delivery to target cells/tissues and high toxicity, the use of functionalized carriers such as nanoparticles or therapeutic polymers would represents an attractive alternative for efficient intracellular release of siRNAs to specific tumor locations. Overall, our findings validate Spindly as a suitable therapeutic target and justify its combination with conventional anticancer drugs in order to enhance their efficacy and potentially overcome resistance, which would represent a promising concept for cancer therapy. Moreover, the results reinforce the concept of exploiting the genomic instability of

tumor cells through therapeutic inhibition of mitotic checkpoints could be a viable strategy. We believe that this strategy has a high likelihood of success given its potential to enhance therapeutic index by targeting tumor-specific vulnerabilities.

In conclusion, the work presented in this thesis contributed to increase the current knowledge concerning the function and regulation of spindle assembly checkpoint and to highlight the potential of Spindly as a therapeutic target for cancer therapy, as an enhancer of paclitaxel and cisplatin-mediated cytotoxicity, making the aims initially proposed fulfilled and, at the same time, opening new lines of research.

CHAPTER 6

REFERENCES

REFERENCES

[1] Pines J. The cell cycle kinases. Semin Cancer Biol. 1994;5(4):305-13.
[2] Harashima H, Dissmeyer N, Schnittger A. Cell cycle control across the eukaryotic kingdom. Trends Cell Biol. 2013;23(7):345-56.
[3] Lim S, Kaldis P. Cdks, cyclins and CKIs: roles beyond cell cycle regulation. Development. 2013;140(15):3079-93.
[4] Sanchez Y, Wong C, Thoma RS *et al.* Conservation of the Chk1 checkpoint pathway in mammals: linkage of DNA damage to Cdk regulation through Cdc25. Science. 1997;277(5331):1497-501.
[5] Murray AW. Recycling the cell cycle: cyclins revisited. Cell. 2004;116(2):221-34.
[6] Morgan DO. The Cell Cycle: Principles of control. Primers in Biology; 2007.
[7] Nigg EA. Cell cycle regulation by protein kinases and phosphatases. Ernst Schering Res Found Workshop. 2001(34):19-46.
[8] Malumbres M, Barbacid M. Cell cycle, CDKs and cancer: a changing paradigm. Nat Rev Cancer. 2009;9(3):153-66.
[9] Hartwell L. Defects in a cell cycle checkpoint may be responsible for the genomic instability of cancer cells. Cell. 1992;71(4):543-6.
[10] Weinert T. DNA damage and checkpoint pathways: molecular anatomy and interactions with repair. Cell. 1998;94(5):555-8.
[11] Visconti R, Della Monica R, Grieco D. Cell cycle checkpoint in cancer: a therapeutically targetable double-edged sword. J Exp Clin Cancer Res. 2016;35(1):153.
[12] Elledge SJ. Cell cycle checkpoints: preventing an identity crisis. Science. 1996;274(5293):1664-72.
[13] Zhou BB, Elledge SJ. The DNA damage response: putting checkpoints in perspective. Nature. 2000;408(6811):433-9.
[14] North S, Hainaut P. p53 and cell-cycle control: a finger in every pie. Pathol Biol (Paris). 2000;48(3):255-70.
[15] Matsuoka S, Huang M, Elledge SJ. Linkage of ATM to cell cycle regulation by the Chk2 protein kinase. Science. 1998;282(5395):1893-7.
[16] Falck J, Mailand N, Syljuasen RG *et al.* The ATM-Chk2-Cdc25A checkpoint pathway guards against radioresistant DNA synthesis. Nature. 2001;410(6830):842-7.
[17] Shieh SY, Ikeda M, Taya Y *et al.* DNA damage-induced phosphorylation of p53 alleviates inhibition by MDM2. Cell. 1997;91(3):325-34.
[18] Banin S, Moyal L, Shieh S *et al.* Enhanced phosphorylation of p53 by ATM in response to DNA damage. Science. 1998;281(5383):1674-7.
[19] Harper JW, Adami GR, Wei N *et al.* The p21 Cdk-interacting protein Cip1 is a potent inhibitor of G1 cyclin-dependent kinases. Cell. 1993;75(4):805-16.
[20] Mailand N, Falck J, Lukas C *et al.* Rapid destruction of human Cdc25A in response to DNA damage. Science. 2000;288(5470):1425-9.
[21] Xiao Z, Chen Z, Gunasekera AH *et al.* Chk1 mediates S and G2 arrests through Cdc25A degradation in response to DNA-damaging agents. J Biol Chem. 2003;278(24):21767-73.
[22] Nigg EA. Mitotic kinases as regulators of cell division and its checkpoints. Nat Rev Mol Cell Biol. 2001;2(1):21-32.
[23] Musacchio A, Salmon ED. The spindle-assembly checkpoint in space and time. Nat Rev Mol Cell Biol. 2007;8(5):379-93.
[24] Doxsey S. Re-evaluating centrosome function. Nat Rev Mol Cell Biol. 2001;2(9):688-98.

[25] Zheng Y, Wong ML, Alberts B *et al.* Nucleation of microtubule assembly by a gamma-tubulin-containing ring complex. Nature. 1995;378(6557):578-83.
[26] Schatten H. The mammalian centrosome and its functional significance. Histochem Cell Biol. 2008;129(6):667-86.
[27] Wang G, Jiang Q, Zhang C. The role of mitotic kinases in coupling the centrosome cycle with the assembly of the mitotic spindle. J Cell Sci. 2014;127(Pt 19):4111-22.
[28] De Martino A, Amato A, Bowler C. Mitosis in diatoms: rediscovering an old model for cell division. Bioessays. 2009;31(8):874-84.
[29] Bornens M. Centrosome composition and microtubule anchoring mechanisms. Curr Opin Cell Biol. 2002;14(1):25-34.
[30] Pickett-Heaps JD. Preprophase microtubule bands in some abnormal mitotic cells of wheat. J Cell Sci. 1969;4(2):397-420.
[31] Karsenti E, Newport J, Kirschner M. Respective roles of centrosomes and chromatin in the conversion of microtubule arrays from interphase to metaphase. J Cell Biol. 1984;99(1 Pt 2):47s-54s.
[32] Maiato H, Rieder CL, Khodjakov A. Kinetochore-driven formation of kinetochore fibers contributes to spindle assembly during animal mitosis. J Cell Biol. 2004;167(5):831-40.
[33] Doxsey S, Zimmerman W, Mikule K. Centrosome control of the cell cycle. Trends Cell Biol. 2005;15(6):303-11.
[34] Kramer A, Lukas J, Bartek J. Checking out the centrosome. Cell Cycle. 2004;3(11):1390-3.
[35] Sun QY, Schatten H. Role of NuMA in vertebrate cells: review of an intriguing multifunctional protein. Front Biosci. 2006;11:1137-46.
[36] Merdes A, Cleveland DW. The role of NuMA in the interphase nucleus. J Cell Sci. 1998;111 (Pt 1):71-9.
[37] Merdes A, Heald R, Samejima K *et al.* Formation of spindle poles by dynein/dynactin-dependent transport of NuMA. J Cell Biol. 2000;149(4):851-62.
[38] Andersen JS, Wilkinson CJ, Mayor T *et al.* Proteomic characterization of the human centrosome by protein correlation profiling. Nature. 2003;426(6966):570-4.
[39] Bernhard OK, Lai J, Wilkinson J *et al.* Proteomic analysis of DC-SIGN on dendritic cells detects tetramers required for ligand binding but no association with CD4. J Biol Chem. 2004;279(50):51828-35.
[40] Ou Y, Rattner JB. The centrosome in higher organisms: structure, composition, and duplication. Int Rev Cytol. 2004;238:119-82.
[41] Bettencourt-Dias M, Glover DM. Centrosome biogenesis and function: centrosomics brings new understanding. Nat Rev Mol Cell Biol. 2007;8(6):451-63.
[42] Zitouni S, Nabais C, Jana SC *et al.* Polo-like kinases: structural variations lead to multiple functions. Nat Rev Mol Cell Biol. 2014;15(7):433-52.
[43] Nogales E, Whittaker M, Milligan RA *et al.* High-resolution model of the microtubule. Cell. 1999;96(1):79-88.
[44] Allen C, Borisy GG. Structural polarity and directional growth of microtubules of Chlamydomonas flagella. J Mol Biol. 1974;90(2):381-402.
[45] Wittmann T, Hyman A, Desai A. The spindle: a dynamic assembly of microtubules and motors. Nat Cell Biol. 2001;3(1):E28-34.
[46] Kline-Smith SL, Walczak CE. Mitotic spindle assembly and chromosome segregation: refocusing on microtubule dynamics. Mol Cell. 2004;15(3):317-27.
[47] Mitchison TJ. Localization of an exchangeable GTP binding site at the plus end of microtubules. Science. 1993;261(5124):1044-7.

[48] Walker RA, O'Brien ET, Pryer NK *et al.* Dynamic instability of individual microtubules analyzed by video light microscopy: rate constants and transition frequencies. J Cell Biol. 1988;107(4):1437-48.
[49] Akhmanova A, Steinmetz MO. Control of microtubule organization and dynamics: two ends in the limelight. Nat Rev Mol Cell Biol. 2015;16(12):711-26.
[50] Margolis RL, Wilson L. Opposite end assembly and disassembly of microtubules at steady state in vitro. Cell. 1978;13(1):1-8.
[51] Tran PT, Walker RA, Salmon ED. A metastable intermediate state of microtubule dynamic instability that differs significantly between plus and minus ends. J Cell Biol. 1997;138(1):105-17.
[52] Scholey JM, Neighbors B, McIntosh JR *et al.* Isolation of microtubules and a dynein-like MgATPase from unfertilized sea urchin eggs. J Biol Chem. 1984;259(10):6516-25.
[53] Mastronarde DN, McDonald KL, Ding R *et al.* Interpolar spindle microtubules in PTK cells. J Cell Biol. 1993;123(6 Pt 1):1475-89.
[54] Sharp DJ, Rogers GC, Scholey JM. Microtubule motors in mitosis. Nature. 2000;407(6800):41-7.
[55] Rieder CL, Salmon ED. The vertebrate cell kinetochore and its roles during mitosis. Trends Cell Biol. 1998;8(8):310-8.
[56] Rieder CL. The structure of the cold-stable kinetochore fiber in metaphase PtK1 cells. Chromosoma. 1981;84(1):145-58.
[57] Akhmanova A, Steinmetz MO. Tracking the ends: a dynamic protein network controls the fate of microtubule tips. Nat Rev Mol Cell Biol. 2008;9(4):309-22.
[58] Komarova Y, De Groot CO, Grigoriev I *et al.* Mammalian end binding proteins control persistent microtubule growth. J Cell Biol. 2009;184(5):691-706.
[59] Zanic M, Widlund PO, Hyman AA *et al.* Synergy between XMAP215 and EB1 increases microtubule growth rates to physiological levels. Nat Cell Biol. 2013;15(6):688-93.
[60] Brouhard GJ, Stear JH, Noetzel TL *et al.* XMAP215 is a processive microtubule polymerase. Cell. 2008;132(1):79-88.
[61] Galjart N. CLIPs and CLASPs and cellular dynamics. Nat Rev Mol Cell Biol. 2005;6(6):487-98.
[62] Komarova YA, Akhmanova AS, Kojima S *et al.* Cytoplasmic linker proteins promote microtubule rescue in vivo. J Cell Biol. 2002;159(4):589-99.
[63] Heald R, Nogales E. Microtubule dynamics. J Cell Sci. 2002;115(Pt 1):3-4.
[64] Barton NR, Goldstein LS. Going mobile: microtubule motors and chromosome segregation. Proc Natl Acad Sci U S A. 1996;93(5):1735-42.
[65] Maiato H, Sampaio P, Sunkel CE. Microtubule-associated proteins and their essential roles during mitosis. Int Rev Cytol. 2004;241:53-153.
[66] Hirokawa N, Noda Y, Okada Y. Kinesin and dynein superfamily proteins in organelle transport and cell division. Curr Opin Cell Biol. 1998;10(1):60-73.
[67] Hirokawa N. The molecular mechanism of organelle transport along microtubules: the identification and characterization of KIFs (kinesin superfamily proteins). Cell Struct Funct. 1996;21(5):357-67.
[68] Hunter AW, Caplow M, Coy DL *et al.* The kinesin-related protein MCAK is a microtubule depolymerase that forms an ATP-hydrolyzing complex at microtubule ends. Mol Cell. 2003;11(2):445-57.
[69] Kashina AS, Baskin RJ, Cole DG *et al.* A bipolar kinesin. Nature. 1996;379(6562):270-2.

[70] Sawin KE, LeGuellec K, Philippe M *et al.* Mitotic spindle organization by a plus-end-directed microtubule motor. Nature. 1992;359(6395):540-3.
[71] Blangy A, Lane HA, d'Herin P *et al.* Phosphorylation by p34cdc2 regulates spindle association of human Eg5, a kinesin-related motor essential for bipolar spindle formation in vivo. Cell. 1995;83(7):1159-69.
[72] Hook P, Vallee RB. The dynein family at a glance. J Cell Sci. 2006;119(Pt 21):4369-71.
[73] Neuwald AF, Aravind L, Spouge JL *et al.* AAA+: A class of chaperone-like ATPases associated with the assembly, operation, and disassembly of protein complexes. Genome Res. 1999;9(1):27-43.
[74] Pfarr CM, Coue M, Grissom PM *et al.* Cytoplasmic dynein is localized to kinetochores during mitosis. Nature. 1990;345(6272):263-5.
[75] Steuer ER, Wordeman L, Schroer TA *et al.* Localization of cytoplasmic dynein to mitotic spindles and kinetochores. Nature. 1990;345(6272):266-8.
[76] Li Y, Yu W, Liang Y *et al.* Kinetochore dynein generates a poleward pulling force to facilitate congression and full chromosome alignment. Cell Res. 2007;17(8):701-12.
[77] Vaughan KT, Mikami A, Paschal BM *et al.* Multiple mouse chromosomal loci for dynein-based motility. Genomics. 1996;36(1):29-38.
[78] Sharp DJ, Rogers GC, Scholey JM. Cytoplasmic dynein is required for poleward chromosome movement during mitosis in Drosophila embryos. Nat Cell Biol. 2000;2(12):922-30.
[79] Yang Z, Tulu US, Wadsworth P *et al.* Kinetochore dynein is required for chromosome motion and congression independent of the spindle checkpoint. Curr Biol. 2007;17(11):973-80.
[80] Barisic M, Aguiar P, Geley S *et al.* Kinetochore motors drive congression of peripheral polar chromosomes by overcoming random arm-ejection forces. Nat Cell Biol. 2014;16(12):1249-56.
[81] Vorozhko VV, Emanuele MJ, Kallio MJ *et al.* Multiple mechanisms of chromosome movement in vertebrate cells mediated through the Ndc80 complex and dynein/dynactin. Chromosoma. 2008;117(2):169-79.
[82] Howell BJ, McEwen BF, Canman JC *et al.* Cytoplasmic dynein/dynactin drives kinetochore protein transport to the spindle poles and has a role in mitotic spindle checkpoint inactivation. J Cell Biol. 2001;155(7):1159-72.
[83] Wojcik E, Basto R, Serr M *et al.* Kinetochore dynein: its dynamics and role in the transport of the Rough deal checkpoint protein. Nat Cell Biol. 2001;3(11):1001-7.
[84] Whyte J, Bader JR, Tauhata SB *et al.* Phosphorylation regulates targeting of cytoplasmic dynein to kinetochores during mitosis. J Cell Biol. 2008;183(5):819-34.
[85] Schroer TA. Dynactin. Annu Rev Cell Dev Biol. 2004;20:759-79.
[86] Bader JR, Vaughan KT. Dynein at the kinetochore: Timing, Interactions and Functions. Semin Cell Dev Biol. 2010;21(3):269-75.
[87] Jaarsma D, Hoogenraad CC. Cytoplasmic dynein and its regulatory proteins in Golgi pathology in nervous system disorders. Front Neurosci. 2015;9:397.
[88] McEwen BF, Dong Y, VandenBeldt KJ. Using electron microscopy to understand functional mechanisms of chromosome alignment on the mitotic spindle. Methods Cell Biol. 2007;79:259-93.
[89] Brinkley BR, Stubblefield E. The fine structure of the kinetochore of a mammalian cell in vitro. Chromosoma. 1966;19(1):28-43.
[90] Jokelainen PT. The ultrastructure and spatial organization of the metaphase kinetochore in mitotic rat cells. J Ultrastruct Res. 1967;19(1):19-44.

[91] McEwen BF, Arena JT, Frank J *et al.* Structure of the colcemid-treated PtK1 kinetochore outer plate as determined by high voltage electron microscopic tomography. J Cell Biol. 1993;120(2):301-12.
[92] McEwen BF, Hsieh CE, Mattheyses AL *et al.* A new look at kinetochore structure in vertebrate somatic cells using high-pressure freezing and freeze substitution. Chromosoma. 1998;107(6-7):366-75.
[93] Vafa O, Sullivan KF. Chromatin containing CENP-A and alpha-satellite DNA is a major component of the inner kinetochore plate. Curr Biol. 1997;7(11):897-900.
[94] Cooke CA, Bazett-Jones DP, Earnshaw WC *et al.* Mapping DNA within the mammalian kinetochore. J Cell Biol. 1993;120(5):1083-91.
[95] Rieder CL. The formation, structure, and composition of the mammalian kinetochore and kinetochore fiber. Int Rev Cytol. 1982;79:1-58.
[96] Maiato H, Hergert PJ, Moutinho-Pereira S *et al.* The ultrastructure of the kinetochore and kinetochore fiber in Drosophila somatic cells. Chromosoma. 2006;115(6):469-80.
[97] Maiato H, Sunkel CE. Kinetochore-microtubule interactions during cell division. Chromosome Res. 2004;12(6):585-97.
[98] Cheeseman IM, Desai A. Molecular architecture of the kinetochore-microtubule interface. Nat Rev Mol Cell Biol. 2008;9(1):33-46.
[99] Silva P, Barbosa J, Nascimento AV *et al.* Monitoring the fidelity of mitotic chromosome segregation by the spindle assembly checkpoint. Cell Prolif. 2011;44(5):391-400.
[100] Foltz DR, Jansen LE, Black BE *et al.* The human CENP-A centromeric nucleosome-associated complex. Nat Cell Biol. 2006;8(5):458-69.
[101] Okada M, Cheeseman IM, Hori T *et al.* The CENP-H-I complex is required for the efficient incorporation of newly synthesized CENP-A into centromeres. Nat Cell Biol. 2006;8(5):446-57.
[102] Hori T, Amano M, Suzuki A *et al.* CCAN makes multiple contacts with centromeric DNA to provide distinct pathways to the outer kinetochore. Cell. 2008;135(6):1039-52.
[103] Kline SL, Cheeseman IM, Hori T *et al.* The human Mis12 complex is required for kinetochore assembly and proper chromosome segregation. J Cell Biol. 2006;173(1):9-17.
[104] Cheeseman IM, Chappie JS, Wilson-Kubalek EM *et al.* The conserved KMN network constitutes the core microtubule-binding site of the kinetochore. Cell. 2006;127(5):983-97.
[105] Holy TE, Leibler S. Dynamic instability of microtubules as an efficient way to search in space. Proc Natl Acad Sci U S A. 1994;91(12):5682-5.
[106] Kirschner M, Mitchison T. Beyond self-assembly: from microtubules to morphogenesis. Cell. 1986;45(3):329-42.
[107] Heald R, Khodjakov A. Thirty years of search and capture: The complex simplicity of mitotic spindle assembly. J Cell Biol. 2015;211(6):1103-11.
[108] DeLuca JG, Dong Y, Hergert P *et al.* Hec1 and nuf2 are core components of the kinetochore outer plate essential for organizing microtubule attachment sites. Mol Biol Cell. 2005;16(2):519-31.
[109] Vaisberg EA, Koonce MP, McIntosh JR. Cytoplasmic dynein plays a role in mammalian mitotic spindle formation. J Cell Biol. 1993;123(4):849-58.
[110] Karess R. Rod-Zw10-Zwilch: a key player in the spindle checkpoint. Trends Cell Biol. 2005;15(7):386-92.

[111] Starr DA, Williams BC, Hays TS *et al.* ZW10 helps recruit dynactin and dynein to the kinetochore. J Cell Biol. 1998;142(3):763-74.
[112] Griffis ER, Stuurman N, Vale RD. Spindly, a novel protein essential for silencing the spindle assembly checkpoint, recruits dynein to the kinetochore. J Cell Biol. 2007;177(6):1005-15.
[113] Gassmann B. [Change opens perspectives]. Krankenpfl Soins Infirm. 2008;101(12):5, 37, 61.
[114] Chan YW, Fava LL, Uldschmid A *et al.* Mitotic control of kinetochore-associated dynein and spindle orientation by human Spindly. J Cell Biol. 2009;185(5):859-74.
[115] Barisic M, Sohm B, Mikolcevic P *et al.* Spindly/CCDC99 is required for efficient chromosome congression and mitotic checkpoint regulation. Mol Biol Cell.21(12):1968-81.
[116] Hanisch A, Sillje HH, Nigg EA. Timely anaphase onset requires a novel spindle and kinetochore complex comprising Ska1 and Ska2. EMBO J. 2006;25(23):5504-15.
[117] Gaitanos TN, Santamaria A, Jeyaprakash AA *et al.* Stable kinetochore-microtubule interactions depend on the Ska complex and its new component Ska3/C13Orf3. EMBO J. 2009;28(10):1442-52.
[118] Guimaraes GJ, Deluca JG. Connecting with Ska, a key complex at the kinetochore-microtubule interface. EMBO J. 2009;28(10):1375-7.
[119] Kops GJ, Saurin AT, Meraldi P. Finding the middle ground: how kinetochores power chromosome congression. Cell Mol Life Sci.67(13):2145-61.
[120] Kapoor TM, Lampson MA, Hergert P *et al.* Chromosomes can congress to the metaphase plate before biorientation. Science. 2006;311(5759):388-91.
[121] Antonio C, Ferby I, Wilhelm H *et al.* Xkid, a chromokinesin required for chromosome alignment on the metaphase plate. Cell. 2000;102(4):425-35.
[122] Funabiki H, Murray AW. The Xenopus chromokinesin Xkid is essential for metaphase chromosome alignment and must be degraded to allow anaphase chromosome movement. Cell. 2000;102(4):411-24.
[123] Wandke C, Barisic M, Sigl R *et al.* Human chromokinesins promote chromosome congression and spindle microtubule dynamics during mitosis. J Cell Biol. 2012;198(5):847-63.
[124] Barisic M, Maiato H. The Tubulin Code: A Navigation System for Chromosomes during Mitosis. Trends Cell Biol. 2016;26(10):766-75.
[125] Barisic M, Silva e Sousa R, Tripathy SK *et al.* Mitosis. Microtubule detyrosination guides chromosomes during mitosis. Science. 2015;348(6236):799-803.
[126] Janke C. The tubulin code: molecular components, readout mechanisms, and functions. J Cell Biol. 2014;206(4):461-72.
[127] Verhey KJ, Gaertig J. The tubulin code. Cell Cycle. 2007;6(17):2152-60.
[128] Forbes DJ, Travesa A, Nord MS *et al.* Reprint of "Nuclear transport factors: global regulation of mitosis". Curr Opin Cell Biol. 2015;34:122-34.
[129] Clarke PR, Zhang C. Spatial and temporal coordination of mitosis by Ran GTPase. Nat Rev Mol Cell Biol. 2008;9(6):464-77.
[130] Zaytsev AV, Grishchuk EL. Basic mechanism for biorientation of mitotic chromosomes is provided by the kinetochore geometry and indiscriminate turnover of kinetochore microtubules. Mol Biol Cell. 2015;26(22):3985-98.
[131] Magidson V, Paul R, Yang N *et al.* Adaptive changes in the kinetochore architecture facilitate proper spindle assembly. Nat Cell Biol. 2015;17(9):1134-44.
[132] Tanaka TU. Chromosome bi-orientation on the mitotic spindle. Philos Trans R Soc Lond B Biol Sci. 2005;360(1455):581-9.

[133] Tanaka TU. Bi-orienting chromosomes: acrobatics on the mitotic spindle. Chromosoma. 2008;117(6):521-33.
[134] Kelly AE, Funabiki H. Correcting aberrant kinetochore microtubule attachments: an Aurora B-centric view. Curr Opin Cell Biol. 2009;21(1):51-8.
[135] Nicklas RB, Ward SC, Gorbsky GJ. Kinetochore chemistry is sensitive to tension and may link mitotic forces to a cell cycle checkpoint. J Cell Biol. 1995;130(4):929-39.
[136] King JM, Nicklas RB. Tension on chromosomes increases the number of kinetochore microtubules but only within limits. J Cell Sci. 2000;113 Pt 21:3815-23.
[137] Liu D, Lampson MA. Regulation of kinetochore-microtubule attachments by Aurora B kinase. Biochem Soc Trans. 2009;37(Pt 5):976-80.
[138] Ruchaud S, Carmena M, Earnshaw WC. The chromosomal passenger complex: one for all and all for one. Cell. 2007;131(2):230-1.
[139] Tanaka TU, Rachidi N, Janke C *et al.* Evidence that the Ipl1-Sli15 (Aurora kinase-INCENP) complex promotes chromosome bi-orientation by altering kinetochore-spindle pole connections. Cell. 2002;108(3):317-29.
[140] Lan W, Zhang X, Kline-Smith SL *et al.* Aurora B phosphorylates centromeric MCAK and regulates its localization and microtubule depolymerization activity. Curr Biol. 2004;14(4):273-86.
[141] Krenn V, Musacchio A. The Aurora B Kinase in Chromosome Bi-Orientation and Spindle Checkpoint Signaling. Front Oncol. 2015;5:225.
[142] Ahonen LJ, Kallio MJ, Daum JR *et al.* Polo-like kinase 1 creates the tension-sensing 3F3/2 phosphoepitope and modulates the association of spindle-checkpoint proteins at kinetochores. Curr Biol. 2005;15(12):1078-89.
[143] Lenart P, Petronczki M, Steegmaier M *et al.* The small-molecule inhibitor BI 2536 reveals novel insights into mitotic roles of polo-like kinase 1. Curr Biol. 2007;17(4):304-15.
[144] Elowe S, Hummer S, Uldschmid A *et al.* Tension-sensitive Plk1 phosphorylation on BubR1 regulates the stability of kinetochore microtubule interactions. Genes Dev. 2007;21(17):2205-19.
[145] Hu M, Liu Q, Song P *et al.* Abnormal expression of the mitotic checkpoint protein BubR1 contributes to the anti-microtubule drug resistance of esophageal squamous cell carcinoma cells. Oncol Rep. 2013;29(1):185-92.
[146] Manning AL, Ganem NJ, Bakhoum SF *et al.* The kinesin-13 proteins Kif2a, Kif2b, and Kif2c/MCAK have distinct roles during mitosis in human cells. Mol Biol Cell. 2007;18(8):2970-9.
[147] Hood EA, Kettenbach AN, Gerber SA *et al.* Plk1 regulates the kinesin-13 protein Kif2b to promote faithful chromosome segregation. Mol Biol Cell. 2012;23(12):2264-74.
[148] Ye AA, Deretic J, Hoel CM *et al.* Aurora A Kinase Contributes to a Pole-Based Error Correction Pathway. Curr Biol. 2015;25(14):1842-51.
[149] Cane S, Ye AA, Luks-Morgan SJ *et al.* Elevated polar ejection forces stabilize kinetochore-microtubule attachments. J Cell Biol. 2013;200(2):203-18.
[150] Drpic D, Pereira AJ, Barisic M *et al.* Polar Ejection Forces Promote the Conversion from Lateral to End-on Kinetochore-Microtubule Attachments on Mono-oriented Chromosomes. Cell Rep. 2015;13(3):460-9.
[151] Kim Y, Holland AJ, Lan W *et al.* Aurora kinases and protein phosphatase 1 mediate chromosome congression through regulation of CENP-E. Cell. 2010;142(3):444-55.

[152] Weaver BA, Cleveland DW. Decoding the links between mitosis, cancer, and chemotherapy: The mitotic checkpoint, adaptation, and cell death. Cancer Cell. 2005;8(1):7-12.
[153] Thompson SL, Bakhoum SF, Compton DA. Mechanisms of chromosomal instability. Curr Biol. 2010;20(6):R285-95.
[154] Khodjakov A, Rieder CL. The nature of cell-cycle checkpoints: facts and fallacies. J Biol. 2009;8(10):88.
[155] Bharadwaj R, Yu H. The spindle checkpoint, aneuploidy, and cancer. Oncogene. 2004;23(11):2016-27.
[156] McCurdy JD, McElroy JS, Kopsell DA *et al.* Effects of mesotrione on perennial ryegrass (Lolium perenne L.) carotenoid concentrations under varying environmental conditions. J Agric Food Chem. 2008;56(19):9133-9.
[157] Sudakin V, Chan GK, Yen TJ. Checkpoint inhibition of the APC/C in HeLa cells is mediated by a complex of BUBR1, BUB3, CDC20, and MAD2. J Cell Biol. 2001;154(5):925-36.
[158] Kramer ER, Gieffers C, Holzl G *et al.* Activation of the human anaphase-promoting complex by proteins of the CDC20/Fizzy family. Curr Biol. 1998;8(22):1207-10.
[159] De Antoni A, Pearson CG, Cimini D *et al.* The Mad1/Mad2 complex as a template for Mad2 activation in the spindle assembly checkpoint. Curr Biol. 2005;15(3):214-25.
[160] Luo X, Yu H. Protein metamorphosis: the two-state behavior of Mad2. Structure. 2008;16(11):1616-25.
[161] Skinner JJ, Wood S, Shorter J *et al.* The Mad2 partial unfolding model: regulating mitosis through Mad2 conformational switching. J Cell Biol. 2008;183(5):761-8.
[162] Yu H. Structural activation of Mad2 in the mitotic spindle checkpoint: the two-state Mad2 model versus the Mad2 template model. J Cell Biol. 2006;173(2):153-7.
[163] Han JS, Holland AJ, Fachinetti D *et al.* Catalytic assembly of the mitotic checkpoint inhibitor BubR1-Cdc20 by a Mad2-induced functional switch in Cdc20. Mol Cell. 2013;51(1):92-104.
[164] Han JS, Vitre B, Fachinetti D *et al.* Bimodal activation of BubR1 by Bub3 sustains mitotic checkpoint signaling. Proc Natl Acad Sci U S A. 2014;111(40):E4185-93.
[165] Diogo V, Teixeira J, Silva PM *et al.* Spindle Assembly Checkpoint as a Potential Target in Colorectal Cancer: Current Status and Future Perspectives. Clin Colorectal Cancer. 2017;16(1):1-8.
[166] Bolanos-Garcia VM, Blundell TL. BUB1 and BUBR1: multifaceted kinases of the cell cycle. Trends Biochem Sci. 2010.
[167] Zich J, Hardwick KG. Getting down to the phosphorylated 'nuts and bolts' of spindle checkpoint signalling. Trends Biochem Sci. 2010;35(1):18-27.
[168] Tang Z, Shu H, Oncel D *et al.* Phosphorylation of Cdc20 by Bub1 provides a catalytic mechanism for APC/C inhibition by the spindle checkpoint. Mol Cell. 2004;16(3):387-97.
[169] Chen RH. Phosphorylation and activation of Bub1 on unattached chromosomes facilitate the spindle checkpoint. EMBO J. 2004;23(15):3113-21.
[170] Yamaguchi S, Decottignies A, Nurse P. Function of Cdc2p-dependent Bub1p phosphorylation and Bub1p kinase activity in the mitotic and meiotic spindle checkpoint. EMBO J. 2003;22(5):1075-87.
[171] Mao Y, Abrieu A, Cleveland DW. Activating and silencing the mitotic checkpoint through CENP-E-dependent activation/inactivation of BubR1. Cell. 2003;114(1):87-98.

[172] Huang H, Yen TJ. BubR1 is an effector of multiple mitotic kinases that specifies kinetochore: microtubule attachments and checkpoint. Cell Cycle. 2009;8(8):1164-7.
[173] Malureanu LA, Jeganathan KB, Hamada M *et al.* BubR1 N terminus acts as a soluble inhibitor of cyclin B degradation by APC/C(Cdc20) in interphase. Dev Cell. 2009;16(1):118-31.
[174] Zhang J, Ahmad S, Mao Y. BubR1 and APC/EB1 cooperate to maintain metaphase chromosome alignment. J Cell Biol. 2007;178(5):773-84.
[175] Dorer RK, Zhong S, Tallarico JA *et al.* A small-molecule inhibitor of Mps1 blocks the spindle-checkpoint response to a lack of tension on mitotic chromosomes. Curr Biol. 2005;15(11):1070-6.
[176] Schmidt M, Budirahardja Y, Klompmaker R *et al.* Ablation of the spindle assembly checkpoint by a compound targeting Mps1. EMBO Rep. 2005;6(9):866-72.
[177] Yamagishi Y, Yang CH, Tanno Y *et al.* MPS1/Mph1 phosphorylates the kinetochore protein KNL1/Spc7 to recruit SAC components. Nat Cell Biol. 2012;14(7):746-52.
[178] Nijenhuis W, Vallardi G, Teixeira A *et al.* Negative feedback at kinetochores underlies a responsive spindle checkpoint signal. Nat Cell Biol. 2014;16(12):1257-64.
[179] Santaguida S, Tighe A, D'Alise AM *et al.* Dissecting the role of MPS1 in chromosome biorientation and the spindle checkpoint through the small molecule inhibitor reversine. J Cell Biol. 2010;190(1):73-87.
[180] Jelluma N, Brenkman AB, van den Broek NJ *et al.* Mps1 phosphorylates Borealin to control Aurora B activity and chromosome alignment. Cell. 2008;132(2):233-46.
[181] Hardwick KG, Weiss E, Luca FC *et al.* Activation of the budding yeast spindle assembly checkpoint without mitotic spindle disruption. Science. 1996;273(5277):953-6.
[182] Fuller BG, Stukenberg PT. Cell division: righting the check. Curr Biol. 2009;19(14):R550-3.
[183] Vanoosthuyse V, Hardwick KG. Overcoming inhibition in the spindle checkpoint. Genes Dev. 2009;23(24):2799-805.
[184] Sivaram MV, Wadzinski TL, Redick SD *et al.* Dynein light intermediate chain 1 is required for progress through the spindle assembly checkpoint. EMBO J. 2009;28(7):902-14.
[185] Etemad B, Kops GJ. Attachment issues: kinetochore transformations and spindle checkpoint silencing. Curr Opin Cell Biol. 2016;39:101-8.
[186] Gassmann R, Holland AJ, Varma D *et al.* Removal of Spindly from microtubule-attached kinetochores controls spindle checkpoint silencing in human cells. Genes Dev. 2010;24(9):957-71.
[187] Barisic M, Sohm B, Mikolcevic P *et al.* Spindly/CCDC99 is required for efficient chromosome congression and mitotic checkpoint regulation. Mol Biol Cell. 2010;21(12):1968-81.
[188] Moudgil DK, Westcott N, Famulski JK *et al.* A novel role of farnesylation in targeting a mitotic checkpoint protein, human Spindly, to kinetochores. J Cell Biol. 2015;208(7):881-96.
[189] Holland AJ, Reis RM, Niessen S *et al.* Preventing farnesylation of the dynein adaptor Spindly contributes to the mitotic defects caused by farnesyltransferase inhibitors. Mol Biol Cell. 2015;26(10):1845-56.
[190] Barisic M, Geley S. Spindly switch controls anaphase: spindly and RZZ functions in chromosome attachment and mitotic checkpoint control. Cell Cycle. 2011;10(3):449-56.

[191] Xia G, Luo X, Habu T *et al.* Conformation-specific binding of p31(comet) antagonizes the function of Mad2 in the spindle checkpoint. EMBO J. 2004;23(15):3133-43.
[192] Yang M, Li B, Tomchick DR *et al.* p31comet blocks Mad2 activation through structural mimicry. Cell. 2007;131(4):744-55.
[193] Wassmann K, Liberal V, Benezra R. Mad2 phosphorylation regulates its association with Mad1 and the APC/C. EMBO J. 2003;22(4):797-806.
[194] Vanoosthuyse V, Hardwick KG. A novel protein phosphatase 1-dependent spindle checkpoint silencing mechanism. Curr Biol. 2009;19(14):1176-81.
[195] Espert A, Uluocak P, Bastos RN *et al.* PP2A-B56 opposes Mps1 phosphorylation of Knl1 and thereby promotes spindle assembly checkpoint silencing. J Cell Biol. 2014;206(7):833-42.
[196] Rosenberg JS, Cross FR, Funabiki H. KNL1/Spc105 recruits PP1 to silence the spindle assembly checkpoint. Curr Biol. 2011;21(11):942-7.
[197] Suijkerbuijk SJ, Vleugel M, Teixeira A *et al.* Integration of kinase and phosphatase activities by BUBR1 ensures formation of stable kinetochore-microtubule attachments. Dev Cell. 2012;23(4):745-55.
[198] Xu P, Raetz EA, Kitagawa M *et al.* BUBR1 recruits PP2A via the B56 family of targeting subunits to promote chromosome congression. Biol Open. 2013;2(5):479-86.
[199] Kruse T, Zhang G, Larsen MS *et al.* Direct binding between BubR1 and B56-PP2A phosphatase complexes regulate mitotic progression. J Cell Sci. 2013;126(Pt 5):1086-92.
[200] Overlack K, Primorac I, Vleugel M *et al.* A molecular basis for the differential roles of Bub1 and BubR1 in the spindle assembly checkpoint. Elife. 2015;4:e05269.
[201] Marques S, Fonseca J, Silva PM *et al.* Targeting the spindle assembly checkpoint for breast cancer treatment. Curr Cancer Drug Targets. 2015;15(4):272-81.
[202] Cahill DP, Lengauer C, Yu J *et al.* Mutations of mitotic checkpoint genes in human cancers. Nature. 1998;392(6673):300-3.
[203] Kops GJ, Weaver BA, Cleveland DW. On the road to cancer: aneuploidy and the mitotic checkpoint. Nat Rev Cancer. 2005;5(10):773-85.
[204] Michel LS, Liberal V, Chatterjee A *et al.* MAD2 haplo-insufficiency causes premature anaphase and chromosome instability in mammalian cells. Nature. 2001;409(6818):355-9.
[205] Babu JR, Jeganathan KB, Baker DJ *et al.* Rae1 is an essential mitotic checkpoint regulator that cooperates with Bub3 to prevent chromosome missegregation. J Cell Biol. 2003;160(3):341-53.
[206] Dai W, Wang Q, Liu T *et al.* Slippage of mitotic arrest and enhanced tumor development in mice with BubR1 haploinsufficiency. Cancer Res. 2004;64(2):440-5.
[207] Logarinho E, Bousbaa H. Kinetochore-microtubule interactions "in check" by Bub1, Bub3 and BubR1: The dual task of attaching and signalling. Cell Cycle. 2008;7(12):1763-8.
[208] Logarinho E, Resende T, Torres C *et al.* The human spindle assembly checkpoint protein Bub3 is required for the establishment of efficient kinetochore-microtubule attachments. Mol Biol Cell. 2008;19(4):1798-813.
[209] Meraldi P, Sorger PK. A dual role for Bub1 in the spindle checkpoint and chromosome congression. EMBO J. 2005;24(8):1621-33.
[210] Lampson MA, Kapoor TM. The human mitotic checkpoint protein BubR1 regulates chromosome-spindle attachments. Nat Cell Biol. 2005;7(1):93-8.
[211] Tighe A, Johnson VL, Albertella M *et al.* Aneuploid colon cancer cells have a robust spindle checkpoint. EMBO Rep. 2001;2(7):609-14.

[212] Gascoigne KE, Taylor SS. Cancer cells display profound intra- and interline variation following prolonged exposure to antimitotic drugs. Cancer Cell. 2008;14(2):111-22.
[213] Janssen A, Kops GJ, Medema RH. Elevating the frequency of chromosome mis-segregation as a strategy to kill tumor cells. Proc Natl Acad Sci U S A. 2009;106(45):19108-13.
[214] Basu J, Bousbaa H, Logarinho E *et al.* Mutations in the essential spindle checkpoint gene bub1 cause chromosome missegregation and fail to block apoptosis in Drosophila. J Cell Biol. 1999;146(1):13-28.
[215] Kops GJ, Foltz DR, Cleveland DW. Lethality to human cancer cells through massive chromosome loss by inhibition of the mitotic checkpoint. Proc Natl Acad Sci U S A. 2004;101(23):8699-704.
[216] Bolanos-Garcia VM. Assessment of the mitotic spindle assembly checkpoint (SAC) as the target of anticancer therapies. Curr Cancer Drug Targets. 2009;9(2):131-41.
[217] Perez EA. Microtubule inhibitors: Differentiating tubulin-inhibiting agents based on mechanisms of action, clinical activity, and resistance. Mol Cancer Ther. 2009;8(8):2086-95.
[218] Fanale D, Bronte G, Passiglia F *et al.* Stabilizing versus destabilizing the microtubules: a double-edge sword for an effective cancer treatment option? Anal Cell Pathol (Amst). 2015;2015:690916.
[219] Fauzee NJ. Taxanes: promising anti-cancer drugs. Asian Pac J Cancer Prev. 2011;12(4):837-51.
[220] Altmann KH. Epothilone B and its analogs - a new family of anticancer agents. Mini Rev Med Chem. 2003;3(2):149-58.
[221] Li J, Ren J, Sun W. Systematic review of ixabepilone for treating metastatic breast cancer. Breast Cancer. 2017;24(2):171-9.
[222] Jordan MA, Thrower D, Wilson L. Mechanism of inhibition of cell proliferation by Vinca alkaloids. Cancer Res. 1991;51(8):2212-22.
[223] Jordan MA, Toso RJ, Thrower D *et al.* Mechanism of mitotic block and inhibition of cell proliferation by taxol at low concentrations. Proc Natl Acad Sci U S A. 1993;90(20):9552-6.
[224] Rieder CL, Maiato H. Stuck in division or passing through: what happens when cells cannot satisfy the spindle assembly checkpoint. Dev Cell. 2004;7(5):637-51.
[225] Gascoigne KE, Taylor SS. How do anti-mitotic drugs kill cancer cells? J Cell Sci. 2009;122(Pt 15):2579-85.
[226] Topham CH, Taylor SS. Mitosis and apoptosis: how is the balance set? Curr Opin Cell Biol. 2013;25(6):780-5.
[227] Rowinsky EK, Wright M, Monsarrat B *et al.* Taxol: pharmacology, metabolism and clinical implications. Cancer Surv. 1993;17:283-304.
[228] Rowinsky EK, Eisenhauer EA, Chaudhry V *et al.* Clinical toxicities encountered with paclitaxel (Taxol). Semin Oncol. 1993;20(4 Suppl 3):1-15.
[229] McGuire WP, Rowinsky EK, Rosenshein NB *et al.* Taxol: a unique antineoplastic agent with significant activity in advanced ovarian epithelial neoplasms. Ann Intern Med. 1989;111(4):273-9.
[230] Gornstein E, Schwarz TL. The paradox of paclitaxel neurotoxicity: Mechanisms and unanswered questions. Neuropharmacology. 2014;76 Pt A:175-83.
[231] Rouzier R, Rajan R, Wagner P *et al.* Microtubule-associated protein tau: a marker of paclitaxel sensitivity in breast cancer. Proc Natl Acad Sci U S A. 2005;102(23):8315-20.

[232] Ahmed AA, Mills AD, Ibrahim AE *et al.* The extracellular matrix protein TGFBI induces microtubule stabilization and sensitizes ovarian cancers to paclitaxel. Cancer Cell. 2007;12(6):514-27.
[233] Whitehurst AW, Bodemann BO, Cardenas J *et al.* Synthetic lethal screen identification of chemosensitizer loci in cancer cells. Nature. 2007;446(7137):815-9.
[234] Pusztai L, Jeong JH, Gong Y *et al.* Evaluation of microtubule-associated protein-Tau expression as a prognostic and predictive marker in the NSABP-B 28 randomized clinical trial. J Clin Oncol. 2009;27(26):4287-92.
[235] Juul N, Szallasi Z, Eklund AC *et al.* Assessment of an RNA interference screen-derived mitotic and ceramide pathway metagene as a predictor of response to neoadjuvant paclitaxel for primary triple-negative breast cancer: a retrospective analysis of five clinical trials. Lancet Oncol. 2010;11(4):358-65.
[236] Wertz IE, Kusam S, Lam C *et al.* Sensitivity to antitubulin chemotherapeutics is regulated by MCL1 and FBW7. Nature. 2011;471(7336):110-4.
[237] Njiaju UO, Gamazon ER, Gorsic LK *et al.* Whole-genome studies identify solute carrier transporters in cellular susceptibility to paclitaxel. Pharmacogenet Genomics. 2012;22(7):498-507.
[238] Russell RA, Crabb DP, Malik R *et al.* The relationship between variability and sensitivity in large-scale longitudinal visual field data. Invest Ophthalmol Vis Sci. 2012;53(10):5985-90.
[239] Jackson JR, Patrick DR, Dar MM *et al.* Targeted anti-mitotic therapies: can we improve on tubulin agents? Nat Rev Cancer. 2007;7(2):107-17.
[240] Mayer TU, Kapoor TM, Haggarty SJ *et al.* Small molecule inhibitor of mitotic spindle bipolarity identified in a phenotype-based screen. Science. 1999;286(5441):971-4.
[241] Kapoor TM, Mayer TU, Coughlin ML *et al.* Probing spindle assembly mechanisms with monastrol, a small molecule inhibitor of the mitotic kinesin, Eg5. J Cell Biol. 2000;150(5):975-88.
[242] Marcus AI, Peters U, Thomas SL *et al.* Mitotic kinesin inhibitors induce mitotic arrest and cell death in Taxol-resistant and -sensitive cancer cells. J Biol Chem. 2005;280(12):11569-77.
[243] Huszar D, Theoclitou ME, Skolnik J *et al.* Kinesin motor proteins as targets for cancer therapy. Cancer Metastasis Rev. 2009;28(1-2):197-208.
[244] Brier S, Lemaire D, DeBonis S *et al.* Molecular dissection of the inhibitor binding pocket of mitotic kinesin Eg5 reveals mutants that confer resistance to antimitotic agents. J Mol Biol. 2006;360(2):360-76.
[245] Tcherniuk S, van Lis R, Kozielski F *et al.* Mutations in the human kinesin Eg5 that confer resistance to monastrol and S-trityl-L-cysteine in tumor derived cell lines. Biochem Pharmacol. 2010;79(6):864-72.
[246] Maliga Z, Mitchison TJ. Small-molecule and mutational analysis of allosteric Eg5 inhibition by monastrol. BMC Chem Biol. 2006;6:2.
[247] Tanenbaum ME, Macurek L, Janssen A *et al.* Kif15 cooperates with eg5 to promote bipolar spindle assembly. Curr Biol. 2009;19(20):1703-11.
[248] Boss DS, Beijnen JH, Schellens JH. Clinical experience with aurora kinase inhibitors: a review. Oncologist. 2009;14(8):780-93.
[249] Lens SM, Voest EE, Medema RH. Shared and separate functions of polo-like kinases and aurora kinases in cancer. Nat Rev Cancer. 2010;10(12):825-41.
[250] Malumbres M. Physiological relevance of cell cycle kinases. Physiol Rev. 2011;91(3):973-1007.

[251] Gharwan H, Groninger H. Kinase inhibitors and monoclonal antibodies in oncology: clinical implications. Nat Rev Clin Oncol. 2016;13(4):209-27.
[252] Cicenas J. The Aurora kinase inhibitors in cancer research and therapy. J Cancer Res Clin Oncol. 2016;142(9):1995-2012.
[253] Cicenas J, Cicenas E. Multi-kinase inhibitors, AURKs and cancer. Med Oncol. 2016;33(5):43.
[254] van de Weerdt BC, Medema RH. Polo-like kinases: a team in control of the division. Cell Cycle. 2006;5(8):853-64.
[255] Cheng MW, Wang BC, Weng ZQ *et al.* Clinicopathological significance of Polo-like kinase 1 (PLK1) expression in human malignant glioma. Acta Histochem. 2012;114(5):503-9.
[256] Ito Y, Miyoshi E, Sasaki N *et al.* Polo-like kinase 1 overexpression is an early event in the progression of papillary carcinoma. Br J Cancer. 2004;90(2):414-8.
[257] Knecht R, Elez R, Oechler M *et al.* Prognostic significance of polo-like kinase (PLK) expression in squamous cell carcinomas of the head and neck. Cancer Res. 1999;59(12):2794-7.
[258] Kneisel L, Strebhardt K, Bernd A *et al.* Expression of polo-like kinase (PLK1) in thin melanomas: a novel marker of metastatic disease. J Cutan Pathol. 2002;29(6):354-8.
[259] Takahashi T, Sano B, Nagata T *et al.* Polo-like kinase 1 (PLK1) is overexpressed in primary colorectal cancers. Cancer Sci. 2003;94(2):148-52.
[260] Tokumitsu Y, Mori M, Tanaka S *et al.* Prognostic significance of polo-like kinase expression in esophageal carcinoma. Int J Oncol. 1999;15(4):687-92.
[261] Weichert W, Denkert C, Schmidt M *et al.* Polo-like kinase isoform expression is a prognostic factor in ovarian carcinoma. Br J Cancer. 2004;90(4):815-21.
[262] Weichert W, Kristiansen G, Winzer KJ *et al.* Polo-like kinase isoforms in breast cancer: expression patterns and prognostic implications. Virchows Arch. 2005;446(4):442-50.
[263] Weichert W, Schmidt M, Gekeler V *et al.* Polo-like kinase 1 is overexpressed in prostate cancer and linked to higher tumor grades. Prostate. 2004;60(3):240-5.
[264] Ramani P, Nash R, Sowa-Avugrah E *et al.* High levels of polo-like kinase 1 and phosphorylated translationally controlled tumor protein indicate poor prognosis in neuroblastomas. J Neurooncol. 2015;125(1):103-11.
[265] Tut TG, Lim SH, Dissanayake IU *et al.* Upregulated Polo-Like Kinase 1 Expression Correlates with Inferior Survival Outcomes in Rectal Cancer. PLoS One. 2015;10(6):e0129313.
[266] Zhang R, Shi H, Ren F *et al.* Misregulation of polo-like protein kinase 1, P53 and P21WAF1 in epithelial ovarian cancer suggests poor prognosis. Oncol Rep. 2015;33(3):1235-42.
[267] de Oliveira JC, Brassesco MS, Pezuk JA *et al.* In vitro PLK1 inhibition by BI 2536 decreases proliferation and induces cell-cycle arrest in melanoma cells. J Drugs Dermatol. 2012;11(5):587-92.
[268] Bu Y, Yang Z, Li Q *et al.* Silencing of polo-like kinase (Plk) 1 via siRNA causes inhibition of growth and induction of apoptosis in human esophageal cancer cells. Oncology. 2008;74(3-4):198-206.
[269] Holtrich U, Wolf G, Brauninger A *et al.* Induction and down-regulation of PLK, a human serine/threonine kinase expressed in proliferating cells and tumors. Proc Natl Acad Sci U S A. 1994;91(5):1736-40.
[270] Gray PJ, Jr., Bearss DJ, Han H *et al.* Identification of human polo-like kinase 1 as a potential therapeutic target in pancreatic cancer. Mol Cancer Ther. 2004;3(5):641-6.

[271] McCarroll JA, Dwarte T, Baigude H *et al.* Therapeutic targeting of polo-like kinase 1 using RNA-interfering nanoparticles (iNOPs) for the treatment of non-small cell lung cancer. Oncotarget. 2015;6(14):12020-34.
[272] Tyagi S, Bhui K, Singh R *et al.* Polo-like kinase1 (Plk1) knockdown enhances cisplatin chemosensitivity via up-regulation of p73alpha in p53 mutant human epidermoid squamous carcinoma cells. Biochem Pharmacol. 2010;80(9):1326-34.
[273] Spankuch B, Heim S, Kurunci-Csacsko E *et al.* Down-regulation of Polo-like kinase 1 elevates drug sensitivity of breast cancer cells in vitro and in vivo. Cancer Res. 2006;66(11):5836-46.
[274] Harris PS, Venkataraman S, Alimova I *et al.* Polo-like kinase 1 (PLK1) inhibition suppresses cell growth and enhances radiation sensitivity in medulloblastoma cells. BMC Cancer. 2012;12:80.
[275] Gleixner KV, Ferenc V, Peter B *et al.* Polo-like kinase 1 (Plk1) as a novel drug target in chronic myeloid leukemia: overriding imatinib resistance with the Plk1 inhibitor BI 2536. Cancer Res. 2010;70(4):1513-23.
[276] Gutteridge RE, Ndiaye MA, Liu X *et al.* Plk1 Inhibitors in Cancer Therapy: From Laboratory to Clinics. Mol Cancer Ther. 2016;15(7):1427-35.
[277] Haupenthal J, Bihrer V, Korkusuz H *et al.* Reduced efficacy of the Plk1 inhibitor BI 2536 on the progression of hepatocellular carcinoma due to low intratumoral drug levels. Neoplasia. 2012;14(5):410-9.
[278] Mao Y, Desai A, Cleveland DW. Microtubule capture by CENP-E silences BubR1-dependent mitotic checkpoint signaling. J Cell Biol. 2005;170(6):873-80.
[279] Guo Y, Kim C, Ahmad S *et al.* CENP-E--dependent BubR1 autophosphorylation enhances chromosome alignment and the mitotic checkpoint. J Cell Biol. 2012;198(2):205-17.
[280] Weaver BA, Silk AD, Montagna C *et al.* Aneuploidy acts both oncogenically and as a tumor suppressor. Cancer Cell. 2007;11(1):25-36.
[281] Wood KW, Lad L, Luo L *et al.* Antitumor activity of an allosteric inhibitor of centromere-associated protein-E. Proc Natl Acad Sci U S A. 2010;107(13):5839-44.
[282] Uzdensky A, Demyanenko S, Bibov M *et al.* Expression of proteins involved in epigenetic regulation in human cutaneous melanoma and peritumoral skin. Tumour Biol. 2014;35(8):8225-33.
[283] Espinosa AM, Alfaro A, Roman-Basaure E *et al.* Mitosis is a source of potential markers for screening and survival and therapeutic targets in cervical cancer. PLoS One. 2013;8(2):e55975.
[284] Yang CP, Liu L, Ikui AE *et al.* The interaction between mitotic checkpoint proteins, CENP-E and BubR1, is diminished in epothilone B-resistant A549 cells. Cell Cycle. 2010;9(6):1207-13.
[285] Schafer-Hales K, Iaconelli J, Snyder JP *et al.* Farnesyl transferase inhibitors impair chromosomal maintenance in cell lines and human tumors by compromising CENP-E and CENP-F function. Mol Cancer Ther. 2007;6(4):1317-28.
[286] Kang J, Yu H. Kinase signaling in the spindle checkpoint. J Biol Chem. 2009;284(23):15359-63.
[287] Stupp R, Mason WP, van den Bent MJ *et al.* Radiotherapy plus concomitant and adjuvant temozolomide for glioblastoma. N Engl J Med. 2005;352(10):987-96.
[288] Daniel J, Coulter J, Woo JH *et al.* High levels of the Mps1 checkpoint protein are protective of aneuploidy in breast cancer cells. Proc Natl Acad Sci U S A. 2011;108(13):5384-9.

[289] Landi MT, Dracheva T, Rotunno M *et al.* Gene expression signature of cigarette smoking and its role in lung adenocarcinoma development and survival. PLoS One. 2008;3(2):e1651.
[290] Salvatore G, Nappi TC, Salerno P *et al.* A cell proliferation and chromosomal instability signature in anaplastic thyroid carcinoma. Cancer Res. 2007;67(21):10148-58.
[291] Yuan B, Xu Y, Woo JH *et al.* Increased expression of mitotic checkpoint genes in breast cancer cells with chromosomal instability. Clin Cancer Res. 2006;12(2):405-10.
[292] Xie Y, Wang A, Lin J *et al.* Mps1/TTK: a novel target and biomarker for cancer. J Drug Target. 2016:1-7.
[293] Kato T, Daigo Y, Aragaki M *et al.* Overexpression of MAD2 predicts clinical outcome in primary lung cancer patients. Lung Cancer. 2011;74(1):124-31.
[294] Ko YH, Roh JH, Son YI *et al.* Expression of mitotic checkpoint proteins BUB1B and MAD2L1 in salivary duct carcinomas. J Oral Pathol Med. 2010;39(4):349-55.
[295] Tanaka K, Mohri Y, Ohi M *et al.* Mitotic checkpoint genes, hsMAD2 and BubR1, in oesophageal squamous cancer cells and their association with 5-fluorouracil and cisplatin-based radiochemotherapy. Clin Oncol (R Coll Radiol). 2008;20(8):639-46.
[296] Gladhaug IP, Westgaard A, Schjolberg AR *et al.* Spindle proteins in resected pancreatic head adenocarcinomas: BubR1 is an independent prognostic factor in pancreatobiliary-type tumours. Histopathology. 2010;56(3):345-55.
[297] Michel L, Diaz-Rodriguez E, Narayan G *et al.* Complete loss of the tumor suppressor MAD2 causes premature cyclin B degradation and mitotic failure in human somatic cells. Proc Natl Acad Sci U S A. 2004;101(13):4459-64.
[298] Yu L, Guo WC, Zhao SH *et al.* Mitotic arrest defective protein 2 expression abnormality and its clinicopathologic significance in human osteosarcoma. APMIS. 2010;118(3):222-9.
[299] Teixeira JH, Silva P, Faria J *et al.* Clinicopathologic significance of BubR1 and Mad2 overexpression in oral cancer. Oral Dis. 2015;21(6):713-20.
[300] Kaestner P, Aigner A, Bastians H. Therapeutic targeting of the mitotic spindle checkpoint through nanoparticle-mediated siRNA delivery inhibits tumor growth in vivo. Cancer Lett. 2011;304(2):128-36.
[301] Wang L, Yin F, Du Y *et al.* Depression of MAD2 inhibits apoptosis and increases proliferation and multidrug resistance in gastric cancer cells by regulating the activation of phosphorylated survivin. Tumour Biol. 2010;31(3):225-32.
[302] Furlong F, Fitzpatrick P, O'Toole S *et al.* Low MAD2 expression levels associate with reduced progression-free survival in patients with high-grade serous epithelial ovarian cancer. J Pathol. 2012;226(5):746-55.
[303] Hao X, Zhou Z, Ye S *et al.* Effect of Mad2 on paclitaxel-induced cell death in ovarian cancer cells. J Huazhong Univ Sci Technolog Med Sci. 2010;30(5):620-5.
[304] Prencipe M, Fitzpatrick P, Gorman S *et al.* Cellular senescence induced by aberrant MAD2 levels impacts on paclitaxel responsiveness in vitro. Br J Cancer. 2009;101(11):1900-8.
[305] Du Y, Yin F, Liu C *et al.* Depression of MAD2 inhibits apoptosis of gastric cancer cells by upregulating Bcl-2 and interfering mitochondrion pathway. Biochem Biophys Res Commun. 2006;345(3):1092-8.
[306] Otake K, Uchida K, Tanaka K *et al.* HsMAD2 mRNA expression may be a predictor of sensitivity to paclitaxel and survival in neuroblastoma. Pediatr Surg Int. 2011;27(2):217-23.

[307] Nascimento AV, Singh A, Bousbaa H *et al.* Overcoming cisplatin resistance in non-small cell lung cancer with Mad2 silencing siRNA delivered systemically using EGFR-targeted chitosan nanoparticles. Acta Biomater. 2017;47:71-80.
[308] Kastl J, Braun J, Prestel A *et al.* Mad2 Inhibitor-1 (M2I-1): A Small Molecule Protein-Protein Interaction Inhibitor Targeting the Mitotic Spindle Assembly Checkpoint. ACS Chem Biol. 2015;10(7):1661-6.
[309] Morales AG, Pezuk JA, Brassesco MS *et al.* BUB1 and BUBR1 inhibition decreases proliferation and colony formation, and enhances radiation sensitivity in pediatric glioblastoma cells. Childs Nerv Syst. 2013;29(12):2241-8.
[310] Haruki N, Saito H, Harano T *et al.* Molecular analysis of the mitotic checkpoint genes BUB1, BUBR1 and BUB3 in human lung cancers. Cancer Lett. 2001;162(2):201-5.
[311] Lee CS, Jang ER, Kim YJ *et al.* Casein kinase 2 inhibition differentially modulates apoptotic effect of trichostatin A against epithelial ovarian carcinoma cell lines. Mol Cell Biochem. 2010;338(1-2):157-66.
[312] Nagao K, Yamamoto Y, Hara T *et al.* Ki67 and BUBR1 may discriminate clinically insignificant prostate cancer in the PSA range <4 ng/ml. Jpn J Clin Oncol. 2011;41(4):555-64.
[313] Cirak Y, Sarsik B, Cakar B *et al.* Predictive and prognostic values of Tau and BubR1 protein in prostate cancer and their relationship to the Gleason score. Med Oncol. 2013;30(2):526.
[314] Wada N, Yoshida A, Miyagi Y *et al.* Overexpression of the mitotic spindle assembly checkpoint genes hBUB1, hBUBR1 and hMAD2 in thyroid carcinomas with aggressive nature. Anticancer Res. 2008;28(1A):139-44.
[315] Ando K, Kakeji Y, Kitao H *et al.* High expression of BUBR1 is one of the factors for inducing DNA aneuploidy and progression in gastric cancer. Cancer Sci. 2010;101(3):639-45.
[316] Liu AW, Cai J, Zhao XL *et al.* The clinicopathological significance of BUBR1 overexpression in hepatocellular carcinoma. J Clin Pathol. 2009;62(11):1003-8.
[317] Yamamoto Y, Matsuyama H, Chochi Y *et al.* Overexpression of BUBR1 is associated with chromosomal instability in bladder cancer. Cancer Genet Cytogenet. 2007;174(1):42-7.
[318] Grabsch H, Takeno S, Parsons WJ *et al.* Overexpression of the mitotic checkpoint genes BUB1, BUBR1, and BUB3 in gastric cancer--association with tumour cell proliferation. J Pathol. 2003;200(1):16-22.
[319] Chen H, Lee J, Kljavin NM *et al.* Requirement for BUB1B/BUBR1 in tumor progression of lung adenocarcinoma. Genes Cancer. 2015;6(3-4):106-18.
[320] Xu HZ, Huang Y, Wu YL *et al.* Pharicin A, a novel natural ent-kaurene diterpenoid, induces mitotic arrest and mitotic catastrophe of cancer cells by interfering with BubR1 function. Cell Cycle. 2010;9(14):2897-907.
[321] Silva PM, Tavares AA, Bousbaa H. Co-silencing of human Bub3 and dynein highlights an antagonistic relationship in regulating kinetochore-microtubule attachments. FEBS Lett. 2015;589(23):3588-94.
[322] Kalitsis P, Fowler KJ, Griffiths B *et al.* Increased chromosome instability but not cancer predisposition in haploinsufficient Bub3 mice. Genes Chromosomes Cancer. 2005;44(1):29-36.
[323] Morais da Silva S, Moutinho-Santos T, Sunkel CE. A tumor suppressor role of the Bub3 spindle checkpoint protein after apoptosis inhibition. J Cell Biol. 2013;201(3):385-93.

[324] Bieche I, Vacher S, Lallemand F *et al.* Expression analysis of mitotic spindle checkpoint genes in breast carcinoma: role of NDC80/HEC1 in early breast tumorigenicity, and a two-gene signature for aneuploidy. Mol Cancer. 2011;10:23.
[325] Shackney SE, Singh SG, Yakulis R *et al.* Aneuploidy in breast cancer: a fluorescence in situ hybridization study. Cytometry. 1995;22(4):282-91.
[326] Shigeishi H, Yoneda S, Taki M *et al.* Correlation of human Bub1 expression with tumor-proliferating activity in salivary gland tumors. Oncol Rep. 2006;15(4):933-8.
[327] Xu M, Takanashi M, Oikawa K *et al.* Identification of a novel role of Septin 10 in paclitaxel-resistance in cancers through a functional genomics screen. Cancer Sci. 2012;103(4):821-7.
[328] Diaz-Martinez LA, Tian W, Li B *et al.* The Cdc20-binding Phe box of the spindle checkpoint protein BubR1 maintains the mitotic checkpoint complex during mitosis. J Biol Chem. 2015;290(4):2431-43.
[329] Kim Y, Choi JW, Lee JH *et al.* MAD2 and CDC20 are upregulated in high-grade squamous intraepithelial lesions and squamous cell carcinomas of the uterine cervix. Int J Gynecol Pathol. 2014;33(5):517-23.
[330] Ding ZY, Wu HR, Zhang JM *et al.* Expression characteristics of CDC20 in gastric cancer and its correlation with poor prognosis. Int J Clin Exp Pathol. 2014;7(2):722-7.
[331] Chang DZ, Ma Y, Ji B *et al.* Increased CDC20 expression is associated with pancreatic ductal adenocarcinoma differentiation and progression. J Hematol Oncol. 2012;5:15.
[332] Moura IM, Delgado ML, Silva PM *et al.* High CDC20 expression is associated with poor prognosis in oral squamous cell carcinoma. J Oral Pathol Med. 2014;43(3):225-31.
[333] Taniguchi K, Momiyama N, Ueda M *et al.* Targeting of CDC20 via small interfering RNA causes enhancement of the cytotoxicity of chemoradiation. Anticancer Res. 2008;28(3A):1559-63.
[334] Kidokoro T, Tanikawa C, Furukawa Y *et al.* CDC20, a potential cancer therapeutic target, is negatively regulated by p53. Oncogene. 2008;27(11):1562-71.
[335] Liu M, Zhang Y, Liao Y *et al.* Evaluation of the Antitumor Efficacy of RNAi-Mediated Inhibition of CDC20 and Heparanase in an Orthotopic Liver Tumor Model. Cancer Biother Radiopharm. 2015;30(6):233-9.
[336] Famulski JK, Vos LJ, Rattner JB *et al.* Dynein/Dynactin-mediated transport of kinetochore components off kinetochores and onto spindle poles induced by nordihydroguaiaretic acid. PLoS One. 2011;6(1):e16494.
[337] Efimov VP, Morris NR. A screen for dynein synthetic lethals in Aspergillus nidulans identifies spindle assembly checkpoint genes and other genes involved in mitosis. Genetics. 1998;149(1):101-16.
[338] Lo KW, Kogoy JM, Pfister KK. The DYNLT3 light chain directly links cytoplasmic dynein to a spindle checkpoint protein, Bub3. J Biol Chem. 2007;282(15):11205-12.
[339] Stehman SA, Chen Y, McKenney RJ *et al.* NudE and NudEL are required for mitotic progression and are involved in dynein recruitment to kinetochores. J Cell Biol. 2007;178(4):583-94.
[340] Varma D, Monzo P, Stehman SA *et al.* Direct role of dynein motor in stable kinetochore-microtubule attachment, orientation, and alignment. J Cell Biol. 2008;182(6):1045-54.
[341] Silva PM, Reis RM, Bolanos-Garcia VM *et al.* Dynein-dependent transport of spindle assembly checkpoint proteins off kinetochores toward spindle poles. FEBS Lett. 2014;588(17):3265-73.

[342] Gassmann R, Holland AJ, Varma D *et al.* Removal of Spindly from microtubule-attached kinetochores controls spindle checkpoint silencing in human cells. Genes Dev. 2010;24(9):957-71.
[343] Bauer C, Groger I, Rupprecht R *et al.* Intrasession reliability of force platform parameters in community-dwelling older adults. Arch Phys Med Rehabil. 2008;89(10):1977-82.
[344] Waters JC, Skibbens RV, Salmon ED. Oscillating mitotic newt lung cell kinetochores are, on average, under tension and rarely push. J Cell Sci. 1996;109 (Pt 12):2823-31.
[345] Maresca TJ, Salmon ED. Intrakinetochore stretch is associated with changes in kinetochore phosphorylation and spindle assembly checkpoint activity. J Cell Biol. 2009;184(3):373-81.
[346] Uchida KS, Takagaki K, Kumada K *et al.* Kinetochore stretching inactivates the spindle assembly checkpoint. J Cell Biol. 2009;184(3):383-90.
[347] Reis R, Feijao T, Gouveia S *et al.* Dynein and mast/orbit/CLASP have antagonistic roles in regulating kinetochore-microtubule plus-end dynamics. J Cell Sci. 2009;122(Pt 14):2543-53.
[348] Maia AF, Lopes CS, Sunkel CE. BubR1 and CENP-E have antagonistic effects upon the stability of microtubule-kinetochore attachments in Drosophila S2 cell mitosis. Cell Cycle. 2007;6(11):1367-78.
[349] Foley EA, Kapoor TM. Microtubule attachment and spindle assembly checkpoint signalling at the kinetochore. Nat Rev Mol Cell Biol. 2013;14(1):25-37.
[350] Kops GJ, Shah JV. Connecting up and clearing out: how kinetochore attachment silences the spindle assembly checkpoint. Chromosoma. 2012;121(5):509-25.
[351] Howell BJ, Hoffman DB, Fang G *et al.* Visualization of Mad2 dynamics at kinetochores, along spindle fibers, and at spindle poles in living cells. J Cell Biol. 2000;150(6):1233-50.
[352] Howell BJ, Moree B, Farrar EM *et al.* Spindle checkpoint protein dynamics at kinetochores in living cells. Curr Biol. 2004;14(11):953-64.
[353] Lara-Gonzalez P, Westhorpe FG, Taylor SS. The spindle assembly checkpoint. Curr Biol. 2012;22(22):R966-80.
[354] Cheeseman IM, Desai A. A combined approach for the localization and tandem affinity purification of protein complexes from metazoans. Sci STKE. 2005;2005(266):pl1.
[355] Nakano H, Funasaka T, Hashizume C *et al.* Nucleoporin translocated promoter region (Tpr) associates with dynein complex, preventing chromosome lagging formation during mitosis. J Biol Chem. 2010;285(14):10841-9.
[356] Yan X, Li F, Liang Y *et al.* Human Nudel and NudE as regulators of cytoplasmic dynein in poleward protein transport along the mitotic spindle. Mol Cell Biol. 2003;23(4):1239-50.
[357] Toledo CM, Herman JA, Olsen JB *et al.* BuGZ is required for Bub3 stability, Bub1 kinetochore function, and chromosome alignment. Dev Cell. 2014;28(3):282-94.
[358] Jiang H, He X, Wang S *et al.* A microtubule-associated zinc finger protein, BuGZ, regulates mitotic chromosome alignment by ensuring Bub3 stability and kinetochore targeting. Dev Cell. 2014;28(3):268-81.
[359] Martinez-Exposito MJ, Kaplan KB, Copeland J *et al.* Retention of the BUB3 checkpoint protein on lagging chromosomes. Proc Natl Acad Sci U S A. 1999;96(15):8493-8.
[360] Waters JC, Chen RH, Murray AW *et al.* Localization of Mad2 to kinetochores depends on microtubule attachment, not tension. J Cell Biol. 1998;141(5):1181-91.

[361] Lara-Gonzalez P, Scott MI, Diez M *et al.* BubR1 blocks substrate recruitment to the APC/C in a KEN-box-dependent manner. J Cell Sci. 2011;124(Pt 24):4332-45.
[362] Buschhorn BA, Petzold G, Galova M *et al.* Substrate binding on the APC/C occurs between the coactivator Cdh1 and the processivity factor Doc1. Nat Struct Mol Biol. 2011;18(1):6-13.
[363] Kuijt TE, Omerzu M, Saurin AT *et al.* Conditional targeting of MAD1 to kinetochores is sufficient to reactivate the spindle assembly checkpoint in metaphase. Chromosoma. 2014.
[364] Ohi MD, Feoktistova A, Ren L *et al.* Structural organization of the anaphase-promoting complex bound to the mitotic activator Slp1. Mol Cell. 2007;28(5):871-85.
[365] Visconti R, Palazzo L, Grieco D. Requirement for proteolysis in spindle assembly checkpoint silencing. Cell Cycle. 2010;9(3):564-9.
[366] Famulski JK, Chan GK. Aurora B kinase-dependent recruitment of hZW10 and hROD to tensionless kinetochores. Curr Biol. 2007;17(24):2143-9.
[367] Zeng X, Sigoillot F, Gaur S *et al.* Pharmacologic inhibition of the anaphase-promoting complex induces a spindle checkpoint-dependent mitotic arrest in the absence of spindle damage. Cancer Cell. 2010;18(4):382-95.
[368] Diaz-Rodriguez E, Sotillo R, Schvartzman JM *et al.* Hec1 overexpression hyperactivates the mitotic checkpoint and induces tumor formation in vivo. Proc Natl Acad Sci U S A. 2008;105(43):16719-24.
[369] Lin YT, Chen Y, Wu G *et al.* Hec1 sequentially recruits Zwint-1 and ZW10 to kinetochores for faithful chromosome segregation and spindle checkpoint control. Oncogene. 2006;25(52):6901-14.
[370] Gascoigne KE, Cheeseman IM. CDK-dependent phosphorylation and nuclear exclusion coordinately control kinetochore assembly state. J Cell Biol. 2013;201(1):23-32.
[371] Kuijt TE, Omerzu M, Saurin AT *et al.* Conditional targeting of MAD1 to kinetochores is sufficient to reactivate the spindle assembly checkpoint in metaphase. Chromosoma. 2014;123(5):471-80.
[372] Musacchio A. The Molecular Biology of Spindle Assembly Checkpoint Signaling Dynamics. Curr Biol. 2015;25(20):R1002-18.
[373] Reddy SK, Rape M, Margansky WA *et al.* Ubiquitination by the anaphase-promoting complex drives spindle checkpoint inactivation. Nature. 2007;446(7138):921-5.
[374] Wang Y, Jin F, Higgins R *et al.* The current view for the silencing of the spindle assembly checkpoint. Cell Cycle. 2014;13(11):1694-701.
[375] Westhorpe FG, Tighe A, Lara-Gonzalez P *et al.* p31comet-mediated extraction of Mad2 from the MCC promotes efficient mitotic exit. J Cell Sci. 2011;124(Pt 22):3905-16.
[376] Bekier ME, Fischbach R, Lee J *et al.* Length of mitotic arrest induced by microtubule-stabilizing drugs determines cell death after mitotic exit. Mol Cancer Ther. 2009;8(6):1646-54.
[377] Huang HC, Shi J, Orth JD *et al.* Evidence that mitotic exit is a better cancer therapeutic target than spindle assembly. Cancer Cell. 2009;16(4):347-58.
[378] Bennani-Baiti B, Bennani-Baiti IM. Gene symbol precision. Gene. 2012;491(2):103-9.
[379] Zasadil LM, Andersen KA, Yeum D *et al.* Cytotoxicity of paclitaxel in breast cancer is due to chromosome missegregation on multipolar spindles. Sci Transl Med. 2014;6(229):229ra43.

[380] Huisman C, Ferreira CG, Broker LE *et al.* Paclitaxel triggers cell death primarily via caspase-independent routes in the non-small cell lung cancer cell line NCI-H460. Clin Cancer Res. 2002;8(2):596-606.
[381] Fonseca J, Marques S, Silva PM *et al.* Prenylated Chalcone 2 Acts as an Antimitotic Agent and Enhances the Chemosensitivity of Tumor Cells to Paclitaxel. Molecules. 2016;21(8).
[382] Hou J, Aerts J, den Hamer B *et al.* Gene expression-based classification of non-small cell lung carcinomas and survival prediction. PLoS One. 2010;5(4):e10312.
[383] Lee SK, Kumar P. Conditional RNAi: towards a silent gene therapy. Adv Drug Deliv Rev. 2009;61(7-8):650-64.
[384] Nascimento AV, Bousbaa H, Ferreira D *et al.* Non-Small Cell Lung Carcinoma: An Overview on Targeted Therapy. Curr Drug Targets. 2015;16(13):1448-63.
[385] Wang TH, Wang HS, Soong YK. Paclitaxel-induced cell death: where the cell cycle and apoptosis come together. Cancer. 2000;88(11):2619-28.
[386] Ikui AE, Yang CP, Matsumoto T *et al.* Low concentrations of taxol cause mitotic delay followed by premature dissociation of p55CDC from Mad2 and BubR1 and abrogation of the spindle checkpoint, leading to aneuploidy. Cell Cycle. 2005;4(10):1385-8.
[387] Brito DA, Rieder CL. Mitotic checkpoint slippage in humans occurs via cyclin B destruction in the presence of an active checkpoint. Curr Biol. 2006;16(12):1194-200.
[388] Knox JJ, Gill S, Synold TW *et al.* A phase II and pharmacokinetic study of SB-715992, in patients with metastatic hepatocellular carcinoma: a study of the National Cancer Institute of Canada Clinical Trials Group (NCIC CTG IND.168). Invest New Drugs. 2008;26(3):265-72.
[389] Chan KS, Koh CG, Li HY. Mitosis-targeted anti-cancer therapies: where they stand. Cell Death Dis. 2012;3:e411.
[390] Janssen A, Medema RH. Mitosis as an anti-cancer target. Oncogene. 2011;30(25):2799-809.
[391] Manchado E, Guillamot M, Malumbres M. Killing cells by targeting mitosis. Cell Death Differ. 2012;19(3):369-77.
[392] Yamada HY, Gorbsky GJ. Spindle checkpoint function and cellular sensitivity to antimitotic drugs. Mol Cancer Ther. 2006;5(12):2963-9.
[393] Neville BW, Day TA. Oral cancer and precancerous lesions. CA Cancer J Clin. 2002;52(4):195-215.
[394] Jemal A BF, Center MM, Ferlay J, Ward E, Forman D. Global cancer statistics. CA Cancer J Clin 2011;61:69-90.
[395] Fandi A, Altun M, Azli N *et al.* Nasopharyngeal cancer: epidemiology, staging, and treatment. Semin Oncol. 1994;21(3):382-97.
[396] Gassmann R, Essex A, Hu JS *et al.* A new mechanism controlling kinetochore-microtubule interactions revealed by comparison of two dynein-targeting components: SPDL-1 and the Rod/Zwilch/Zw10 complex. Genes Dev. 2008;22(17):2385-99.
[397] Barbosa J NA, Faria J, Silva P, Bousbaa H. The spindle assembly checkpoint: perspectives in tumorigenesis and cancer therapy. Front Biol. 2011;6: 147–55.
[398] Monteiro LS, Delgado ML, Ricardo S *et al.* EMMPRIN expression in oral squamous cell carcinomas: correlation with tumor proliferation and patient survival. Biomed Res Int. 2014;2014:905680.
[399] Monteiro LS, Delgado ML, Ricardo S *et al.* Phosphorylated mammalian target of rapamycin is associated with an adverse outcome in oral squamous cell carcinoma. Oral Surg Oral Med Oral Pathol Oral Radiol. 2013;115(5):638-45.

[400] Zhang P, Zhang Z, Zhou X *et al.* Identification of genes associated with cisplatin resistance in human oral squamous cell carcinoma cell line. BMC Cancer. 2006;6:224.
[401] Lengauer C, Kinzler KW, Vogelstein B. Genetic instabilities in human cancers. Nature. 1998;396(6712):643-9.
[402] Bockmuhl U, Petersen I. DNA ploidy and chromosomal alterations in head and neck squamous cell carcinoma. Virchows Arch. 2002;441(6):541-50.
[403] Saunders WS, Shuster M, Huang X *et al.* Chromosomal instability and cytoskeletal defects in oral cancer cells. Proc Natl Acad Sci U S A. 2000;97(1):303-8.
[404] Sheltzer JM, Amon A. The aneuploidy paradox: costs and benefits of an incorrect karyotype. Trends Genet. 2011;27(11):446-53.
[405] Cohen SM, Lippard SJ. Cisplatin: from DNA damage to cancer chemotherapy. Prog Nucleic Acid Res Mol Biol. 2001;67:93-130.
[406] Dasari S, Tchounwou PB. Cisplatin in cancer therapy: molecular mechanisms of action. Eur J Pharmacol. 2014;740:364-78.
[407] Karlsson MO, Molnar V, Freijs A *et al.* Pharmacokinetic models for the saturable distribution of paclitaxel. Drug Metab Dispos. 1999;27(10):1220-3.
[408] Chen JG, Horwitz SB. Differential mitotic responses to microtubule-stabilizing and -destabilizing drugs. Cancer Res. 2002;62(7):1935-8.

APPENDIX

MOVIES LEGENDS

MOVIES LEGENDS

CHAPTER 3. SHEDDING LIGHT ON SPINDLE ASSEMBLY CHECKPOINT REGULATION AND FUNCTION

Dynein-dependent transport of spindle assembly checkpoint proteins off kinetochores toward spindle poles

Movie 3.1. Control (Saline G) HeLa cells stably expressing EGFP-Bub3 showed normal mitosis timing and normal localization pattern of Bub3. Maximum projections of 7 Z-stacks at 1 μm intervals are displayed. Time is shown in hours:minutes.

Movie 3.2. ATP reduction induced relocalization of EGFP-Bub3 to spindle poles in metaphase-arrested cells. HeLa cells stably expressing EGFP-Bub3 were treated with MG132 and filmed for 30 minutes, then AZ/DOG was added and the cells were further filmed for 60 minutes. EGFP-Bub3 relocalized to spindle poles within minutes of adding AZ/DOG. Maximum projections of 7 Z-stacks at 1 μm intervals are displayed. Time is shown in hours:minutes.

CHAPTER 4. EXPLORING THE POTENTIAL THERAPEUTIC IMPLICATIONS OF SPINDLE ASSEMBLY CHECKPOINT FOR CANCER THERAPY

Spindly Delays Mitotic Exit and Exacerbates Cell Death Response of Cancer Cells Treated with Low Doses of Paclitaxel

Movie 4.1. Time-lapse imaging (DIC microscopy) of a typical mitosis in untreated NCI-H460 cells. Time is shown in hours:minutes.

Movie 4.2. Time-lapse imaging (DIC microscopy) showing a typical Spindly-depleted cell undergoing death in mitosis after >13 h spent in mitosis. Time is shown in hours:minutes.

Movie 4.3. Time-lapse imaging (DIC microscopy) showing a typical mitosis in 10 nM paclitaxel-treated NCI-H460 cells. Time is shown in hours:minutes.

Movie 4.4. Time-lapse imaging (DIC microscopy) of Spindly-depleted plus 10 nM paclitaxel-treated cells; the cell at the middle of field arrests in mitosis, initiates mitotic exit at 11h:00min, and dies at 26h:10min. Time is shown in hours:minutes.